Isolation and proteomic characterization of the mid-infection inclusion of *Chlamydia trachomatis*

D i s s e r t a t i o n

zur Erlangung des akademischen Grades
doctor rerum naturalium
(Dr. rer. nat.)
im Fach Biologie

eingereicht an der
Lebenswissenschaftlichen Fakultät
der Humboldt-Universität zu Berlin

von
Lukas Aeberhard

Präsident der Humboldt-Universität zu Berlin
Prof. Dr. Jan Hendrik Olbertz

Dekan der Lebenswissenschaftlichen Fakultät
Prof. Dr. Richard Lucius

Gutachter:
1. Prof. Dr. Thomas Meyer
2. Prof. Dr. Kai Matuschewski
3. PD Dr. Klaus Heuner

eingereicht am: 16.09.14

Tag der mündlichen Prüfung: 15.12.14

Für Lilly, Hugo, Wilhelma und Siegfried

Zusammenfassung

Chlamydia trachomatis ist ein obligat intrazelluläres Humanpathogen, welches sich, nach der Einnistung in seiner Wirtszelle, innerhalb einer membranumhüllten Vakuole, der sogenannten Inklusion, befindet. Die Inklusionsmembran stellt dabei die primäre Kontaktfläche für Pathogen–Wirtszell-Interaktionen dar und definiert dadurch die Nische, in welcher sich die Bakterien vermehren können. Eine immer größer werdende Anzahl von Wirtszellproteinen wurde bereits als inklusionslokalisiert beschrieben, wobei viele dieser Proteine entscheidende Funktionen in der Biogenese und Erhaltung der Inklusion übernehmen. Die Zusammensetzung des Wirtszellproteoms der Inklusion von *C. trachomatis* ist demnach von zentralem Interesse für die Forschungsgemeinschaft, welche dessen Wirtszellinteraktionen untersucht, ist zurzeit aber nicht umfassend bekannt.

Zum ersten Mal beschreiben wir in dieser Arbeit die Isolation und biochemische Charakterisierung der Inklusion von *C. trachomatis*, mittels herkömmlicher Organellaufreiniungsverfahren und massenspektrometrischer Proteomanalyse an einem zentralen Zeitpunkt der Infektion. Die relative Quantifizierung von Proteinen mittels stabiler isotopenmarkierter Aminosäuren in Zellkultur (SILAC) und die zusätzliche markierungsfreie Quantifizierung erlaubten uns die Darstellung dieses subzellulären Proteoms mit hohem Konfidenzniveau. Mithilfe dieser Methoden haben wir über dreihundert Wirtszellproteine identifiziert und quantifiziert, welche noch nicht als inklusionslokalisiert bekannt waren. Diese Daten erlauben es zum ersten Mal eine unbeeinflusste und quantitative Aussage über das Inklusionsproteom von *C. trachomatis* zu machen und sind eine wichtige Ressource für alle Arbeitsgruppen, welche sich mit Wirtszellinteraktionen von Chlamydien beschäftigen.

Die globale Analyse dieser Daten bestätigte die Rekrutierung vieler Proteine, welche in verschiedenen Membrantransportwegen involviert sind. Zudem fanden sich viele Proteine des retrograden Transportweges, welcher bislang nicht im Zusammenhang mit Chlamydien-Infektionen untersucht wurde. Die detaillierte Analyse dieser Proteine zeigte, dass Sorting Nexine sehr spezifisch zur Inklusion rekrutiert werden. Zudem haben wir mithilfe des unlängst beschriebenen Inhibitors Retro-2^{cycl} gezeigt, dass retrograder Transport essenziell für die effiziente intrazelluläre Replikation von *C. trachomatis* ist.

Zusammengefasst haben wir eine große Anzahl zuvor unbekannter inklusionsassoziierter Proteine identifiziert und quantifiziert, was das Wissen über die Interaktionen von *C. trachomatis* mit der Wirtszelle entscheidend vertieft. Auf Basis unserer Daten schlagen wir retrograden Transport als neues potenzielles Angriffsziel von Therapeutika zur Behandlung von *C. trachomatis* Infektionen vor.

Abstract

Chlamydia trachomatis is an obligate intracellular human pathogen which, after invasion of its host cell, resides within a membrane bounded vacuole called the inclusion. The inclusion membrane represents the main host-pathogen interface of *Chlamydiae* and thereby defines the environment in which the bacteria thrive. A growing number of proteins have been found to be inclusion localized, many of which serve important functions in the establishment and maintenance of the inclusion. The proteome composition of the inclusion of *C. trachomatis* is therefore of central interest for the research community involved in the investigation of host-pathogen interactions of *Chlamydia* but is yet unknown.

Here we describe for the first time the isolation and biochemical characterization of the mid-infection inclusion of *C. trachomatis* using mass spectrometry based proteomics in combination with traditional organelle purification techniques. Relative quantification by Stable isotope labeling by amino acids in cell culture (SILAC) and additional label free quantification allowed the generation of a high confidence subcellular proteome. Using this approach, we were able to identify and quantify over three hundred host cell proteins that were not reported previously to be inclusion localized. These data for the first time allow an unbiased and quantitative assessment of the inclusion proteome and are an important resource for all groups involved in the research of host-pathogen interactions of *Chlamydia.*

By analyzing the obtained data on a global scale, we were able to confirm previous reports on the recruitment of proteins implied in several membrane trafficking pathways. Detailed analysis of proteins identified to be involved in retrograde trafficking, a pathway that has not been described previously in the context of chlamydial infections, showed that sorting nexins are specifically recruited to the inclusion. We furthermore identified retrograde trafficking to be essential for the efficient intracellular replication of *C. trachomatis* using the recently described inhibitor Retro-2^{cycl}, which drastically reduced bacterial progeny formation upon treatment.

Taken together, we identified and quantified a large number of previously unknown inclusion associated proteins and thereby significantly increased the knowledge of the interactions of *C. trachomatis* with the host cell. Based on our findings, we propose retrograde trafficking as a novel potential drug target for the treatment of infections with *C. trachomatis*.

Table of contents

1. Introduction

1.1 Chlamydiales

Chlamydiae are Gram-negative, obligate intracellular bacteria with a unique biphasic developmental cycle (Abdelrahman and Belland 2005) and infect a wide range of host organisms. In humans, they are responsible for a number of different diseases ranging from infections of the urogenital tract to the eye and the lungs (Peeling and Brunham 1996).

In addition to being pathogens of humans, *Chlamydia*-like organisms have been found to infect amoebae and other eukaryotic hosts; however, no close free-living relative is known (Collingro, Tischler *et al.*). Several *Chlamydia*-like organisms have been described, all of which originated from the same common ancestor as evidenced by the available genome sequences (Collingro, Tischler *et al.* 2011). *Chlamydiales* therefore represent a unique branch of bacteria. The order *Chlamydiales* branched approximately 2 billion years ago from the major bacterial phyla while the so called environmental *Chlamydia*, endosymbionts in free-living amoebae, diverged approximately 700 million years ago from the present-day pathogenic *Chlamydiaecae* (Horn, Collingro *et al.* 2004).

Not surprisingly, *Chlamydiales* have a long history of co-evolution with their eukaryotic hosts (Schmitz-Esser, Linka *et al.* 2004, Horn 2008), which is manifested in the intricate interplay between the pathogen and the infected host. The study of these interactions may contribute to the development of novel therapeutic approaches and is therefore of great medical importance. Furthermore, the basic research on host-pathogen interactions is an important contributor to our understanding of basic functions and regulatory mechanisms of the eukaryotic cell.

1.1.1 Taxonomy of Chlamydia

Based on the sequencing of 16S and 23S rRNA, a phylogenetic tree for the bacterial phylum *Chlamydia*e was put forward by Everett *et al.* (Everett, Bush *et al.* 1999), of which the only order is *Chlamydiales,* consisting of the families *Parachlamydiaecae*, *Waddliaecae*, *Simkaniaceae* and *Chlamydiaceae.* In this proposed taxonomy, the genus *Chlamydia* was assigned to two genera, *Chlamydia* and *Chlamydophila* as the 16S rRNA genes clustered differentially. However, this view was not broadly accepted as several aspects other than the 16S rRNA gene phylogeny did not support the distinction (Schachter, Stephens *et al.* 2001). In 2009 it was proposed to reunite the family *Chlamydiacae* into the single genus *Chlamydia,* based on the natural history of the organism as revealed by genome comparisons (Stephens, Myers *et al.* 2009). This thesis and the majority of recent publications adhere to the revised taxonomy by Stephens *et al.* 2009 (see Figure 1.1 A and B).

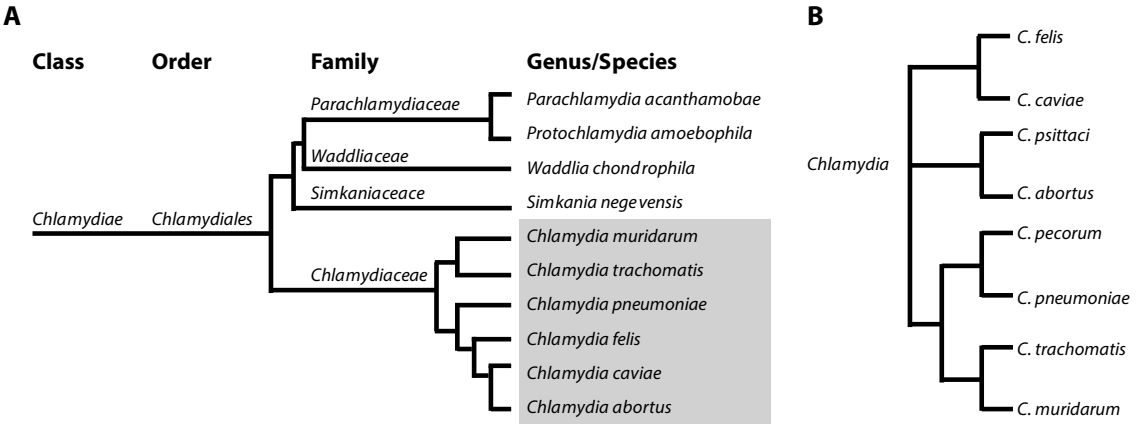

Figure 1.1: Taxonomy and phylogeny of the phylum *Chlamydiae*
Schematic representation of the phylogenetic tree and taxonomy of **A)** the phylum *Chlamydiae* based on (Everett, Bush *et al.* 1999, Collingro, Tischler *et al.* 2011), taking into account the revision of the family *Chlamydiaceae* (Stephens, Myers *et al.* 2009) and **B)** the phylogenetic tree of *Chlamydiaceae* according to Stephens *et al.* 2009 with additional species and a slightly different phylogeny. The length of the lines is arbitrary and does not represent phylogenetic distances.

1.1.2 Clinical relevance of Chlamydia infections

In humans, *Chlamydia trachomatis* is the most frequently diagnosed disease causing species of the *Chlamydiaceae*. With approximately 90 million infections a year it is also the most widespread bacterial sexually transmittable disease (Brunham and Rey-Ladino 2005). Three groups of serovars that display different tissue tropism and clinical outcomes have been described.

Trachoma, the leading infectious cause of blindness world-wide is caused by the ocular serovars A through C. Repeated infection of the epithelium of the conjunctive leads to the development of scar tissue. The scarred tissue leads to a contraction of the epithelium, which in turn causes the eyelids to roll inwards, where the eyelashes scratch the ocular surface. This condition is called trichiasis and eventually leads to blindness (Burton and Mabey 2009).

Serovars D-K on the other hand only occasionally cause conjunctivitis and are most commonly associated with sexually transmittable disease due to infections of the mucosal epithelial cells of the urogenital tract. Most infections go unnoticed, but acute diseases include urethritis, cervicitis and in rare cases, when a newborn is infected during birth, neonatal pneumonia. More importantly, sequelae due to chronic infections, can lead to pelvic inflammatory disease, ectopic pregnancy, proctitis and tubal infertility (Peeling and Brunham 1996). Complications arising from these infections are a main cause of preventable infertility in the developed world (Faro 1985, Haggerty, Gottlieb *et al.* 2010).

Serovars L1, L2, and L3 cause the more systemic infection lymphogranuloma venereum (LGV). This sexually transmitted infection causes inflammation of the inguinal lymph nodes by infection of monocytes and macrophages (Schachter and Osoba 1983, Mabey and Peeling 2002). The infection has a strong acute manifestation which presents itself in three stages. The first stage is a painless

genital ulcer which often goes unnoticed followed by the second stage where the infections spreads to the lymph nodes, which leads to painful lymphadenopathy. The third stage is characterized by chronic inflammatory lesions which lead to scarring of the genital tract and often spread to the eyes. Sequelae of chronic infections includes lymphatic obstruction (Mabey and Peeling 2002).

Once detected, treatment of *Chlamydia* is relatively straightforward by a single dose administration of Azithromycin or 7 days treatment with Doxycycline, Erythromycin, Levofloxacin or Ofloxacin (Centers for Disease Control and Prevention 2010). However, most infections in industrialized nations remain asymptomatic and therefore without diagnosis, necessitating the use of additional measures to reduce infections in the general population. These include education on protected sexual intercourse and screening for *Chlamydia* infections (Belland, Ojcius *et al.* 2004). In less developed countries which are mostly affected by Trachoma, efforts focus on access to surgical intervention for late stage infections, distribution of antibiotics for treatment of acute infections, improved facial hygiene and environmental change, such as access to water and sanitation (SAFE-strategy). These efforts are bundled in the GET2020 (Global elimination of trachoma by 2020) alliance by the world health organization (Mecaskey, Knirsch *et al.* 2003).

1.1.3 The developmental cycle of *Chlamydiaceae*

All members of the family *Chlamydiaceae* share a biphasic developmental cycle (Figure 1.2) that involves two distinct developmental forms and three distinct intracellular stages (early, mid and late), that are distinguishable by different transcriptional programs (Shaw, Dooley *et al.* 2000). These three traditional gene sets were extended by at least another class (tardy) in microarray studies of the *C. pneumoniae* developmental cycle (Maurer, Mehlitz *et al.* 2007). The elementary body (EB) is the infectious form of the bacteria whereas the reticulate body (RB) is the replicative and metabolically highly active form (Moulder 1991). EBs are characterized by their relative tolerance to environmental stress which is attributed to their outer membrane proteins that are highly cross linked by disulfide bonds (Hatch, Miceli *et al.* 1986). Their DNA is condensed due to the binding of the histone H1 like proteins Hc1 and Hc2 (Perara, Ganem *et al.* 1992, Brickman, Barry *et al.* 1993).

EBs attach to the cell surface and are internalized by endocytosis (Hybiske and Stephens 2007).

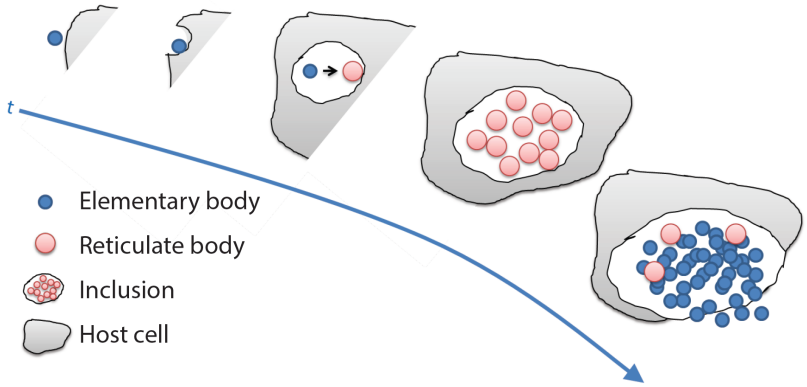

Figure 1.2: Chlamydial cycle of development
The cycle of development starts with the attachment of *Chlamydia* to the cell surface when present in the infectious form, the elementary body (EB). The nascent vacuole containing the bacterium is called an inclusion. After the inclusion has been transported to the peri-Golgi region, the EB transforms into the replicative form, the reticulate body (RB). The RBs divide by binary fission while the inclusion grows and start to redifferentiate into EBs towards the end of the bacterial life cycle. The bacteria are then released either by extrusion of the inclusion or lysis of the host cell. The whole cycle takes approximately 48 h to complete in the case of *C. trachomatis* L2 but is considerably longer for other serovars and strains of *Chlamydia*.

Once inside the cell, the bacteria reside within a membrane bounded organelle called the inclusion. After uptake, unknown signals trigger extensive changes in the metabolic and morphologic properties of the bacteria. This stage of conversion from EB to RB is called the early stage. Hc1 and Hc2 dissociate from the DNA (Grieshaber, Fischer *et al.* 2004), thereby enabling the transcription of early genes. Outer membrane disulfide bonds are cleaved (Hatch, Miceli *et al.* 1986), concomitant with an increase of the diameter from 0.3 to 1 µm (Wyrick 2000).

During the mid-stage of the infection, the RBs divide by binary fission while the inclusion grows in size considerably (Moulder 1991).

The late stage starts at approximately mid-point of the infection, which for infections of *C. trachomatis* L2 is around 24 h *post infectionem* (*p.i.*), when RBs start to redifferentiate into the infectious form of the bacteria (Moulder 1991). 26 genes that correspond to the late stage of transcription have functions specifically related to EBs (Belland, Zhong *et al.* 2003). These include hctA and hctB which encode Hc1 and Hc2 as well as omcAB, which encodes two small cystein-rich outer membrane proteins (Omc A and OmcB) that are presumably involved in the structural rigidity of the EB outer membrane.

The end of the cycle is marked by the release of the bacteria either by lysis of the host cell or extrusion of the intact inclusion (Hybiske and Stephens 2007).

1.2 Host pathogen interactions

1.2.1 Gaining entrance

Although attachment to and entry of the host cell are key steps in the development of *Chlamydia,* the mechanisms in place for these interactions are not completely known. For entry of the host cell, several bacterial adhesins have been proposed. Glycosaminoglycan (Menozzi, Pethe *et al.* 2002), the major outer membrane protein (MOMP) (Su, Raymond *et al.* 1996), OmcB (Fadel and Eley 2007) and polymorphic membrane protein D (PmpD) (Wehrl, Brinkmann *et al.* 2004) all might be involved as either adhesins or receptor ligands. Surprisingly, MOMP was found to be glycosylated (Swanson and Kuo 1991) and bacterial N-linked glycan was shown to be required for infectivity in vivo (Campbell, Lee *et al.* 2006).

Among the proposed host receptors for different species of *Chlamydia* are heparan sulfate receptor (Su, Raymond *et al.* 1996), cation independent mannose 6-phosphate receptor (CI-M6PR) (Puolakkainen, Kuo *et al.* 2005), and the estrogen receptor complex (Davis, Raulston *et al.* 2002). Most recently, the entry of *C. pneumoniae* has been shown to be mediated by the invasin-receptor interaction of epidermal growth factor receptor (EGFR) and Pmp21 (Molleken, Becker *et al.* 2013), but the requirement for EGFR is not absolute, indicating several different mechanisms of uptake.

Among the proteins identified to be involved in attachment of *Chlamydia* to the cell surface, only protein disulfide isomerase (PDI) was identified as necessary for multiple species. PDI was shown to be necessary for two distinct mechanisms, structurally for attachment whereas its oxido-reductive enzymatic activity was required for entry (Abromaitis and Stephens 2009).

Taken together, the attachment and entry of *Chlamydia* is likely to be governed by multiple redundant mechanisms that ensure efficient infection of a wide range of host cells.

1.2.2 Early modification of the host cell

After attachment, the bacteria actively modify the host cell by means of a type three secretion system (T3SS), a multiprotein complex that acts as a molecular syringe which translocates bacterial effector proteins across the plasma membrane (PM) into the cytosol of the infected cells (Beeckman and Vanrompay 2010). One of the best known early effectors of *C. trachomatis* is TARP (translocated actin-recruiting phosphoprotein) which actively contributes to bacterial internalization by modifying the actin cytoskeleton (Jewett, Fischer *et al.* 2006). Reorganization of the actin skeleton is a hallmark of the entry of *Chlamydia* and has been shown to be dependent on small GTPases such as Rac1 (Ras-related C3 botulinum toxin substrate 1) in addition to bacterial factors (Scidmore 2011).

Inclusions are then transported along microtubules to the microtubule organizing center (MTOC) in a dynein dependent, dynactin independent manner which indicates that a bacterial effector protein links the inclusion to dynein (Clausen, Christiansen *et al.* 1997, Grieshaber, Grieshaber *et al.* 2003, Grieshaber, Grieshaber *et al.* 2006). Once at the MTOC, the inclusion maintains this link to the centrosome, even during the cell cycle, which results in several defects including supernumerary centrosomes, segregation defects and abnormal spindle poles (Grieshaber, Grieshaber *et al.* 2006, Johnson, Tan *et al.* 2009).

1.2.3 Living inside the inclusion – obtaining nutrients

At approximately 6 h – 8 h *p.i.* the inclusion of *C. trachomatis* L2 is positioned at the MTOC and ready for expansion. When the transformation of the EB into the replicative RB is completed (Belland, Zhong *et al.* 2003), *Chlamydiae* depend on the supply of external nutrients for growth. The genome sequence of *Chlamydia trachomatis* revealed massive genome condensation in the evolution of *Chlamydia* (Stephens, Kalman et al. 1998). The apparent lack of several core biosynthetic pathways suggests that most nutrients are delivered across the inclusion membrane to the bacteria. In a study by Heinzen and Hackstadt, fluorescent tracer molecules of varying molecular weight were tested for diffusion from the cytosol to the inclusion lumen. The membrane was not passively permeable for tracers as small as 520 Da, indicating a lack of open pores in the membrane (Heinzen and Hackstadt 1997). Although smaller compounds were never tested, it is assumed that the inclusion membrane is also impermeable for metabolites smaller than 520 Da such as certain sugars, amino acids and nucleotides, therefore necessitating active transport across the membrane. So far, only one host derived nutrient transporter has been shown to be recruited to the inclusion, namely the mammalian sodium multivitamin transporter (SMVT) which, in non-infected host cells, transports lipoic acid, biotin and pantothenic acid across the PM into the cell (Fisher, Fernandez *et al.* 2012).

Using ratiometric imaging with membrane-permeant, ion-selective fluoresecent dyes, the physical environment within the inclusion was probed. Ion concentrations of H^+, Na^+, K^+, and Ca^{2+} were comparable to cytoplasmic concentrations and the inclusion membrane appeared to be freely permeable for cytoplasmic ions (Grieshaber, Swanson *et al.* 2002).

C. trachomatis depends on pyrimidine and purine nucleotides for energy transduction and nucleic acid biosynthesis, as it is unable to synthesize them *de novo*. Although the enzymatic pathways to generate ATP via substrate level phosphorylation and CTP from UTP via a CTP synthetase exist (Stephens, Kalman *et al.* 1998), *Chlamydia* are auxotrophic for ATP, GTP and UTP (Tipples and McClarty 1993). To overcome this limitation, these nucleotides are imported to the bacteria by an unusual nucleotide transporter system. At least two proteins for nucleotide transport are found in

C. trachomatis: Npt1 (Nucleoside triphosphate transport protein 1) and Npt2. Biochemical analyses in *Escherichia coli* indicated that Npt1 serves as ATP/ ADP exchanger whereas Npt2 catalyzes the uptake of all ribonucleoside triphosphates for anabolic reactions (Tjaden, Winkler *et al.* 1999). In addition, *Chlamydiae* are unable to synthesize nicotinamide adenine dinucleotide (NAD) and therefore must scavenge it from the host. Surprisingly Npt1 of *C. trachomatis* seems to serve this purpose by having evolved the ability to also transport NAD in addition to ATP (Fisher, Fernandez *et al.* 2013). In a recent study, Npt1 was proposed as a putative inclusion membrane localized secreted protein (Saka, Thompson *et al.* 2011), suggesting it could serve as a bacterial transporter across the inclusion membrane.

A few genes involved in amino acid biosynthesis have been found in the genome. Surprisingly, most pathways are incomplete and therefore might serve other purposes than de novo amino acid biosynthesis. Among the more complete pathways is the tryptophan biosynthesis operon although with two missing enzymes (trpD and trpE). A gene encoding the tryptophan repressor was present too, indicating the capacity of *C. trachomatis* to respond to changes in intracellular tryptophan concentrations.

13 ABC (ATP-binding cassette) transporters primarily associated with amino acid and oligopeptide transport have been identified in the *C. trachomatis* genome which is in line with their limited amino acid biosynthetic ability (Stephens, Kalman *et al.* 1998).

C. trachomatis is able to de novo synthesize lipids normally found in prokaryotic membranes such as phosphatidyletahnolamine, phosphatidylglycerol and phosphatidylserine (Wylie, Hatch *et al.* 1997). Surprisingly, the analysis of the total lipid composition of *C. trachomatis* revealed a number of lipids typically only found in eukaryotic cells, including phosphatiylcholine, phosphatidylinositol (PtdIns), sphingomyelin (SM) and cholesterol (Hatch and McClarty 1998). Due to the lack of the enzymes necessary for synthesis of these lipids (Stephens, Kalman *et al.* 1998), they are most likely obtained from the host cell.

The inclusion membrane itself has not been analyzed for its lipid composition yet. Immunofluorescence (IF) studies have indicated that several host lipids including SM, ceramide, cholesterol, phosphatidic acid, PtdIns, phosphatidyletahnolamine and phosphatidylserine are present in the inclusion membrane (Elwell, Jiang *et al.* , Hackstadt, Scidmore *et al.* 1995, Hackstadt, Rockey *et al.* 1996, Carabeo, Mead *et al.* 2003, Beatty 2008). Indeed, a lot of the research in host-pathogen interactions of *Chlamydia* has focused on the transport of lipids across the inclusion membrane. This has revealed extensive interactions with several membrane trafficking pathways and the majority of host cell organelles.

1.2.4 Interaction with host organelles

The original observation by Hackstadt *et al.* (Hackstadt, Scidmore *et al.* 1995) indicated a close association of the Golgi apparatus (GA) with the inclusion and the trafficking of a fluoresecent ceramide analogue to the inclusion and the bacteria contained within. Subsequent analysis of the bacteria indicated that the fluorescent ceramide analogue was converted to SM. Endogenous SM is synthesized from ceramide in the GA prior to its transport to the PM in non-infected cells. Blocking vesicular transport with Brefeldin A (BFA) decreased the acquisition of SM by *C. trachomatis* and decreased inclusion size (Hackstadt, Rockey *et al.* 1996). It was therefore concluded that *C. trachomatis* intercepts an exocytic pathway that traffics SM rich vesicles from the *trans*-Golgi to the PM. Further research showed that only a subset of exocytic vesicles from the GA is intercepted as the SM related lipid glycosylceramide, which is also synthesized in the GA, was not trafficked to the inclusion (Moore, Fischer *et al.* 2008).

Similar to SM, cholesterol is transported from the GA to the inclusion and taken up by the bacteria. As the susceptibility of this trafficking to pharmacological inhibitors is identical to that of SM acquisition, it is thought to be maintained by the same mechanism (Carabeo, Mead *et al.* 2003). Two studies further underline the absolute necessity of host SM biosynthesis for the development of *Chlamydia* (van Ooij, Kalman *et al.* 2000, Robertson, Gu *et al.* 2009). Chemical inhibition of SM synthesis by inhibitors of serine palmitoyltransferase, the first enzyme in the biosynthetic pathway of host cell SM, leads to loss of inclusion membrane integrity followed by disruption of inclusion development and premature redifferentiation to EBs and release from the host cell (Robertson, Gu *et al.* 2009). Furthermore, inhibitor treated infections showed inhibition of homotypic fusion of inclusions (Robertson, Gu *et al.* 2009).

In a study by Heuer *et. al.* it was shown that *C. trachomatis* fragments the GA, likely by cleavage of the Golgi matrix protein golgin 84, into discrete ministacks which surround the inclusion (Heuer, Rejman Lipinski *et al.* 2009). The fragmentation of the GA enhanced infectious progeny formation presumably by improved lipid acquisition from the fragmented GA. Further work indicated that the Rab (Ras-like protein from rat brain) GTPases Rab11A and Rab6A are involved in this mechanism as their depletion inhibited fragmentation of the GA (Rejman Lipinski, Heymann *et al.* 2009).

In addition to the aforementioned vesicular transport pathways of lipid acquisition, ceramide has been shown to be delivered to the inclusion of *C. trachomatis* and *C. muridarum* by a non-vesicular, BFA insensitive pathway which relies on the ceramide transfer protein CERT (Derre, Swiss *et al.* 2011, Elwell, Jiang *et al.* 2011). CERT is recruited to the inclusion by its interaction with IncD (inclusion protein D) (Derre, Swiss *et al.* 2011, Agaisse and Derre 2014) and participates in interactions of the inclusion membrane with the endoplasmic reticulum (ER), so called membrane

contact sites (MCS) which have been described more extensively by Dumoux *et al*. (Dumoux, Clare *et al.* 2012).

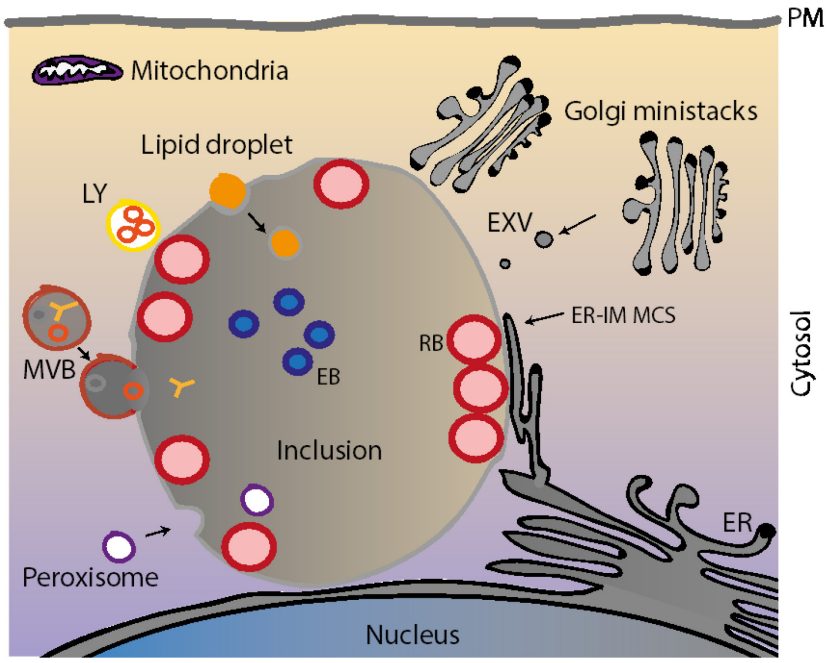

Figure 1.3: Interactions of the inclusion of *C. trachomatis* with cellular organelles
Details and references can be found in the text. EXV = exocytic vesicle, ER = endoplasmic reticulum, MVB = multivesicular body, IM = inclusion membrane, MCS = membrane contact site, LY = lysososme, PM = plasma membrane.

Lipid droplets, storage organelles for neutral lipids, are targeted by bacterial effectors and have been shown to be translocated into the lumen of *C. trachomatis* inclusions, where they associated with RBs (Kumar, Cocchiaro *et al.* 2006, Cocchiaro, Kumar *et al.* 2008). Pharmacological inhibition of lipid droplet formation furthermore led to attenuated growth, indicating this source of neutral lipids to be important for chlamydial expansion (Kumar, Cocchiaro *et al.* 2006).

Recently the interaction of the *C. trachomatis* inclusion with peroxisomes was described (Boncompain, Muller *et al.* 2014). Similar to lipid droplets, they are translocated into the lumen of the inclusion from where the bacteria presumably acquire plasmalogens, peroxisome synthesized ether phospholipids, and incorporate them to their cells. However, the requirement for peroxisomes was not essential for the generation of infectious progeny.

Proteins and lipids of multivesicular bodies (MVBs), intermediates of the endosome-lysosome pathway are recruited directly to the inclusion at late time points of the infection (Beatty 2006, Beatty 2008). The functional consequences of this interaction remain unknown

Lysosomes (LYs) are known to be closely associated with the inclusion and their function supports the growth of the bacteria by supplying free amino acids which are taken up by *Chlamydia* (Ouellette, Dorsey *et al.* 2011).

The direct fusion of the inclusion with autophagosomes was excluded (Al-Younes, Brinkmann *et al.* 2004), although an autophagy independent function of the autophagy associated proteins MAP1-LC3 (Microtubule-associated protein 1 light chain 3) is relevant for chlamydial propagation (Al-Younes, Al-Zeer *et al.* 2011).

Interactions of *C. trachomatis* with mitochondria, for example to prevent apoptosis, are well known (Perfettini, Reed *et al.* 2002). Direct associations of the inclusion with these organelles have not been described whereas they were observed in the avian strain *C. psittaci* (Matsumoto, Bessho *et al.* 1991). An overview of the interactions of the inclusion of *C. trachomatis* with cellular organelles is given in Figure 1.3.

1.3 Modification of the inclusion membrane

As described for the entry of the bacteria, *Chlamydia* encode for an extensive repertoire of putative effector proteins, most of which are believed to be secreted by the T3SS (Peters, Wilson *et al.* 2007, Jehl, Arnold *et al.* 2011). Many putative effector proteins belong to the class of Inc proteins, which are characterized by a bi-lobed hydrophobic domain (Bannantine, Griffiths *et al.* 2000). Inc proteins share relatively low sequence homology between species and most species encode their own complement of Incs (Lutter, Martens *et al.* 2012). In the case of *C. trachomatis,* it consists of between 39 and 59 proteins, depending on the prediction algorithms (Bannantine, Griffiths *et al.* 2000, Toh, Miura *et al.* 2003, Dehoux, Flores *et al.* 2011). A large part of the more than twenty experimentally verified Inc proteins of *C. trachomatis* localize to the inclusion membrane where they are thought to actively modify this intracellular niche (Bannantine, Griffiths *et al.* 2000, Rockey, Scidmore *et al.* 2002, Li, Chen *et al.* 2008). The ectopic expression of several different Inc proteins from *C. trachomatis* in HeLa cells led to the formation of membranous vesicular structures which did not colocalize with a wide range of organellar markers (Mital, Miller *et al.* 2013). This indicates that Inc proteins can indeed induce the formation of novel compartments without additional active modification of the compartment by live bacteria.

The most notable proposed functional mechanism of Inc proteins is the mimicry of SNARE (soluble NSF attachment factor receptor) proteins, which are essential for membrane fusion events in many vesicular trafficking events (Sudhof and Rothman 2009). By this mechanism, Inc proteins can either induce fusion with certain vesicles and compartments or inhibit it (Delevoye, Nilges *et al.* 2008, Paumet, Wesolowski *et al.* 2009).

1.4 Parasitophorous vacuoles are unique niches within the endomembrane system

The route of entry is similar for most intracellular pathogens. The organism is taken up by the host cell either actively by phagocytosis or by the subversion of endocytic pathways. Both mechanisms eventually lead to the pathogen to be contained in a membrane bounded vacuole that is derived from the PM. Once inside the cell, there are two options for the invading organism: escaping into the cytosol or altering the fate of the endosome/phagosome maturation to convert it into a hospitable environment for replication.

The majority of intracellular pathogens reside within a cytosolic vacuole generally termed parasitophorous vacuole (PV) (Casadevall 2008). Not surprisingly, they all evolved different strategies to avoid their degradation in the endolysosome (EL) or phagolysosome repectively.

1.4.1 The endomembrane system

The endomembrane system of eukaryotic cells is a large composite of membrane bounded organelles that form a functional unit, either by being interconnected or by direct interchange of material through vesicular transport. These organelles include the nuclear envelope, the ER, the GA, LYs, vacuoles, vesicles, endosomes, the PM and several intermediate compartments (Bonifacino and Glick 2004). The two primary functional subunits of the endomembrane system are the secretory system and the endosomal-lysosomal system, which both interact extensively (Bonifacino and Glick 2004).

The secretory system is composed of the ER, the ER – Golgi intermediate compartment (ERGIC), the GA which is itself composed of several cisternae, organized from cis over medial to trans and the trans Golgi network (TGN), a number of secretory vesicles and the PM (Bonifacino and Glick 2004). Proteins that are targeted for delivery to organelles of the secretory or endosomal-lysosomal systems or for secretion into the extracellular space, are moved unidirectionally along the secretory pathway, which starts at the ER with essentially one route up to the TGN, from where the proteins are sorted to their different destinations (Griffiths and Simons 1986). This flow is called the anterograde transport and is the standard route of delivery of newly synthesized proteins. Retrograde flow of proteins occurs from proteins that follow the endocytic pathway or retrograde trafficking routes. Both retrograde and anterograde flow of proteins are highly regulated to maintain the identity and functionality of the organelles of the endomembrane system (Bonifacino and Rojas 2006). In Figure 1.4, a schematic overview of the endosomal-lysosomal system and the secretory pathway is given.

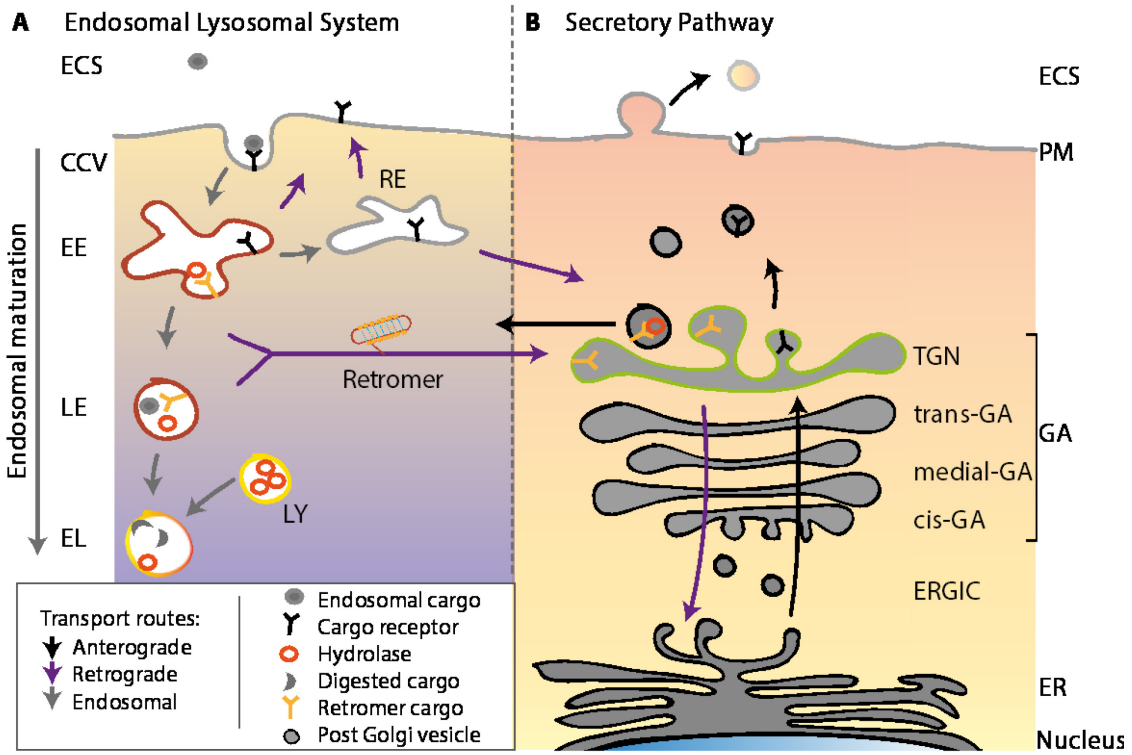

Figure 1.4: Trafficking pathways in the endomembrane system

Schematic overview of the main trafficking pathways within the endomembrane system. For explanation see text. ECS = extracellular space, CCV = clathrin coated vesicle, EE = early endosome, LE = late endosome, EL = endolysosome, LY = lysosome, PM = plasma membrane, TGN = trans Golgi network, GA = Golgi apparatus, ER = endoplasmic reticulum, ERGIC = ER – Golgi intermediate compartment **A)** Schematic overview of the endosomal-lysosomal system. **B)** Schematic overview of the secretory pathway.

Endocytosis is the process by which a cell absorbs extracellular material. Depending on the size and nature of the absorbed material, different pathways come into play. The endosomal-lysosomal system is composed of a number of organelles which serve different functions: The early endosomes (EEs), the recycling endosome (REs), the late endosomes (LEs) (essentially identical to MVBs), LYs and ELs (Huotari and Helenius 2011).

Nascent endosomes are membranous vacuoles derived from the plasmalemma which lack degradative and microbicidal activity. In the cytoplasm they fuse with EE, from which recycling of receptors to the PM either directly or via the RE takes place (Huotari and Helenius 2011). The endosomes start to mature into LE after 8 -15 minutes. Endosomal maturation involves the recruitment of Rab5 (EE) followed by a transition to Rab7 (LE) (Rink, Ghigo *et al.* 2005). During maturation, endosomes move along microtubules towards the MTOC (Aniento, Emans *et al.* 1993), while they receive cargo from the secretory pathway, especially hydrolases, which supports their maturation. Eventually they deliver a mixture of endocytic material and secretory cargo to the LYs, with which they ultimately fuse to form the EL. After degradation of the endocytosed material, the EL converts into a LY by another maturation step (Huotari and Helenius 2011), see also Figure 1.4 A.

Phagocytosis, a specialized form of endocytosis is the engulfment and subsequent elimination of particles larger than approximately 0.5 µm by a cell. It is primarily carried out by specialized cell types called professional phagocytes such as macrophages and dendritic cells but also occurs in other cell types. The mechanisms of phagosome maturation, although similar, are partly distinct from those of traditional endosomal maturation but also involve the transition from Rab5 to Rab7 (Kinchen and Ravichandran 2008). In the course of their maturation, they acquire the capacity to digest their contents and inactivate bacteria.

1.4.2 Retrograde trafficking

Retrograde trafficking acts on cargo which originally is targeted from the GA to endosomes or from the PM to endosomes by transporting it against the anterograde membrane flow from the endosomes to the TGN, the GA or, in a few exceptions to the ER (Johannes and Popoff 2008).

The prototypical retrograde trafficking is that of acid hydrolase receptors, for example Mannose-6-phosphate receptors. These sorting receptors are responsible for the delivery of newly synthesized acid hydrolase precursor proteins from the TGN to endosomes. The receptors bind the hydrolases, which carry a mannose-6-phosphate residue, at the TGN and transfer them to the endosomes, where they are released from the receptor due to a shift to low pH (Munier-Lehmann, Mauxion *et al.* 1996). The hydrolases eventually mature with the endosomes to late endosomes and lysosomes, where they become fully active. The receptors, after detachment of the hydrolases, are recycled back to the TGN. This mechanism is conserved in mammalians for the so-called multiligand type-I receptor family (Mari, Bujny *et al.* 2008) which includes sortilin, sorLA and sorCS among others.

Other proteins also depend on cycling from the endosome to the TGN including SNARE proteins such as VAMP4 and, which both have been reported to be associated to the chlamydial inclusion (Delevoye, Nilges *et al.* 2008, Pokrovskaya, Szwedo *et al.* 2012). In addition to this, several other cellular functions have been reported to depend on retrograde trafficking, for example the polarized secretion of matrix metalloproteases (Wang, Ma *et al.* 2004). Most importantly there does not seem to be a single route for retrograde trafficking but it can occur from several different stages of maturation along the endsomal pathway to the TGN (Johannes and Wunder 2011).

1.4.3 The retromer

The retromer is a complex that functions centrally in retrograde trafficking. It accumulates cargo in tubules that emanate from the EEs, most probably at the transition to LEs (Rojas, van Vlijmen *et al.* 2008, van Weering, Verkade *et al.* 2012) . These tubules progress to scission from the EE/LE, from where they are transported along microtubules to the TGN.

The retromer was first described in yeast, where it is composed of two subcomplexes. One subcomplex, termed the cargo selective complex, consists of a heterotrimer of vacuolar protein sorting-associated protein 26 (VPS26p), VPS29p and VPS35p (Seaman, McCaffery *et al.* 1998). VPS35p is responsible for the cargo recognition via a sorting motif on the cytoplasmic domain of the respective cargo. The second subcomplex consists of members of the sorting nexin (SNX) family, Vps5p and VPS17p, which dimerize via interactions on their C-termini while Vps5p solely interacts with the cargo selective complex on its N-terminus (Seaman and Williams 2002, Attar and Cullen 2010). It is called the membrane-deforming subcomplex due to its ability to induce and/or stabilize membrane tubules via the BAR (Bin/amphiphysin/Rvs) domain.

As a result of several gene duplications, the composition of the mammalian retromer is more complex. The VPS26/VPS29/VPS35 complex is expanded in by an additional copy of VPS26 (named VPS26A and VPS26B) (Bugarcic, Zhe *et al.* 2011). The role of Vps5p is fulfilled by SNX1 and SNX2 (Carlton, Bujny *et al.* 2005, Griffin, Trejo *et al.* 2005, Rojas, Kametaka *et al.* 2007) while there are two clear Vps17p homologs, SNX5 and SNX6 (Wassmer, Attar *et al.* 2007). Additionally, also SNX32 has been suggested as Vps17p homolog but not yet experimentally tested. This classical composition of the retromer is called the SNX-BAR retromer as all mentioned sorting nexins contain the characteristic BAR domain in addition to the PtdIns-binding PX (phox homology) domain, which is found in all members of the SNX family (Attar and Cullen 2010). For proper positioning of the SNX-BAR subcomplex, an avidity based coincidence sensing mechanism, involving both the PtdIns binding capacity and the membrane curvature sensing of the BAR domain, was suggested (Cullen and Korswagen 2012).

The cargo selective subcomplex has been shown to be recruited to membranes via Rab7 (Rojas, van Vlijmen *et al.* 2008, Seaman, Harbour *et al.* 2009) and possibly SNX3 (Harrison, Hung *et al.* 2014) in addition to binding to cargo either directly or via adapter proteins. SNX-BAR proteins always form heterodimers of one Vps5 homolog (SNX1, SNX2) and one Vps17 homolog (SNX5, SNX6) (Hong, Yang *et al.* 2009), while all four can bind to the cargo recognition complex independently (Wassmer, Attar *et al.* 2009).

Upon assembly of the SNX-BAR retromer complex at cargo containing sites at the endosome and tubularisation of the membrane, accessory factors that mediate pathway progression bind to the nascent tubulues. These include the WASH (Wiskott-Aldrich syndrome protein and Scar

homologue) complex and a regulatory complex. WASH binds to VPS35 via a component of its regulatory complex and induces actin polymerization which generates a force pushing the tubule away from the vacuolar compartment (Gomez and Billadeau 2009, Harbour, Breusegem *et al.* 2010). Additionally SNX5 and SNX6 interact with the p150^{glued} subunit of dynactin (Hong, Yang *et al.* 2009, Wassmer, Attar *et al.* 2009) to couple it to dynein which in turn binds to microtubules to generate an additional pulling force on the tubules.

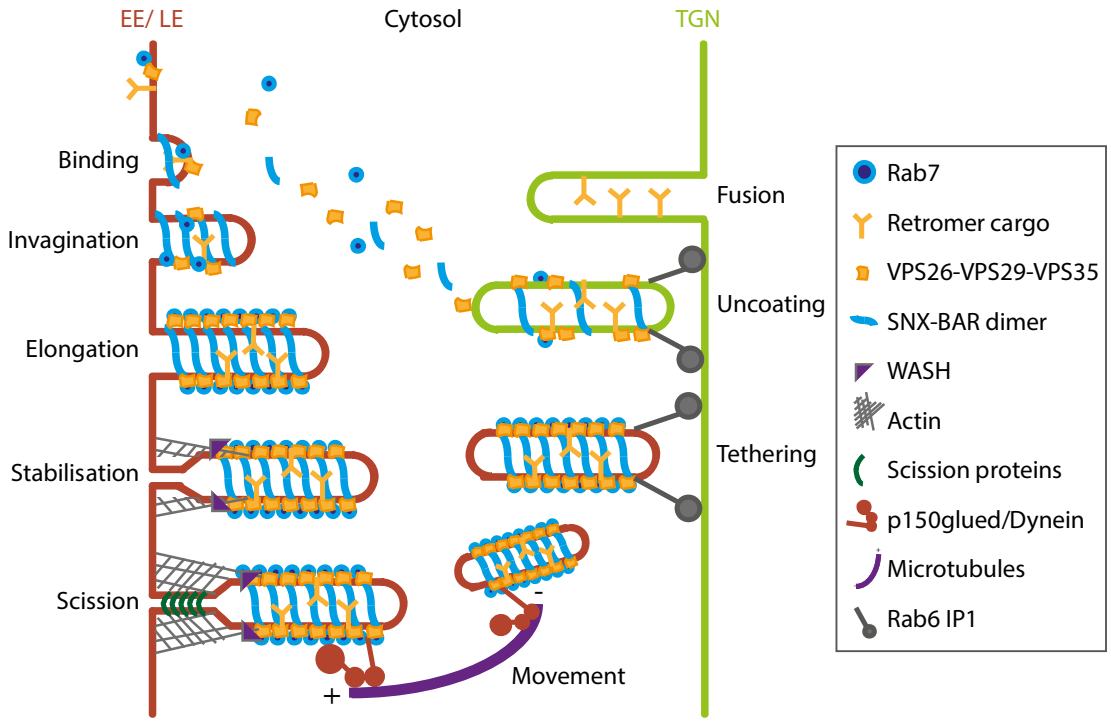

Figure 1.5: Function of the SNX-BAR retromer
The process starts in the upper left corner with binding of the VPS complex to Rab7 and association with the SNX-BAR dimer followed by invagination over elongation, stabilization by actin and scission from the endosomal membrane, followed by movement along microtubules towards the TGN where the tublues are tethered to the membrane via Rab6 IP1, followed by uncoating and fusion with the TGN membrane. Red and green membranes indicate different membrane PtdIns compositions. For more details see text. Adapted from (McGough and Cullen 2011) and (Cullen and Korswagen 2012). TGN = trans Golgi network, EE = early endosome, LE = late endosome.

Fission of the tubule is achieved by a yet unknown mechanism which releases the retromer tubule from the endosome from where it is transported along microtubules to the TGN. In yeast, Vps1 has been shown to be involved in fission (Chi, Liu *et al.* 2014), along with Mvp1, a homolog of SNX8. The disruption of the SNX-p150^{glued} interaction leads to extended SNX positive tubules (Wassmer, Attar *et al.* 2009) which do not progress to fission, which is also observed upon knockdown of the WASH complex (Gomez and Billadeau 2009). Once at the TGN, the tubules are tethered to the membrane by Rab6 interacting protein 1 (Rab6 IP1) (Wassmer, Attar *et al.* 2009), followed by uncoating and fusion with the target membrane. See Figure 1.5 for a schematic overview of retromer function.

In comparison to the retromer complex of yeast, the composition of the mammalian retromer has a large diversity and independent functions of each subcomplex are beginning to emerge.

Recently, an alternative composition of the retromer complex composed of SNX3 and the cargo recognition complex has been described (Harterink, Port *et al.* 2011, Zhang, Wu *et al.* 2011). SNX3 does not contain a BAR domain and in this composition the SNX3-retromer mediates the recycling of Wnt and Wntless proteins but also exists in yeast, where it recycles an iron transporter (Strochlic, Setty *et al.* 2007), a function also maintained in mammalian cells (Niu, Zhang *et al.* 2013). The retromer is also involved in non-retrograde transport activities such as the transcytotic transport of polymeric immunoglobulin receptors from the basolateral to the apical surface of polarized epithelial cells which requires the cargo recognition complex but is independent of SNX1 and SNX2 (Verges, Luton *et al.* 2004).

1.4.3.1 SNX proteins bind PtdIns via the PX domain

The PtdIns-binding PX domain is found in all members of the SNX family. The SNX-PX subclass contains only a PX domain (9 members), whereas the SNX-BAR class (12 members) contains an additional BAR domain. The combination of PX domains with additional domains other than BAR is grouped to SNX-Other (12 members). (Attar and Cullen 2010)

SNX1 was originally reported to bind to PtdIns 3,4,5-triphosphate (PtdIns(3,4,5)P(3)) (Zhong, Lazar *et al.* 2002) but these observations were based on protein-lipid overlay assays. In subsequent investigation using liposome-based assays, binding was only observed to PtdIns(3)P and (PtdIns(3,5)P(2) but not to PtdIns(3,4,5)P(3) (Cozier, Carlton *et al.* 2002). Similarly SNX2 binds to PtdIns(3)P and (PtdIns(3,5)P(2), while also interacting with PtdIns(4)P and PtdIns(3,4,)P(2) albeit slightly less pronounced (Carlton, Bujny *et al.* 2005). GFP tagged versions of SNX1 and SNX2 are relocalized to the cytoplasm from endosomes upon inhibition of phosphoinositide-3-kinases (PI3K) by wortmannin (Cozier, Carlton *et al.* 2002, Carlton, Bujny *et al.* 2005). This is in line with their binding characteristics to PtdIns phosphorylated at the 3 position of the inositol ring, although SNX2 could principally also bind to PtdIns(4)P rich membranes, which are mostly found at the GA, upon inhibition of PI3K. SNX5 has been shown to bind PtdIns(3)P and PtdIns(3,4)P(2) (Merino-Trigo, Kerr *et al.* 2004) although the latter finding was called into question as it could not be reproduced upon trial (Attar and Cullen 2010) and another report indicated binding to PtdIns(4,5)P(2) while dismissing PtdIns(3)P binding altogether (Koharudin, Furey *et al.* 2009). The PX domain of SNX6 was found to bind PtdIns(4)P in liposome assay with very weak binding to PtdIns(3)P and (PtdIns(4,5)P(2) (Niu, Zhang *et al.* 2013).

1.4.3.2 The BAR domain senses membrane curvature

The BAR domain senses membrane curvature upon dimerization when the dimer assumes a crescent shaped surface by which it interacts with the membrane by electrostatic interactions (Peter, Kent *et al.* 2004). The binding of certain BAR domains can lead to extensive membrane remodeling, causing tubulation (Frost, Unger *et al.* 2009). Overexpression of SNX1 leads to extensive endosome tubulation (Carlton, Bujny *et al.* 2004) with a size of SNX1 positive retromer tubules of 30-55 nm in vitro and 20-50 nm in vivo (Carlton, Bujny *et al.* 2004, Mari, Bujny *et al.* 2008). Surprisingly, SNX2 does not induce membrane tubulation in vitro or in vivo and, unlike SNX1, is not essential for endosome to TGN recycling of CI-M6PR (Carlton, Bujny *et al.* 2005) which is one of the standard readouts for retromer functioning.

1.4.4 Isolation of PVs

In recent years, the isolation and proteomic characterization of phagosomes has led to considerable insight into the biology of their maturation (Li, Jagannath *et al.* 2010). The isolation of phagosome membranes has been aided largely by their relative ease of isolation using phagocytosis of latex beads, a method that has been used as early as 1971 (Ulsamer, Wright *et al.* 1971).

The isolation of phagosome/endosome related PVs has proven to be more difficult due to the heterogeneity of PVs. Surprisingly, one of the first reports on an isolated PV was the partial purification of mid-infection inclusions isolated from *C. psittaci* infected cells (Matsumoto 1981), but, the procedure proved difficult to reproduce. The technique employed in that study was isotonic lysis of cells with a dounce homogenizer followed by filtration using a metal mesh to separate the inclusions from the remaining cellular debris. The obtained relatively pure inclusions were visualized by electron microscopy but not characterized further (Matsumoto 1981). Using the same strain, early inclusions and phagosomes derived from inactivated bacteria were isolated shortly thereafter (Zeichner 1982, Zeichner 1983).

The PVs of *Listeria* (Alvarez-Dominguez, Barbieri *et al.* 1996), *Rhodococcus*, *Afipia, Bordtella* (Luhrmann and Haas 2000), *Salmonella*, *Yersinia* (Mills and Finlay 1998) and *Mycobacteria* (Sturgill-Koszycki, Schlesinger *et al.* 1994) have all been isolated using various protocols, yet their proteomes have not been analyzed in depth due to technical limitations at the time.

Traditionally, the purification of organelles such as mitochondria and nuclei involves several density gradient centrifugation steps. More recently, isolation using antibody based affinity purification has been developed for the isolation of mitochondria (Hornig-Do, Gunther *et al.* 2009). In the same year, Urwyler *et al*. introduced an analogous method to the study of intracellular bacteria by purifying *Legionella* containing vacuoles (LCVs) from infected

Dictyostelium discoideum (Urwyler, Nyfeler *et al.* 2009) This method involves a two-step procedure in which the lysate of infected cells was incubated with an antibody directed against the bacterial effector substrate of Icm/Dot transporter C (SidC). SidC localizes to the cytoplasmic side of LCVs by binding the host lipid Ptdins(4)P exclusively on LCVs (Ragaz, Pietsch *et al.* 2008). LCVs were then labeled with a secondary antibody coupled to supraparamagnetic micro-beads and purified by applying a magnetic field followed by density gradient centrifugation.

In the proteomics era, the LCV of *L. pneuomophila* has been isolated and analyzed by two independent groups in the same year (Shevchuk, Batzilla *et al.* 2009, Urwyler, Nyfeler *et al.* 2009). The latter study greatly improved the knowledge of proteins associated with the LCV, especially in regard to the recruitment of Rab proteins. The study was further complemented with the analysis of the LCV isolated from macrophages as opposed to amoebae (Hoffmann, Finsel *et al.* 2013).

Using a novel method for isolation, the proteome of the PV or *Brucella abortus* has been analyzed which revealed the two host proteins GAPDH and Rab2 to be essential for its infection (Fugier, Salcedo *et al.* 2009). The MCV (*Mycobacteria* containing vacuole) was isolated from macrophages and dendritic cells have been compared using label free proteomics (Li, Singh *et al.* 2011). In addition, the sole proteome of MCVs from macrophages (Lee, Jethwaney *et al.* 2010) and the comparative proteome of two different strains of *Mycobacteria* isolated from macrophages (Rao, Singh *et al.* 2009) have been analyzed. The inclusion of *C. trachomatis* or any other *Chlamydia* species has not been isolated in sufficient quantities for global proteome analysis.

1.5 Proteome analysis of *Chlamydia* infections

Several proteomics studies have been published in the *Chlamydia* field. The earliest reports, employing two dimensional polyacrylamide gel electrophoresis (2D-PAGE) for protein separation identified proteins of EBs from *C. pneumonia* (Vandahl, Birkelund *et al.* 2001) and several different strains of *C. trachomatis* (Shaw, Gevaert *et al.* 2002). These studies focused mainly on the identification of proteins and the conformation of expression of previously hypothetical proteins. Further studies examined the influence of the induction of persistent states in *C. pneumoniae* infections, either by iron starvation (Wehrl, Meyer *et al.* 2004) or treatment with IFN-γ (Mukhopadhyay, Miller *et al.* 2004).

Comparative proteomics was first used in a study by Skipp *et al*. when *C. trachomatis* EBs and RBs were compared with a combination of three different proteomics technologies including 2D-PAGE and two liquid chromatography coupled to tandem mass spectrometry (LC-MS/MS) based methods (Skipp, Robinson *et al.* 2005).

The *C. trachomatis* outer membrane complex (COMC) was purified and analyzed by LC-MS/MS and compared to EB and Sarkosyl-soluble fractions which revealed 17 proteins to be specifically enriched in the COMC (Liu, Afrane *et al.* 2010).

The most recent study by Saka *et al.* also compared EBs and RBs isolated from *C. trachomatis* L2 infected cells and for the first time used an absolute quantification approach to compare the two proteomes (Saka, Thompson *et al.* 2011). This revealed clearly distinct sets of proteins are present in each developmental form, where the EBs are mainly composed of proteins involved in central metabolism and glucose metabolism and a large number of T3SS proteins and effectors, whereas the RBs expressed a large number of proteins necessary for ATP generation, protein synthesis and nutrient transport. Additionally, membranes isolated from infected cells which were enriched for the inclusion membrane markers IncG and IncA by density gradient centrifugation were analyzed. The authors, however, did not publish the host cell derived proteome of these membranes, but used only the information on bacterial proteins, which confirmed a number of predicted and previously reported inclusion membrane proteins. In addition the inclusion membrane localization of several proteins annotated as periplasmic and cytosolic such as the arginine transporter J (ArtJ), the zinc transporting ATPase A (zntA) and the ATP/ADP/NAD translocase Npt1 were suggested.

1.6 Aim of this thesis

After invasion of the host cell, *Chlamydiae* reside within a membrane bounded vacuole called the inclusion. The inclusion membrane represents the main host-pathogen interface of *Chlamydia,* thus one of the central questions in the research of host-pathogen interactions is the composition of the host protein complement that is recruited to the inclusion in the course of an infection and thereby defines the environment in which the bacteria thrive. A growing number of proteins have been found to be inclusion localized, many of which serve important functions in the establishment and maintenance of the inclusion. However, the identification of these proteins and the associated pathways has mostly relied on an educated guess approach followed by analysis using microscopy and therefore represents only a limited and strongly biased view of the total proteome of the inclusion.

The first and foremost goal of this thesis is therefore identification of the host cell derived proteome of mid-infection inclusion of *C. trachomatis* L2 in an unbiased, systematic approach by developing a novel method to isolate this compartment and subsequent analysis by proteomics. The global analysis of this information will contribute substantially to our understanding of the nature and biogenesis of the inclusion and might lead to the identification of targets for the development of novel therapeutic approaches against *Chlamydia*.

2. Materials and Methods

2.1 Materials

2.1.1 Bacterial strains

Chlamydiales

C. trachomatis L2	lymphatic isolate 434 Bu (ATCC: VR-902B)

Escherichia coli

Rosetta 2	Merck
Top 10	Invitrogen
DH5α	New England Biolabs

2.1.2 Cell lines

HeLa	isolated from human cervix carcinoma (ATCC: CCL-2)

2.1.3 Plasmids

From previous publications:

Expressed insert	**Plasmid name**	**Provider**	**Reference**
GST	pGEX-3X	GE Healthcare	-
-	pUC19	University of California	-
eGFP	peGFP-C1	Invitrogen	
YFP-Rab3D WT	peYFP-C1-Rab3D	Gerke, V.	(Knop, Aareskjold *et al.* 2004)
YFP-Rab3D T35N	peYFP-C1-Rab3DT35N	Gerke, V.	(Knop, Aareskjold *et al.* 2004)
VCP-eGFP	VCP(wt)-EGFP	Addgene: 23971	(Tresse, Salomons *et al.* 2010)
GFP-Sec61β	pAc-GFPC1-Sec61beta	Addgene: 15108	(Voeltz, Prinz *et al.* 2006)
STIM1-YFP	human STIM1 YFP	Addgene: 19754	(Prakriya, Feske *et al.* 2006)
eGFP-SYNGR2	peGFP- cellugyrin	Kandror, K.V.	(Li, Bakirtzi *et al.* 2009)
Rab11A-eGFP	peGFP-Rab11A	Zerial, M.	(Sonnichsen, De Renzis *et al.* 2000)

***Cloned for this thesis*:**

Expressed insert	Internal name	Protein	Domain	Backbone
GST-IncA	pLA011	IncA	cytosolic domain	pGEX-3X
eGFP-SNX2[1]	pSK102	SNX2	Full length	pEGFP-C1
eGFP-SNX5[1]	pSK103	SNX5	Full length	pEGFP-C1
eGFP-PX(SNX5)[1]	pSK111	SNX5	PX-domain (AA29-169)	pEGFP-C1

[1]*These constructs were cloned by Sophia Koch, RKI, Berlin*

2.1.4 Primers

Primers for cloning

Expressed insert	Restriction site	Primer sequence (5' to 3')	Direction
GST-IncA	BamHI	cccggGGATCCATAATTTCATGCTGAGCG	FW
	EcoRI	cccggGAATTCCTAGGAGCTTTTTGTAGAGG	RV
eGFP-SNX2	EcoRI	gaatGAATTCAATGGCGGCCGAGAGGGAAC	FW
	SalI	gttaGTCGACCTAGGCAATGGCTTTGGCTTC	RV
eGFP-SNX5	EcoRI	cttaGAATTCAATGGCCGCGGTTCCCGAG	FW
	SalI	caatGTCGACTCAGTTATTCTTGAACAAGTCAATACAGC	RV
eGFP-PX(SNX5)	HindIII	gataAAGCTTTATCGCTTCAGATTGACATACCTG	FW
	BamHI	ctatGGATCCATCATATTCCAGGAAAACATGAAAG	RV

2.1.5 Small Interfering RNAs

Target	Sequence (5' to 3')	Manufacturer	Reference/ Catalog Nr.
Luciferase	AACUUACGCUGAGUACUUCGA	Qiagen	(Rejman Lipinski, Heymann *et al.* 2009)
SNX1	CGCGGTGGTCAGTAAACATCA	Qiagen	Hs_SNX1_1, SI00047775
SNX1	CTCGGGTGACTCAATATGAAA	Qiagen	Hs_SNX1_2, SI00047782
SNX2	TGCTCCTAGAATTGAATCAAA	Qiagen	Hs_SNX2_6, SI04190907
SNX2	TAGGTAATTCTGAGGATCATA	Qiagen	Hs_SNX2_7, SI04206475
SNX2	CTGCCTAGAGCAGTTAATACA	Qiagen	Hs_SNX2_8, SI04258394

SNX5	ACAGGTATATATGGAAACAAA	Qiagen	Hs_SNX5_1, SI00729015
SNX5	CCCGACTTTGATGGTCCTCGA	Qiagen	Hs_SNX5_6, SI03184342
SNX5	CCCGTAGTTCGTCTTTAGTTA	Qiagen	Hs_SNX5_7, SI03186190
SNX6	GCCACTCTTATTTACCTTTAA	Qiagen	Hs_SNX6_7, SI02644698
SNX6	CCGAAACTTCCCAACAATTAT	Qiagen	Hs_SNX6_8, SI02644705

2.1.6 Media and Solutions

Cell Culture Media

Application	**Composition**	**Manufacturer**
Cell growth	RPMI 1640	Gibco
	10 % FCS, heat inactivated	Biochrom
	1 mM sodium pyruvate	Gibco
	5 mM L-glutamine	Gibco
Infection	DMEM high glucose (4.5 g/l)	Gibco
	1 mM sodium pyruvate	Gibco
	5 mM L-glutamine	Gibco
SILAC “light” cell growth	SILAC DMEM	PAA
	10 % dialyzed FCS, heat inactivated	Biochrom
	L- arginine (42 mg/ml)	SILANTES
	L- lysine (96 mg/l)	SILANTES
SILAC “light” infection	SILAC DMEM	PAA
	5 % FCS	Biochrom
	L- arginine (42 mg/ml)	SILANTES
	L- lysine (96 mg/l)	SILANTES
SILAC “heavy” cell growth	SILAC DMEM	PAA
	5 % dialyzed FCS, heat inactivated	Biochrom
	$^{13}C_6{}^{15}N_4$ L- arginine (42 mg/ml)	SILANTES
	$^{13}C_6{}^{15}N_2$ L-Lysine (96 mg/l)	SILANTES
SILAC “heavy” infection	SILAC DMEM	PAA
	5 % dialyzed FCS, heat inactivated	Biochrom

	$^{13}C_6{}^{15}N_4$ L- arginine (42 mg/ml)	SILANTES
	$^{13}C_6{}^{15}N_2$ L-Lysine (96 mg/l)	SILANTES
Transfection	OptiMEM	Gibco
Passaging	Trypsin EDTA	Gibco
LB medium	10 g/l trypton, 5 g/l yeast extract, 5 g/l NaCl	RKI
LB-agar plates	LB medium, 1.5 % bacto agar	RKI

Buffers and solutions

Buffer	**Composition**
PBS	137 mM NaCl, 2.7 mM KCl, 10 mM Na_2HPO_4 + 2 H_2O, 1.76 mM KH_2PO_4
TBS	137 mM NaCl, 10 mM Tris/HCl,
TBST	TBS, 0.05 % Tween 20
TBST-M	TBST, 3 % milk powder
5 x Stacking gel SDS-PAGE buffer	1 M Tris/HCl pH 6.8
5 x Separating gel SDS-PAGE buffer	1 M Tris/HCl pH 9.0
6 x SDS-PAGE loading buffer (Lämmli)	375 mM Tris/HCl pH 6.8, 48 % glycerol, 9 % β-mercaptoethanol, 6% SDS, 0.03 % bromphenol blue
SDS-PAGE running buffer	25 mM Tris/HCl, 192 mM glycine, 0.1 % SDS
Coomassie staining solution	0.1 % Coomassie Blue R-250, 10 % acetic acid,
Destaining solution	10 % acetic acid, 40% ethanol
Western blot wet transfer buffer	25 mM Tris/HCl, 192 mM glycine, 0.1 % SDS, 20 % methanol
Western blot semi dry transfer buffer	48 mM Tris/HCl, 30 mM glycine, 1.3 mM SDS, 20 % methanol
Stripping buffer	62.5 mM Tris/HCl, 100 mM β- mercaptoethanol, 2% SDS
IF permeabilisation buffer	0.2 % BSA, 0.2 % Triton X-100
Stocking buffer	PBS, 250 mM sucrose
6 x FASP lysis buffer	16% SDS, 400 mM Tris/HCl, pH 7.6, 0.4 M DTT
UA	8 M Urea in 0.1 M Tris/HCl pH 8.5
IAA solution FASP	50 mM iodoacetamide in UA

AmBic	50 mM NH_4HCO_3
Britton and Robinson universal buffer	20 mM acetic acid, 20 mM phosphoric acid, 20 mM boric acid
SAX fractionation buffers	1 x Britton and Robinson universal buffer, pH adjusted with NaOH for pH = 3, 4, 5, 6, 8, 11, 250 mM NaCl added for pH = 3
HSMG	20 mM HEPES, 250 mM sucrose, 1.5 mM $MgCl_2$, 0.5 mM EGTA, pH 7.4 adjusted with KOH
HSM	20 mM HEPES, 250 mM sucrose, 1.5 mM $MgCl_2$, pH 7.4 adjusted with KOH
HSMG+	HSMG, c0mplete EDTA free protease inhibitors
Buffer A (aqueous)	0.1 % formic acid in H_2O
Buffer B (organic)	0.1 % formic acid in ACN
Buffer A_2 (aqueous)	0.1 % acetic acid, 2 % ACN
Buffer B_2 (organic)	0.1 % acetic acid in ACN
TBE	89 mM Tris/HCl, 89 mM borat, 2 mM EDTA, pH 8.0
6 x DNA loading buffer	0.25 % brom phenol blue, 0.25% xylen cyanol, 30% glycerol, 1 mM EDTA
Mowiol mounting media	2.4 g Mowiol 4-88, 6 g glycerol, 6 ml H_2O, 12 ml 0.2 M Tris pH 8.5
4% PFA	4 % PFA, 4 % sucrose in PBS

2.1.7 Kits and consumables

Name	Use	Manufacturer/ Vendor
Plastic ware cell culture	Cell culture	TPP
Plastic ware other	General use	Sarstedt/ TPP/ BD
VenorGeM	Mycoplasma detection	Biochrom
MB Taq DNA Polymerase	Mycoplasma detection	Biochrom
Wizard SV	Molecular cloning	Promega
Qiagen Plasmid Mini Kit	Plasmid isolation	Qiagen
QuantiTect Reverse Transcription Kit	Reverse transcription	Qiagen
T4 ligase	Molecular cloning	New England Biolabs
Restriction Enzymes	Molecular cloning	New England Biolabs
Glutathione HiCap Matrix	Protein purification	Qiagen
cOmplete EDTA free	Protease inhibition	Roche
RNAiFect	Transfection	Qiagen
Lipofectamine 2000	Transfection	Invitrogen
4 x PageRuler Plus Prestained	SDS-PAGE	Fermentas
2-Log DNA Ladder	Agarose gel electrophoresis	New England Biolabs
MACS-LS separation columns	MACS separation	Miltenyi
Sequencing grade modified trypsin	Tryptic digest	Promega
µ-Dish 35 mm low	Live cell microscopy	ibidi
$^{12}C_6{}^{14}N_4$L- arginine	SILAC	SILANTES
$^{13}C_6{}^{15}N_4$ L- arginine	SILAC	SILANTES
$^{12}C_6{}^{14}N_2$ L-Lysine	SILAC	SILANTES
$^{13}C_6{}^{15}N_2$ L-Lysine	SILAC	SILANTES
Dialyzed FCS	SILAC	Biochrom
Pierce Protein A/G Magnetic Beads	Magnetic separation	Pierce
Immobilon-P	Western blot	Millipore
Standard Microscopy Slide	Microscopy	Roth
KOVA Glasstic Slides 10	Cell counting	Hycor
Steritop-GP Filter Unit 250	Sterile filtration	Millipore

Sterican 26 G	Needle	Braun
Injekt Solo 5 ml	Syringe	Braun
Parafilm	Immunofluorescence	Pechiney Plastic Packaging
Rotiphorese® Gel 30 (37,5:1)	SDS-PAGE	Carl Roth
Vivacon 500 30.000 MWCO	Tryptic digest	Sartorius Stedim
Phusion Polymerase	PCR	New England Biolabs
dNTPs	PCR	New England Biolabs
Electroporation cuvette BRIDGE 2 mm	Transformation	Carl Roth
Lysozyme	Protein purification	Carl Roth
Glutathione	Protein purification	Carl Roth
Rotiquant Bradford assay	Protein quantification	Carl Roth
Litmus paper	pH measurement	Macherey Nagel
LoBind 1.5 ml tubes	Proteomics	Eppendorf
PepMap100 C_{18} 10 cm column	Proteomics	Dionex
PepMap Precolumn	Proteomics	Dionex
Glass cover slips	Immunofluorescence	Marienfeld
Glass beads 2.2 mm	Cell lysis	Roth
RNAeasy Kit	RNA extraction	Qiagen
Primers	PCR	MWG

2.1.8 Antibodies

Primary antibodies

Antigen	**From species**	**Source**	**Catalog Nr.**
SNX1	mouse	BD Bioscience	611482
SNX2	mouse	BD Bioscience	611308
SNX5	goat	Santa Cruz	sc-10625
SNX6	goat	Santa Cruz	sc-8679
VPS35	goat	Imgenex	IMG-3575
VPS35	mouse	Abcam	ab57632
CI-M6PR	mouse	AbD seroTec	MCA2048
IncA	rabbit	This thesis	

GAPDH	mouse	Pierce	MA5-15738
Sam68	mouse	Santa Cruz	sc-1238
Hsp60	mouse	Enzo Life Sciences	ALX-804-072
Hsp60	mouse	Enzo Life Sciences	ALX-804-071
COXI	mouse	Santa Cruz	sc-58347
GRP94	mouse	GeneTex	40016
p62	mouse	BD Biosciences	610497
LAMP-1	mouse	BD Biosciences	611042
Bcl-2	mouse	BD Biosciences	610538
Annexin II	mouse	BD Biosciences	610068
MOMP	mouse	(Gurumurthy, Maurer *et al.* 2010)	

Secondary antibodies

Name	**Use**	**Manufacturer**
ECL anti-mouse IgG, HRP conjugated	WB	Amersham Biosciences
ECL anti-rabbit IgG, HRP conjugated	WB	Amersham Biosciences
Cy2: Goat anti-mouse IgG	IF	Dianova
Cy2: Goat anti-rabbit IgG	IF	Dianova
Cy3: Goat anti-mouse IgG	IF	Dianova
Cy3: Goat anti-rabbit IgG	IF	Dianova
Cy5: Goat anti-mouse IgG	IF	Dianova
Alexa Fluor 488: goat anti mouse IgG	IF	Dianova
Alexa Fluor 647: goat anti rabbit IgG	IF	Dianova
MACS goat anti-rabbit IgG micro-beads	MACS	Miltenyi

2.1.9 Chemicals

Name	**Manufacturer/ Vendor**
Agarose	Carl Roth
IPTG	Carl Roth
Aktivkohle	Carl Roth
Acetone	Carl Roth

Formaldehyde 37 %	Carl Roth
Glycin	Carl Roth
Glycerol	Carl Roth
TRIS	Carl Roth
Tween 20	Carl Roth
Triton X-100	Carl Roth
Ammoniumpersulfate	Carl Roth
Ampicillin	Carl Roth
Kanamycinsulfate	Carl Roth
Bromophenol blue	Carl Roth
Calcium chloride	Carl Roth
Ethanol	Carl Roth
Nuclease free water	Carl Roth
Dipotassium phosphate	Carl Roth
Monopotassium phosphate	Carl Roth
DMSO	Carl Roth
DTT	Carl Roth
SDS	Carl Roth
EDTA	Carl Roth
Acetic acid	Carl Roth
Potassium chloride	Carl Roth
Methanol	Carl Roth
NaCl	Carl Roth
NaOH	Carl Roth
Paraformaldehyde	Carl Roth
KCl	Carl Roth
KOH	Carl Roth
HCl	Carl Roth
TEMED	Carl Roth
Magnesium chloride	Carl Roth
Mowiol 4-88	Carl Roth

Monosodium phosphate	Carl Roth
Milk powder	Carl Roth
Bovine Serum Albumin (BSA) Fraction V	Carl Roth
Coomassie Brillant Blue R 250	Carl Roth
EGTA	Carl Roth
Trichloracetic acid	Carl Roth
GelRed	VWR
Benzonase Nuclease HC	Novagen
ECL Reagent	Pierce
β- mercaptoethanol	Carl Roth
Sucrose	Carl Roth
Boric acid	Carl Roth
Phosphoric acid	Carl Roth
HEPES	Sigma Aldrich
Xylene cyanol	Carl Roth
Ethidium bromide	Carl Roth
Sodium azide	Carl Roth
TBE Buffer (10x)	Sigma Aldrich
Iodoacetamide	Sigma Aldrich
Urea	Sigma Aldrich
3M Empore C18 Disk	3M
3M Empore Anion Exchange-SR Disk	3M
Ammonium bicarbonate	Sigma Aldrich
TFA	Sigma Aldrich
Acetonitrile	Sigma Aldrich
Water for LC/MS	Sigma Aldrich
Formic acid	Pierce
Percoll	Sigma Aldrich
Poly-D-Lysine	Sigma Aldrich
Dextran, Alexa Fluor 647, 10,000 MW	Molecular Probes
DAPI	Sigma Aldrich

Osmium tetroxide	Sigma Aldrich
Epon	Sigma Aldrich
Hoechst 33342	Sigma Aldrich
Uranyl acetate	Merck
Lead citrate	Merck
Tannin	Merck
Propylene oxide	Merck

2.1.10 Equipment

Name	Type	Manufacturer/ Vendor
Allegra X-15 R	Benchtop centrifuge	Beckman Coulter
RC-6	High speed centrifuge	Beckman Coulter
Centrifuge 5417 R	Microfuge	Eppendorf
FlexCycler	PCR thermocycler	analytikjena
Perfect Blue Mini / Midi	Electrophoresis chamber	Peqlab
HS2020	Safety cabinet	Thermo
CB 150	Incubator	Binder
Ecotron	Incubator	Infors HT
Thermotron	Incubator	Infors HT
Vibrofix VF1 Electronic	Vortex mixer	IKA
Vortex mixer SA8	Vortex mixer	Stuart
GenePulser	Electroporator	BioRad
HL-2000 HybriLinker	Hybridization oven	UVP
PowerPac HC	Power Supply	BioRad
Trans-Blot SD	Semi-dry transfer cell	Biorad
Mini-Protean Tetra	Electrophoresis cell	BioRad
Scanjet G4050	Flatbed scanner	Hewlett Packard
Vibramax 100	Shaker	Heidolph
RM 50	Rotating mixer	Assistent
S-2002	Scale	Denver Instrument

Orion 2 Star	pH meter	Thermo
Thermomixer compact	Thermomixer	Eppendorf
Standard Power Pack P25	Power Supply	Biometra
Severin 700 & Grill	Microwave oven	Severin
Dynamag-2	Magnetic particle concentrator	Invitrogen
Orbitrap Discovery	Mass spectrometer	Thermo
Orbitrap Q-Exactive	Mass spectrometer	Thermo
EASY nLC II	nano HPLC	Proxeon
Mr. Frosty	Freezing container	Nalgene
Axiovert 40	Microscope	Zeiss
CURIX 60	Developer	Agfa HealthCare
Branson Sonifier 450	Sonicator	Branson
Nanodrop ND-8000	Spectrophotometer	Nanodrop
Infinite 200 Pro	Microplate reader	Tecan
SpeedVac	Centrifugal evaporator	Eppendorf
Mx3000 P	Real time PCR thermocycler	Stratagene
QuadroMACS Separator	MACS magnet	Miltenyi
Tecnai 12	TEM	FEI
USB Digital Camera	Digital Camera for microscopy	Realtime Imaging
UC7	Ultramicrotome	Leica
Megaview III	Digital Camera for TEM	OSIS

2.1.11 Software

Name	**Use**	**Manufacturer/ Reference**
Photoshop CS6	Image processing	Adobe
Illustrator CS6	Image processing	Adobe
XCalibur	Mass spectrometry	Thermo
MaxQuant 1.3.0.5	Mass spectrometry	(Cox and Mann 2008)
Perseus 1.3.0.5	Bioinformatics	(Cox and Mann 2008)
R	Bioinformatics	The R Foundation
Excel 2010	Data processing	Microsoft

Word 2010	Word processing	Microsoft
EndNote X7	Literature management	Thomson Reuters
Graph Pad Prism 5	Data processing	Graph Pad Software
Geneious 7.0.6	Data processing	Biomatters
Stratagene MxPro 4.1	Data processing	Stratagene
DAVID 6.7	Bioinformatics	(Huang da, Sherman *et al.* 2009)
GOrilla	Bioinformatics	(Eden, Navon *et al.* 2009)
STRING 9.1	Bioinformatics	(Franceschini, Szklarczyk *et al.* 2013)
Cytoscape 3.1.0	Bioinformatics	(Shannon, Markiel *et al.* 2003)

2.2 Methods

2.2.1 Cell culture

Cell culture

HeLa cells were grown in Roswell Park Memorial Institute medium (RPMI) 1640 supplemented with 5 mM L-glutamine and 1 mM sodium pyruvate and 10 % fetal calf serum (FCS) in absence of antibiotics if not stated otherwise. Cells were propagated in 75 cm^2 cell culture flasks and passaged at confluency after two to three days. For passaging, cells were washed with phosphate buffered saline (PBS) and incubated with trypsin-ethylenediaminetetraacetic acid (trypsin-EDTA) for 5 minutes at 37 °C before dilution with fresh media. Cells were cultured for a maximum of ten passages. Cells were grown in a humidified incubator in 5 % CO_2 at 37 °C. The cells were routinely tested for *Mycoplasma* contamination via polymerase chain reaction (PCR) using the VenorGeM kit according to manufacturer's instructions.

Stock of SILAC (Stable isotope labeling by amino acids in cell culture) cells

HeLa cells were labeled by culturing for 6 passages in SILAC (Stable isotope labeling by amino acids in cell culture) DMEM (Dulbecco's modified Eagle's medium) containing either isotope labeled ($^{13}C_6{}^{15}N_4$ L- arginine, $^{13}C_6{}^{15}N_2$ L-Lysine) or unlabeled ($^{12}C_6{}^{14}N_4$ L-arginine, $^{12}C_6{}^{14}N_2$ L-Lysine) L-lysine and L-arginine and 10 % dialyzed FCS (dFCS). All SILAC media was sterile filtered before use. To reduce metabolic proline to arginine conversion due to oversupply of arginine in the growth medium (Blagoev and Mann 2006), the concentration of L-arginine and L-lysine was titrated to conditions where the growth rate of cells was equal to standard DMEM concentrations over 10 passages.

Cells were expanded for stock preparation and were stocked in dFCS supplemented with 10 % Dimethyl sulfoxide (DMSO). Cells were frozen using Nalgene Mr. Frosty freezing containers according to manufacturer's instructions. Samples of these cells were taken, tryptic peptides prepared by FASP (filter aided sample preparation) and desalted by STAGE (stop and go extraction) tip before analysis with LC-MS/MS to control for complete incorporation of isotope labeled amino acids.

Transfections

For transfections, HeLa cells were grown in 12 well plates to 80 % confluency and transfected with 0.5 µg plasmid DNA and 1 µl Lipofectamine 2000. For higher cell numbers the procedure was scaled up accordingly. DNA and Lipofectamine 2000 were mixed in 100 µl OptiMEM each before

mixing, vortexing briefly and incubating 20 min at room temperature (RT). Cells were washed once and incubated with 300 µl fresh media followed by dropwise addition of the liposome/DNA mixture.

siRNA (short inhbiting RNA) mediated knockdowns

For specific knockdown of target host cell proteins, HeLa cells were transfected with target specific siRNAs. Cells were grown in 12 well plates to around 80 % confluency and transfected with a total of 80 pmol siRNA (approximately 1 µg). The siRNA was dissolved in 100 µl Qiagen RNAi transfection buffer followed by addition of 6 µl RNAi Fect transfection reagent and incubation for 20 minutes at RT to allow formation of Liposomes. Cells were washed once and incubated with 600 µl fresh media before dropwise addition of the siRNA transfection mixture. Cells were grown for 72 h and successful knockdown was assessed by RT-QPCR or western blot.

2.2.2 Chlamydial infections

Chlamydial infections

Infections were performed with the strain *C. trachomatis* serovar L2. HeLa cells were grown to 70-80 % confluency and infected 40 h after seeding. All standard infections were done in DMEM (4.5 g/l glucose) supplemented with 1 mM sodium pyruvate containing 5 % FCS at 35 °C, using half the culture volume. Infected cells were washed and incubated with fresh infection medium (standard culture volume) at two hours *p.i.*

Preparation of *Chlamyida* stock solution

For preparation of bacterial stocks, HeLa cells were grown in 150 cm^2 culture flasks to 80 % confluency and infected with a multiplicity of infection (MOI) of 3. At 48 h *p.i.*, the cells were harvested by scraping and transferred to 50 ml plastic tubes containing sterile glass beads. Lysis was achieved by vortexing for 3 minutes. Cellular debris was pelleted for 10 minutes at 500 x *g* at 4 °C and the EBs contained in the supernatant were pelleted by centrifugation (48'000 x *g*, 60 min, 4 °C). EBs were washed once with cold stocking buffer and resuspended in the same buffer. The EB solution was homogenized by multiple passages through a 26 G syringe. Small aliquots of *Chlamydia* stock solution were stored at 4 °C for 3h before freezing at -80 °C.

Determination of infectious titer

HeLa cells were seeded into 24 well cell culture plates which were prepared with glass cover slips and grown to 80 % confluency. Cells were infected with serial dilutions of *Chlamydia* stock solution for 24 h, before fixation with 2 % paraformalydehyde (PFA) in PBS for 30 min at RT. Fixed cells were immunostained for bacterial heat shock protein 60 (Hsp60). Inclusions in 10 fields of view (FOV) were counted in the appropriate dilution (10-50 per FOV) with a Zeiss Axiovert 40 inverted microscope using the ID Plan Neofluar 40x/0.6 objective. Inclusions per FOV were transformed into inclusion forming units (IFU) per ml with the following formula: [IFU/ml = inclusions per FOV x 454 x dilution factor x 4], which takes into account the number of cells per FOV (454) and the dilution of the inoculum corrected to 1 ml volume (x 4 from 250 µl).

Reinfection assay

The reinfection assay was used to determine the amount of infectious progeny formed after an indicated amount of time, usually 48 h for *Chlamydia trachomatis* L2 (one full developmental cycle). By this method, the effect of different treatment for example by addition of a chemical inhibitor or knockdown of a certain mRNA can be assessed. In practice, treated or mock treated cells were infected with the indicated MOI (mostly 2), the cells lysed after the indicated time point using glass beads in 15 ml plastic tubes with 3 minutes of vortexing. Newly formed IFU were titrated as described. In time course analyses, samples of different time points were frozen at -80 °C before processing for titration in batch. This significantly reduces viable progeny and therefore precludes comparison to directly titered experiments.

Morphology assay

For morphology assays, cells were treated as indicated in six well plates and fixed with glutaraldehyde fixing solution (2.5 % glutaraldehyde, 50 mM HEPES). Samples were harvested by scraping and processed as pellet for analysis by transmission electron microscopy (TEM). The samples were post fixed in 1 % osmium tetroxide followed by block contrasting with tannin (0.1 % in 50 mM HEPES) followed by dehydration through a series of increasing ethanol concentrations. The samples were infiltrated with propylenoxide before embedding in Epon. Epon was allowed to polymerize for 48 h at 60 °C. Samples were analyzed by TEM as described below. Randomized pictures were taken from each sample. The morphology of the bacteria was assessed by manual counting of at least 500 bacteria per condition.

2.2.3 Nucleic acids

Separation of nucleic acids by agarose gel electrophoresis

The analysis of DNA in the different steps of molecular cloning was done by horizontal agarose gel electrophoresis. Separation of DNA strands was achieved in 0.5-2 % agarose gels in TBE buffer at 80-120 V for 30-120 min. All samples were stained by 6 x DNA loading buffer before loading into the wells of the gel. DNA was stained either with GelRed (6 µl per 50 ml gel) in gel or by post staining in a 0.5 µg/ml ethidium bromide solution. Intercalated fluorescing dye was visualized on a transilluminator. For size reference we used NEB 2-Log DNA Ladder (0.1-10.0 kb).

Polymerase chain reaction (PCR)

DNA fragments were amplified for molecular cloning using polymerase chain reaction (PCR). All PCR reactions were perfomed in a Jena Biosciences Flexcycler thermocycler. The PCR mixture is shown in Table 2.1.

Table 2.1: Standard mixture for polymerase chain reaction

Reagent	Final concentration	50 µl reaction
5 x Buffer HF	1 x	10 µl
H_2O	-	28 µl
dNTPs (2.5 mM each)	200 µM each	4 µl
Phusion Polymerase	20.0 u/ml	0.5 µl
Primer forward (10 µM)	0.5 µM	2.5 µl
Primer reverse (10 µM)	0.5 µM	2.5 µl
Template DNA	<250 ng	2.5 µl

The standard PCR cycling conditions were as follows:

1.) Initial denaturation for 30 s at 98 °C
2.) 35 cycles of:
    a. 10 s denaturation at 98 °C
    b. annealing at 52 °C – 60 °C for 30 s, depending on the primers
    c. elongation (30 s/kb) at 72 °C
3.) Final elongation 10 min at 72 °C

PCR conditions were optimized where necessary by changing the annealing temperature, number of cycles, addition of DMSO and longer elongation times.

Preparation and transformation of electrocompetent *E. coli*

Electrocompetent *E. coli* were prepared by inoculation of 200 ml Luria-Bertani (LB) media containing the appropriate antibiotics with 2 ml overnight culture. Bacteria were grown to $A_{600\,nm}$

= 0.4 at 37 °C. The flask was shaken for 15 min in ice cold water before bacteria were pelleted for 10 minutes at 4750 x *g* at 4 °C. Bacteria were washed three times in ice cold H_2O and resuspended in 3 ml 10 % glycerol. 55 µl aliquots were snap frozen in liquid N_2 and stored at -80 °C until further use. Competency was assessed by transforming with the pUC19 control plasmid under ampicillin selection (100 µg/ml).

E. coli were transformed using 25 µl electrocompetent bacteria mixed with plasmid DNA in electroporation cuvettes (2 mm gap). Electroporation was done with the following settings: 2500 V, 25Ω, 250 µF in a BioRad GenePulser. Transformed bacteria were taken up in 1 ml warm LB media and incubated at for 1 h at 37 °C, 300 rpm in a thermomixer before plating on LB-agar plates containing selective antibiotics for transformed bacteria, on which they were grown overnight at 37 °C.

Preparation of plasmid DNA

Freshly picked colonies of the desired *E. coli* strains were grown over night in 10 ml (Miniprep) or 50 ml (Midiprep) LB medium containing the appropriate antibiotic(s) at 37 °C in an orbital shaker. The DNA was extracted using Qiagen Plasmid Mini Kit (Miniprep) or Qiagen Plasmid Midi Kit (Midiprep) according to the manufacturer's instructions. The yield and quality of the extracted DNA was assessed by ultraviolet-visible spectrophotometry taking into account the absorption of DNA at 260 nm (1 $A_{260\,nm}$ = 50 µg /ml) and the absorption of tryptophan and tyrosine at 280 nm, where a ratio of $A_{260\,nm}/A_{280\,nm}$ above 1.8 was considered to be sufficiently pure DNA.

DNA purification, restriction digest and ligations of DNA

Where necessary, DNA was directly cleaned up or gel purified or using the Promega Wizard SV Kit according to manufacturer's instructions. The DNA restriction digests were performed according to manufacturer's instructions with standard digest duration of 3 h at 37 °C.

Ligations using T4 ligase were performed for 3 h at 16 °C with an equimolar vector to insert ratio and a total amount of 50 ng DNA in 10 µl reaction volume, followed by clean up using the Wizard SV Kit. One third of the ligation reaction was typically used for transformation of electrocompetent bacteria. Correct insertion of the insert was verified by control digest. All final constructs were verified by Sanger sequencing using Big Dye according to manufacturer's instructions by the in house sequencing facility of the Robert Koch Institute (RKI), Berlin.

Preparation of complementary DNA (cDNA)

For preparation of cDNA, the QuantiTect Reverse Transcription kit from Qiagen was used according to manufacturer's instructions.

2.2.4 Standard protein methods

SDS-PAGE

Standard discontinuous sodium dodecyl sulfate – PAGE (SDS-PAGE) according to Lämmli was performed as described (Laemmli 1970). The stacking gel was used at 5 % acrylamide concentration throughout. The concentration of acrylamide of the separating gels was chosen between 8 % and 15 % depending on the apparent molecular weight of the proteins to be analyzed. Ammonium persulfate was used at a final concentration of 0.1 %, tetramethylethylenediamine at 0.01 %. The ratio of acrylamide to bis-acrylamide was 37.5:1 (Rotiphorese Gel 30). As size reference we used Fermentas Page Ruler Plus Prestained protein ladder. Proteins were electrophoretically separated in BioRad Mini-Protean Tetra electrophoresis cells at 160 V for 1 h using SDS-PAGE running buffer. SDS-PAGE gels were then either stained using Coomassie blue staining or used for western blot. Coomassie blue staining was done by heating the gel for 1 minute in a microwave in coomassie staining solution followed by 1 h staining on an orbital shaker. The staining solution was then exchanged by destaining solution, heated in the microwave and incubated on an orbital shaker until the protein bands were clearly visible. The gels were scanned on a Hewlett Packard Scanjet G4050 flatbed scanner when necessary.

Preparation of protein extracts for SDS-PAGE/ western blot

For samples containing Percoll, protein extract was prepared by addition of 6 x SDS-PAGE loading buffer, heating to 95 °C for 5 minutes, followed by pelleting insoluble material and Percoll at 20’000 x *g* for 10 minutes.

Whole cell extracts were prepared by washing cells twice in well with cold PBS and direct addition of 100 µl 1 x SDS-PAGE loading buffer per 10^6 cells. Protein extract was heated to 95 °C for 5 minutes and insoluble material pelleted by centrifugation at 20’000 x *g* for 10 minutes. Equal cell numbers corresponding to 15-20 µg protein were used for western blot.

E. coli protein extracts were prepared by addition of 6 x SDS-PAGE loading buffer and heating to 95 °C for 5 minutes.

Western blot and Immunodetection

Proteins separated by SDS-PAGE were transferred to a Millipore Immobilon-P polyvinylidene difluoride (PVDF) membrane either by semi dry blot or wet blot. For semi-dry blot, the membrane was wetted by methanol followed by equilibration in semi-dry blot transfer buffer. Proteins were transferred at 70 mA per gel for 1 h in a BioRad Trans-Blot SD semi-dry transfer cell at RT. For wet blot, the membrane was wetted by methanol and equilibrated in wet blot transfer buffer.

Proteins were transferred in a BioRad Mini-Protean Tetra electrophoresis cell at 250 mA for 2 h at 4 °C with additional cooling supplied by cold packs. After transfer, the PVDF membrane was incubated in tris buffered saline supplemented with tween and 3 % milk (TBST-M) for 1 h at RT to block unspecific binding, followed by incubation with the primary antibody over night at 4 °C or for 3 h at RT on a rotating mixer. The membrane was washed 3 x 10 min with TBST followed by incubation with a species specific horse radish peroxidase linked secondary antibody for 1 h at RT. The membrane was washed again (3 x 10 min) with TBS-T before the antibody was detected by enhanced chemiluminescence (ECL) using the Pierce ECL Plus Kit to expose an X-ray film. The film was developed in a Agfa Citrix 60 developer and scanned on a Hewlett Packard Scanjet G4050 flatbed scanner for digitalization.

To detect several antigens sequentially, the first antibody complex was removed by stripping of the membrane in stripping buffer at 56 °C for 20 minutes in a hybridization oven, followed by two washes in TBS. The membrane was blocked again in TBST-M before incubation with the next primary antibody.

Protein expression and purification

For protein expression of glutathione S-transferase (GST) fusion proteins, an overnight *E. coli* culture grown from a freshly transformed single colony of bacteria was diluted 1/20 into 500 ml LB media containing ampicillin and grown to OD_{600} = 0.35. Cold shock was induced by 10 minutes incubation in ice water. Expression was induced by addition of 0.1 mM isopropyl β-D-1-thiogalactopyranoside. The culture was incubated over night at 18 °C, shaking at 160 rpm in an orbital shaker. The culture was pelleted by centrifugation at 5000 x *g* for 10 minutes. Bacteria were lysed in PBS supplemented with with cOmplete EDTA free protease inhibitor cocktail, 1 mM EDTA, 0.1 % Triton X-100 and 1 mg/ml lysozyme for 45 min on ice. $MgCl_2$ was added to a concentration of 2 mM and the solution supplemented with 250 u Benzonase after the first 15 min of incubation. Three freeze thaw cycles were performed using a 37 °C water bath and N_2 (l.).

The lysate was cleared by centrifugation at 15´000 x *g* and soluble GST tagged protein was purified using Qiagen Glutathione HiCap Matrix slurry according to manufacturer's instructions. The protein was eluted with glutathione, protein concentration was estimated by Bradford assay according to manufacturer's instructions using BSA standards and the final eluate was used as antigen for immunization.

Antibody production

Polyclonal rabbit anti–IncA antibody was produced by immunization of New Zealand White rabbits with the C-terminal cytoplasmic fragment of IncA (N80-S246) fused to GST (GST-IncA). All

animal handling was done by Biogenes, Germany. The antigen was produced in *E. coli* (Rosetta 2) using the pGEX-3X N-terminal GST expression vector (GE Healthcare, USA) as described above. Cloning was done by using *Eco*RI and *Bam*HI restriction sites in *E. coli* DH5α with the primers listed in the materials section.

Affinity purification

GST-IncA and GST-only (purified from empty pGEX-3X vector) were washed and crosslinked to Qiagen Glutathione HiCap Matrix using BS3 (Suberic acid-bis-(3-sulfo-N-hydroxysuccinimide ester)) at a molar protein to crosslinker ratio of 1:40 by incubation overnight at 4 °C in PBS. Free BS3 was saturated by TBS; non-cross-linked proteins were removed by washing with 0.2 M glycine pH 2.0.

The antibody was affinity purified by depleting inactivated (56 °C, 30 minutes) rabbit serum from GST specific antibodies for 8 h, followed by binding to the crosslinked GST-IncA beads overnight. Beads were washed with 0.1 M borate, 0.5 M NaCl, pH 8.0 and eluted with 0.2 M glycine pH 2.0 into 2 M Tris to neutralize the pH. Purified antibody was dialyzed against PBS and diluted 1:1 in glycerol, 0.06 % sodium azide for storage at -20 °C.

2.2.5 Mass spectrometry and related methods

Sample preparation by FASP

For sample preparation for LC-MS/MS of both whole cell lysates and isolated inclusions, we used a method that allows for the essentially complete recovery of a protein sample, including transmembrane proteins and other very hydrophobic proteins which presents a challenge to most other sample preparation methods (Wisniewski, Zougman *et al.* 2009).

Total protein of samples (approximately 40 µg protein) was extracted by heating to 95 °C in 1 x FASP lysis buffer (4 % SDS, 0.1 M DTT, 100 mM Tris/HCl pH 7.6) for 5 minutes. DNA was sheared by sonication in a Branson 450 water cooled (4 °C) sonicator for 30 seconds at 100 % amplitude, 50 % on/off cycle, followed by centrifugation at 20'000 x *g* to pellet debris. The supernatant was mixed with 200 µl UA (Urea buffer) in a Vivacon 500 centrifugal ultrafiltration device with a 30 kDa molecular weight cut off and centrifuged for 15 min at 14'000 x *g.* To alkylate free thiol groups on cysteines, 100 µl iodoacetamide (IAA) solution was added, mixed for 1 minute in a thermo mixer and incubated for 20 min at RT in the dark. The proteins in the ultrafiltration device were washed three times with UA to remove IAA, followed by three washes with ammonium bicarbonate buffer (AmBic) to remove urea. Proteins were then digested by addition of 40 µl AmBic containing sequencing grade trypsin (1 µg per sample, 1:40 protein to enzyme ratio) and

incubation over night at 37 °C in a wet chamber. Digested peptides were eluted by centrifugation at 14'000 x *g* for 10 minutes which was repeated after addition of 40 µl AmBic. Peptide yield was determined by absorption reading at 280 nm using a Nanodrop ND-8000 spectrophotometer assuming 1 mg/ml peptides to have A_{280} = 1.1. Depending on the sample, the peptides were either acidified with trifluoracetic acid (TFA) for desalting by STAGE tip or used directly for fractionation by strong anion exchange chromatography.

STAGE tip

For desalting of tryptic peptides we used a method based on Stop and Go extraction (STAGE) tips (Rappsilber, Ishihama *et al.* 2003, Rappsilber, Mann *et al.* 2007). STAGE tips are composed of small disks of C_{18}.- linked silica beads embedded in a Teflon mesh material (C18 Empore Disk, 3M) inserted into standard plastic pipet tips. Desalting is based on reversed phase extraction. 200 µl tips with three layers of C18 material were packed as described (Rappsilber, Mann *et al.* 2007). Loading and washing was done in a table top centrifuge at 3000 x *g* for 1 min at RT with STAGE tips assembled in a 2 ml plastic tube. Before loading with tryptic peptides, tips were conditioned with 50 µl methanol followed by 80 % acetonitrile (ACN) / 3 % TFA and 50 µl H_2O. Tryptic digest of peptides after FASP elution was acidified with TFA and pH was tested by probing minute amounts on litmus paper. The tryptic digest was loaded on the conditioned STAGE tip and washed twice with 50 µl 0.1 % TFA in H_2O. Desalted peptides were eluted with 60 % ACN directly into glass vials or 96 well plates. Peptides were dried in a SpeedVac and resuspended in 20 µl buffer A.

Strong anion exchange (SAX) chromatography

Where indicated, tryptic peptides were fractionated into six fractions using SAX chromatograhy in STAGE tip format (Ishihama, Rappsilber *et al.* 2006, Wisniewski, Zougman *et al.* 2009). SAX tips were prepared by stacking six layers of 3M Empore Anion Exchange disks in a 200 µl pipet tip. Loading and washing was done in a table top centrifuge at 3000 x *g* for 1 min at RT with SAX tips assembled in a 2 ml plastic tube. The SAX tip was conditioned with 100 µl methanol followed by 100 µl 1 M NaOH. The pH was equilibrated by passing 100 µl SAX fractionation buffer pH 11 twice. The peptide solution was diluted with SAX fractionation buffer pH 11 before assembling the conditioned SAX tip into a freshly conditioned STAGE tip. The peptide solution was then loaded by centrifugation at 3000 x *g* for 1 min followed by a wash with 100 µl SAX fractionation buffer pH 11. The STAGE tip was replaced and the SAX fractions were eluted subsequently with the buffer of pH 8, 6, 5, 4 and 3 into individual STAGE tips. STAGE tips were washed with 50 µl 0.1 % TFA before

elution with 60 % ACN directly into glass vials or 96 well plates. Fractionated peptides were dried in a SpeedVac and resuspended in 20 µl buffer A.

SILAC incorporation rate

For determination of the SILAC incorporation rate, tryptic peptides were analyzed on a Thermo Orbitrap Discovery mass spectrometer coupled to a Proxeon nLC1000 nano high performance liquid chromatograph (nHPLC). Peptides were ionized by electrospray ionization (ESI). Approximately 1 µg of peptides were loaded on a Thermo Acclaim PepMap 100 precolumn (0.75 µm inner diameter, packed with 3 µm C_{18} particles). Separation by reversed phase chromatography was achieved on a 10 cm PepMap100 C_{18} column packed with 5 µm particles, 75 µm inner diameter using a 95 min linear gradient from 5 % to 40 % buffer A in buffer B at a flow rate of 300 nl/ min. The mass spectra were acquired in a data-dependent "top 10" method which dynamically chooses the most abundant precursor ions from the survey scan (300-1700 m/z, 30'000 resolution). Precursors above the threshold of 2000 counts were isolated within a 2 m/z window and fragmented by collision induced dissociation using normalized collision energy of 35 % and activation time of 30 ms. Dynamic exclusion was defined by a repeat count of 1, a list size of 500 features and exclusion duration of 30 s. The lock mass option was used on 445.120026 for ions of polydimethylcyclosiloxane. Raw data was analyzed by MaxQuant 1.3.0.5 in standard settings with the requantify feature disabled using the human reviewed reference proteome .FASTA file obtained from uniprot.org at 12.09.12. Incorporation of heavy labeled amino acids to peptides was above 98 % (average) with 88 % of peptides appearing only in the heavy labeled state. Complete labeling was therefore assumed for all bioinformatic purposes.

Measurements of SILAC inclusions and lysates

Tryptic peptides were analyzed on a Thermo Q Exactive mass spectrometer coupled to an Advion TriVersa NanoMate source. Ten µl of tryptic peptides were separated with a Dionex UltiMate 3000 nHPLC. Peptides were ionized by ESI. Approximately 1 µg of peptides were loaded on Thermo Acclaim PepMap 100 precolum (0.75 µm inner diameter, packed with 3 µm C_{18} particles). Separation by reversed phase chromatography was achieved on a 25 cm Thermo Acclaim PepMap RSLC C_{18} column with 2 µm C_{18} particles using a 120 min linear gradient from 2 % to 25 % buffer A_2 in buffer B_2 at a flow rate of 300 nl/ min. The column was heated to 40 °C. The mass spectra were acquired in a data-dependent "top 10" method which dynamically chooses the ten most abundant precursor ions from the survey scan (300-1650 m/z, 70'000 resolution, 120 ms injection time, automatic gain control target value of 3×10^6). Precursors with a charge of ≥2 were isolated within a 3 m/z window and fragmented by higher energy collisional dissociation using normalized

collision energy of 27.5 %, automatic gain control target value of 2 x 10^5 and 17'500 resolution, 100 m/z fixed first mass. Dynamic exclusion was defined by exclusion duration of 30 s.

2.2.6 Bioinformatic analysis

Analysis of raw data

Raw data was analyzed with MaxQuant Version 1.3.0.5 (Cox and Mann 2008) in standard settings with the requantify feature disabled using a false discovery rate (FDR) of < 1%. Quantification by intensity based absolute quantification (iBAQ) was enabled (Schwanhausser, Busse *et al.* 2011), without introduction of external reference peptides (iBAQ logarithmic fit disabled). The human reviewed reference proteome .FASTA file (organism 9606, keyword 1185) and the reference proteome for *C. trachomatis* serovar L2 (strain 434/Bu / ATCC VR-902B) were retrieved from uniprot.org on September 12, 2012 and concatenated. The .raw files for the lysates (3 .raw files) were processed independently of the .raw files of the fractionated and full inclusion measurements. All six SAX fractions plus the overview fraction of each experiment were treated as a single experiment and analyzed together (21 .raw files).

Initial filtering

The data obtained from MaxQuant was filtered initially by removing common contaminations included in the common contaminations FASTA file provided by MaxQuant 1.3.0.5 (Cox and Mann 2008), as well as identifications based solely on proteins from the decoy database (reverse database from .FASTA file). Furthermore only proteins that were found in all three experiments of a triplicate were retained.

For the bacterial proteome filtering of at least two unique peptides per protein group per experiment was used.

For determination of the host cell derived proteome of the inclusion, all bacterial proteins were filtered. Protein groups that had less than two unique+ razor peptides in at least one experiment were filtered.

Statistical test for enrichment (SILAC exclusion approach)

Each host protein in the inclusion fraction data set that showed three (first test, n = 1095) or two (second test, n = 305) SILAC ratios was tested for a significant shift of its ratios compared to the empirical lysate distribution.

SILAC ratios of all the proteins after filtering were transformed by taking the logarithm. An empirical distribution was calculated based on the lysate SILAC ratios of proteins which were measured in both data sets (lysate and inclusion fractions, each in three replicates). A two-sided Wilcoxon test was applied to determine the differentially enriched proteins in the inclusion fraction data. P-values were adjusted for multiple testing by the Benjamini-Hochberg approach and all proteins below an adjusted p-value of 0.01 were considered if three SILAC ratios were detected, whereas this threshold was lowered to 0.04 for proteins which showed only two SILAC ratios.

For the first test with three SILAC ratios, the overlap of proteins between the data sets corresponded to 724 proteins of 1095 proteins and overall 1882 lysate ratios contributed to the distribution since not all lysate proteins showed a SILAC ratio in all of the 3 replicates. As a result, 744 human proteins were reported to be differentially enriched, among these, 253 were enriched in the inclusion fraction with a p-value of below 0.01.

In the second test, the overlap between proteins with either two or three SILAC ratios in the inclusion fraction was used for the empirical lysate distribution, resulting in a total of 903 proteins with 2344 contributing SILAC ratios from the lysate fraction. As a result, an additional 181 proteins were differentially enriched, among these, 92 proteins were enriched in the inclusion fraction with p-value below 0.04.

The statistical analysis was performed by M. Fischer in the group of Dr. B. Renard, RKI, Berlin.

Abundance analyses

For the lysate proteome, the relative abundance of each protein group was determined by dividing the iBAQ intensity of a protein group by the summed the iBAQ intensity of all protein groups that were found in all three experiment after initial filtering and had a reported iBAQ intensity. For proteins that had a standard deviation below 0.5 times the average, the protein group was flagged as only limited quantitative (n = 621 of 2003). For the gene ontology (GO) distribution and enrichment analyses also non-quantitative protein groups were considered as their total percentage was neglectable (10 % of total iBAQ intensity).

For the abundance of proteins in the inclusion proteome, only proteins that passed the SILAC based cutoff were considered. The L iBAQ intensity was first normalized with the average SILAC ratio of the respective experiment in the lysate (after filtering as described above) to account for differences in initial protein abundance, before normalizing to the average SILAC ratio of the inclusion fractions to account for the proportion of contaminating protein. After this, the relative abundance of each protein group was determined by dividing the normalized iBAQ intensity of a

protein group by the summed normalized iBAQ intensity of all protein groups. Proteins which were limited quantitative according to the above rule were also flagged (n = 145 of 345).

iBAQ enrichment score

The iBAQ enrichment score equals the ratio of the relative contributions of inclusion vs. lysate as described above. For proteins that were never found in in the lysates, we used a published dataset in which HeLa cells were prepared with the same protocols we used and analyzed with a similar proteomics platform but in more depth, to approximate the relative abundance of these proteins in the samples (Nagaraj, Wisniewski *et al.* 2011). Only proteins that were identified based on tryptic peptides were used and these proteins were also flagged. In total, 228 protein groups of the inclusion dataset were found in the lysate in all three experiments with at least 2 unique + razor peptides per experiment. An additional 33 with less than 2 unique + razor peptides per experiment and 44 in less than three experiments. 40 were not quantified nor found in the lysate, all of which were reliably quantified in the inclusion dataset and the published dataset. Three protein groups were neither found in the published dataset (SH3TC1, SH3TC2; PRAMEF4, 5, 6, 9, 20, 23 and DNAH6). In all cases protein groups were matched by their Majority protein identifiers (IDs) among different datasets and, if necessary, matched by the first identifier (n = 10) or by hand due to different .FASTA files used for processing (n = 2).

Organellar contribution analysis and enrichment analysis

The organellar contribution of proteins from both datasets (inclusion and lysate) were calculated individually. Subcellular localization data was retrieved from UniprotKB (UniProt 2014) for all proteins. The first protein ID was used in the case of protein groups consisting of multiple IDs.

GO enrichment analyses were performed with GOrilla (Eden, Navon *et al.* 2009), GO data (Ashburner, Ball *et al.* 2000) was current as of May 17, 2014. The dataset of the HeLa proteome from Nagaraj *et al.* (Nagaraj, Wisniewski *et al.* 2011) was used of as background after filtering for 2 or more unique tryptic peptides (n = 6331) of which 5970 proteins were mappable to GO terms.

Protein protein interaction analysis

Protein-protein interactions of inclusion associated proteins annotated with the highly enriched GO term “protein localization” (GO:0008104, n = 84) were analyzed using STRING 9.1 (Franceschini, Szklarczyk *et al.* 2013) with standard settings in confidence view as of May 25, 2014. The interaction network was imported to Cytoscape 3.1.0 and annotated with quantitative experimental data.

2.2.7 Inclusion isolation and associated methods

Gradient purification of crude inclusions

HeLa cells were cultured in 75 or 150 cm^2 flasks and infected with MOI = 4 at 70-90 % confluence. For standard isolations, 6 x 10^7 cells were used. All steps were done on ice or in a cold room at 4 °C. Cells were washed once with PBS and subsequently with ice cold 4-(2-hydroxyethyl)-1-piperazineethanesulfonic acid (HEPES) sucrose magnesium ethylene glycol tetraacetic acid (EGTA) buffer (HSMG). Cells were scraped into 6 ml lysis buffer (33 % Percoll solution, HSMG) supplemented with cOmplete EDTA free protease inhibitors according to manufacturer's instructions. Lysis was performed by repeated passage through a ball homogenizer using 16 µm clearance and 11-13 passages.

The lysate was then separated on a self-forming Percoll gradient in a total volume of 16 ml by centrifugation at 35'000 x *g* for 30 minutes at 4 °C (Beckmann RC-6 with Thermo Scientific F21-8x50y rotor). The lower 6 ml of the gradient were either used for MACS (magnet assisted cell sorting) purification or crude inclusions were diluted six fold in HSMG and pelleted at 1500 x *g* for 10 minutes, followed by another wash and centrifugation at 1200 x *g* for 10 minutes.

MACS purification of inclusions

The lower 6 ml of the gradient (crude inclusions) were taken and incubated with affinity purified rabbit αIncA (1:1000) antibody for 1.5 h at 4 °C followed by incubation with MACS secondary goat anti-rabbit antibody (1:100) for another 1.5 hours. Inclusions were mixed gently by inversion every 30 minutes. Inclusions were then purified by MACS separation on an LS separation column. The crude inclusions were loaded on the column in steps of 2 ml and washed with three times the input volume of HSMG buffer. Inclusions were then eluted with 3 ml HSMG buffer after removal of the magnet, aided by gentle pushing using the supplied plunger. Where indicated, inclusions were concentrated by centrifugation at 1200 *x g* for 10 minutes at 4 °C. Fractions at each step were taken for analysis by counting and western blot.

Inclusion counting

Inclusions in HSMG lysis buffer were counted by hand on a Zeiss Axiovert 40 phase contrast microscope using KOVA Glasstic 10 slides. Inclusions were identified by eye by a characteristic halo surrounding the spheres in solution. No size exclusion was performed, counted inclusion diameters ranged from approximately 3 to 15 µm. At least five fields were counted for each sample with a minimum of 50 counted inclusions in total.

Small scale isolations for validations by confocal microscopy

Two wells of a six well plate (3 x 10^6 cells) were each transfected with 1 µg of the respective plasmid using Lipofectamine2000 as described above. 4 hours after transfection, cells were infected with MOI = 2 for 24 h. After removal of the media, cells were washed with PBS, followed by a wash with HSMG buffer. The cells were then scraped into 2 ml lysis buffer containing 33 % Percoll and lysed by 13 passages in a ball homogenizer using 16 µm clearance. The lysate was split into two 2 ml tubes and each taken to 1.6 ml. The lysate was then centrifuged at 19´000 x *g* for 55 minutes at 4 °C in a R5417R centrifuge (Eppendorf, Germany). The top 1 ml was removed and the lower fractions pooled, diluted 1:2 with HSMG and spun down on a Poly-D-Lysine coated live cell dish for microscopic analysis at 1500 x *g* for 10 minutes.

Immunofluorescence of inclusions

Inclusions were centrifuged (1200 x *g* for 10 minutes) on Poly-D-Lysine coated live cell dishes. The specimen was fixed with 4 % PFA in HSM buffer and the dish incubated over night at 4 °C. The buffer was exchanged with PBS and IF was performed in well essentially as described for whole cells.

Electron Microscopy of isolated inclusions

Inclusions were centrifuged (1200 x *g*, 10 minutes) on Poly-D-Lysine coated live cell dishes. The specimen was fixed with 4 % PFA in HSM buffer and the dish incubated at RT for 1h. The buffer was exchanged with glutaraldehyde fixing solution (2.5 % glutaraldehyde, 50 mM HEPES) and incubated at 4 °C overnight. For analysis by transmission electron microscopy (TEM), the samples were post fixed in 1 % osmium tetroxide followed by dehydration through a series of increasing ethanol concentrations. The samples were infiltrated with acetone before embedding in Epon. Epon was allowed to polymerize for 48 h at 60 °C.

Dextrane permeability assay

Inclusions were centrifuged (1200 x *g* for 10 minutes) on Poly-D-Lysine coated live cell dishes and incubated with 1 µM of Alexa Fluor 647 conjugated 10 kDa dextran. Confocal images of isolated inclusions were acquired using an LSM 780 LSCM.

SILAC MACS inclusion isolation

SILAC labeled cells were thawed and passaged for a maximum of 4 passages and cultured in the appropriate media containing 10 % dFCS with growth conditions and handling equal to normal cell culture.

For infections, cells were washed with SILAC DMEM, and infected with *C. trachomatis* L2 at an MOI of 4 for 24 h at 35 °C in SILAC DMEM supplemented with 5 % non-dialyzed FCS (infection, H label) or 5 % dialyzed FCS (mock controls, L label) and the appropriate amino acids using half the culture volume of media. The inoculum was replaced with fresh infection media (standard volume) after washing once with SILAC DMEM at 2 h *p.i.*

Inclusions were isolated as described above but 6 x 10^7 infected cells were mixed with the same amount of mock infected cells before lysis. The protocol was carried out in twice the volume (32 ml total gradient volume) and 2 x 6 ml crude inclusions were loaded on one column before washing with 3 x 12 ml HSMG.

Isolated inclusions were concentrated to 30 µl by spinning down at 1200 *x g* for 10 minutes. Purified inclusions were always handled at 4 °C or on ice unless specified otherwise. Inclusion samples were prepared for LC-MS/MS by FASP. 10 % of the sample was used for direct injection after desalting by STAGE tip. The remaining peptides were separated by strong anion exchange chromatography into 6 fractions before desalting by STAGE tip followed by LC-MS/MS as described above.

2.2.8 Microscopy

Immunostaining

HeLa cells were seeded into 12 or 24 well cell culture plates which were prepared with glass cover slips. After the indicated experimental procedure, cells were washed with PBS twice and fixed with 2 % PFA for 30 minutes at RT. Preferentially the confluency was at 90 % at the time of fixation. After washing with PBS, cells were blocked and permeablilized with 0.2 % BSA/0.2 % Triton X-100 in PBS for 20 minutes at RT. The cells were then incubated for 1 h with primary antibody solution at the appropriated dilution in 0.2 % BSA in PBS by placing the cover slip upside down on a 25 µl drop of antibody solution on parafilm. After incubation, cover slips were washed three times for 10 minutes on an orbital shaker before incubation with the appropriate fluorophore coupled secondary antibody solution containing DAPI in 0.2 % BSA in PBS. This incubation was carried out for 1 h protected from light to avoid photobleaching of the fluorophore. After an additional three times 10 minutes washing, the cover slips were mounted on microscopy slides with mowiol and dried over night at RT before storage at 4 °C in the dark.

Confocal microscopy

Immunostained samples and live cell samples were analyzed on a Zeiss LSM 780 laser scanning confocal microscope (LSCM) equipped with Zeiss Zen software. Images were processed with Adobe Photoshop CS6 for image corrections (brightness, contrast, intensity) where necessary. Figures were assembled in Adobe Illustrator CS6.

Phase contrast microscopy

For analysis by conventional phase contrast microscopy without staining, samples were either mounted on a standard microscopy slide with cover slip and imaged directly, or imaged from a KOVA Glasstic Slide 10. The microscope used was a Zeiss Axiovert 40 equipped with a camera from Realtime Imaging.

Electron microscopy

Ultra-thin sectioning of Epon embedded samples at approximately 60 nm per slice was performed using a Leica UC7 ultramicrotome and sections were stained with 2 % uranyl acetate (20 minutes) and 2 % lead citrate (3 minutes) to increase contrast. The sections were examined using a FEI Tecnai12 TEM operated at 120 kV. Digital images were taken with an OSIS Megaview III Camera.

3. Results

After invasion of the host cell, *Chlamydiae* reside within a membrane bounded vacuole called the inclusion. Both host derived and bacterial proteins are found to be present at the inclusion and its membrane throughout the bacterial developmental cycle. The aim of this thesis was the identification and analysis of the host cell proteome of the inclusion of *C. trachomatis*. In the first part of this this section, we describe a novel procedure for the purification of the mid-infection inclusion of cells infected with *C. trachomatis.* In the second part of this section we analyzed the proteome of the inclusion. The analysis of these data led us to the in depth investigation of the relevance of retrograde trafficking for *C. trachomatis* which is presented in the last part.

3.1 Isolation of intact mid-infection inclusions

The protocol described by Urwyler *et al.* for the isolation of the LCV (*Legionella* containing vacuole) (Urwyler, Nyfeler *et al.* 2009) was the starting point to develop a method to isolate the mid-infection inclusion of *C. trachomatis* L2. Our interest in the mid-infection inclusion and especially in the 24 h *p.i.* time point is founded by a number of different observations. Firstly, the developmental cycle of *C. trachomatis* L2 reaches its midpoint (Nicholson, Olinger *et al.* 2003). The inclusion is still in considerable growth while the RBs divide extensively. One can assume that at this point all mechanisms that contribute to bacterial growth and the growth of the inclusion are fully developed to support this expansion. Secondly, only a small fraction of RBs has transformed into EBs, keeping the infections synchronous as opposed to later time points. Thirdly, the size of the inclusion, although considerable, still does not occupy the majority of the cytoplasmic space which increases the chances of successful isolation.

3.1.1 Antibody generation

For the immunomagnetic separation and analyses by western blot and IF, we generated an antibody directed against the bacterial effector protein IncA. IncA is a type III secreted protein involved in homotypic vesicle fusion (Hackstadt, Scidmore-Carlson *et al.* 1999). It is expressed from 12 h *p.i.* and shows a rim like staining of the inclusion membrane in LSCM (Hackstadt, Scidmore-Carlson *et al.* 1999). The antibody was generated by expressing and purifying the cytoplasmic part of IncA fused to GST (Figure 3.1 A). A New Zealand White rabbit was immunized with the purified protein. The antibody was further affinity purified from serum against GST-IncA. Visualization by LSCM after immunostaining showed a clear rim like staining of the inclusion membrane (Figure 3.1B), while cells stained with preimmune serum of the rabbit did not show any specific staining, even at very high concentrations (data not shown).

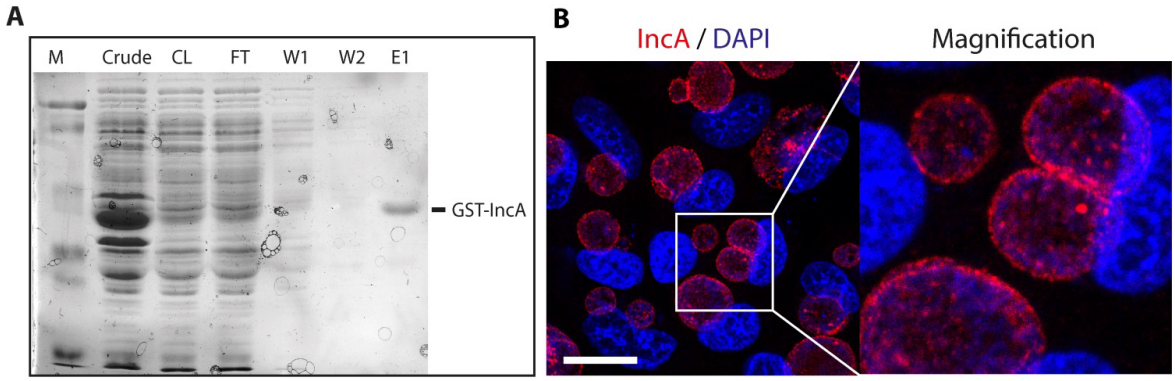

Figure 3.1: IncA antibody generation
A) Coomassie stained SDS-PAGE gel showing the purification of the cytosolic domain of IncA fused C-terminally to GST. (CL = Cleared lysate, FT = Flow through, W1 = first wash fraction, W2 = second wash fraction). E1 indicates the final eluate used for immunization **B)** LSCM image of HeLa cells infected for 24 h with *C. trachomatis* L2 with MOI = 2 after immunostaining using affinity purified anti IncA antibody (red). DNA was stained using DAPI (blue). Scale bar = 20 µm.

3.1.2 Density gradient separation

First of all, we wanted to establish a lysis procedure that allows the recovery of intact inclusions in solution. To this end, we chose an isoosmolar lysis buffer to reduce osmotic stress on the fragile inclusions. We then lysed the cells in a ball homogenizer. The ball homogenizer allows adaptation of the lysis conditions by adjustment of the size of the ball. We determined the least harsh conditions that lysed non-infected cells to approximately 90% in around ten strokes. This condition was then used to lyse cells infected with *C. trachomatis* L2 at different time points after infection. Spheres with a distinct halo were released into the lysis buffer. The size of the spheres increased with the time post infection (Figure 3.2) and the spheres were not observable in mock infected cells which further supported their bacterial origin.

To separate these putative inclusions from cellular debris, we tried several different methods, including filtration and differential centrifugation, but most methods proved to be too harsh or inefficient for practical use. Eventually we found density gradient centrifugation to be an efficient means to separate the majority of inclusions form most of the cellular debris.

As density gradient medium, we chose Percoll as it is isoosmolar and chemically inert. Isoosmolarity was of particular importance, as it is crucial to maintain the highly fragile compartment intact. The chemical inertness is highly desirable for analysis by electron microscopy as it reduces interference with chemicals during sample preparation which is often a problem with more reactive media such as Histodenz.

Percoll furthermore allows the formation of in-situ gradients in which the average density of the media is the area of highest resolving power. In preliminary experiments, we found that the density of inclusions is highly variable at 24 h *p.i.* and thus do not settle in a single band in isopycnic centrifugation. We therefore searched for a condition that allowed the separation of most inclusions primarily from nuclei and intact cells as we found these to clog the MACS column

in preliminary experiments, presumably due to free DNA from ruptured nuclei. To further counteract this issue, we additionally used $MgCl_2$ in the lysis buffer as its absence destabilizes free nuclei (Doyle, Price *et al.* 1981).

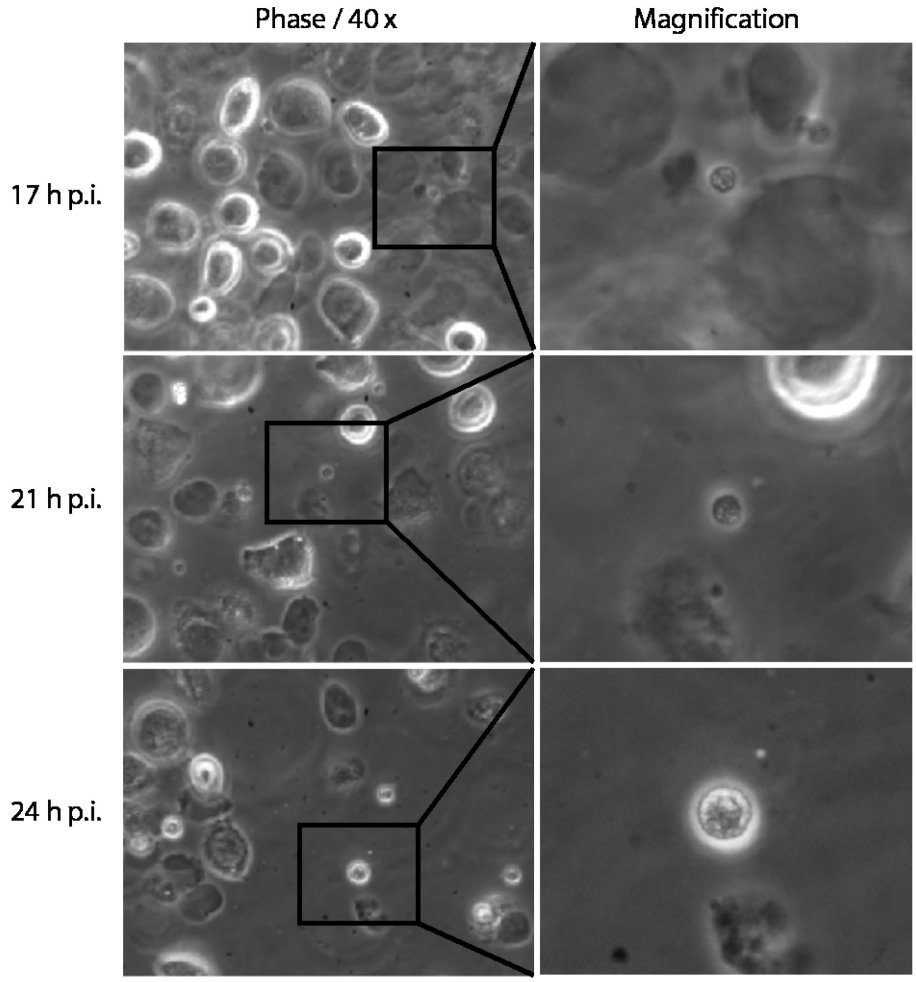

Figure 3.2: Floating spheres are released into solution upon lysis of *C. trachomatis* infected cells
HeLa cells infected with *C. trachomatis* L2 (MOI = 1.2) were lysed in osmostabilizing buffer at three different time points *p.i.* Phase contrast images (left) were taken at 40 x magnification on a Zeiss Axiovert 40 cell culture microscope. Magnifications of the indicated rectangle are displayed on the right of each image.

After testing several conditions between 25 % and 50 % Percoll which we analyzed by phase contrast microscopy (data not shown), we settled for an in situ generated gradient of 33 % Percoll by centrifugation for 30 minutes at 35'000 *x g* at 4 °C. The gradient was split into 16 fractions and fractions analyzed for presence of inclusions. The primarily inclusion containing fractions (1-4) were pooled and concentrated by pelleting after dilution of the gradient media. Each fraction was prepared for SDS-PAGE and probed by western blot for different organelle markers as shown in Figure 3.3 A.

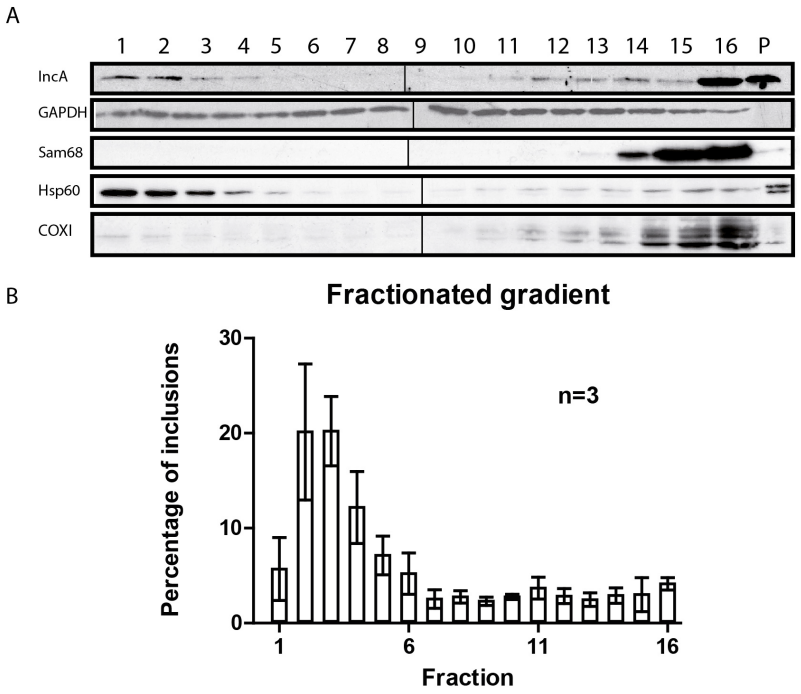

Figure 3.3: The inclusion membrane marker IncA sediments to high density fractions in a Percoll gradient
A) 6 x 10^7 HeLa cells were infected for with *C. trachomatis* L2 for 24 h with MOI = 2. Cells were lysed in a ball homogenizer (16 µm clearance, 13 strokes) and subsequently fractionated on an in-situ formed 33% Percoll gradient in HSMG buffer. The gradient was fractionated into 16 fractions of equal volume (fraction 1: bottom, fraction 16: top). Fractions 1-4 were pooled, diluted in HSMG and washed twice (P). Equal volumes of each fraction (1-16) or concentrated washed inclusions (P) were prepared, separated on a 10% SDS-PAGE gel, western blotted and probed with specific antibodies against the indicated proteins. **B)** The majority of intact inclusions sediments to high density fractions in a Percoll gradient. Intact inclusions were counted for each fraction of a gradient prepared as described in A) but MOI = 3, and the percentage was plotted. Error bars indicate standard deviation of three independent replicates.

The inclusion marker protein IncA was enriched in the lower fractions of the gradient. However, a large proportion of total IncA was found in the highest fractions of the gradient. This proportion of IncA presumably stems from ruptured inclusions and inclusions that are still attached to the cytoskeleton. Sam68 (Src associated in mitosis of 68 kDa), a protein that is primarily found in the nucleus was highly enriched in the lower density region of the gradient and no signal was observed in the high density fractions, which correlated with visual inspection of the fractions by phase contrast microscopy (data not shown). The soluble cytosolic marker GAPDH was found distributed across all fractions as expected as we used an in situ generated gradient without layering the lysate on the gradient medium. The mitochondrial marker Cytochrome C Oxidase Subunit I (COXI) was found primarily in the upper (low density) part of the gradient, although some signal was also observed overlapping with the IncA enriched fractions.

To understand the distribution of the inclusions on the gradient in more detail, we counted inclusions in each fraction of the fractionated gradient (Figure 3.3 B). The intact inclusions were enriched mainly in the lower part of the gradient with a clear peak at fraction two whereas in the upper section there was no pronounced accumulation into one fraction. We observed that some relatively large inclusions preferentially localize to the upper (lower density) fractions of the gradient (data not shown).

The total yield of the optimized gradient purification protocol was assessed by counting the number of intact inclusions. Approximately 60% of total inclusions are recovered after gradient density centrifugation. This number was reduced to only 35 % after one round of washing (Figure 3.4 B) underlining the extreme fragility of this compartment, thus dismissing repeated pelleting as efficient means of further enrichment.

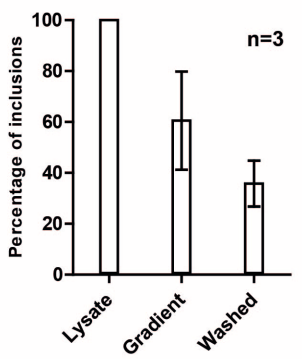

Figure 3.4: Yield of gradient purified inclusions
Yield of final gradient purification protocol. 6 x 10^7 HeLa cells were infected with *C. trachomatis* L2 for 24 h with MOI = 4. Cells were lysed by a ball homogenizer (16 µm clearance, 13 strokes) and subsequently fractionated on an in-situ formed 33 % Percoll gradient in HSMG buffer. The gradient was separated into two fractions. The upper fraction was discarded while intact inclusions were counted in the the lower 4 ml (Gradient). The gradient fraction was further diluted 1:6 with HSMG. Inclusions were pelleted at 1500 *x g* for 10 minutes, resuspended in HSMG and counted (Washed). Counted inclusions were normalized to inclusions in the lysate for each of three independent experiments. Standard deviation is indicated by error bars.

3.1.3 Quality control of density gradient purified inclusions

To judge the integrity of the gradient purified inclusions, we performed TEM (transmission electron microscopy) (Figure 3.5). Inclusions were isolated at 24 *p.i.*, washed once and spun on live cell dishes. Inclusions were then fixed and prepared for TEM.

Visualized inclusions clearly showed a single membrane surrounding the contained bacteria. The bacteria were distinguishable into EB and RB form, but their morphology did appear to be markedly different from bacteria visualized from cells without prior lysis described in the literature. Especially, the number of bacteria with condensed DNA, appearing as electron dense regions in the cytoplasm, was significantly higher than expected for this time point. Furthermore the average size and number of inclusions that remained intact during the preparation was considerably smaller than what we observed in live cell microscopy, indicating a significant loss during sample preparation for TEM (data not shown).

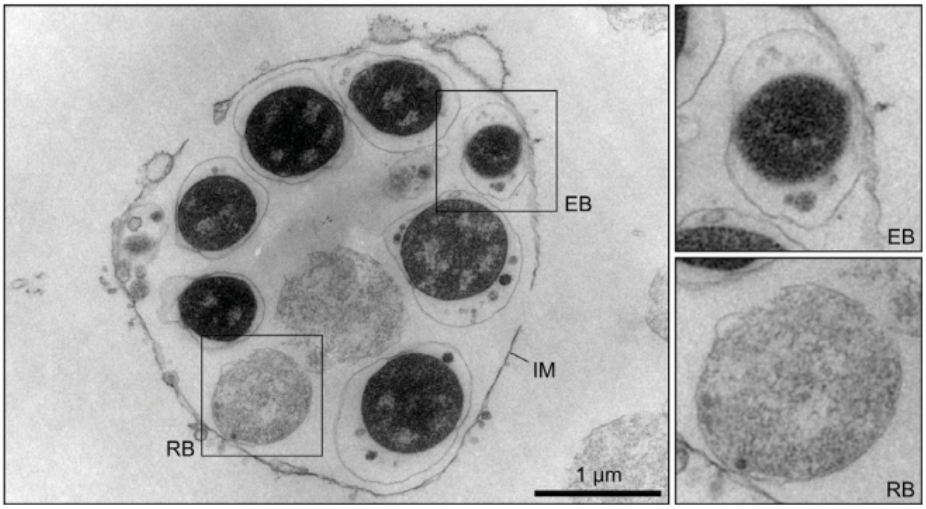

Figure 3.5: Percoll gradient purified inclusions retain a single membrane
Electron micrograph of gradient purified and washed inclusions. Inclusions were gradient purified after 24 h of infection as described. High density fractions containing inclusions were washed once and spun on live cell dish before fixation in 4% PFA /HSM for 30 minutes at room temperature, followed by fixation with glutaraldehyde and processing for TEM. IM = inclusion membrane, EB= elementary body, RB = reticulate body. *Preparation of sample for TEM after fixation and imaging were performed in the group of Dr. M. Laue, RKI, Berlin*.

In the next experiment, we assessed if proteins associated with the inclusion membrane remain attached during the purification procedure. To this end, we transfected cells with an eGFP tagged variant of Rab11A, a protein that is strongly recruited to the inclusion at 24 h *p.i*. (Rzomp, Scholtes *et al.* 2003). After gradient purification, the inclusions were spun onto a live cell dish and fixed before immunostaining. Confocal microscopy relevealed that Rab11A-eGFP was retained on the inclusion membrane and showed a clear rim-like staining (Figure 3.6). The majority of the Rab11A-eGFP signal colocalized with the inclusion membrane marker IncA, suggesting that inclusion associated proteins remain attached to the inclusion membrane during the purification procedure.

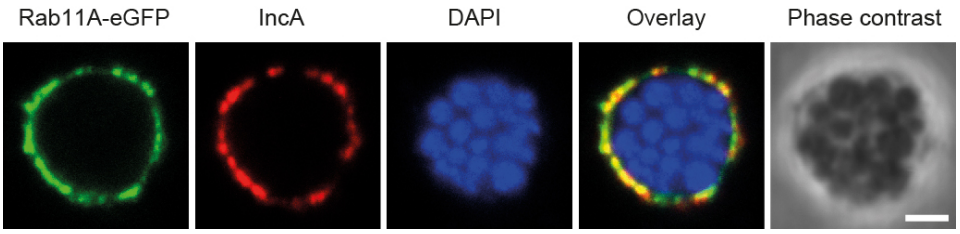

Figure 3.6: Inclusion associated proteins remain attached during purification
Inclusions were gradient purified at 24 h *p.i*. from *C. trachomatis* L2 infected HeLa cells transiently expressing the inclusion associated protein Rab11A-eGFP. Inclusions were fixed with 4% PFA in HSM and subsequently immunostained with specific antibodies against IncA. The DNA was stained with DAPI. Scale bar = 2 µm.

The structural integrity, especially the intactness of the surrounding membrane, of freshly gradient purified inclusions was assessed in the following experiment: Gradient purified inclusions were prepared for live cell microscopy and incubated with a high molecular weight (10 kDa) dextran compound, labeled with AlexaFluor 647. If the compound enters the luminal space of the

inclusion, the membrane is presumably ruptured, otherwise intact (Figure 3.7 A). Only inclusions that appeared sphere shaped and in focus in LSCM images were considered. We observed an intact membrane in 85% of the inclusions that passed the above criteria (Figure 3.7 B).

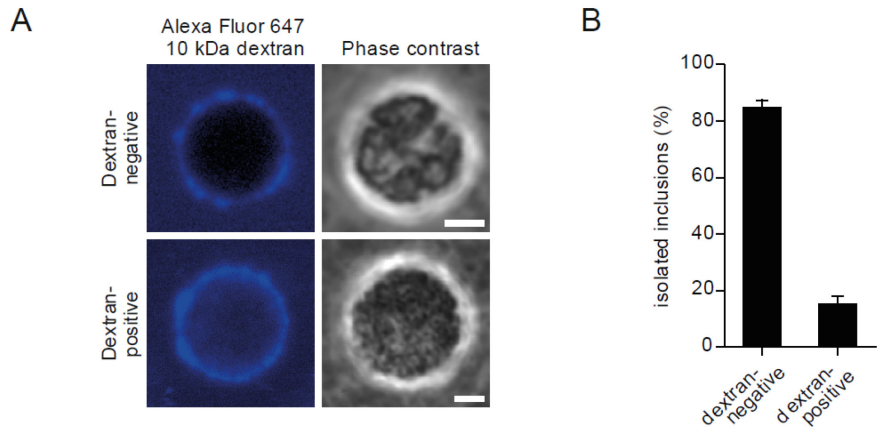

Figure 3.7: Integrity of gradient purified inclusions
Inclusions were gradient purified after 24h of infection and spun on a live cell dish. **A)** Inclusions were incubated with 10 kDa Dextran coupled to Alexa Fluor 647 and visualized by LSCM. **B)** Intact and ruptured inclusions were quantified as indicated. Indicated are mean percentages of three biological replicates. Error bars indicate standard deviation.

Taken together, we show that the lysis procedure followed by density gradient centrifugation allows the reproducible recovery of intact mid-infection inclusions from *C. trachomatis* L2 infected HeLa cells.

3.1.4 Immunomagnetic sorting of gradient purified inclusions

To further improve the purity of the isolated compartment, we subjected the gradient purified inclusions to immunomagnetic sorting (Figure 3.8 A). Gradient purified inclusions were incubated with the previously generated antibody directed against IncA (see Figure 3.1), followed by incubation with a secondary antibody coupled to supraparamagnetic micro-beads. The inclusions were then loaded onto a Miltenyi MACS LS column with a suitable magnet attached. Inclusions were washed with three times the input volume. Inclusions were eluted after removal of the magnet.

Secondary and primary antibody concentrations were titrated to retain 80% + inclusions during loading with minimal amount of each antibody (data not shown).

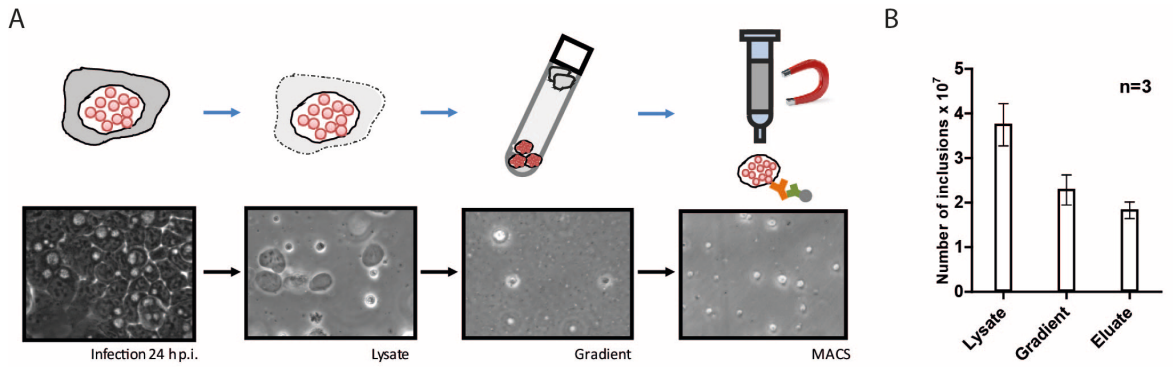

Figure 3.8: Workflow and yield of MACS purification
A) Complete workflow of the MACS purification procedure and purity assessment by phase contrast microscope. Different fractions of the purification procedure from infection over lysis, density gradient centrifugation and MACS separation were analyzed by phase contrast microscopy at 40 x magnification. Inclusions were isolated from 6 x 10^7 HeLa cells that were infected with *C. trachomatis* L2 for 24 h with an MOI of 4. The gradient fraction represents the lower 6 ml of the density gradient and was used as input for MACS separation. Eluate is the fraction of pure inclusions obtained after extensive washing on the MACS LS column. **B)** Visually intact inclusions were counted in different fractions. Numbers given are means of three independent replicates. Error bars indicate standard deviation.

The yield of the complete procedure was calculated by counting the inclusions contained in each fraction of the protocol (Figure 3.8 B). After the gradient 60.9 %(+-9.0 %) of inclusions were recovered of a total of 3.75 x 10^7 inclusions that were in the total lysate fraction. 80.0 % (+-8.1 %) of inclusions were recovered from the gradient fraction after MACS purification. The total yield of the protocol is 48.8% (+-4.9 %) of inclusions in solution.

The biochemical purity of the MACS purified inclusions was assessed by immunoblotting (Figure 3.9). We used a number of markers for different intracellular compartments to determine their depletion during the purification procedure. The ER marker Glucose regulated protein of 94 kDa (GRP94) appeared as a double band after infection with *C. trachomatis* L2. Nuclei are removed almost entirely in the density gradient purification step as indicated by the removal of p62. The same is true for the lysosomal marker lysosomal associated membrane protein 1 (LAMP-1) as well as Annexin II, a marker for the PM. GAPDH, a soluble cytosolic protein is also quantitatively removed by the MACS step, indicating sufficient washing during the procedure.

The bacterial marker IncA is highly enriched in the MACS 5X lane, indicating successful enrichment and purification of inclusion membranes. Hsp60 on the other hand is markedly increased after gradient centrifugation, as free bacteria co-sediment with the inclusion fractions but are not retained in the MACS fraction.

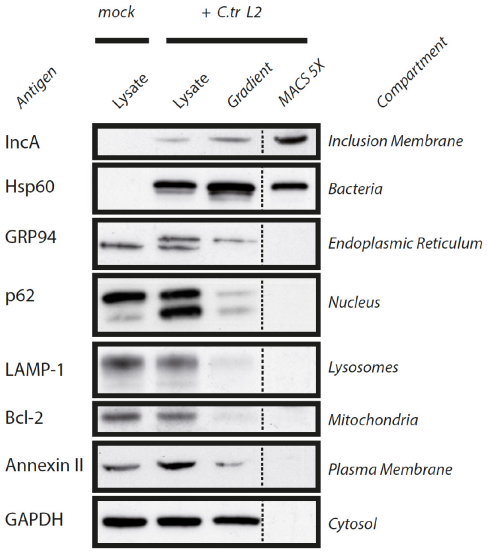

Figure 3.9: MACS purified inclusions are depleted of cellular organelles
Western blot analysis of different steps of the inclusion purification procedure. Inclusions were isolated from cells infected with *C. trachomatis* L2 for 24 h with MOI = 4 (+*C.tr L2*). Inclusions were gradient purified and the lower 6 ml (Gradient) were used for MACS purification. In the first three fractions, equal volumina of approximately equal protein amounts were loaded, the MACS 5X lane contains 5X the number of inclusions contained in the infected cell lysate lane. The indicated proteins were detected with specific antibodies. The subcellular compartments indicate the primary location of the probed proteins. GRP94 = glucose regulated protein of 94 kDa, Hsp60 = Heat shock protein of 60 kDa, p62 = Nucleoporin 62, Bcl-2 = B-cell lymphoma 2, GAPDH = Glyceraldehyde 3-phosphate dehydrogenase.

In summary, we here show for the first time the biochemical purification and partial characterization of mid-infection inclusions from *C. trachomatis* using a novel protocol. Furthermore, we established a toolbox for the analysis of inclusions in absence of the host cellular context by phase contrast microscopy, LSCM and electron microscopy.

3.2 Proteome analysis of mid-infection inclusions

After successfully purifying the inclusion of *C. trachomatis* L2 from HeLa cells at 24 h *p.i.*, we determined the host cell derived proteome of the isolated inclusions. We used SILAC (stable isotope labeling with amino acids in cell culture) as control for non-specific co-purifying proteins during the inclusion purification procedure (Ong, Blagoev *et al.* 2002). Furthermore, we used a label free quantification approach to determine the enrichment of proteins in isolated inclusions compared to total cell lysate.

The complete workflow for the SILAC experiment is described in Figure 3.10. We labeled cells differentially with heavy labeled (H) or unlabeled light (L) arginine and lysine. The L population of cells was then infected for 24 h with *C. trachomatis* L2 while the H population was mock infected. At 24 h *p.i.,* the cells were mixed 1:1 after scraping and samples were taken for total proteome measurement (Lysate). The mixed cells were subjected to the inclusion isolation protocol as described (Figure 3.8 A, p. 62). The final elution of MACS purified inclusions was pelleted and prepared for LC-MS/MS.

The proteins that are *bona fide* constituents of the inclusion are expected to have a high ratio of L label vs. H label (SILAC ratio) of one peptide species, whereas contaminants are expected to have ratios close to 1:1 in the inclusion fraction. The enrichment score for proteins detected in both lysate and inclusion fractions is based on iBAQ which was used to approximate the relative contribution of each protein to the total composition of each fraction.

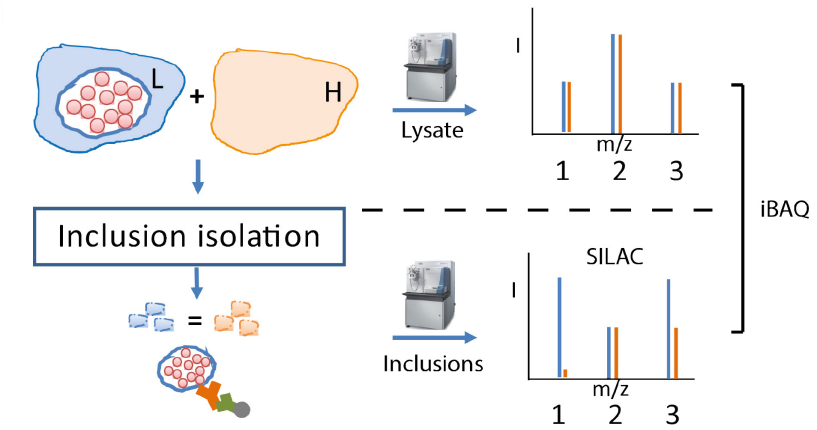

Figure 3.10: Workflow of inclusion host proteome analysis
HeLa cells were differentially labeled with heavy (H) or light (L) isotope labeled amino acids. Cells were infected with *C. trachomatis* L2 for 24 h and lysed for inclusion isolation. Samples of total lysate were taken and prepared for measurement by LC-MS/MS after tryptic digest (Lysate). Inclusions were isolated from the remaining lysate and similarly prepared for LC-MS/MS (Inclusions). The scheme of three different peptides (1-3) measured by LC-MS/MS shows idealized SILAC ratios for peptides derived from different classes of proteins. (1) corresponds to the ideal inclusion associated protein which has a high L/H ratio. Contaminations introduced by the isolation procedure are expected to be identical for H and L labeled cells, corresponding to peptide (2). Proteins that are in part contaminations as well as inclusion associated have a lower L/H ratio (3). The enrichment of proteins in the inclusion fraction compared to the total lysate is calculated based on label free iBAQ. *LC-MS/MS was performed by Dr. Frank Schmidt and Dr. Nico Jehmlich, Universität Greifswald*.

3.2.1 Proteome measurement and initial data analysis

We isolated inclusions in triplicate and subjected the proteins of both the lysate and the inclusions to LC-MS/MS. Protein lists were generated by MaxQuant as described in the methods section. For reasons of simplicity, the term “protein group” will be substituted by “protein” in the remainder of this thesis if not indicated specifically.

3.2.2 Bacterial proteome

We first analyzed the bacterial proteins found at the 24 h inclusion. After primary filtering (2 or more unique peptides in all three replicates), we identified 602 proteins of the 884 contained in the Uniprot database for *C. trachomatis* L2 434 Bu (68 % of total ORFs). An additional 106 were found in all three replicates, but with less than two peptides in at least one of the replicates (80 % of total ORFs).

Of the 62 Inc proteins predicted for *C. trachomatis* D (Bannantine, Griffiths *et al.* 2000, Toh, Miura *et al.* 2003, Dehoux, Flores *et al.* 2011), 21 were reliably identified whereas an additional 11 were identified with less stringent filtering of one peptide per experiment. We listed the Inclusion proteins we identified and ranked them according to their proportional intensity, for completeness we also listed the abundance as determined by iBAQ (Table 3.1). It must be noted that the second most abundant protein (CT241) was found in the outer membrane complex (Liu, Afrane *et al.* 2010) and therefore most likely is not an inclusion membrane protein. Of the bacterial 22 proteins identified at the inclusion membrane by Li *et al*. (Li, Chen *et al.* 2008) we identified 16 (18 with less stringent filtering) including two additional non-classical Inc proteins (CT089, CT529).

In a recent bioinformatics screen, 96 *C. trachomatis* L2 proteins were predicted to be T3SS substrates (Jehl, Arnold *et al.* 2011) of which we identified 51 (67 with less stringent filtering). 20 of the 29 that were never identified were annotated as hypothetical proteins

Taken together, we identified a significant proportion of the total encoded proteome of *C. trachomatis* L2, including seven out of eight virulence plasmid encoded proteins (pL2) and a large number of predicted effector proteins.

Table 3.1: Abundance of predicted inclusion membrane proteins identified in the proteome

For each protein, the abundance was approximated based on summed intensity (i) or reported iBAQ values (iBAQ) and normalized to 20000 total arbitrary units. Standard deviation is indicated (SD) and was derived from triplicate experiments. Where no abundance is indicated, less than two unique peptides were detected in at least one of the experiments. Total number of unique peptides (P) and numbers of unique peptides identified in each experiment are indicated (P1-3). Gene identifiers for *C. trachomatis* D UW-3 (D UW-3) and *C. trachomatis* L2 Bu 434 (L2 Bu 434) are listed.

D UW-3	L2 Bu 434	Protein names	P	P1	P2	P3	iBAQ	iBAQ SD	i	i SD
CT223	CTL0476	Candidate inclusion membrane protein	17	15	15	12	63	4	60	9
CT241	CTL0493	Outer membrane protein	38	27	37	28	17	4	48	11
CT118	CTL0373	Inclusion membrane protein G	9	8	8	8	99	11	44	16
CT147	CTL0402	Putative integral membrane protein	65	47	53	39	7	1	41	5
CT618	CTL0882	Putative membrane protein	10	8	9	7	35	4	28	2
CT116	CTL0371	Inclusion membrane protein E	3	3	3	3	109	39	24	18
CT813	CTL0184	Candidate inclusion membrane protein	13	8	12	7	31	5	21	6
CT228	CTL0480	Candidate inclusion membrane protein	10	9	10	5	13	3	11	3
CT115	CTL0370	Inclusion membrane protein D	4	3	3	3	10	1	5	2
CT229	CTL0481	Candidate inclusion membrane protein	7	6	6	5	8	1	4	1
CT728	CTL0097	Putative integral membrane protein	5	2	4	2	6	5	4	4
CT249	CTL0500A		3	2	2	3	12	1	3	1
CT616	CTL0880	Putative integral membrane protein	13	4	7	8	1	0	2	0
CT232	CTL0484	Inclusion membrane protein B	3	3	3	3	8	2	2	1
CT233	CTL0485	Inclusion membrane protein C	4	3	2	3	6	1	2	1
CT850	CTL0223	Putative integral membrane protein	12	3	11	4	1	1	1	1
CT288	CTL0540	Candidate inclusion membrane protein	14	5	10	5	1	0	1	0
CT005	CTL0260	Putative membrane protein	6	2	4	3	2	1	1	1
CT214	CTL0466	Candidate inclusion membrane protein	10	5	4	4	1	0	1	0
CT226	CTL0478	Candidate inclusion membrane protein	3	2	2	2	2	1	1	0
CT018	CTL0273	Putative membrane protein	6	2	3	5	1	0	1	0
CT119	CTL0374	Inclusion membrane protein A	9	7	7	1	-	-	-	-
CT058	CTL0314	Putative membrane protein	6	4	4	1	-	-	-	-
CT101	CTL0356	Putative membrane protein	3	2	2	1	-	-	-	-
CT134	CTL0389		2	1	2	1	-	-	-	-
CT192	CTL0444	Candidate inclusion membrane protein	4	1	3	3	-	-	-	-
CT222	CTL0475	Candidate inclusion membrane protein	2	2	2	1	-	-	-	-
CT324	CTL0576		2	1	2	1	-	-	-	-
CT442	CTL0701	Cysteine-rich membrane protein	3	2	3	1	-	-	-	-
CT556	CTL0819	Putative membrane protein	2	1	2	1	-	-	-	-
CT642	CTL0010	Putative membrane protein	5	2	4	1	-	-	-	-
CT788	CTL0156	Putative exported protein	2	2	2	1	-	-	-	-

3.2.3 Host cell-derived inclusion proteome

3.2.3.1 SILAC exclusion approach

To be able to distinguish host proteins associated with the inclusion from contaminants and co-purifying proteins, we performed a statistical test to determine enrichment in the inclusion fraction based on the SILAC ratio distribution in the lysate and the SILAC ratios of the inclusions (SILAC exclusion approach) (Figure 3.11). The protein lists obtained from MaxQuant were filtered stringently (1 unique + razor peptide minimum per protein group in all three replicates, two or more unique + razor peptides in at least one replicate, false discovery rate < 1%, filtered common contaminations, proteins identified solely from the decoy database and bacterial proteins) before being used in further analyses if not indicated otherwise. We detected 1472 host proteins that passed this initial filtering in the inclusion fraction, while 2003 were detected in the lysates.

As a large number of proteins in the inclusion fraction was detected in triplicates but did not show SILAC ratios in all three replicates either due to primarily being in the L labeling state or too few SILAC ratio counts due to low abundance in one of the replicates, in addition to proteins that had SILAC ratios reported in all three experiments (Figure 3.11 A), we performed a test for enrichment with these proteins (Figure 3.11 B).

For the test, SILAC ratios of all proteins were transformed by computing the logarithm. An empirical distribution was calculated based on the lysate ratios of proteins which were measured in both data sets (lysate and inclusion fractions, each in three replicates). A two-sided Wilcoxon test was applied to determine the differentially enriched proteins in the inclusion fraction data. Each protein in the inclusion fraction data set was tested for a significant shift of its ratios compared to the empirical lysate distribution. P-values were adjusted for multiple testing by the Benjamini-Hochberg approach and all protein groups below an adjusted p-value of 0.01 were considered in the first test. As a result, 746 proteins were reported to be differentially enriched, among these 253 were enriched in the inclusion fraction (Figure 3.11 A). In the second test proteins below an adjusted p-value of 0.04 were considered and the empirical distribution of the lysate SILAC ratios was based on both, proteins with two and three SILAC ratios. In this second test, an additional 92 proteins were found to be enriched in the inclusion fraction. In total, 345 host proteins were considered to be inclusion associated based on their isotope label ratio.

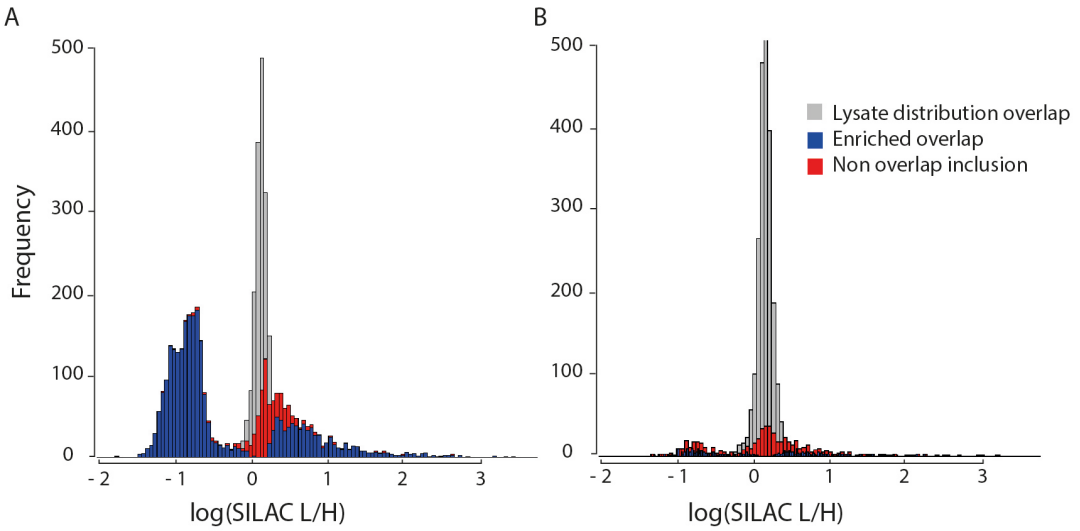

Figure 3.11: Statistical test for enrichment in the inclusion fraction/ SILAC exclusion approach
Proteins were tested for enrichment in the inclusion fraction as described in the text. The graph shows a bar diagram with the empirical distribution of the logarithm of the SILAC ratios of proteins that were found in both the inclusion and lysate fraction. The grey bars indicate the SILAC ratios of proteins found in the lysate which overlap with inclusion proteins, blue bars show proteins that are differentially enriched in the inclusion fraction. Red bars show proteins which were only found in inclusion dataset. Proteins enriched in the inclusion fraction are expected to have positive (L/H) SILAC ratios. **A**) Proteins of the inclusion fraction which show three SILAC ratios (blue and red) **B**) Proteins of the inclusion fraction which only show two SILAC ratios (blue and red). The highest bar was capped at 500. More proteins were used for the empirical lysate distribution compared to A, because the overlap for both proteins with two and three SILAC ratios was used. *Statistical test was performed by M. Fischer, Robert Koch Institut (RKI), Berlin.*

3.2.3.2 Contaminants

To characterize possible organellar contaminations we retrieved subcellular location data from UniprotKB (UniProt 2014) of all proteins which were reliably quantified (SILAC ratio in at least 2 of 3 experiments) in the inclusion fraction (n = 1399) and plotted these in bins of 0.125 of their corresponding SILAC ratios. As shown in Figure 3.12, the proteins that showed a low L/H ratio are predominantly annotated as mitochondrial. Indeed 85 % percent of the proteins that pass the cutoff for enrichment in the mock isolation are annotated as mitochondrial. Similar to mitochondrial proteins yet less pronounced, also a significant amount of lysosomal proteins showed a slight shift towards low L/H ratios which exceeded the minimal change observed in lysates (average SILAC ratio of lysates = 1.12, average of lysosomal proteins in lysates = 1.06, average of non-inclusion lysosomal proteins in inclusion fraction = 0.89). Apart from the mitochondrial contamination, we did not observe large amounts of contaminating proteins. In support of this, there is a local minimum of proteins per organelle around the region of the cutoff, with local maxima on both sides of the cutoff suggesting a relatively clear separation of contaminations versus true inclusion proteins (Figure 3.12).

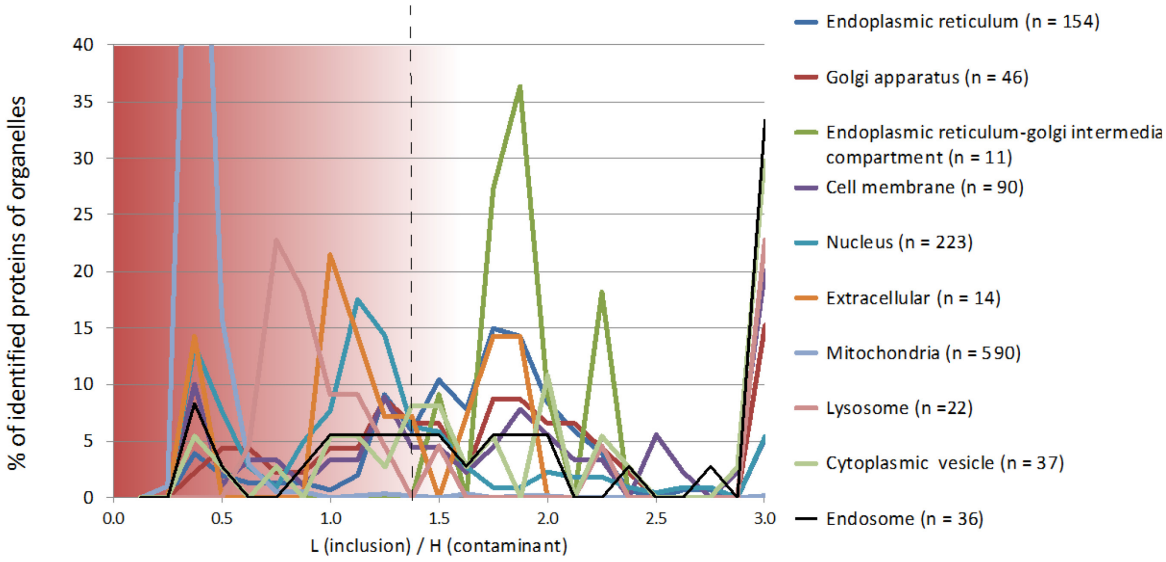

Figure 3.12: The distribution of annotated organellar proteins along the SILAC ratios
Mean SILAC ratios of proteins after primary filtering were pooled into bins of 0.125 (n = 1399). The total number of proteins mapping to the subcellular localization term was determined and the percentage in each bin plotted along against the SILAC ratios. Data points were connected for better visibility. The approximate cutoff for enrichment is indicated with a dashed line. Values above 3 were pooled in the 3.0 bin.

3.2.3.3 Enrichment score

To identify proteins that are enriched at the inclusion in comparison to their abundance in the whole cell, we used iBAQ to approximate the abundances of proteins in our samples (Schwanhausser, Busse *et al.* 2011). As opposed to the original publication, we did not introduce standards for absolute quantification but quantified only relative to the total summed intensity of an individual experiment. Despite limited accuracy, this method provides additional information especially for highly abundant proteins in addition to the SILAC based exclusion approach. Based on this method, we quantified the relative contribution of each protein to the total proteome of the lysate and the inclusion. Only proteins that passed the SILAC exclusion approach were considered. The quotient of the values for the inclusion and the lysate resulted in the enrichment score for proteins which were overlapping in the two datasets (iBAQ enrichment score). For proteins that were not found in our lysate proteome, we used a recently published very high coverage dataset of the HeLa proteome (Nagaraj, Wisniewski *et al.* 2011) for approximation of the protein abundance in the cell lysate. All identified host proteins are listed in the appendix with their SILAC ratio and iBAQ enrichment score, if available (Table 6.1, p. 144).

3.2.3.4 Known inclusion associated proteins

As an intrinsic validation of our dataset, we compared it to proteins that were reported in the literature to be associated with the inclusion of *C. trachomatis* at mid-infection stages (see Table 4.1, p. 102 for a complete overview). Of these 52 proteins in total (Rab subgroups were not counted separately), we found 23 in our dataset after stringent filtering and applying the SILAC exclusion approach (Figure 3.13). Only one previously reported inclusion protein was removed by the SILAC exclusion approach (Vimentin).

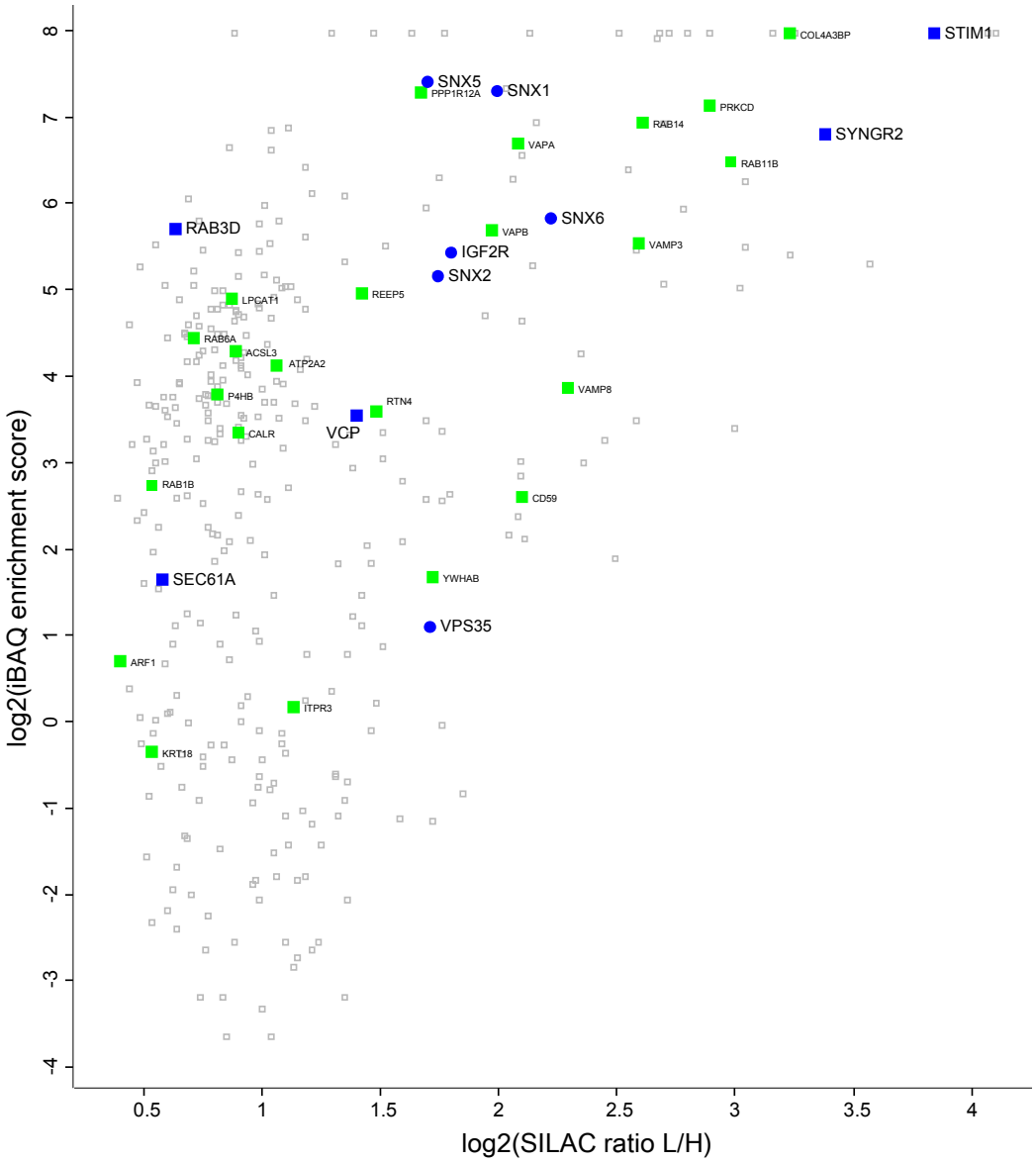

Figure 3.13: iBAQ enrichment and SILAC ratios of identified proteins

Overview of iBAQ based enrichment and SILAC ratios of identified proteins. Proteins reported in the literature to be inclusion associated are shown in green. Proteins validated in this thesis are shown in blue. All other host proteins that passed the SILAC based cutoff are shown in grey. Identifiers show the official gene symbol of the respective proteins. iBAQ enrichment scores were capped at 250 fold.

3.2.3.5 Validation

To further validate our proteomics approach, we selected several proteins with varying SILAC ratios and enrichment scores for further analysis. A graphic overview of the iBAQ enrichment score and SILAC ratios of the literature reported identified proteins and the proteins selected for validation and further experiments is given in Figure 3.13.

We developed a small scale variant of the gradient purification protocol which we used to isolate inclusions from cells transfected with fluorescent fusion proteins in addition to IF staining of infected cells. This validation by purified inclusions (VPI) is especially helpful when validating proteins that are not exclusively recruited to the inclusion but are found in other organellar structures surrounding the inclusions such as the ER. In these instances LSCM imaging of intact cells shows ambiguous localization.

To validate the VPI approach, we transfected HeLa cells with wild type (WT) YFP-Rab3D and the dominant negative mutant T36N (Chen, Edwards *et al.* 2002, Knop, Aareskjold *et al.* 2004) and performed IF and VPI at 24 *p.i*. The dominant negative mutant is deficient in guanine nucleotide binding and therefore cannot assume the GTP bound conformation necessary for membrane association (Chen, Garcia-Santos *et al.* 2013). As expected, inclusions isolated from cells expressing YFP-Rab3D WT showed a rim like staining when visualized by live cell LSCM, while the dominant negative mutant did not associate with the inclusion membrane (Figure 3.14). As an additional control, we performed the experiment with cells expressing eGFP only, where we also did not observe fluorescent signal originating from the isolated inclusions (data not shown). Rab3D is therefore a novel inclusion associated protein that interacts with the inclusion in a GTP dependent manner.

Valinosin-containing protein (VCP) is involved in a large number of cellular processes including mitochondrial quality control, autophagy, vesicle transport and fusion, 26S proteasome function and DNA damage repair (Baek, Cheng *et al.* 2013). It has a cytosolic localization but associates with the ER (Ye, Shibata *et al.* 2004) where it is involved in retro-translocation of misfolded proteins across the ER membrane. Expression of VCP-eGFP in cells infected for 24 h did not lead to a redistribution of the cellular pools of VCP compared to non-infected cells but co-localization with the inclusion membrane marker IncA was evident. VPI further confirmed this association and showed a rim-like staining of the inclusion membrane.

Synaptogyrin-2 (SYNGR2), also known as cellugyrin, is a relatively poorly characterized protein that localizes to synaptic-like microvesicles (Janz and Sudhof 1998, Belfort and Kandror 2003, Mital, Miller *et al.* 2010). Expression in non-infected cells leads to a clearly membrane associated distribution reminiscent of the ER. The infection did not lead to a redistribution of the total

protein but only a slight association with the inclusion. VPI confirmed the inclusion membrane association.

The Sec61 complex is involved in co-translational protein targeting to the ER membrane (Park and Rapoport 2012). Although Sec61β was not in the set of positively enriched proteins (p = 0.01067, cutoff = 0.01), we found another protein of the Sec61 complex, Sec61α which led us to believe that Sec61β might share its localization. Indeed, Sec61β did localize to the inclusion in the VPI experiment indicating that the whole complex might be localized there.

Stromal interaction molecule 1 (STIM1) which forms homooligomers or heterooligomers with STIM2, which was also found at the inclusion, is involved in mediating store-opened Ca^{2+} entry and is dually localized to the ER and the PM, depending on intracellular Ca^{2+} levels (Zhang, Yu *et al.* 2005). When imaging the YFP-fusion protein, the association with the inclusion was rather weak, while no YFP positive inclusions were found in the VPI experiment.

In sum, we tested five different proteins for inclusion association in IF and VPI and were able to verify four of them positively while the localization of one remained ambiguous.

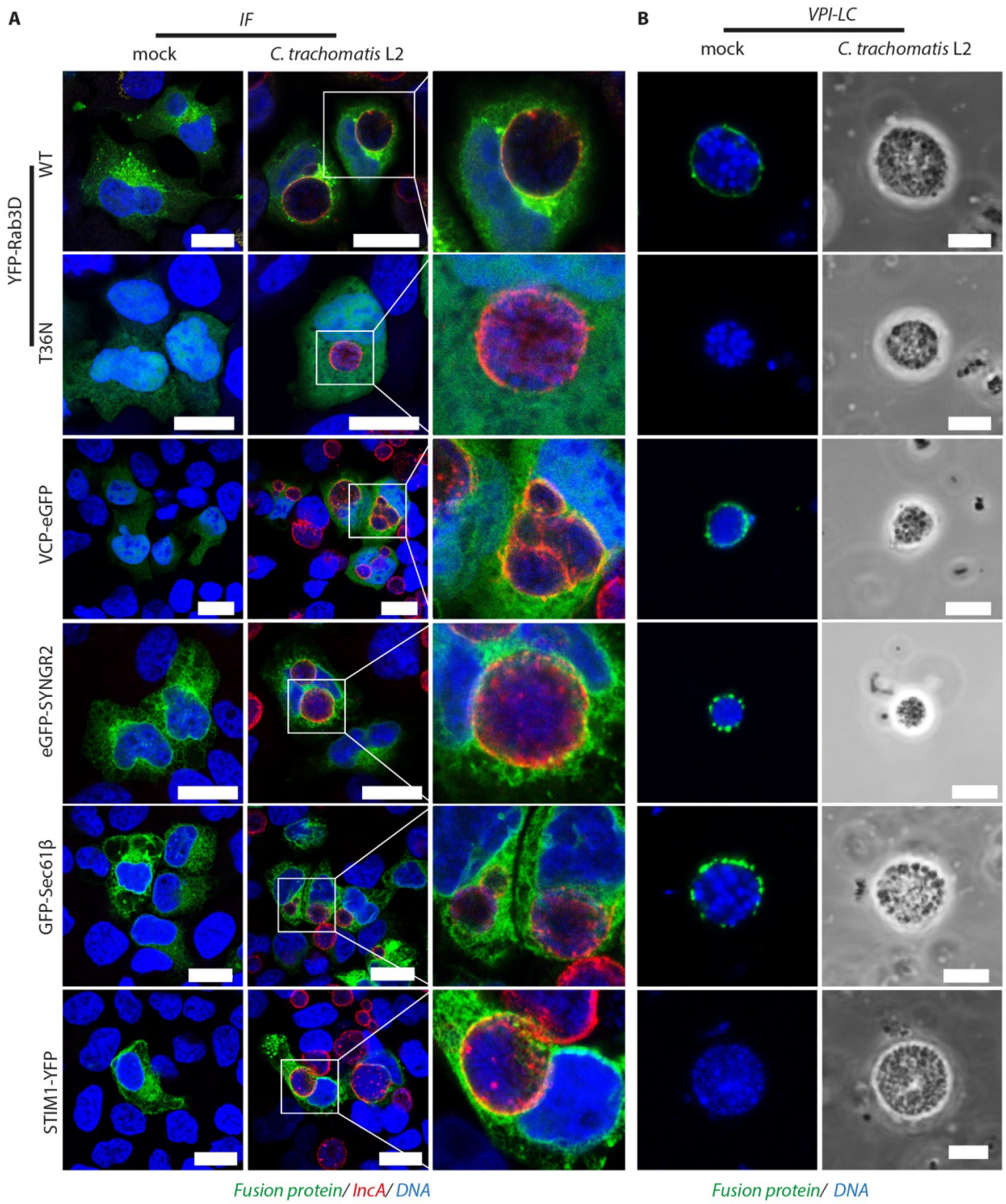

Figure 3.14: Validation of inclusion associated proteins using fluorescent fusion proteins

A) IF images showing HeLa cells expressing the indicated fluorescent fusion proteins (green), infected with *C. trachomatis* L2 (MOI = 2). Cells were fixed 24 h *p.i.* with 2 % PFA and stained for IncA (inclusion membrane, red) and DNA (DAPI, blue). Scale bar, 20 µm. **B)** Validation by purified inclusions in live cell microscopy (VPI-LC): Inclusions were gradient purified from cells expressing the indicated fusion protein using a small scale protocol and analyzed by LSCM, DNA was stained with DAPI. Scale bar = 5 µm.

3.3 Global analysis of the host cell derived inclusion proteome

After validating the proteome data by IF studies, we performed a global analysis of the 345 proteins that passed the filtering and SILAC based exclusion approach for inclusion association.

3.3.1 Organellar contributions

Although it is known that the inclusion interacts extensively with many cellular organelles in the course of its development cycle, the contribution of host organellar protein pools to the total proteome is unknown. Also, the acquisition of membranes necessary for the rapid expansion of the inclusion is not understood, despite our knowledge of several mechanisms that might be involved in this process simultaneously.

To address these questions, we determined the relative contribution of the major subcellular organelles to the host cell derived proteome of the inclusion and the total cell lysate. We obtained subcellular location data from UniprotKB (UniProt 2014) and calculated the contribution of each major organelle to the total proteome of the inclusion and the lysate both in number of proteins (Figure 3.15 A), and absolutely quantified (Figure 3.15 B). There was not a single compartment that contributed the overwhelming majority of proteins but the composition is a patchwork organelle of different sources, both numerical and absolutely quantified.

With the exception of cytosolic proteins, the largest number and percentage of inclusion proteins was annotated as components of the ER (35.1 % by number and 35.9 % by iBAQ percentage) with a low contribution in the total cell lysate (7.7 % and 4.0 %, respectively). Another, rather unexpected but significant contribution came from the PM (16.6 % and 13.8 % vs. 7.7 % and 7.7 % in the lysate). One term, cytoplasmic vesicle (CV), showed a large difference between the two quantification strategies in the inclusion fraction. The quantification on the basis of numbers of proteins in the inclusion fraction was 8.0 %, whereas based on iBAQ it was found in 12.2 % of the total protein, indicating that these proteins are highly enriched in stoichiometric abundance. The GA, endosomes and ERGIC also were only annotated in a rather low percentage in the inclusion fraction but were highly enriched compared to total cell lysate (Figure 3.15), which was even more pronounced in the iBAQ percentage.

In the inclusion fraction, only 3 proteins were annotated as mitochondrial (0.9 % and 0.4 %, respectively).

Lysosomal proteins were, at 2.2 % and 0.9 %, respectively also low, although the contribution in inclusions was slightly higher than in the cell lysate.

Taken together, both methods of quantification show a similar composition of the inclusion, with the ER, CVs and the PM being the main contributors among the major intracellular organelles.

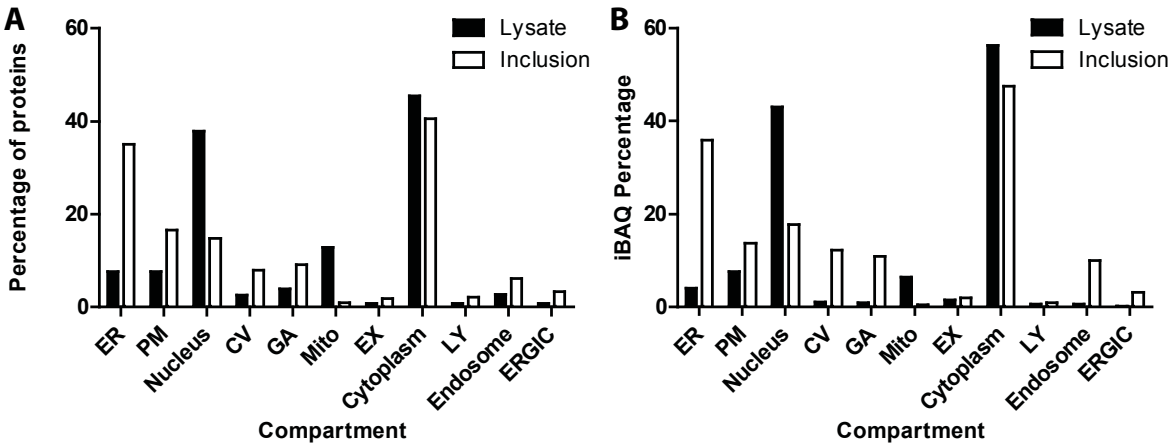

Figure 3.15: **Organellar distribution of proteins in lysate and inclusions**
Proteins that were reliably found and quantified in the inclusion and the total cell lysate (Lysate: n = 2002; Inclusion: n = 345) were annotated with subcellular localization data from UniprotKB. One protein can have annotations for several subcellular organelles. **A)** The percentage of proteins annotated with the indicated term is shown. **B)** Proteins were quantified according to their iBAQ intensity and the stoichiometric abundance of proteins annotated with the indicated subcellular localization term was summed. ER = endoplasmic reticulum, PM = plasma membrane, CV = cytoplasmic vesicle, GA = Golgi apparatus, Mito = mitochondria, EX = extracellular, LY = lysosome, ERGIC = ER – Golgi intermediate compartment.

3.3.2 Enrichment analyses

To further characterize the composition of the inclusion, we used enrichment analysis based on GO terms using GOrilla (Eden, Navon *et al.* 2009). For all GO enrichment analyses, we used a background generated from the tryptic peptides detected by Nagaraj *et al.* in the deep proteome of HeLa cells (Nagaraj, Wisniewski *et al.* 2011) to account for detection bias introduced by mass spectrometry based proteomics. Tables of GO enrichment analyses can be found in the appendix (Table 6.3, Table 6.4 and Table 6.5, p. 155 ff.).

3.3.2.1 Cellular components

The first analysis was based on the GO of cellular components (GOCC) similar to what we showed in the first analysis or organellar contributions, but using GO terms, which annotate proteins more broadly than the manually curated UniprotKB database. In this analysis, the most highly enriched term was “vesicle” with a p-value of 6.95×10^{-55} and 2.61 fold enrichment (212 proteins mapping to the term). The more granular terms were mapped to “cytoplasmic membrane-bounded vesicle” (a subcategory of CV) with 68 proteins and “extracellular vesicular exosome” with 196 proteins of the total 345. In the same range of enrichment and a similar p-value was “endoplasmic reticulum part” followed by “plasma membrane”, thereby confirming the quantification shown in Figure 3.15. 207 proteins were annotated with “membrane” ($p = 4.02 \times 10^{-29}$) thereby indicating that we do have a good coverage of membrane proteins. Highly enriched GO terms that are presumably irrelevant to our biological system were “melanosome”, “zona pellucida receptor

complex", the latter overlapping completely with "chaperonin-containing T-complex", a large chaperone complex of 900 kDa typically found in the cytosol (Dunn, Melville *et al.* 2001), for which we only found low iBAQ based enrichment despite high SILAC ratios (average iBAQ enrichment 0.57 +-0.17 standard deviation), suggesting limited functional relevance.

3.3.2.2 Functional categories and complexes

We analyzed the dataset for GO terms of biological processes (GOBP) that were overrepresented in our dataset. As expected for the high abundance of ER derived proteins in our dataset, several ER specific processes were highly enriched such as "protein folding" ($p = 8.01 \times 10^{-19}$), "response to ER stress" ($p = 1.01 \times 10^{-14}$) and "response to unfolded protein" ($p = 1.29 \times 10^{-16}$). Surprisingly, the term "blood coagulation" was also one of the most highly enriched ($p = 3.09 \times 10^{-9}$), however, has possibly little relevance to inclusion formation in our biological setting.

The most highly enriched single term apart from the above mentioned was "establishment of protein localization" (GO:0045184) with a p-value of 2.53×10^{-13} and a total of 85 proteins contributing to this category. As we are interested in the biogenesis of the inclusion, we decided to look at these proteins in more detail. Analysis of these proteins for specific complexes of interacting proteins using STRING 9.1 (Search Tool for the Retrieval of Interacting Genes/Proteins) (Franceschini, Szklarczyk *et al.* 2013) revealed four clusters of highly interacting proteins (Figure 3.16 A-D). The first cluster is composed of components of the SNX-BAR retromer, a complex involved in retrograde trafficking from endosomes to the TGN. Four proteins found in this complex are among the most highly enriched accoring to their iBAQ enrichment score and SILAC ratio (Figure 3.13). The second cluster is composed of the 14-3-3 protein family, of which one member, 14-3-3 β, has previously been reported be be inclusion localized (Scidmore and Hackstadt 2001). The third cluster consists of a number of proteins invloved in co-translational protein import to the ER including Sec61β, Sec63, SRPB, VCP and others. The last cluster consists of three Rab proteins, VAMP3 and VAMP8, two syntaxins, and additional proteins, some of which form a SNARE complex involved in membrane fusion, primarily of exocytic vesicles with the PM (Wade, Bryant *et al.* 2001, Ruepp, Brauner *et al.* 2008).

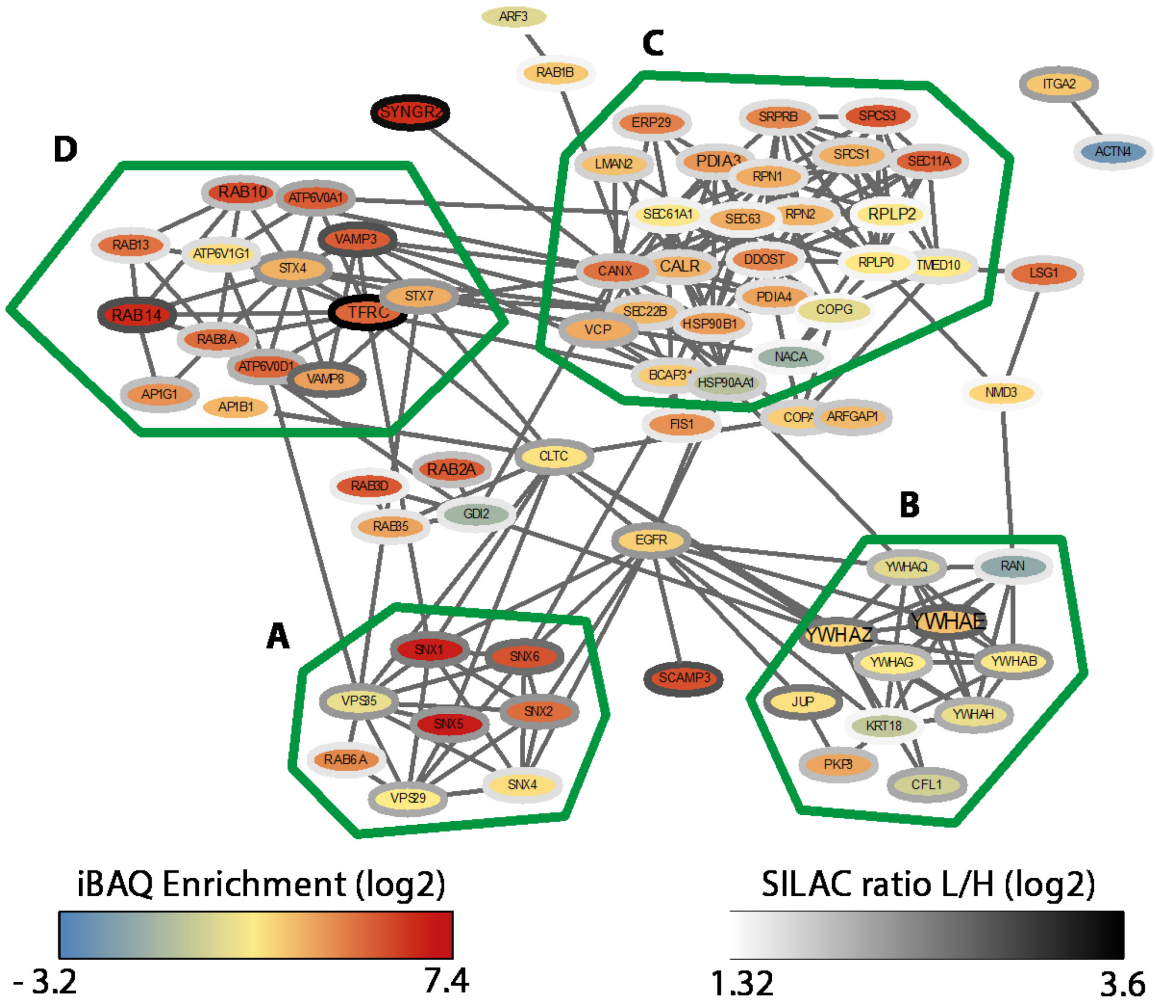

Figure 3.16: **Protein-protein interaction network of proteins involved in protein localization**
Protein-protein interactions of inclusion associated proteins annotated with the highly enriched GO term "establishment of protein localization" (GO:0045184, n = 85) were analyzed. Connecting lines indicate interactions as reported by STRING database in standard settings. Color of the node represents the enrichment score, the color of border of the nodes are colored according to the SILAC ratio. The font size indicates the relative abundance in the inclusion proteome. Main clusters of interacting proteins are encircled with a green line and labeled A –D.

The most granular (i.e. highly resolved) GO term that was resolved apart from ER related processes was "vesicle mediated transport" (GO:0016192, n = 71). To further characterize these trafficking pathways that are putatively involved in the maintenance of the inclusion, we analyzed the contribution of proteins involved in anterograde and retrograde transport to the proteome (Figure 3.17). Proteins involved in retrograde trafficking constitute 40 % of the proteins involved in either process, with retrograde transport from endosomes to the GA being the largest group within the retrograde trafficking group (18 % of total). Within the group of anterograde trafficking proteins, those involved post Golgi trafficking and its subcategories contribute the majority of proteins (25 %).

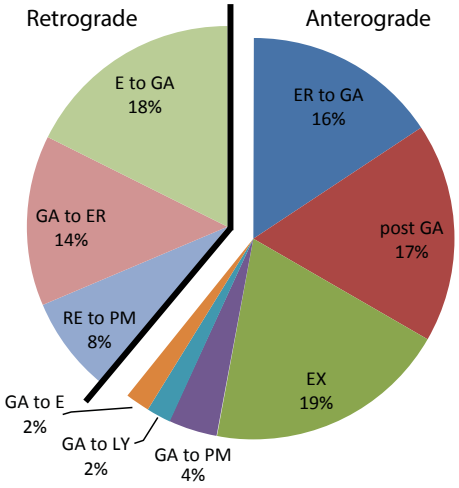

Figure 3.17: Proteins involved in retrograde and anterograde trafficking
Proteins annotated with the GO term „vesicle mediated transport"(GO:0016192, n = 71) and child terms were extracted from the host proteome. Three proteins with incomplete GO annotation were added manually (Rab1B, Rab12, VPS29). 35 of these proteins were further classified as involved in retrograde or anterograde transport, and respective subcategories. Five proteins were annotated with both retrograde and anterograde transport pathways (LMAN1, Rab11B, Rab14, TMED10 and VAMP3). Two additional proteins were annotated with two subcategories (STX7, VAMP8, both anterograde). E = endosome, ER = endoplasmic reticulum, GA = Golgi apparatus, EX = exocytosis, PM = plasma membrane, LY = lysosome, RE= recycling endosome.

3.3.2.3 Known protein motifs and domains

Proteins that localize to the inclusions have a large number of recruitment phenotypes, ranging from complete relocalization to the inclusion membrane over more subtle recruitment to subdomains of the inclusion membrane to complete translocation of the protein into the inclusion lumen (see Table 4.1, p. 102). The mechanisms of recruitment to the inclusion have only been studied for a handful of proteins and are diverse. However, this does not exclude that certain groups of proteins could be recruited for example by common motifs. We therefore analyzed if protein motifs and domains indexed in several databases were enriched in our dataset using DAVID (Huang da, Sherman *et al.* 2009).

The highest ranking INTERPRO (Hunter, Jones *et al.* 2012) terms were "Endoplasmic reticulum, targeting sequence" (n = 18, p = 6.6 x 10^{-13}) and "Thioredoxin-like proteins" (n = 15, p = 1.8 x 10^{-11}). Apart from these proteins that are typically enriched in the ER, "Chaperonin TCP-1, conserved site", which was also identified in the GOCC analysis, was enriched as eight proteins found in our proteome are part of this complex. Furthermore 14-3-3 (n = 7, p = 1.3 x 10^{-7}) proteins and Ras GTPases (n = 15, p = 5.4 x 10^{-7}) were highly enriched, both of which members were previously reported to be associated with the inclusion (Table 4.1). "RNA polymerase sigma factor 54, interacting" proteins (n = 5, p = 4.4 x 10^{-4}), "Calcium-binding EF-hand" domain containing proteins (n = 9, p = 3.6 x 10^{-3}) and "VPS5 C-terminal" (n = 3, p = 7.9 x 10^{-3}) were although less enriched, still

highly significant. All of the"VPS5 C-terminal" proteins are part of the SNX-BAR protein complex identified in Figure 3.16.

Taken together, apart from Ras GTPases, there is no large group of proteins containing enriched known protein motifs or domains. The PX domain containing proteins of the SNX-BAR retromer complex will be studied in more detail in the next chapter as the retromer and has not been previously investigated in the context of *Chlamydia* infections; yet is among the most prominent functional complexes at the inclusion based on our analyses (see section 3.4, p. 81).

3.3.3 Rab proteins

Rab proteins are important contributors to organellar identity and play a key role in a majority of known vesicle mediated transport processes (Behnia and Munro 2005). Furthermore, the modulation of Rab proteins by bacterial effector proteins is a well-known intracellular survival strategy of intracellular pathogens (Alix, Mukherjee *et al.* 2011). As the enrichment analysis indicated that Ras GTPases and especially Rab GTPases are highly abundant in the inclusion proteome, we decided to further investigate these.

Based on iBAQ, all Rab proteins have a combined stoichiometric abundance of 11.64 % of total host protein on the inclusion of which Rab11B and Rab14 contribute over half (Table 3.2). Also, they were, apart from Rab1B/C highly enriched compared to total lysate but their SILAC ranged widely.

Table 3.2: Rab proteins and their abundance at the inclusion
Known = the inclusion localization of the proteins has been described previously, SG =subgroup, indicated when only a subgroup member of the proteins has been reported to be inclusion localized. Percentage = Percentage of total iBAQ intensity of inclusion fraction. Compartment = Primary localization of Rab protein in non-infected cells. References for indicated compartments: (Galvez, Gilleron *et al.* 2012). RE= recycling endosome, EE = early endosome, TGN = trans Golgi network, ER = endoplasmic reticulum, GA = Golgi apparatus, G4V = Glut4 containing vesicles, LY = Lysosome, CCV = clathrin coated vesicles, EX = exocytic vesicles.

Gene names	Known	Percentage	iBAQ enrichment	SILAC ratio (L/H)	Compartment
RAB11B	Yes(SG)	3.89	88.82	7.91	RE
RAB14	Yes	2.34	122.36	6.12	EE, TGN
RAB2A	No	1.8	48.85	2.26	ER/GA
RAB10	No	1.39	69.34	2.32	TGN, G4V
RAB6A	Yes	1.08	21.68	1.64	GA
RAB8A;RAB8B	No	0.38	35.89	2.01	RE, G4V
RAB1B;RAB1C	Yes (SG)	0.31	6.68	1.45	GA/Exosome/Mitochondria
RAB12	No	0.13	122.19	4.47	RE/LY
RAB27B	No	0.12	37.35	1.63	EX
RAB13	No	0.1	31.83	1.74	EE
RAB35	No	0.07	13.42	1.66	PM/ CCV/ EE
Rab3D	No	0.03	52.13	1.55	EX

3.3.4 Nutrient transporters

Nutrient transport across the inclusion membrane is still widely enigmatic (chapter 1.2.3, p. 6). Although we did expect to find a number of solute transporters to be recruited to the inclusion membrane, after stringent filtering, only three members of the solute carrier (SLC) group of solute transporters were reliably identified, while no member of the ABC transporter family was identified. Two proteins, namely the heavy chain of the cell surface antigen 4F2 (SLC3A2) and the Large neutral amino acids transporter 1 (LAT1 aka. SLC7A5), one of the possible light chains in complex with 4F2, were found to be enriched at the inclusion. 4F2 is involved in the transport of large neutral amino acids such as phenylalanine, tyrosine, leucine, arginine and tryptophan across the PM but is only active as transporter when associated with a light chain, which can be one of several different SLCs (Kanai, Segawa *et al.* 1998, Mastroberardino, Spindler *et al.* 1998). The 4F2/LAT1 heterodimer is therefore a possible transporter of neutral amino acids across the inclusion membrane. The third identified SLC family protein is Monocarboxylate transporter 4 (SLC16A3) which normally transports e.g. pyruvate and lactate across the PM. Taken together, a surprisingly low number of host cell solute transporters were identified in our proteome.

3.4 Importance of retrograde transport for *Chlamydia trachomatis*

In the global analysis of the inclusion proteome (see chapter 3.3), we found that proteins involved in protein localization are highly enriched. Analysis of these proteins further revealed retrograde trafficking and specifically the retromer complex to be one of four major clusters of proteins that contribute to this function (Figure 3.16 and Figure 3.17).

3.4.1 The retromer complex is recruited to the inclusion of *C. trachomatis*

The retromer is a pentameric complex composed of two functional subcomplexes. One subcomplex is the cargo recognition complex, consisting of the proteins Vps26, Vps29 and Vps35 while the second subcomplex is composed of two sorting nexins (SNX) which is responsible for membrane binding (Attar and Cullen 2010) (see also chapter 1.4.3., p. 15)

When ranking by the enrichment score for inclusion associated proteins, all SNX-BAR retromer-associated SNX proteins (SNX1, SNX2, SNX5 and SNX6) are highly enriched in the inclusion fraction (Figure 3.18), while the non-canonical SNX4 was less enriched. Two components of the VPS subcomplex (VPS29 and VPS35) were also found in the proteome but considerably less enriched. The two human homologs of VPS26, VPS26A and VPS26B were each only found in two of three experiments and therefore filtered from the list.

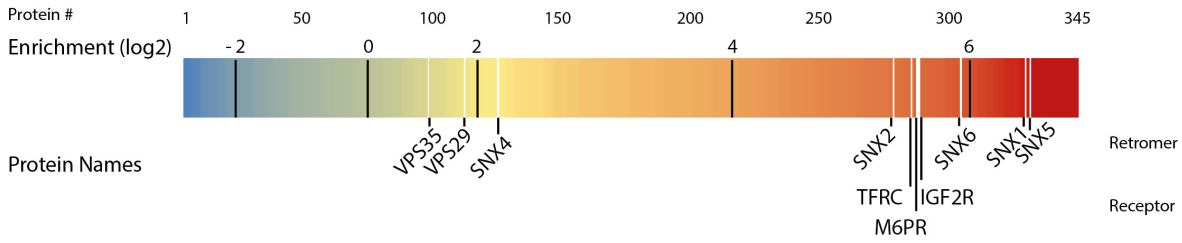

Figure 3.18: Enrichment of components of the retromer complex and retrograde trafficking at the inclusion.
The enrichment of inclusion associated proteins compared to total cell lysate was calculated using iBAQ. Each protein is represented by a line colored according to its enrichment score. Black lines indicate the ranges of log2 transformed fold enrichment. Proteins of interest of are represented as white lines. Proteins of the SNX-BAR subcomplex are among the 80 most highly enriched proteins.

The retromer cargo, receptors that are retrieved from endosomes to the TGN, are involved in several physiological processes of which CI-M6PR and M6PR are the most well studied. M6PR and CI-M6PR recognize newly synthesized mannose 6-phosphate tagged lysosomal enzymes at the TGN which it shuttles to the endosomal pathway from where it is retrogradely transported back to the TGN (Ghosh, Dahms *et al.* 2003). Indeed, the two cargoes we found in the inclusion proteome were the CI-M6PR (aka IGF2R) and M6PR. They were highly enriched (Figure 3.18), although both carry the quantitative flag in the lysate proteome and therefore the enrichment score is likely inaccurate (Appendix, Table 6.1, p. 144). Transferrin receptor (TFRC) is recycled by a non-canonical retromer complex composed of SNX3 and VPS35 (Chen, Garcia-Santos *et al.* 2013) and is also highly enriched in our proteome, SNX3, however, was not found.

To confirm our proteomics data on the recruitment of the retromer complex, we immunostained infected cells with antibodies that recognize SNX1, SNX2, CI-M6PR and VPS35 (Figure 3.19) and analyzed them by LSCM. The stainings showed a clear redistribution of SNX1 and SNX2 to the inclusion membrane with almost no protein remaining at the endosomal localization observed in non-infected cells. The signal colocalized strongly with IncA and had a pronounced rim-like staining. Furthermore, the intensity of the fluorescence signal was clearly stronger in infected cells than in their non-infected counterparts, this effect was more pronounced for SNX2 than for SNX1. CI-M6PR on the other hand showed no rim-like staining of the inclusion membrane and very little staining of the inclusion lumen. Sometimes vesicles in the luminal space of the inclusion were visible. VPS35 also localized to vesicular cytoplasmic structures and more often than CI-M6PR stained vesicles within the inclusion lumen. We furthermore observed SNX-positive tubular structure emanating from the inclusion, which were often directed towards the nucleus and interconnected separate inclusions in the same cells (Figure 3.20).

We therefore conclude that the SNX-BAR subunit of the retromer complex is strongly recruited to the inclusion; its localization, however, is independent of its cargo as well as the cargo recognition subcomplex.

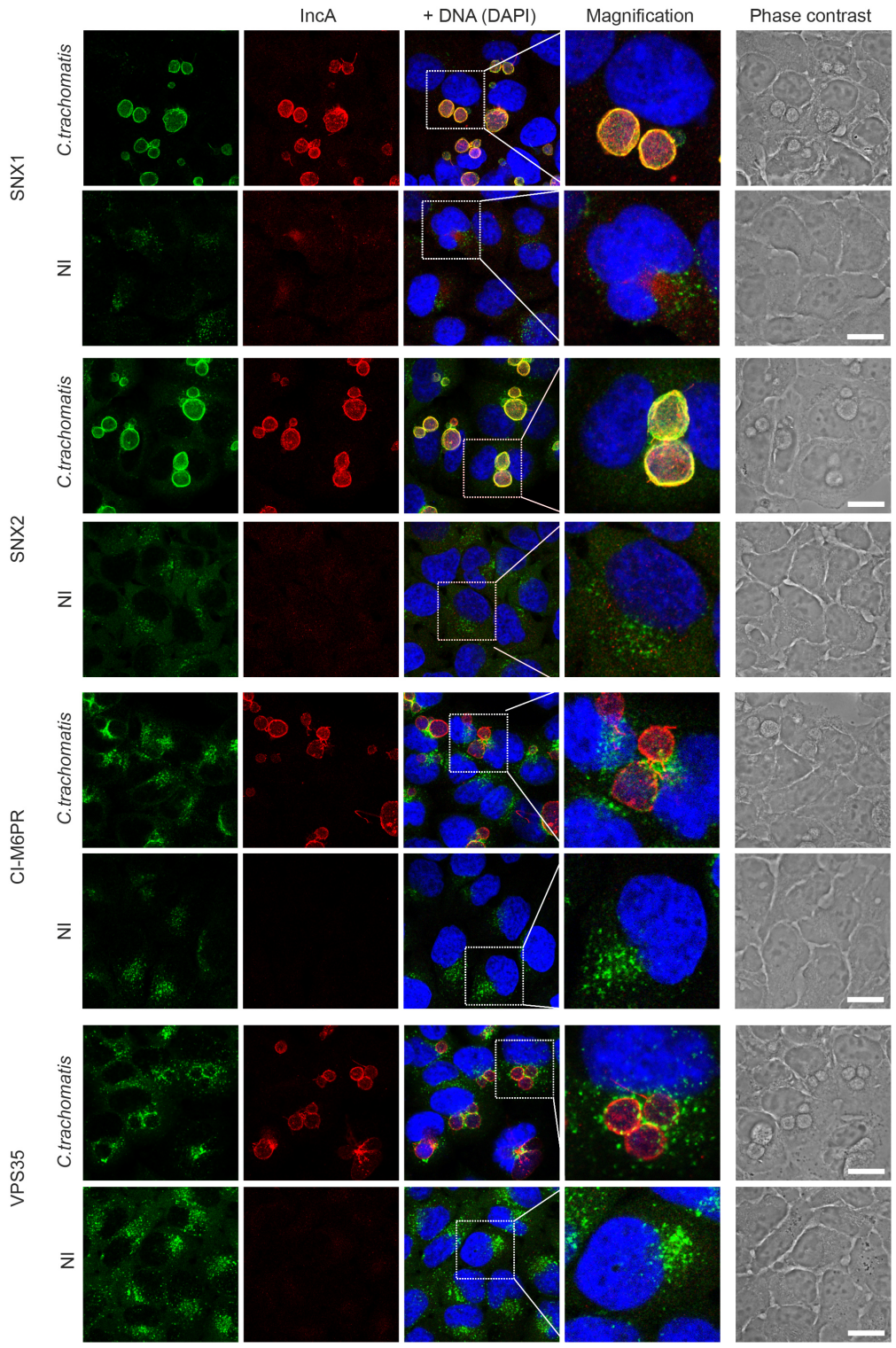

Figure 3.19: Recruitment of SNX-BAR retromer components and cargo to the inclusion
Confocal IF images of Hela cells. Cells were infected for 24 h with *C. trachomatis* L2 at an MOI of 5 or not infected (NI) as indicated. Cells were stained with specific antibodies after fixation with 2 % PFA. Scale bar = 20 µm. *The experiment was performed by Dr. Sebastian Banhart, RKI Berlin.*

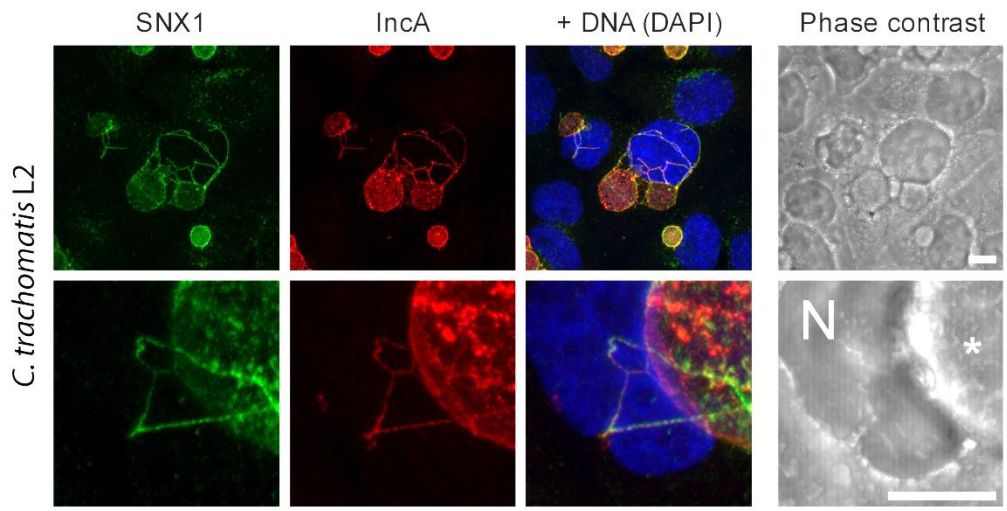

Figure 3.20: SNX1 positive fibres extend from the inclusion
Confocal IF images of Hela cells. Cells were infected for 24 h with *C. trachomatis* L2 at MOI = 2. Cells were stained with specific antibodies after fixation with 2 % PFA. Scale bar = 10 µm. Displayed is a maximum intensity projection of a z-stack comprised of 13 slices of 3.83 µm total z distance (upper panels) or 15 slices, 4.47 µm total z distance (lower panels). The lower panels show higher magnification of a different area than the upper panels. N= nucleus, asterisk indicates inclusion. *The experiment was performed by Dr. Sebastian Banhart, RKI Berlin*.

3.4.2 Effect of SNX-BAR depletion on bacterial progeny formation

To determine if the retromer complex is directly involved in the development of the inclusion, we tested the influence of protein knockdowns with all SNX-BAR proteins on the bacterial infection (Figure 3.21 A). The knockdown efficiency was verified by western blot (Figure 3.21 B). The assay was performed with three different MOI (0.25, 0.5 and 2) and showed the same effect in all three experiments. The knockdown of SNX1, SNX2 and SNX6 had only minimal influence on the infection, while the knockdown of SNX5 slightly increased bacterial progeny formation. The knockdown of SNX5 and SNX6 also reduced the steady state levels of SNX1 and SNX2 as determined by western blot (Figure 3.21 B), an effect that was previously reported for SNX5/SNX6 knockdowns on SNX1 levels (Wassmer, Attar *et al.* 2007).

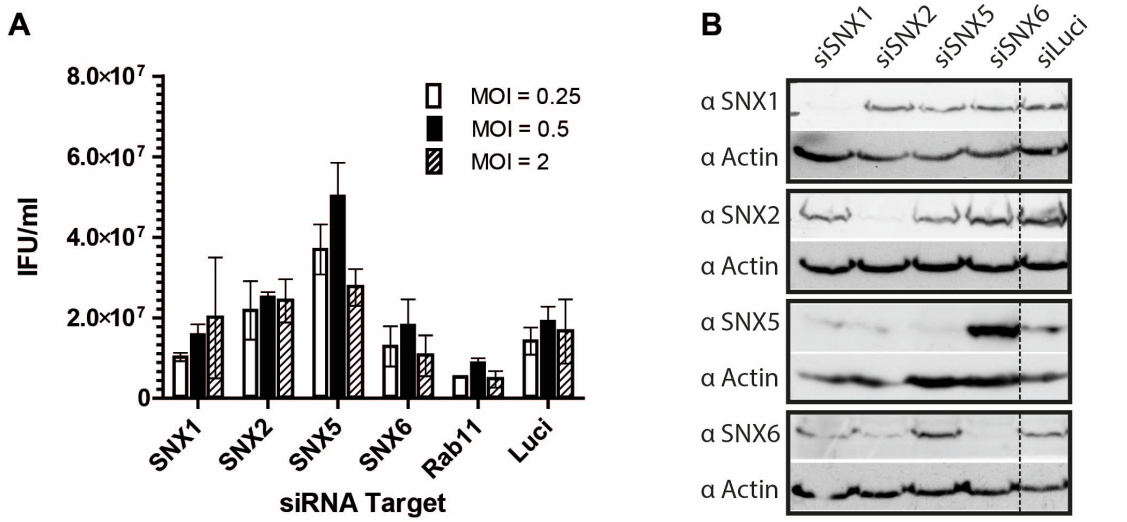

Figure 3.21: Knockdown of SNX-BAR compontents does not ablate bacterial progeny formation
A) Progeny formation was assessed in cells that were siRNA treated to deplete the indicated target proteins. HeLa cells were transfected with siRNAs for 72 h before infection and infected for 48 h before harvest. IFU were determined by titration on fresh HeLa cells. As non-targeting control we used siLuci, siRab11A was used as positive control. Shown are mean values of three biological replicates, error bars indicate standard deviation. For the experiments performed at MOI = 2, individual experiments were done using two (SNX1, SNX6) or three (SNX2, SNX5) individual siRNAs and averaged, for all other experiments the two respectively three targeting siRNAs were pooled. **B)** Knockdowns were verified by western blot after 72 h of induction using specific antibodies against the targeted proteins. Representative blots are shown. Actin protein levels were monitored as loading control.

3.4.3 Determinants of SNX-BAR recruitment to the inclusion

Despite the lack of severe effects on bacterial progeny formation after knockdown of SNX-BAR proteins, we were interested in the mechanisms by which these proteins are recruited to the inclusion.

Cells expressing full length eGFP fusion constructs of SNX2 and SNX5 were analyzed by LSCM and showed a clear rim like staining of the inclusion membrane after 24 h of infection (Figure 3.23), similar to what we observed in IF studies of fixed cells (Figure 3.19). This confirmed the association of SNX5 with the inclusion and additionally showed that the eGFP fusion does not interfere with inclusion recruitment of SNX proteins. Cells expressing eGFP fusion constructs at high levels showed aggregation of fusion proteins and increased cytosolic fluorescence (data not shown).

The recruitment of SNX proteins to the endosomal membrane is primarily mediated by binding to endosome localized PtdIns species; the specificity of binding differs for each SNX protein (see 1.4.3.1, p. 17). The PtdIns binding is mediated by their PX domain. To determine if the PX domain of the SNX-BAR proteins is sufficient to mediate recruitment to the inclusion membrane, we constructed an eGFP-fusion protein carrying the PX domain of SNX5. In cells expressing the the eGFP-PX(SNX5) fusion protein we observed clear recruitment to the inclusion membrane in cells expressing the protein at a medium level (Figure 3.23, 2) while cells expressing the protein at

higher levels showed strong cytosolic and nuclear staining (Figure 3.23, 3). Co-staining with SNX1 indicated that the binding of PX(SNX5) and SNX1 is competitive, as cells expressing the PX fusion protein had severely reduced SNX1 recruitment compared to cells not expressing the protein (Figure 3.23, 1 vs. 2 and 3). Similar results were also obtained for the combination of SNX2 and PX(SNX5) as well as full length constructs of SNX2 and SNX5 (data not shown).

These data clearly indicate that the PX domain is sufficient for recruitment to the inclusion membrane and recruitment of SNX1/2 and SNX5 proteins likely occurs via the same binding site.

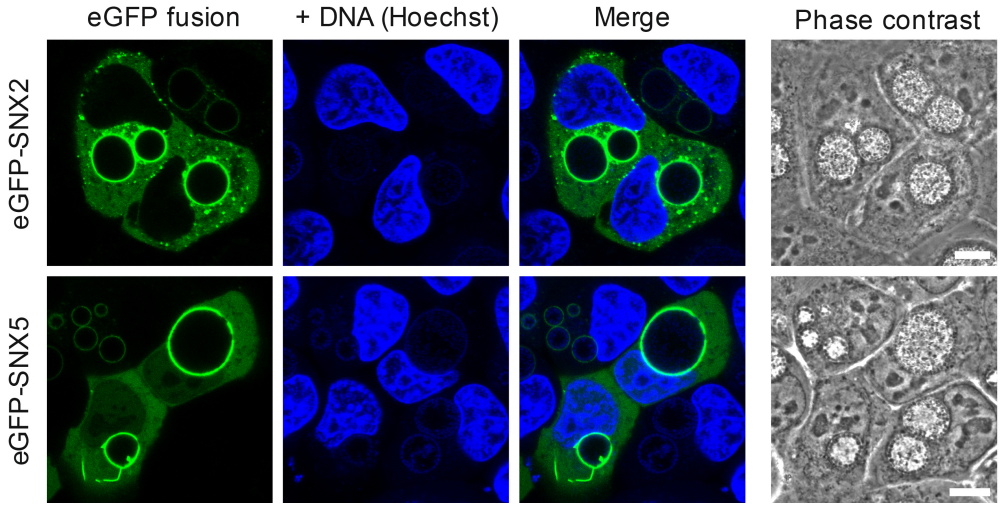

Figure 3.22: eGFP fusion proteins of SNX2 and SNX5 are recruited to the inclusion
Localization of eGFP-SNX fusion proteins in in infected HeLa cells. Indicated SNX-eGFP fusion proteins were expressed in HeLa cells and infected with *C. trachomatis* L2 at an MOI of 2. At 24 h p.i. DNA was stained using Hoechst 33342 and samples were analyzed under live conditions using a LSCM. Under these conditions, DNA staining of bacteria inside the inclusion is very weak. Inclusions are visualized in the phase contrast. Scale bar = 10 µm. *Experiment was performed by Dr. Sebastian Banhart, RKI Berlin.*

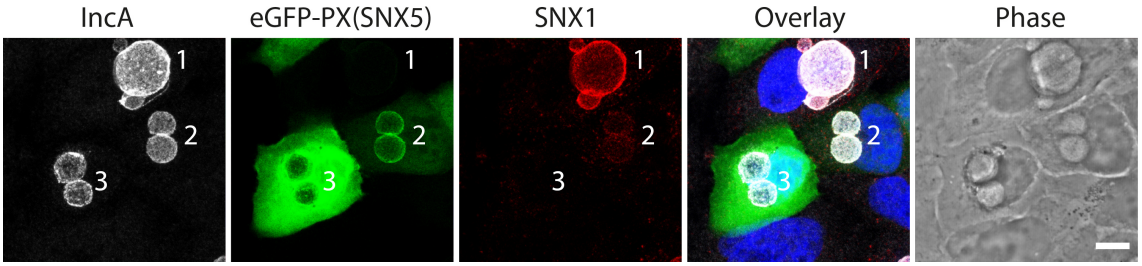

Figure 3.23: The PX domain of SNX5 is sufficient to mediate inclusion recruitment
Confocal images of HeLa cells transiently expressing eGFP-PX(SNX5). Cells were infected for 24 h with *C. trachomatis* L2 at an MOI of 2. Cells were stained with the indicated specific antibodies and DAPI (blue) after fixation with 2 % PFA. Numbers indicate cells expressing the eGFP fusion construct at different levels. 1: no expression, 2: medium expression, 3: high expression. Scale bar = 10 µm. The panel showing the fusion protein only has increased brightness levels compared to the overlay to improve visibility. *Experiment was performed by Dr. Sebastian Banhart, RKI Berlin.*

3.4.4 The retrograde trafficking inhibitor Retro-2 inhibits bacterial growth

As the knockdown of retromer proteins did not have a strong effect on bacterial progeny formation, we considered alternative approaches to probe the dependence of *C. trachomatis* on retrograde transport.

To date, no specific inhibitor of the retromer complex exists. Retro-2 a compound that inhibits retrograde trafficking of bacterial toxins from the endosomes to the TGN was described recently (Stechmann, Bai *et al.* 2010). Retro-2 cyclizes to its biologically active form Retro-2^{cycl} in aqueous and organic solvents and the term Retro-2 will refer to Retro-2^{cycl} throughout this thesis if not specified (Park, Kahn *et al.* 2012, Nelson, Carney *et al.* 2013).

To test if the intracellular development of *C. trachomatis* depends on a Retro-2 inhibited retrograde pathway, we performed a reinfection assay in which we compared the formation of infectious progeny at 48 h *p.i.* in cells incubated with 20 µM Retro-2 and mock treated (Figure 3.24 A). The treatment was started at 8 h *p.i.*, a time point at which essentially all nascent inclusions have relocalized to the perinuclear region (Clausen, Christiansen *et al.* 1997) and the EB has transformed into an RB (Belland, Zhong *et al.* 2003). We observed a very strong reduction of IFU by more than one order of magnitude in Retro-2 treated cells, indicating that the compound targets mechanisms necessary for chlamydial development .

To more accurately define the time frame in which Retro-2 interferes with the intracellular development of *C. trachomatis*, we performed a time course analysis of the progression of the infection upon inhibitor treatment (Figure 3.24 B). In non-treated cells, the formation of infectious progeny peaks around 48 h *p.i.,* at the completion of the infectious cycle, whereas for Retro-2 treatment the peak of infectious progeny formation is reached between 24 h *p.i.* and 36 h *p.i.* To exclude a direct toxic effect of Retro-2 on the bacteria, we treated EB stocks with high concentrations (200 µM) of Retro-2 before infecting cells, which did not lead to reduced progeny formation in comparison to DMSO treated control cells (Figure 3.24 C).

To determine if the treatment with Retro-2 directly influences the developmental cycle of the bacteria, we analyzed cells infected with *C. trachomatis* L2 at 48 h *p.i.* with and without treatment with Retro-2 on the ultrastructral level using TEM (Figure 3.25). We did not observe a dramatic shift of the bacterial morphology away from infectious EBs that could explain the strong growth inhibition observed, yet the abundance of intermediate bodies was significantly higher in Retro-2 treated cells.

These results indicate that the infection of *C. trachomatis* L2 depends on a retrograde trafficking route inhibited by Retro-2 but the EB to RB transition is not strongly affected by the inhibitory effect of the compound.

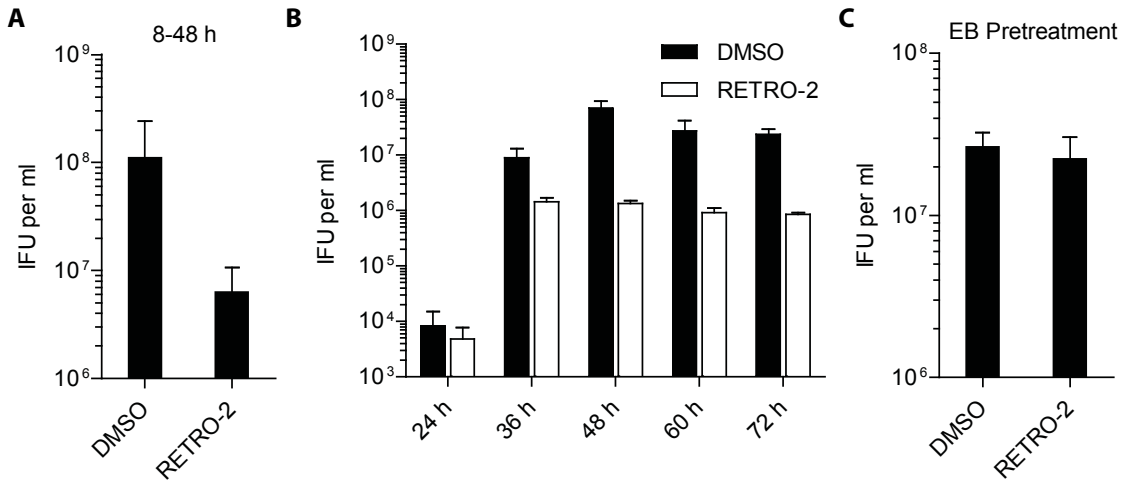

Figure 3.24: Retro-2 treatment inhibits chlamydial growth
Reinfection assay assessing the effect of Retro-2 on infectious progeny formation. HeLa cells were infected with *C. trachomatis* L2 at MOI = 2. At 8 h *p.i.*, cells were either treated with 20 µM Retro-2 or DMSO as solvent control. Cells were harvested **A)** at 48 h *p.i.* in three independent replicates or **B)** at different time points after infection in two independent replicates. **C)** *C. trachomatis* L2 elementary bodies (EBs) were treated with 200 µM Retro-2 or DMSO as solvent control for 30 minutes at room temperature before pelleting, followed by washing with infection medium and infection of HeLa cells at MOI = 2 for 48 h. This assay was performed in four independent replicates. A, B and C) IFU was titrated on fresh HeLa monolayers after mechanical lysis with glass beads. The number of inclusion forming units (IFU) per ml was determined after immunostaining for Hsp60. Error bars indicate standard deviation.

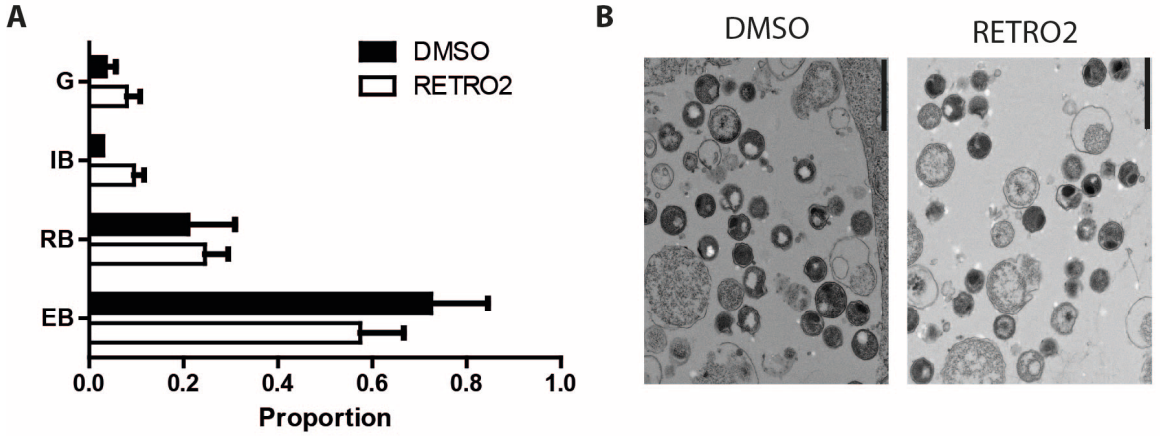

Figure 3.25: **Retro-2 treatment does not significantly affect the distribution of morphologies of bacteria**
Hela cells were infected for 48 h with C. trachomatis L2 at an MOI of 2. The cells were treated with 20 µM Retro-2 at 8 h p.i. or mock treated with DMSO. Cells pelleted and fixed with glutaraldehyde before processing for TEM. **A)** Randomized images were taken from slices and the images were analyzed by eye for the distribution of different morphologies of *C. trachomatis*. G = Ghost, IB = intermediate body, RB = reticulate body, EB = elementary body. Experiment was performed in biological duplicates; bars indicate standard deviation **B)** Representative TEM images. Scale bar = 1 µm. *Electron microscopy was performed in the group of Dr. M. Laue, RKI, Berlin.*

Having established the importance of retrograde trafficking for the infection of *C. trachomatis* L2 we were interested if the retrograde trafficking route inhibited by Retro-2 is due to a direct effect on the SNX-BAR retromer. Retro-2 treatment has been shown to relocalize the SNARE proteins Syntaxin 5 and Syntaxin 6 in non-infected cells by an unknown mechanism from perinuclear Golgi membranes (Stechmann, Bai *et al.* 2010). We therefore reasoned that the intracellular localization of additional proteins could be altered due to treatment with Retro-2.

We focused on the SNX-BAR retromer proteins after Retro-2 treatment. Immunostaining of infected cells showed that treatment with Retro-2 does not influence the intracellular localization to the inclusion (Figure 3.26), in line with previous reports for VPS26, SNX1 and SNX2 in non-infected cells (Stechmann, Bai *et al.* 2010).

Taken together we show that Retro-2 strongly inhibits bacterial growth, possibly via a mechanism which influences retrograde trafficking events downstream of SNX-BAR recruitment.

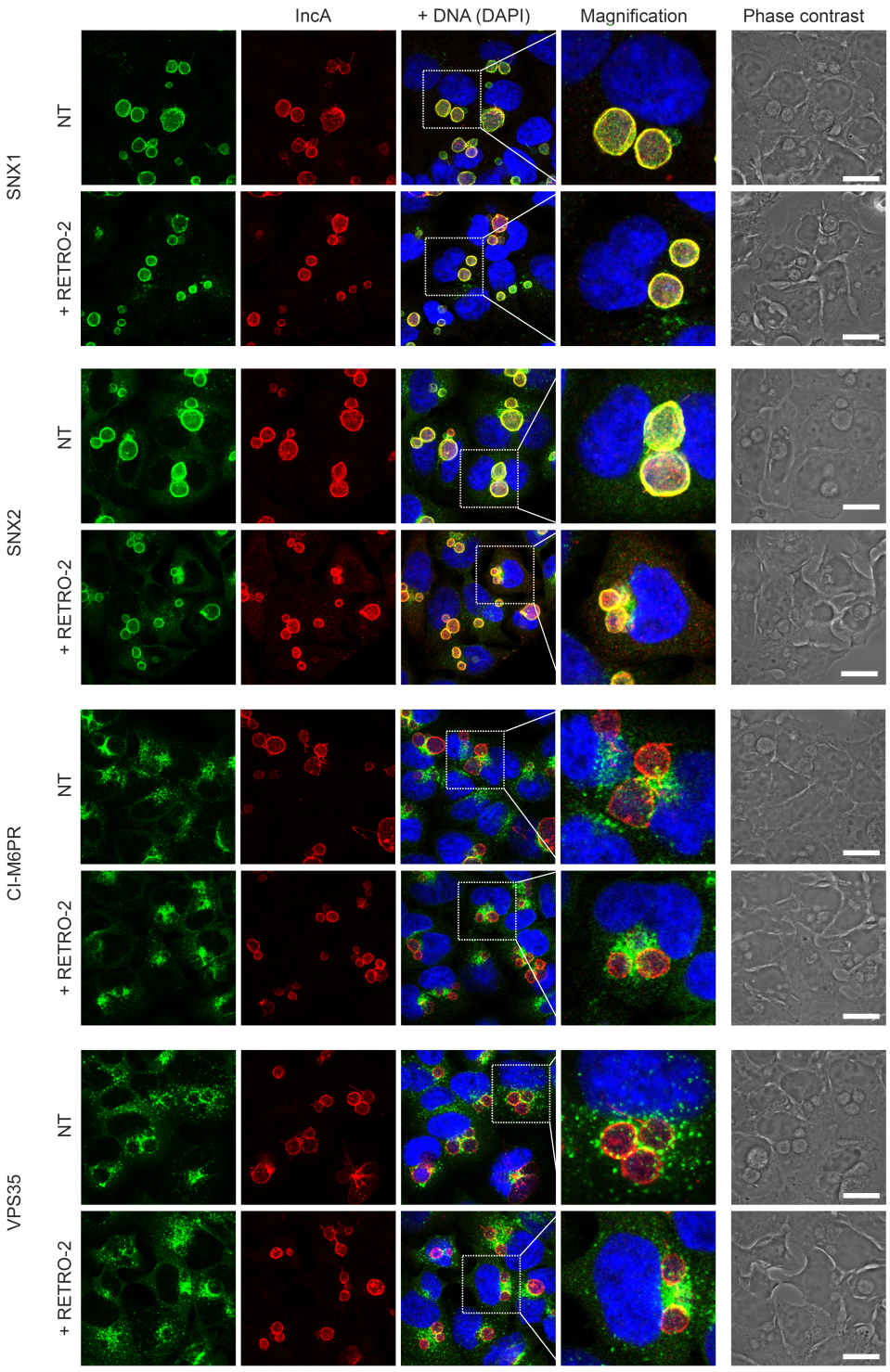

Figure 3.26: Retro-2 treatment does not alter the intracellular distribution of SNX-retromer associated proteins
Confocal images of Hela cells. Cells were infected for 24 h with *C. trachomatis* L2 at an MOI of 2. Infected cells were either not treated (NT) or treated with 20 µM Retro-2 from 8 h *p.i.* as indicated. Cells were stained with specific antibodies after fixation with 2 % PFA. Scale bar = 20 µm. *Experiment was performed by Dr. Sebastian Banhart, RKI Berlin*.

4. Discussion

After uptake, the inclusion of *Chlamydia* is the niche in which these obligate intracellular bacteria thrive and its membrane is the main host-pathogen interface for the duration of the infection. Understanding the interactions of the host cell and the pathogen in molecular detail is a powerful strategy towards the development of novel therapeutic agents beyond the reach of conventional antibiotics. The host derived proteome composition of the inclusion of *C. trachomatis* is therefore of central interest for the community involved in research of this infectious agent and an important milestone for the systematic analysis of chlamydial infections on a molecular level.

Here we described for the first time the isolation and biochemical characterization of the mid-infection inclusion of *C. trachomatis* L2. At this stage, the bacteria grow exponentially, while the inclusion expands considerably. This growth relies on the successful delivery nutrients and membranes to the inclusion, making this a central time point in the development of *Chlamydia.* However*,* the underlying mechanisms are poorly understood. To improve our knowledge of the nature of the inclusion, we analyzed the host derived proteome of the fully established intracellular niche. The data confirmed a significant proportion of previously reported inclusion associated proteins and its global analysis revealed the quantitative contribution of intracellular organelles to the composition of the inclusion. This indicated the presence of a significant amount of ER derived proteins and in general a heterogeneous proteome composition, suggesting it to be it a patchwork of organelles of the endomembrane system. We identified proteins involved in retrograde trafficking to be highly enriched at the inclusion by global analysis of our data. In subsequent experimental validations we found the SNX-BAR retromer complex to be strongly recruited to the inclusion, despite the absence of markers that are involved in SNX-BAR recruitment in non-infected cells such as PtdIns(3)P and Rab7A. In additional experiments, we found a strong inhibition of bacterial progeny formation by the inhibitor Retro-2, a compound that interferes with retrograde trafficking of exogenous toxins.

Taken together, we identified and quantified a large number of previously not identified inclusion associated proteins and thereby significantly increased our knowledge of the interactions of *C. trachomatis* with the host cell and the nature of the inclusion.

4.1 Inclusion isolation

In the first part of this thesis, we established a novel procedure that allows the isolation of intact *C. trachomatis* L2 inclusions at mid-infection stages. The protocol was loosely based on a previously published method for the isolation of the LCV (*Legionella* containing vacuole) from infected *D. discoideum* (Urwyler, Nyfeler *et al.* 2009). Due to the extremely fragile nature of the chlamydial inclusion, the method was heavily modified.

The first goal was to find a method to release visually intact inclusions from infected cell culture in sufficient quantity for the subsequent purification steps. We initially showed that inclusions containing *C. trachomatis* L2 can be released into solution using optimal lysis conditions at several different time points after infection (Figure 3.2). The majority of inclusions were ruptured during the lysis procedure with only about 15 % of the theoretical amount of total inclusions going into solution despite efforts to increase the total yield (data not shown). The inclusion has been described to be surrounded by a cytoskeletal framework composed of actin fibers and intermediate filaments (Kumar and Valdivia 2008) which are thought to stabilize the organelle during growth. A more recent report showed that actin recruitment during *C. trachomatis* infection is not universal and only observed in a subpopulation of cells (Chin, Kirker *et al.* 2012). The actin scaffold could therefore be a major contributor to the more stable subpopulation that can be retrieved from infected cells into solution in addition so a bias towards smaller inclusions which are intrinsically more stable. Supporting the first hypothesis, we did find F-actin to be present in the inclusion fractions in our proteome analysis and additionally found several proteins that are known to interact with actin, either as capping factors or at branching nodes. However, actin is known to be highly abundant both in cells and as an environmental contamination in proteomics, therefore its presence in the inclusion fraction may be of limited significance.

The second challenge was to find an optimal strategy for initial purification of the visually intact inclusions from cellular debris. To this end, we developed a method to separate the inclusions from cellular debris at 24 h *p.i.* by density gradient centrifugation. Apparently the buoyant density of inclusions is very diverse, distributed across the range of densities of intracellular organelles. Although we did recover the majority of inclusions in solution by fractionation of the gradient (Figure 3.3 B), a subpopulation escaped our analysis which was distributed over the whole gradient without apparent peaks. We can only speculate about the nature of this subpopulation. It seems likely these are inclusions that either contain large amounts of glycogen (Chiappino, Dawson *et al.* 1995) or lipid droplets which are known to be translocated into the lumen of inclusions (Cocchiaro, Kumar *et al.* 2008) which could have a considerable effect on their overall density. This speculation is also supported by the absence of markers for the two compartments in our proteome analysis and by a slightly different morphology of these inclusions as observed in

our experiments. The yield of the gradient purification at over 60 % was high and reproducible, but further enrichment by differential centrifugation ("washing") proved to be extremely inefficient as inclusions were easily ruptured upon resuspending (Figure 3.4), due to their intrinsic fragility towards mechanical forces.

In quality control experiments by TEM, we found that inclusions were surrounded by a single membrane and an additional experiment using LSCM confirmed this membrane to contain the secreted bacterial membrane protein IncA (Figure 3.5). These experiments showed that we can recover inclusions that are surrounded by a single membrane, the IncA decorated inclusion membrane. This is important, as the *Chlamydia* use two different exit strategies for release from the host cell, one of them being the extrusion of intact inclusion (Hybiske and Stephens 2007) where extruded inclusions are surrounded by an additional membrane derived from the PM that is pinched off from the cell upon extrusion. The recovered inclusions are therefore not an artefact of preliminary extrusion, which has been shown to be chemically inducible also at time points significantly before the end of the developmental cycle (Hybiske and Stephens 2007) and would have led to a significant amount of false positives in the proteome analysis due to the additional membrane derived from the PM.

The retention of Rab11A-eGFP on gradient purified inclusions showed that recruited proteins are retained during the inclusion purification procedure (Figure 3.6). Although it is not clear how Rab11A is recruited in infections with *C. trachomatis*, an Inc protein has been reported in *C. pneumoniae* (Cortes, Rzomp *et al.* 2007) that directly interacts with RabGTPases, with the strongest interaction being with Rab11. In addition to this direct binding, RabGTPases are generally retained at membranes by their C-terminal prenyl anchor (Pfeffer and Aivazian 2004). It is therefore not clear whether proteins that are only loosely attached to the inclusion membrane are retained during the procedure. Examples include binding indirectly to an Inc-recruited protein, proteins that dynamically associate and dissociate from the membrane, or depend on co-factors for binding that are not present in the lysis buffer. However, the proteome analysis confirmed that a large number of host proteins are retained in sufficient amount for proteome analysis.

In the last part of the establishment of the purification procedure, we improved the purity of the preparation considerably by an additional antibody based affinity purification step using MACS (Figure 3.8) and our newly made antibody against the cytosolic portion of IncA (Figure 3.1). Analysis by western blot clearly showed a derichment of all major cellular organelles and an enrichment of the inclusion membrane localized effector IncA (Figure 3.9), thereby underlining the successful purification observed by phase contrast microscopy (Figure 3.8 A). MACS purification proved to be highly specific as seen in the western blot, but additionally had very high yield, as over 80 % of visually intact inclusions were retained (Figure 3.8 B).

Taken together this protocol allows the specific straightforward isolation of inclusions from *C. trachomatis* L2 from infected HeLa cells in cell culture. The total time from harvest of cells to the collection of purified inclusions is around 6 hours and therefore rapid. The yield allows for the use of moderate amounts of cells (6×10^7 cells for standard isolations). Parallel processing of several samples by one experimenter is possible and the number of samples is primarily limited by the initial lysis step, a bottleneck that can be overcome by the use of an additional homogenizer. All steps were designed to allow comparative analyses of inclusions isolated from cells which were for example treated with siRNAs or inhibitors. To this end we tried to reduce the overall influence of handling on the yield and quality of the isolation. This intention in combination with the inability to repeatedly concentrate the inclusions by pelleting due to their fragility, led us to adopt a gradient purification technique in which we use an in situ generated gradient as opposed to a layered or preformed gradient. This drastically reduces the error introduced by the collection of interlayer fractions in layered gradients. The downside of this approach is the extended incubation time of the inclusions in cell lysate which potentially influences the protein composition of the inclusion by selective cleavage of proteins by proteases, or the association of unspecific proteins with the inclusion. To limit degradation and deterioration of the isolated proteins and other components of the inclusions, protease inhibitors were used upon lysis and all steps of the protocol were performed at 4 °C or on ice. To control for unspecific protein binding, and to control for remaining co-purifying cellular debris, we adopted a SILAC based method for the proteome measurement (see Figure 3.10, p. 64 and section 4.2.2, p. 99).

4.2 Proteome analysis of mid-infection inclusions

Using the newly established protocol for the isolation of mid-infection inclusions of *C. trachomatis* L2, we were able to analyze for the first time the proteome of this unique intracellular compartment. With a combination of label free absolute quantification and SILAC-based relative quantification, we used a novel strategy to distinguish specific components of the bacterial compartment from co-purifying nonspecific proteins which yielded a high confidence set of inclusion associated proteins. Furthermore, we obtained an almost complete coverage of the predicted bacterial proteome with semi-quantitative information for the majority of identified proteins, including many Inc proteins.

4.2.1 Bacterial proteome

As a first analysis, we looked at the coverage of the bacterial proteome in our dataset. Due to the size of the chlamydial inclusion at 24 h *p.i.* and the quantity of bacteria contained therein, the majority of proteins, based on cumulative intensity, were of bacterial origin. Presumably due to this high abundance, we achieved a very high coverage of the bacterial proteome of 68 % of predicted proteins with stringent filtering (2 unique peptides in all three experiments) and up to 80 % with only one unique peptide per experiment of the total of 884 predicted proteins.

In a recent study, the proteome of purified EBs and RBs was absolutely quantified (Saka, Thompson *et al.* 2011). 66 proteins were identified by Saka *et al*. which we did not find (43 when filtering was less stringent), of which all were only found in the EB fraction. 133 proteins were not found in either study (15 % of all predicted proteins), while 265 proteins were found in our study but not in theirs. An additional five proteins were identified in a study by Skipp *et al.*, which was performed on isolated EBs and RBs of *C. trachomatis* D in which a total of 322 proteins were identified (Skipp, Robinson *et al.* 2005). Our dataset is therefore the most comprehensive proteome of *C. trachomatis* to date. Additionally, as the chlamydial developmental cycle is composed of at least three to four main transcriptional classes (Shaw, Gevaert *et al.* 2002, Maurer, Mehlitz *et al.* 2007), it is likely that the remaining proteins are expressed only at a very low level or not at all at mid infection or are secreted into the host cell cytosol and therefore escape our analysis.

To compare our bacterial dataset to the published absolutely quantified dataset of Saka *et al.*, we used a method for quantification of the bacterial proteins based on total intensity per protein vs. summed intensity as reported by MaxQuant, which is based on extracted ion current (XIC) (Cox and Mann 2008). The correlation of the three replicates based on Pearson's R-squared correlation coefficient (R^2) was significantly better than when using the iBAQ method for quantification (R^2 =

0.90, 0.93, 0.79 for intensity, R^2 = 0.77, 0.82, 0.62 for iBAQ). Also, the intensity derived abundance correlated significantly better with the absolute quantification performed by Saka *et al.* despite lack of correction for stoichiometric abundance. As expected, the bacterial proteome of the inclusion more closely matches the composition of RBs (R^2 = 0.56) than EBs (R^2 = 0.27), see Figure 4.1. This is further supported by the finding that none of the proteins that were quantified by Saka *et al.* but we did not reliably identify (n = 35) were quantified in RBs while the remaining were only identified by a single peptide (n = 32). Unfortunately, the correlation of the two datasets was too low to directly compare abundances, which might be further complicated by the fact that our proteome was derived from infections at 24 h *p.i*. while the RB proteome was determined at 18 h *p.i.*

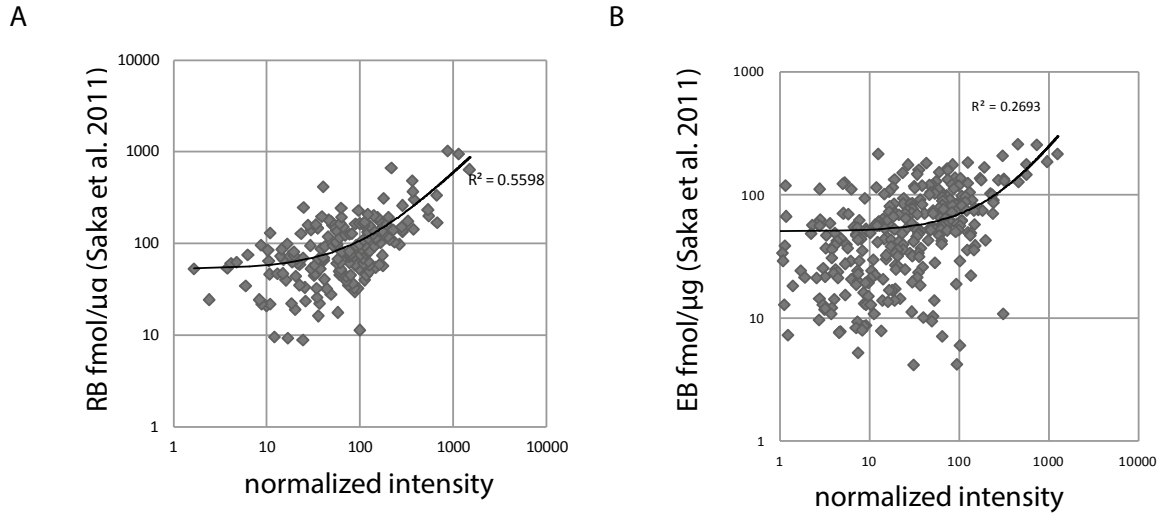

Figure 4.1: Correlation of the bacterial proteome of RBs and EBs and the inclusion

The overlap of the absolutely quantified bacterial proteome of RBs and EBs retrieved from Saka *et al*. 2011 and our inclusion proteome was normalized to the summed intensity of peptides for each protein**.** Overlap and correlation with **A)** RB proteome (n=181) and **B)** EB proteome (n = 303). The Pearson's R-squared correlation coefficient (R^2) for the linear values is indicated.

As in our approach, it was not possible to distinguish proteins that are localized to the inclusion membrane from proteins in the inclusion lumen or the bacteria, we only focused on the relative abundance of predicted Inc proteins which are listed in Table 3.1. We found a total of 32 of the 62 predicted Inc proteins which is, given the hydrophobic nature and low abundance of these membrane proteins (1.5 % of total intensity of bacterial proteins), a considerable amount. According to a microarray study, all predicted Inc proteins are expressed on RNA level from 16 h *p.i.* in *C. trachomatis* D (Belland, Zhong *et al.* 2003), suggesting lack of sufficient sensitivity in measurement as opposed to inexistence of the remaining Inc proteins to be the reason for their incomplete coverage. The abundance of Inc proteins will be further discussed in section 4.2.2.5, p. 106.

4.2.2 Host cell derived inclusion proteome

4.2.2.1 SILAC exclusion approach

The main goal of this thesis was to identify host cell proteins that are associated with the inclusion. The high sensitivity of modern LC-MS/MS based proteomics demands an experimental design which includes a strategy to distinguish between *bona fide* components of the isolated compartment as well as co-purified contaminations (Drissi, Dubois *et al.* 2013). To this end we used a SILAC-based exclusion approach to control for non-specific co-purifying host cell derived proteins during the inclusion purification procedure (Figure 3.10 and Figure 3.11). For SILAC, cell populations are differentially labeled by amino acids which are themselves labeled with the stable isotopes deuterium (^{2}H), ^{15}N and ^{13}C (Ong, Blagoev *et al.* 2002). This allows accurate relative quantification of proteins in shotgun proteomics experiments. Furthermore, we used a label free quantification approach to determine the enrichment of proteins in isolated inclusions compared to total cell lysate. A similar method was successfully used in a recent study by Campbell-Valois *et al*. to identify contaminants in latex bead purified phagosome preparations (Campbell-Valois, Trost *et al.* 2012).

SILAC labeling of cells mandates the use of dFCS (dialyzed FCS) to allow complete metabolic labeling of the cells in culture because nFCS (normal FCS) contains unspecified amounts of non–labeled amino acids. To test the influence of dFCS on the infection with *C. trachomatis* L2, we monitored an infection by phase contrast microscopy in presence of dFCS or nFCS and observed smaller inclusions than usual (data not shown). To minimize the influence of dFCS on the infection we decided to perform the infections in presence of nFCS in non -labeled cells and only mock infected cells in dFCS with heavy isotope label. The drawback of this strategy is that the measurements of the total lysate cannot be used to identify changes in protein abundance that occur upon infection as the observed effects are always a mixture of the influence of dFCS/ nFCS and the infection. Furthermore, this strategy precluded a so called label-swap which would have helped to rule out environmental contaminations and any influence of the isotope label by swapping the SILAC labeling state of infected and non-infected cells.

When applying the SILAC exclusion approach, we found 345 host proteins to be enriched in the inclusion fraction of which 253 were in the very high confidence range ($p < 0.01$) and an additional 92 which had slightly less confidence ($p < 0.04$) due to only two SILAC ratios for the proteins that were tested in the second set (Figure 3.11). This number seems low in comparison to published datasets of PVs. For example, in the isolation of the LCV from mouse macrophages, 1156 host proteins were reported (Hoffmann, Finsel *et al.* 2013). It must be taken into account that in the study by Hoffman *et al*., no control for contaminating proteins was performed and proteins that were found in only one of three experiments were reported as well. When reducing the list to

only those proteins found in all three replicates, 555 remain, of which 266 are annotated as mitochondrial. In the proteome of MCVs (*M. tuberculosis* vacuoles), depending on the publication, 321 (Rao, Singh *et al.* 2009) or approximately 800 host proteins were detected (Li, Singh *et al.* 2011) with the same caveat of not controlling for contaminating co-purifying protein and in the latter case only technical duplicate analyses and a comparably high false discovery rate (5 %) for peptide identifications. Therefore the number of proteins detected in other studies of bacterial phagosomes is in the same range of what we here report after the SILAC exclusion approach and stringent filtering.

In the proteome of latex bead purified phagosomes, where a similar SILAC approach was used, depending on the filtering approximately 1200 to 1700 proteins were detected in triplicates, of which almost all showed high SILAC ratios (Campbell-Valois, Trost *et al.* 2012). Phagosome preparations are, due to the inertness of latex beads and their very high uniformity, considered to be the purest organelle preparations (Ulsamer, Wright *et al.* 1971, Li, Jagannath *et al.* 2010). The detection of significantly more genuine vacuole proteins in these preparations is therefore not surprising. As opposed to bacterial PVs, neither are bacterial proteins present, which significantly obscure mass spectrometric detection of host cell derived proteins in our proteome. The cumulated intensity of bacterial proteins compared to proteins that pass the approximate SILAC cutoff is around tenfold higher in the inclusion fraction. Furthermore, the SILAC exclusion approach has limitations for example with proteins that have a high dissociation constant, which reduces the SILAC ratio due to exchange of L for H labeled proteins during the extended incubation time in cell lysate before MACS separation, thereby increasing the number of false negative detections. All these factors influence the number of reported proteins but apart from the latter mostly will be resolved with improved sensitivity in mass spectrometric detection.

Taken together, despite the difficulties of isolating this compartment in very high purity, our workflow delivers a high confidence set of proteins for further analysis with sufficient depth for global analyses.

4.2.2.2 Contaminants

The first analysis of the host cell derived proteome was geared towards identifying contaminating proteins in our dataset (Figure 3.11). Proteins from co-purifying organelles that stably associate with the inclusion before cell lysis cannot be directly excluded by the SILAC exclusion approach. To investigate this possibility, we analyzed the distribution of proteins from different organelles along the SILAC ratios (Figure 3.12). Proteins from co-purifying organelles associated before lysis would be expected to be represented by a single peak in the high L/H range. The appearance of a major peak around the SILAC ratio of 1:1 for all organelles apart from mitochondria and the ERGIC

confirmed the absence of such contaminations for most organelles Only 11 proteins were annotated as ERGIC proteins, which all had varying iBAQ enrichment scores, favoring independent recruitment over organellar contamination. Latter, however, cannot be excluded based on our data.

A significant contribution of mitochondrial proteins to the total host derived proteome was found, although the abundance of mitochondrial proteins in the total lysate was not affected (average SILAC ratio of all proteins in lysate = 1.12, of mitochondrial proteins = 1.11). The SILAC ratios in the inclusion fraction revealed that these mitochondrial proteins primarily originate from mock infected control cells with over twofold enrichment compared to infected cells (Figure 3.12), indicating significantly changed properties of the mitochondria. These properties could include changed shape, size or density due to the infection or the use of dFCS, which would lead to changed behavior in the purification protocol. Conversely, active binding of mitochondria from mock infected cells to inclusions could be contributing to the differences observed. In cells infected with *C. psittaci*, inclusions associate intimately with mitochondria which is not observed in infections with *C. trachomatis* (Matsumoto, Bessho *et al.* 1991). The mechanisms governing this association are currently unknown and an active modification of the mitochondria by *C. trachomatis* to reduce their association with the inclusion cannot be ruled out. Such effector mediated interaction with mitochondria has recently been described for the PV of *Toxoplasma gondii* (Pernas, Adomako-Ankomah *et al.* 2014), but further investigation of this matter was beyond the scope of this thesis.

Although we were able to distinguish true inclusion associated proteins from cellular debris and especially mitochondria by the SILAC exclusion approach, the amount of contaminating mitochondria contributed a significant part of the total host cell proteins. It is therefore possible that proteins which are normally associated with mitochondria but are also recruited to the inclusion, are masked by the presence of exceeding amounts of H labeled counterpart proteins and thereby excluded by the SILAC exclusion approach (false negative). Furthermore it might explain the comparably low SILAC ratios we observed for the majority of enriched proteins, when compared to a similar experiment performed with latex bead purified phagosome preparations (Campbell-Valois, Trost *et al.* 2012). Mitochondria are known to bind parts of the ER (as mitochondria associated membranes, MAM) (Fujimoto and Hayashi 2011) and thereby might skew the SILAC ratios of ER localized proteins considerably towards low enrichment. Technically, the indirect association of inclusions with mitochondria and other organelles that are possibly enmeshed in actin/myosin networks due to *rigor mortis* could be further reduced by the addition of ATP to the lysis buffer. In the case of latex bead purified phagosomes, this led to a significant reduction of copurifying ER and mitochondrial proteins (Gotthardt, Warnatz *et al.* 2002).

The absence of several marker proteins which have previously been investigated was confirmed. The latter include the lysosomal markers (average SILAC L/H ratios are indicated in brackets) LAMP1 (0.88) and LAMP2 (1.05), cathepsin D (1.04) (Heinzen, Scidmore *et al.* 1996), the endosomal and lysosomal markers Rab5A (1.02) and Rab7A (1.09) (Rzomp, Scholtes *et al.* 2003), all of which were not enriched in the inclusion fraction as judged by the SILAC exclusion approach. Conversely, we did find three subunits of vacuolar H^+-ATPase (vATPase) to be positively enriched, contradicting an earlier report of its absence (Heinzen, Scidmore *et al.* 1996). However, with the whole complex consisting of 13 subunits it is likely that these are co-purified minor contaminations e.g. as part of MVBs which are known to fuse with the inclusion in the course of an infection (Beatty 2006, Beatty 2008). Among the controversial proteins for which both presence and absence at the inclusion was reported are TFRC and CI-M6PR (Taraska, Ward *et al.* 1996, van Ooij, Apodaca *et al.* 1997). Of TFRC we found copious amounts (1.9 % of total protein), CI-M6PR (0.018 %), however, localized primarily in vesicular structures around the inclusion in our IF studies (Figure 3.19). This is therefore the first biochemical proof that these proteins are indeed closely associated with inclusions even in the absence of the host cell context.

4.2.2.3 Known inclusion associated proteins

Whereas originally the inclusion was thought to be an isolated compartment that acts as a niche devoid of host proteins (Fields and Hackstadt 2002), this picture has changed dramatically in recent years as indicated by the extensive interaction with cellular organelles outlined in the introduction. The list of proteins that directly or indirectly associate with the inclusion has grown rapidly. Associations with proteins at different time points of the infection, in addition to the different strains and serovars used, make it almost impossible to get a complete overview of the inclusion associated proteins identified to date. In Table 4.1 we tried to give an overview of the proteins that associate with the inclusion of *C. trachomatis* at mid-infection stages.

Table 4.1: Overview of proteins that associate with the inclusion of *C. trachomatis* at 24 h *p.i.*
Trivial names were used as reported in the cited manuscripts. The Uniprot identifier (ID) of the reviewed human potein is shown for each protein except for actin where the exact proteins were not defined. ISO indicates if a highly homologous variant was found.

Trivial Name	Uniprot ID	Found	Reference
14-3-3β	P31946	YES	(Scidmore and Hackstadt 2001)
ABCA1	O95477		(Cox, Naher *et al.* 2012)
ACBD6	Q9BR61		(Soupene, Rothschild *et al.* 2012)
ACSL3	O95573	YES	(Soupene, Rothschild *et al.* 2012)
Actin			(Kumar and Valdivia 2008)
ApoA1	P02647		(Cox, Naher *et al.* 2012)
Arf1	P84077	YES	(Moorhead, Jung *et al.* 2010)
BAD	Q92934		(Verbeke, Welter-Stahl *et al.* 2006)
BICD1	Q96G01		(Moorhead, Rzomp *et al.* 2007)
CERT	Q9Y5P4	YES	(Elwell, Jiang *et al.* 2011)
Calreticulin	P27797	YES	(Majeed, Krause *et al.* 1999)
CLA1	Q8WTV0		(Cox, Naher *et al.* 2012)

CD59	P13987	YES	(Hasegawa, Sogo *et al.* 2009)
CD63	P08962		(Beatty 2006, Beatty 2008)
COG3	Q96JB2		(Pokrovskaya, Szwedo *et al.* 2012)
COG8	Q96MW5		(Pokrovskaya, Szwedo *et al.* 2012)
Cytokeratin 18	P05783	YES	(Kumar and Valdivia 2008)
Derlin-1	Q9BUN8		(Dumoux, Clare *et al.* 2012)
DP-1 (REEP5)	Q00765	YES	(Dumoux, Clare *et al.* 2012)
Fyn	P06241		(Mital, Miller *et al.* 2010)
GBP1	P32455		(Elwell, Jiang *et al.* 2011)
GS15	Q9NYM9		(Pokrovskaya, Szwedo *et al.* 2012)
IP3-R	Q14643/Q14573	YES	(Majeed, Krause *et al.* 1999)
LPCAT1	Q8NF37	YES	(Soupene, Rothschild *et al.* 2012)
MAP1-LC3	Q9H492		(Al-Younes, Al-Zeer *et al.* 2011)
MYPT1	O14974	YES	(Lutter, Barger *et al.* 2013)
OCRL1	Q01968		(Moorhead, Jung *et al.* 2010)
PDI	P07237	YES	(Dumoux, Clare *et al.* 2012)
PI4KIIα	Q9BTU6		(Moorhead, Jung *et al.* 2010)
PKCδ	Q05655	YES	(Tse, Mason *et al.* 2005)
Rab1A	P62820	YES (ISO)	(Rzomp, Scholtes *et al.* 2003)
Rab11A	P62491	YES (ISO)	(Rzomp, Scholtes *et al.* 2003)
RAB11FIP2	Q7L804		(Leiva, Capmany *et al.* 2013)
Rab14	P61106	YES	(Capmany, Leiva *et al.* 2011)
Rab4A	P20338		(Rzomp, Scholtes *et al.* 2003)
Rab4B	P61018		(Rzomp, Scholtes *et al.* 2003)
Rab6A	P20340	YES	(Rzomp, Scholtes *et al.* 2003)
Rab6B	Q9NRW1	YES (ISO)	(Rzomp, Scholtes *et al.* 2003)
Raf1	P04049		(Gurumurthy, Maurer *et al.* 2010)
RTN4	Q9NQC3	YES	(Dumoux, Clare *et al.* 2012)
SMS1	Q86VZ5		(Elwell, Jiang *et al.* 2011)
SMS2	Q8NHU3		(Elwell, Jiang *et al.* 2011)
SMVT	Q9Y289		(Fisher, Fernandez et al.)
Syntaxin 6	O43752		(Moore, Mead *et al.* 2011)
SERCA2/ATPA2	P16615	YES	(Majeed, Krause *et al.* 1999)
Src	P12931		(Mital, Miller *et al.* 2010)
VAMP3	Q15836	YES	(Delevoye, Nilges *et al.* 2008)
VAMP4	O75379		(Delevoye, Nilges *et al.* 2008)
VAMP7	P51809		(Delevoye, Nilges *et al.* 2008)
VAMP8	Q9BV40	YES	(Delevoye, Nilges *et al.* 2008)
VAPA	Q9P0L0	YES	(Elwell, Jiang *et al.* 2011)
VAPB	O95292	YES	(Agaisse and Derre 2014)
Vimentin	P08670		(Kumar and Valdivia 2008)
ZNF23	P17027		(Soupene, Rothschild *et al.* 2012)

Underlining the successful purification and application of the SILAC exclusion approach, we found a significant proportion of these previously reported inclusion associated proteins in our dataset (23/52, not counting different subgroup members of Rab proteins, Figure 3.13). A handful of proteins were found in all three replicates with SILAC ratios above the approximate threshold, but were removed either due to filtering of common contaminations (Actin) or too few unique + razor peptides in at least one of the experiments (Rab11FIP1/2, Src/Fyn, PI4KIIα). An additional seven were found but in less than three replicates (CLA1, CD63, MAP1-LC3, Rab4A/B, Raf1, Syntaxin 6 and VAMP7). Of these, only Rab4A and Raf1 had SILAC ratios above the approximate cutoff, while Rab4B, Syntaxin 6 and VAMP7 had no reported SILAC ratios, MAP1-LC3 and CD63 and were below the cutoff, and CLA1 was almost exactly on the approximate cutoff. Sixteen previously reported inclusion associated proteins were not found in any of the experiments (3234 host protein groups identified in total). This indicates that although most of these proteins are possibly retained on the inclusion, the sensitivity of our instrumentation or the measured amount was insufficient to

detect them in all replicates. To further investigate this point, we ranked the proteins detected in the deep proteome of HeLa cells (Nagaraj, Wisniewski *et al.* 2011)by the iBAQ value of tryptic peptides to see if highly abundant proteins are overrepresented in the overlap with previously known inclusion proteins (Figure 4.2). 5 of the 52 proteins were not found in the 8603 proteins detected in the tryptic digest of HeLa cell lysates and an additional five were only detected with one peptide. Our limit for reliable detection of proteins with more than one unique + razor peptide is slightly above the median iBAQ intensity in the HeLa cell lysate (Figure 4.1). This is, considering the technical difficulties due to massive amounts of bacterial peptides present in our samples, satisfying. However, based on these data, the true number of inclusion associated proteins might be significantly higher than what we here report, more specifically around twice the reported number.

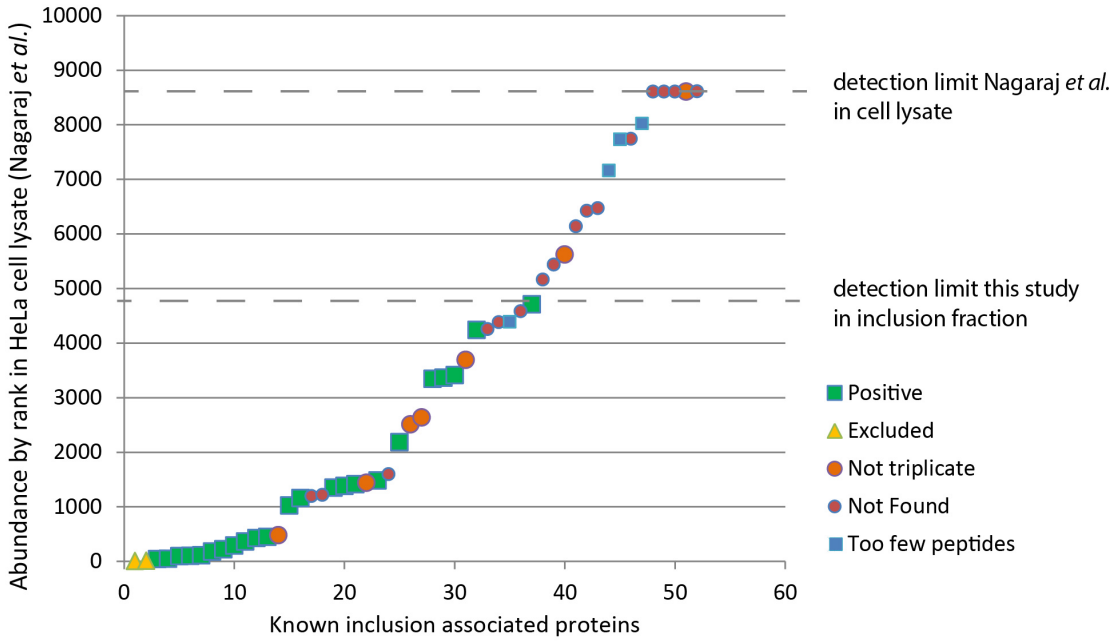

Figure 4.2: Known inclusion associated proteins by abundance in cell lysate

All previously reported inclusion associated proteins were ranked by their abundance in HeLa cell lysates based on iBAQ intensity of tryptic peptides (Nagaraj, Wisniewski *et al.* 2011). Proteins that were not found in the lysate are on the detection limit (rank 8604, n = 5). Positive = proteins that passed the SILAC exclusion approach, Excluded = did not pass the SILAC exclusion approach or were removed by initial filtering of common contaminants. Not triplicate = proteins detected in the inclusion fraction but not in all experiments. Not found = proteins that were never detected in the inclusion fraction. Too few peptides = proteins that were identified with only one peptides in all three experiments.

4.2.2.4 Validation

To further validate the proteome approach, we additionally analyzed five proteins that have previously not been reported to be inclusion localized and had varying SILAC ratios and iBAQ enrichment scores. We validated the presence of VCP, Rab3D, SYNGR2 and Sec61β both in IF and on isolated inclusions using fluorescently tagged fusion proteins (Figure 3.14). Sec61β was

removed from the list of inclusion proteins by the SILAC exclusion approach but it was the first protein to be excluded with a p-value of 0.0107, where 0.01 was the cutoff. In later experiments, in which we investigated the SNX-BAR retromer, we additionally verified SNX1, SNX2, CI-M6PR and VPS35 to be inclusion localized using IF (Figure 3.19), while SNX5 was validated by expression of a fluorescent fusion protein (Figure 3.22).

Of the proteins that were previously reported to be inclusion associated or directly recruited by bacterial factors, we found a wide spread of both SILAC ratios and iBAQ enrichment scores (Figure 3.13). While The SILAC ratios were evenly distributed with several previously known proteins at the lower end of the SILAC ratios, the iBAQ enrichment score had, apart from one exception (Cytokeratin 18), a threshold of iBAQ enrichment score of slightly over 1. The SILAC ratios of the 11 newly identified and validated inclusion proteins are evenly spread among the SILAC ratios, while all iBAQ enrichment scores were above two (Figure 3.13). Only one protein that was previously reported to be inclusion localized and passed our initial filtering was removed due to the SILAC exclusion approach (Vimentin), while one protein we tested positively was also excluded (Sec61β) albeit only by an ace. Conversely only one protein complex that was reported to be absent was positively enriched (vATPase). Based on our data it can therefore be assumed that the SILAC exclusion approach efficiently separates co-purifying contaminants from actual inclusion associated proteins while the iBAQ enrichment score supplements this information.

Surprisingly, we were unable to isolate fluorescent inclusions from cells overexpressing STIM1-YFP (Figure 3.14 B), although STIM1, according to the p–value of the SILAC exclusion approach and the iBAQ enrichment score, is one of the most highly enriched proteins at the inclusion (Figure 3.13). Furthermore, we observed clear colocalisation with IncA in cells expressing STIM1-YFP in IF studies (Figure 3.14 A).

While it cannot be excluded that STIM1 is an environmental contamination, the high iBAQ enrichment score suggests it is not, as these would typically occur in all samples of one batch or show high L/H scores also in the lysate fraction. Also its high abundance (0.45 % of total) suggests it to be a true inclusion protein. The best explanation for this contradicting data is therefore that overexpressed STIM1 as opposed to endogenous STIM1 either does not stably bind the inclusion, leading to dissociation upon lysis, or inclusions from cells overexpressing STIM1 are intrinsically less stable. In a recent report, expression of STIM1-YFP was shown to reduce periphagosomal actin rings (Nunes, Cornut *et al.* 2012), a structure that is reminiscent of the actin coat surrounding inclusion, which is thought to increase its structural integrity (Kumar and Valdivia 2008). A similar mechanism could therefore lead to the destabilization of inclusions isolated from STIM1 overexpressing cells, leading to the inability to isolate intact STIM1-YFP positive inclusions in VPI.

Generally, using fluorescent fusion proteins is an efficient means of validating the intracellular localization of proteins but shows divergence from information obtained by antibody-based staining, with an approximate overlap of 80 % (Stadler, Rexhepaj *et al.* 2013).

Our proteomics approach is a complementary method to further validate previously published data on inclusion localization obtained from both approaches. Yet, the absence of a protein from our dataset does not negate previous findings due to limitations in mass spectrometric detection as discussed above.

4.2.2.5 Active recruitment of proteins by Chlamydia

Although the mechanisms by which host proteins are recruited to the inclusion are unknown for the larger part of known inclusion associated proteins, they were elucidated for some. The protein 14-3-3β was the first host protein found to be recruited to the inclusion of *C. trachomatis* (Scidmore and Hackstadt 2001). It is recruited to the inclusion directly via the Inc protein IncG (CT118) and binds a via conserved phosphorylated serine on position 166 of IncG. Furthermore the direct binding of Raf1 by 14-3-3β was shown by proximity ligation assay (Gurumurthy, Maurer *et al.* 2010). In addition to 14-3-3β, we also found the remaining six members of the 14-3-3 family of proteins in human cells. All of them except for 14-3-3σ are at least twofold enriched at the inclusion based on iBAQ (Table 6.1) and contribute substantially to the total host protein content of the inclusion (10.6 %). As all members of the 14-3-3 family are highly conserved it is likely that several members can bind equally well to the 14-3-3 binding motif of IncG (Scidmore and Hackstadt 2001).

The lipid transfer protein CERT was shown to bind by direct interaction with IncD (CT115), whereas its associated protein VAPB was recruited indirectly via binding to CERT (Agaisse and Derre 2014). An alternative mechanism was found in the recruitment of protein kinase C delta (PKCδ), which is scavenged by highly accumulated diacylglycerol in the vicinity of the inclusion (Tse, Mason *et al.* 2005). The binding of the SNARE protein syntaxin 6 is presumably directly or indirectly mediated by a bacterial effector, as inhibition of chlamydial protein synthesis ablated recruitment. In addition it was demonstrated that the recruitment depends on a PM retrieval signal (Moore, Mead *et al.* 2011). Rab4 is recruited by the Inc protein CT229 (Rzomp, Moorhead *et al.* 2006) while Rab11 is presumably recruited by another Inc protein which has been demonstrated for *C. pneumoniae,* where Cpn0585 binds several Rab proteins but predominantly Rab11 (Cortes, Rzomp *et al.* 2007). The Inc protein CT813 has been shown to interact with VAMP8 and VAMP7 which it probably recruits both (Delevoye, Nilges *et al.* 2008). The Inc CT228 has been shown to recruit Myosin phosphatase target subunit 1 (MYPT1), presumably depending on its phosphorylation state (Lutter, Barger *et al.* 2013).

Taken together, mechanisms of recruitment for inclusion associated proteins are diverse but those identified mostly depend on either direct or indirect binding to Inc proteins. Indeed, we did find all proteins that have been reported to be directly recruited by Inc proteins in our final dataset except for Rab4 and VAMP7 (Table 4.1 and Figure 3.13). Furthermore, the five Inc proteins that mediate these interactions were among the ten most highly abundant predicted Inc proteins (Table 3.1). For four of these top 10 Inc proteins (CT116, CT147, CT223 and CT618) no cellular interaction partners was found to date, although CT223 has been functionally implicated with blocked cytokinesis in *C. trachomatis* infections (Alzhanov, Weeks *et al.* 2009) while CT147 shows homology to early endosomal antigen 1 (EEA1) and was suggested to be involved in the avoidance of the progression of early endosomal maturation (Belland, Zhong *et al.* 2003). CT116 (IncE) and CT618 therefore should be prime candidates for further studies on Inc proteins.

4.3 Global analysis of the host cell derived inclusion proteome

4.3.1 Determinants of organellar identity

One of the most prominent questions in the biology of *Chlamydia* concerns the position of the chlamydial inclusion in the endomembrane system. Despite many years of research, the mechanisms that govern its intracellular fate from endocytosis to the establishment of a replicative niche, including extensive nutrient transport across the inclusion membrane remain poorly characterized.

As acid phosphatase is absent from the inclusion and fusion with lysosomes is not observed, the identity of the chlamydial inclusion is clearly non-lysosomal (Friis 1972, Lawn, Blyth *et al.* 1973, Wyrick and Brownridge 1978). The analysis of the inclusion for markers of the endosomal pathway showed absence of typical markers for LE and LY such as LAMP-1 and 2, cathepsin D and vATPase (Heinzen, Scidmore *et al.* 1996, Taraska, Ward *et al.* 1996, van Ooij, Apodaca *et al.* 1997, Al-Younes, Rudel *et al.* 1999). Also, the lumen of the inclusion is not acidified, in line with undisturbed replication upon treatment with inhbitors of vacuolar acidification (Heinzen, Scidmore *et al.* 1996, Schramm, Bagnell *et al.* 1996). These findings are in agreement with our proteome data in which we found only seven proteins annotated with the subcellular localization term lysosome to be at the inclusion (LDLR, IGF2R, M6PR, PRDX6, SQSTM1, Rab12 and VAMP8), all of which are also found in other organelles (Figure 3.15). In general, the analysis of proteomes based on current databases is not perfect and should be interpreted with care. For example it has been shown in a proteomics study that 39 % of all identified organellar proteins showed multiple distinct localizations (Foster, de Hoog *et al.* 2006), however, well defined quantitative data on the localization of these proteins to different subcompartments is not available yet. For this reason, the manually curated Uniprot annotations were used for the definition of the suborganellar localization of a protein as these are annotated rather conservatively.

4.3.1.1 Organellar contributions

The inclusion is known to interact extensively with host cell organelles (see 1.2.4, Figure 1.3, p. 9). In our global analysis of the individual contribution of organelles to the inclusion proteome, we found a very diverse composition of the inclusion (Figure 3.15). Using absolute quantification of proteins, we approximated the stoichiometric contribution of each organelle in addition to an analysis based only on numbers of identified proteins. In both analyses, we found a significant contribution of ER derived proteins to the total proteome which was further supported by the enrichment of GO terms specific to the ER. Several earlier reports have reported the localization of ER marker proteins to the inclusion. These include Calreticulin, Sarcoplasmic/endoplasmic

reticulum calcium ATPase 2 (ATP2A2) (Majeed, Krause *et al.* 1999) PDI, Reticulon-4, Derlin-1 and Receptor expression-enhancing protein 5 (aka DP1) (Dumoux, Clare *et al.* 2012), of which we found all in our proteome except for Derlin-1 (Figure 3.13). An intimate association beween the rough ER, the inclusion and RBs on the luminal side of the inclusion membrane was described as a pathogen synapse (Dumoux, Clare *et al.* 2012) that is putatively involved in host pathogen interactions of *Chlamydiae,* although the function of this pathogen synapse remains unclear. ER-inclusion MCS have been implicated in ceramide transport across the inclusion membrane via CERT (Derre, Swiss *et al.* 2011, Elwell, Jiang *et al.* 2011).

The source of ER derived proteins and their functional role is elusive, however, it is tempting to speculate that the Sec61 complex and associated proteins might play a role in the localization of these proteins to the inclusion, as we found a large number of proteins involved in co-translational protein transport across the ER membrane to be inclusion associated (see Figure 3.16) in addition to membrane bound Sec61β in a validation experiment (Figure 3.14). Furthermore, Sec61 is involved post translational protein transport across the ER membrane and retro-translocation from the ER lumen to the cytosol (Liao and Carpenter 2007), of which the latter could be a mechanism hijacked by *Chlamydia* for T3SS independent secretion of effector proteins to the cytosol.

The study of the phagosome proteome from dendritic cells and macrophages has also implicated a role of ER derived membranes to the composition of this organelle (Garin, Diez *et al.* 2001, Campbell-Valois, Trost *et al.* 2012), where ER resident proteins are thought to increase the efficiency of antigen cross presentation in a ER-phagosome mix compartment (Guermonprez, Saveanu *et al.* 2003, Houde, Bertholet *et al.* 2003). As epithelial cells are not involved in antigen cross presentation, it is hard to determine if this mix of compartments is induced by the pathogen or as a host defense strategy in the case of *Chlamydia* infections. As opposed to the proposed early fusion with ER membranes after phagocytosis, significant acquisition of ER markers by *Chlamydia* occurs only mid infection (after 20 h *p.i.*) and is dependent on chlamydial translation (Dumoux, Clare *et al.* 2012), thus favoring a bacteria-mediated mechanism.

4.3.2 Enrichment analyses

To identify functions that are enriched in the host derived inclusion proteome comparison to the total cellular proteome of HeLa cells, we used GO term enrichment analysis. Enrichment analyses based on GO of cellular compartments (GOCC) supported our previous findings proteins which are annotated as part of “membrane bounded vesicle”, “plasma membrane” and “endoplasmic reticulum part” are highly enriched. Suprisingly, a large part of the inclusion proteome was annotated with the term “extracellular vesicular exosome” (196 of the 3 proteins, total iBAQ

percentage 79 %). Exosomes are released from the cell when a MVB fuses with the PM. MVBs are known to fuse with the inclusion membrane, while translocating their intraluminal vesicles, into the inclusion lumen (Beatty 2006, Beatty 2008). Although this interaction certainly is important, GO terms, as mentioned earlier, are still a somewhat rough guideline towards organelle identity. For example the GO term "extracellular vesicular exosome" is largely based on three high throughput proteomics studies, which identified over a thousand proteins in exosomes, which is not very informative as marker, if quantitative data is lacking (see references of the Gene Ontology database (Ashburner, Ball *et al.* 2000)). However, it is striking that most compartments derived from the endomembrane system share a base set of proteins with very diverse functions, while the specialized functional role of the compartment is mostly determined by a lower number of highly enriched proteins, a mechanism which hijacked by the selective recruitment of proteins by *C. trachomatis*.

The analysis for enrichment of specific functions using GO enrichment analyses showed, apart from rather high abundance of ER derived processes, a strong enrichment of proteins involved in protein localization. The more specific analysis of these proteins revealed that four main clusters of proteins contribute to this function (Figure 3.16). Of these, proteins that interact with these proteins were partly described previously, namely Rab6A which interacts with VPS29 and VPS35 (complex A, SNX-BAR), 14-3-3β as member of the highly enriched 14-3-3 protein family (complex B), several ER derived proteins in complex C and VAMP3/VAMP8/Rab14 in complex D (see Table 4.1). As most proteins of the SNX-BAR complex showed both high SILAC ratio and iBAQ enrichment scores, these proteins were investigated in more detail (section 4.4, p. 116). Also, retrograde trafficking, the pathway mediated by these proteins, has not previously been investigated in chlamydial infections. Functional analysis of the proteins enriched in vesicle mediated trafficking further supported the involvement of significant amounts of proteins involved in retrograde trafficking events (Figure 3.17).

The analysis for enrichment of specific domains and motifs further suggested that Ras GTPases are highly enriched at the inclusion, with 12 of 15 being Rab GTPases (Table 3.2), which will be discussed in the next section.

4.3.3 Rab proteins

In recent years, the knowledge about determinants of organellar identity has drastically increased and apart from typical marker enzymes, small GTPases including RabGTPases and Arf GTPases in addition to organelle specific PtdIns are now considered crucial factors (Behnia and Munro 2005). Furthermore, the modulation of PtdIns metabolism and GTPase function are established concepts

used by bacteria to create a unique intracellular niche (Alix, Mukherjee *et al.* 2011). The PtdIns composition of the inclusion will be discussed later (Figure 4.4, p. 118).

Rab proteins are proteins of the small GTPase family which are found specific to compartments of the endomembrane system. They can switch between a GDP bound inactive state and a GTP bound active state, in which they are membrane bound and recruit specific effectors to their target membrane. Recruitment of Rab proteins can also be regulated by PtdIns species and *vice versa* effectors of Rab proteins often are involved in PtdIns metabolism, leading to a highly regulated system of activation/inactivation and recruitment which defines the identity of the target membrane combinatorially (Di Paolo and De Camilli 2006).

The recruitment of RabGTPases to the inclusion has been addressed repeatedly, but current studies only analyzed a small subset of the total complement of Rab proteins (Rzomp, Scholtes *et al.* 2003, Rzomp, Moorhead *et al.* 2006, Rejman Lipinski, Heymann *et al.* 2009, Capmany, Leiva *et al.* 2011). Known inclusion associated Rab proteins are Rab11A, a marker for RE, Rab14 which is involved vesicular transport from the GA to EE, Rab4A and B (EE to RE transport) Rab6 (GA) and Rab1 (GA/ER) (Dong, Zhu *et al.* 2012, Galvez, Gilleron *et al.* 2012). Most importantly, the EE marker Rab5A and the LE/LY marker Rab7 are both absent from the inclusion, suggesting an early escape from the endosomal maturation pathway (Rzomp, Scholtes *et al.* 2003). In line with these previous reports, we found a large number of small GTP binding proteins at the inclusion, yet our data do not completely agree with previously published data. Rab10 was reported to be absent from the inclusion of *C. trachomatis* (Rzomp, Scholtes *et al.* 2003) but we found it to be highly enriched; furthermore, we did not identify Rab1A, Rab4A and B and Rab6B which were reported previously, although we did find Rab1B/C and Rab6A, therefore only a homolog of Rab4 was not detected. For Rab1A, Rab11A and Rab6A we did not find sufficient unique peptides, as different subgroups of Rab proteins share high sequence identity this is not surprising. However, due to our filtering for two unique + razor peptides per protein group, they were eliminated from the final list, despite most likely being in the same protein group as their subgroup members.

In Figure 4.3 an overview of all Rab proteins we found in our proteome is given, showing their primary localization in non-infected cells. Newly found Rab proteins were Rab2A which contributed 1.8 % to the total, Rab8A, Rab12, Rab13, Rab27B, Rab35 and Rab3D, which all were significantly less abundant. We validated Rab3D and it clearly localized to the inclusion membrane both in fixed cells and on purified inclusions, when expressed as fluorescent fusion protein (Figure 3.14). We furthermore confirmed that this binding is GTPase dependent by using a dominant negative mutant which did not bind to inclusions. Rab3D, Rab8A and Rab27B are all involved in exocytosis. Although the inclusion is known to intercept basolaterally directed exocytic vesicles (Moore, Fischer *et al.* 2008), still relatively little is known about its interaction with exocytosis and

post Golgi trafficking. Most importantly, the inclusion itself is extruded at the end of the developmental cycle (Hybiske and Stephens 2007) and the association of these Rab proteins could be a preliminary step towards the extrusion of the inclusion which seems to be tightly regulated as it leaves the host cell intact.

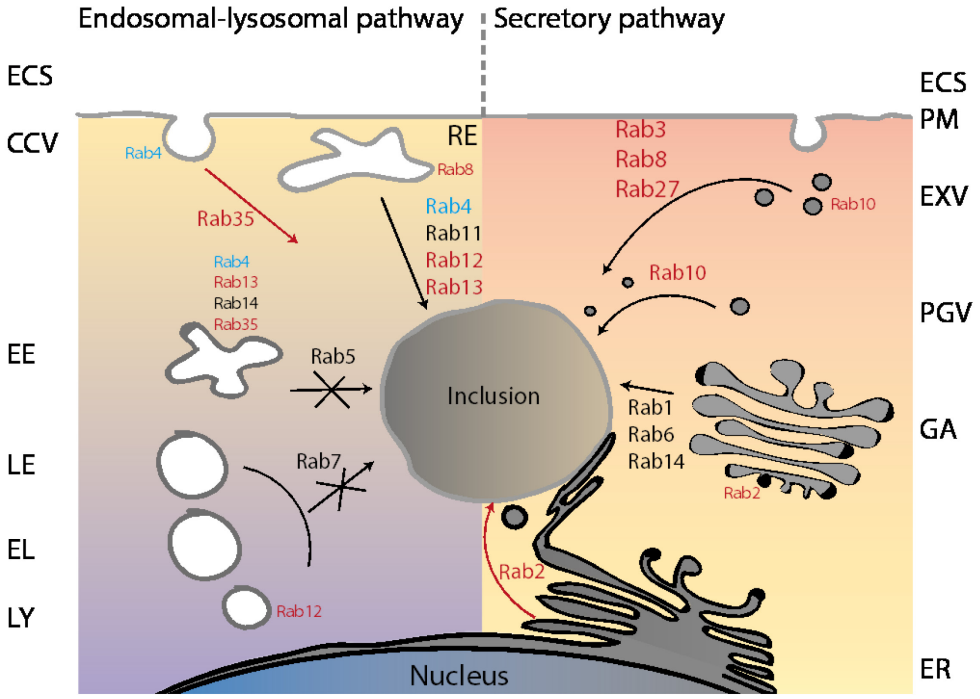

Figure 4.3: Overview of Rab proteins that interact with the inclusion
Overview of Rab proteins that were found in the inclusion proteome and not reported previously (red), previously reported and found in the proteome (black) and reported but not found in the proteome (blue). Where multiple organelles are reported, the minor organellar localization in uninfected cells is represented by smaller legends . Black arrows indicate known intercepted trafficking pathways, red arrows indicate novel intercepted trafficking pathways. Rab5 and Rab7 are not acquired and excluded by their SILAC ratio as previously reported. References can be found in the text. For simplicity subgroups of Rab proteins are not indicated. ECS= Extracellular space, CCV = clathrin coated vesicle, EE = early endosome, LE = late endosome, EL = endolysosome, LY = lysosome, PM = plasma membrane, EXV = exocytic vesicle, PGV = post Golgi vesicle, GA = Golgi apparatus, ER = endoplasmic reticulum. References see (Galvez, Gilleron *et al.* 2012)

Rab2A is involved in membrane trafficking in the early secretory pathway where it associates with vesicular tubular structures to deliver cargo from the ER to the GA (Tisdale, Bourne *et al.* 1992).

The interception of early traffic from the ER in transit to the GA could be an additional way to receive nutrients and might explain the significant contribution of ER derived proteins to the inclusion proteome.

Taken together, we confirmed that the inclusion is indeed a patchwork organelle that receives cargo from essentially all trafficking pathways of the endomembrane system. In addition to the previously described trafficking routes, we also found significant enrichment of proteins involved in retrograde trafficking (Figure 3.17) and proteins destined for the ER and the PM (Figure 3.15) of which the latter two are also supported by the presence of Rab proteins that mediate trafficking

along these pathways (Figure 4.3). Among the more surprising findings was the high abundance of SNX-BAR proteins (Figure 3.16 and Figure 3.18), a group of proteins normally localized to endosomes, which will be discussed in section 4.4, p. 116.

4.3.4 Nutrient transporters

We analyzed our proteome for host cell solute transporters. The main groups of transmembrane transporters are the SLC group of proteins, ABC transporters, water channels, ion channels, and ion pumps, of which only ABC and SLC transporters are considered solute transporters. The SLC group of proteins consists of over 400 members and all SLC are membrane proteins that control the uptake and efflux of a number of most solutes such as sugars, amino acids and drugs independent of ATP hydrolysis (Schlessinger, Matsson *et al.* 2010). ABC transporters on the other hand, transport solutes by ATP hydrolysis (primary transporter activity) (Rees, Johnson *et al.* 2009) of which approximately 50 are encoded by the human genome (Dean, Rzhetsky *et al.* 2001). In our inclusion proteome, we only found three members of the SLC transporter group while no ABC transporters were identified (0, p. 80). The previously reported inclusion associated vitamin transporter SMVT (SLC5A6) (Fisher, Fernandez *et al.* 2012) was not found in our proteome.

The absence of more nutrient transporters from our proteome suggests two alternative scenarios. Either, the sensitivity of our approach is not high enough to identify these proteins which are typically of low abundance and high hydrophobicity (Hediger, Clemencon et al. 2013), with the latter aspect further negatively affecting mass spectrometric analysis. Alternatively, bacterial proteins overtake this function at the inclusion membrane. Slightly less than half of the 107 SLC transporters and half of the 31 ABC transporters detected by Nagaraj *et al.* in their tryptic digest of HeLa lysates were within our sensitivity range determined in Figure 4.2, suggesting absence of most of these proteins, therefore supporting the notion of bacterial transporters being involved in these processes.

4.3.5 Comparison to other PVs

Several species of pathogenic bacteria are known to reside in a PV derived from the endomembrane system in addition to *Chlamydia*. Nutrient transport across their PV membranes is in most cases poorly characterized. *L. pneumophila* are Gram-negative bacteria and the cause of Legionnaire's disease which is transmitted through contaminated water. Once inside the lungs they can infect alveolar macrophages, where they reside within the LCV (Isberg, O'Connor et al. 2009). The replication of *L. pneumophila* has been shown to depend on the expression and functional activity of the host cell neutral amino acid transporter SLC1A5 which is upregulated early in the infection (Wieland, Ullrich et al. 2005). LCV localization of SLC1A5 was not assessed in

the study, but it was found in the macrophage derived LCV proteome in all three replicates (Hoffmann, Finsel et al. 2013). Additionally, a group of bacterial amino acid transporters was identified in *Legionella*, termed phagosomal transporters (Phts), which are required for intracellular survival, although again it is not known whether they localize to the limiting LCV membrane (Sauer, Bachman et al. 2005). The only homologue in *Chlamydia* was detected in the environmental *Protochlamydia amoebophila* UWE25 therefore excluding this protein family as potential transporters in *C. trachomatis* infections.

The high abundance of Rab proteins we found at the inclusion is not unprecedented, as the LCV isolated both from *D. discoideum* and macrophages were both found to interact heavily with Rab proteins (Urwyler, Nyfeler *et al.* 2009, Hoffmann, Finsel *et al.* 2013). Furthermore, the LCV resists fusion with lysosomes (Horwitz 1983) and interacts strongly with ER derived vesicles early after entry (Swanson and Isberg 1995). In the course of its maturation, ribosome decorated ER membranes associate with the LCV (Tilney, Harb *et al.* 2001). To support vacuole growth, the LCV intercepts vesicular traffic directed from the ER to the Golgi apparatus (Kagan and Roy 2002). In the light of our findings concerning the significant contribution of ER proteins to the inclusion proteome, we compared our inclusion proteome to the proteome of LCVs isolated from macrophages. Indeed we found an overlap of 174 proteins out of our 345. As discussed previously, no controls for co-purifying proteins were performed in this study and proteins which were found in only one of three experiments were also considered. Furthermore no quantitative data is available which would help to compare the two datasets. Upon more stringent filtering of their data (found in all three experiments), the overlap was reduced to 100 of 555 proteins of which 45 were annotated as ER proteins (61/174 with less stringent filtering), based on UniprotKB subcellular localization data. Also, 106 of the 174 overlapped with the GO term “extracellular vesicular exosome”.

Mycobacteria tuberculosis is a Gram-positive, facultative intracellular bacterium. In macrophages it grows in the MCV (*Mycobacterium*-containing vacuole) which is decorated with Rab5 but not Rab7, while also excluding vATPase (Russell, Mwandumba *et al.* 2002), therefore remaining in a transition phase of the endosomal-lysosomal pathway while stalling maturation. We compared our dataset to the MCVs isolated form dendritic cells and macrophages infected with wild-type *M. tuberculosis* H37Rv for in which 680 and 693 proteins, respectively, were found and quantified (Li, Singh *et al.* 2011). The overlap of these proteins was rather low at 102 and 100 proteins, respectively. Of the proteins that overlapped, 74 and 75 were annotated as exosomal. When comparing the relative abundances in the inclusion proteome to the two datasets, the correlation was very low (R^2 = 0.07 for both) with rather high correlation in between between the two datasets (R^2 = 0.63).

Taken together, although the proteomes of these three PVs are not directly comparable, we did find a significant proportion of overlapping proteins for LCV proteins and a rather low overlap for MCVs, showing that although the mechanisms of PV establishment are different, similarities exist. A large proportion of overlap observed with exosomes between the three datasets suggests that these proteins constitute a base set of proteins of the endomembrane system.

Additional examples of vacuole dwelling intracellular bacteria of which currently no PV proteomes exists include *Salmonella* and *Coxiella*. *Salmonella spp.* are facultative intracellular Gram-negative bacteria (Grassl and Finlay 2008). The *Salmonella*-containing vacuole (SCV) segregates from the classical phagosomal maturation pathway early on. After entry, the SCV acquires markers of EE, including EEA1, TFRC and Rab5. Subsequently lysosomal markes such as Rab7, LAMP1 and vATPase are recruited probably by fusion with LE while others such as M6PR are removed by a Rab11 dependent recycling pathway (Bakowski, Braun *et al.* 2008). *Coxiella. burnetii* are gram negative obligate intracellular bacteria and the causative agent of Q-Fever. Among the intracellular bacteria that reside within PVs, *C. burnetii* is unique in that it does not avoid phagosome maturation but evolved to live in the harsh acidic environment of the phagolysosome (Akporiaye, Rowatt *et al.* 1983). The endosomal marker Rab5 is acquired as early as 5 minutes after infection (Romano, Gutierrez *et al.* 2007) followed by the recruitment of late endosomal/lysosomal markers Rab7 (Romano, Gutierrez *et al.* 2007), vATPase, LAMP-1, LAMP-2, and LAMP-3 (Ghigo, Colombo *et al.* 2012).

Also compared to these two examples, the inclusion of *C. trachomatis* is indeed unique, as it does not acquire typical markers of EEs, LEs, ELs or LYs, with the possible exception of SNX proteins which are typically found at the EE/LE (see section 4.4, p. 116). With the technical development that proteomics is currently undergoing, it is only a question of time until highly reliable quantitative datasets are available for most PVs, which will allow more reliable comparisons between these unique intracellular niches.

4.4 Importance of retrograde transport for *Chlamydia trachomatis*

In the last part of this thesis, we showed that components of retrograde trafficking machinery SNX-BAR are recruited very specifically to the inclusion of *C. trachomatis.* Furthermore, we showed by inhibitor experiments that retrograde trafficking is essential for efficient intracellular replication of *C. trachomatis.*

4.4.1 Enrichment of the SNX-BAR retromer complex at the inclusion

We initially found that several proteins involved in retrograde trafficking are recruited to the inclusion as they were highly enriched in our proteome (Figure 3.17, Figure 3.18). We further confirmed this association in IF studies for SNX1 and SNX2, which are both part of the SNX-BAR retromer, as well as in live cell imaging experiments using eGFP fusion proteins of SNX2 and SNX5 (Figure 3.19 and Figure 3.22). Components of the cargo recognition subcomplex were less enriched in the proteome and also showed weak to no staining of the inclusion in our validation (Figure 3.19). We therefore reasoned that the SNX-BAR membrane deforming subcomplex associates with the inclusion independently of the cargo recognition complex. The recruitment of the cargo recognition subcomplex is thought to be mediated by binding Rab7 (Rojas, van Vlijmen *et al.* 2008, Seaman, Harbour *et al.* 2009) at the transition of EE to LE (Rab5 to Rab7 switch) (van Weering, Verkade *et al.* 2012). As Rab7 was previously reported to be absent from the inclusion, a finding that we confirmed in our proteome (see also Figure 4.3), it is likely that these two subcomplexes indeed are functionally separated during the infection.

4.4.2 Effect of SNX-BAR depletion on bacterial progeny formation

In RNAi mediated knockdown of SNX-BAR retromer components, we found that infectious progeny formation was not affected by the depletion of SNX-BAR proteins, except for a slight increase of infectious progeny formation in the knockdown of SNX5 (Figure 3.21). The function of the SNX-BAR proteins is, according to published literature, in part redundant. SNX2 is not essential for CI-M6PR retrieval, the central function of the retromer (Carlton, Bujny *et al.* 2005), a finding that was confirmed in a later study (Rojas, Kametaka *et al.* 2007). It was shown that the individual knockdown of SNX5 and SNX6 leads to reduced levels of SNX1 (Wassmer, Attar *et al.* 2007), which we also observed in our knockdown experiments; in addition we also observed a reduction of SNX2 upon individual knockdown of SNX5 and SNX6 (Figure 3.21 B).

In early co-immunoprecipitation experiments, SNX6 was shown to interact with SNX1, while SNX5 did not interact with SNX1 (Wassmer, Attar *et al.* 2007). Further extensive validation of the SNX-BAR interactome by yeast two hybrid screening and, GST pull down and immunoprecipitation

studies (Wassmer, Attar *et al.* 2009) ,however, clearly showed interactions of SNX1 with SNX5 and SNX6 and SNX2 with SNX 5 and SNX6 and ruled out homodimers of SNX1 and SNX2, which were reported earlier (Rojas, Kametaka *et al.* 2007). Judging by the significantly reduced levels of three SNX-BAR proteins upon knockdown of SNX5 and SNX6 (Figure 3.21 B), it is unlikely that the residual function of SNX proteins is sufficient to maintain intact retromer mediated trafficking, given that the functional complex requires a heterodimeric complex of SNX1/2 and SNX5/6. The increase of infectious progeny upon knockdown of solely SNX5 (Figure 3.21) might be explained by the induction fragmentation of the GA, which was reported previously (Wassmer, Attar *et al.* 2007) and is known to be beneficial for bacterial replication (Heuer, Rejman Lipinski *et al.* 2009).
Taken together, our results indicate that the relevance of SNX-BAR proteins for the infection is not detected by our assay, possible due to technical limitations, such as involvement in multiple stages of the infection leading to a combination of beneficial and disruptive effects on development upon depletion of SNX-BAR proteins by siRNA mediated knockdown. Alternatively it is possible that the effects are very subtle in cell culture and depend on additional factors that are possibly only present *in vivo*.

4.4.3 Determinants of SNX-BAR recruitment to the inclusion

The SNX-BAR proteins are characterized by their PtdIns binding PX domain (1.4.3.1). PtdIns are phospholipids that are concentrated at the cytosolic surface of membranes which can be phosphorylated reversibly at the inositol ring at positions 3, 4 and 5, with a total of seven possible PtdIns species. PtdIns contribute only a small percentage (approximately 15 %) of total phospholipids in eukaryotic cells, with a tenfold lower amount for individual species. Specific PtdIns species are enriched at individual organelles where they induce the recruitment of PtdIns binding proteins, which are often effectors in membrane trafficking events. Interconversion of PtdIns is concerted with the maturation of organelles and is for example tightly linked to endosomal-lysosomal maturation. (Di Paolo and De Camilli 2006)
The PtdIns composition of the inclusion has not been analyzed comprehensively to date. Proteins involved in PtdIns(4)P metabolism have been reported to be recruited to the inclusion and the inclusion membrane was found to be enriched in PtdIns(4)P, while PtdIns(3)P and PtdIns(4,5)P(2) were not detected at the inclusion membrane in experiments using fluorescent fusion proteins with PtdIns binding domains (Moorhead, Jung *et al.* 2010). An overview of the PtdIns composition as determined for the inclusion and non-infected cells and the PtdIns binding specificities of SNX-BAR proteins is given in Figure 4.4.

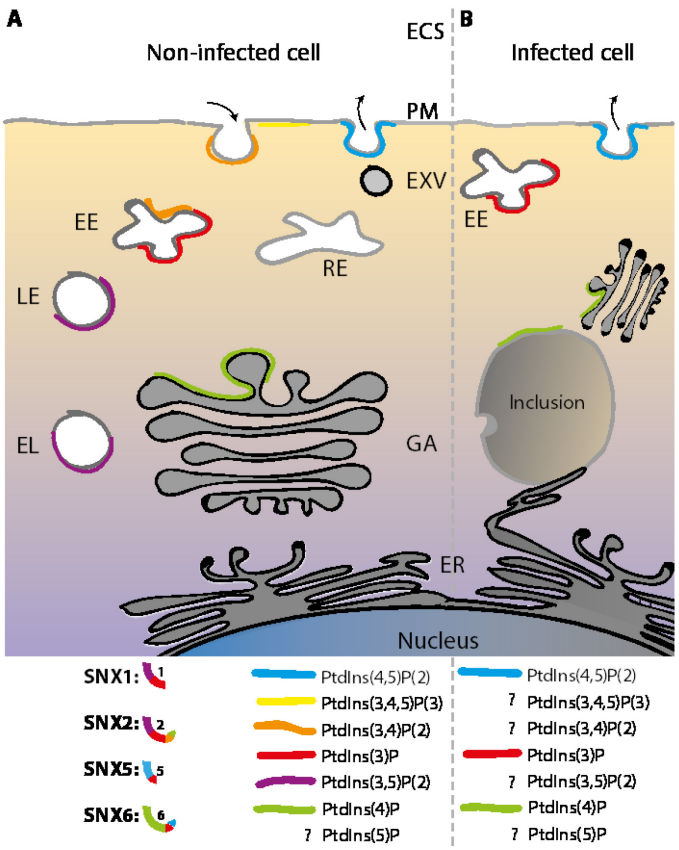

Figure 4.4: PtdIns species in the endomembrane system and the inclusion.
Enrichment of PtdIns species in the endomembrane system in uninfected (**A**) and infected cells (**B**). A question mark indicates that the localization of this PtdIns species is unknown in the respective condition. The PtdIns binding characteristics of SNX1,2,5,6 are indicated by the matching colors that indicate the PtdIns content of the membranes. References: see (1.4.3.1, p. 17) for SNX PtdIns binding specificities and (Di Paolo and De Camilli 2006) for PtdIns species in the endomembrane system.

We showed that the PX domain of SNX5 is sufficient to mediate recruitment to the inclusion membrane and most likely binds to the same binding site that maintain SNX1 and SNX2 at the inclusion (Figure 3.23). These results are surprising in the light that PtdIns(3)P was reported to be absent from the inclusion (Moorhead, Jung *et al.* 2010), although it is thought to be the main PtdIns species contributing to the recruitment of SNX1 and SNX2 to the EE/LE (Cozier, Carlton *et al.* 2002, Carlton, Bujny *et al.* 2005) and inhibition of PtdIns(3)P formation by wortmannin leads to the loss of endosomal localization of SNX1 and SNX2 (Rojas, Kametaka *et al.* 2007). PtdIns(4,5)P(2), which is the main PtdIns binding partner of SNX5 (Koharudin, Furey *et al.* 2009), was neither found at the inclusion (Moorhead, Jung *et al.* 2010).

Taken together, it is still unclear how SNX-BAR proteins are recruited to the inclusion but there are strong indications that a major contributing factor is the binding via PtdIns species, whereas a bacterial factor, for example an Inc protein, cannot be excluded.

4.4.4 Model of SNX-BAR function at the inclusion of C. trachomatis

Based on our data I devised two working models that integrate our data on SNX-BAR involvement in infections with *C. trachomatis* (Figure 4.5). The retromer function in unfected cells is in more detail in Figure 1.5 (p. 16). Both models favor a complete or nearly complete separation of the cargo recognition complex (VPS26/29/35) from the SNX-BAR proteins as a consequence of SNX-BAR recruitment to the inclusion as seen in infections at 24 h *p.i.* (Figure 3.19).

In the first model, the inclusion acts as surrogate for the TGN by initially receiving retromer cargo from endosomes but failing to release the SNX-BAR subcomplex from the inclusion membrane, either by direct binding of SNX proteins via a bacterial effector protein at the inclusion or by perturbing the intrinsic uncoating mechanism after the PtdIns(4)P mediated release from the dynein-dynactin motor complex (Niu, Zhang *et al.* 2013), while the VPS26/29/35 complex is released from the membrane and binds again at the Rab7 enriched EE/LE. This model is further supported by the presence of Rab6 and Rab11 at the inclusion, which both interact with the proposed retromer tubule tethering factor Rab6 IP1 (Miserey-Lenkei, Waharte *et al.* 2007), suggesting that the inclusion could serve as target membrane. Also, the major transport direction of SNX-BAR tubules occurs via minus end directed transport towards the MTOC to the juxtanuclear TGN (Wassmer, Attar *et al.* 2009). The inclusion is known to closely associate with the MTOC (Grieshaber, Grieshaber *et al.* 2006); indeed in our proteomics data we found several centrosomal proteins to be highly enriched, suggesting a direct link to the MTOC. This is further supported by the finding that SNX positive tubules accumulate on distinct spots on the inclusion, therefore giving it a degree of polarity.

In the second model, the inclusion originally assumes the role of the EE/LE in retromer function but, due to the absence of Rab5 and Rab7 at the inclusion, is unable to recruit VPS26/29/35 and its cargo to the extending SNX-BAR tubules. As binding of the WASP complex for actin polymerization at the extending tubule is VPS35 dependent (Gomez and Billadeau 2009, Harbour, Breusegem et al. 2010), the WASP complex is probably not recruited to the tubules either as we did not find it in the proteome. The binding of SNX5 and SNX6 to $p150^{glued}$ on the other hand should not be influenced, thereby allowing the tubules to extend along microtubules, leading to the strong tubulation phenotype we observed in the infected cell (Figure 3.20). The tubulation phenotype is also observed upon knockdown of the WASH complex (Gomez and Billadeau 2009), which supports this model.

The functional consequence of both models would be the inhibition of retrograde trafficking and a concomitant reduction of CI-M6PR recycling, which would lead to significantly decreased delivery of hydrolases to maturing endosomal compartments and LY, possibly extending the time available for *Chlamydia* to escape the endosomal maturation route early in the infection.

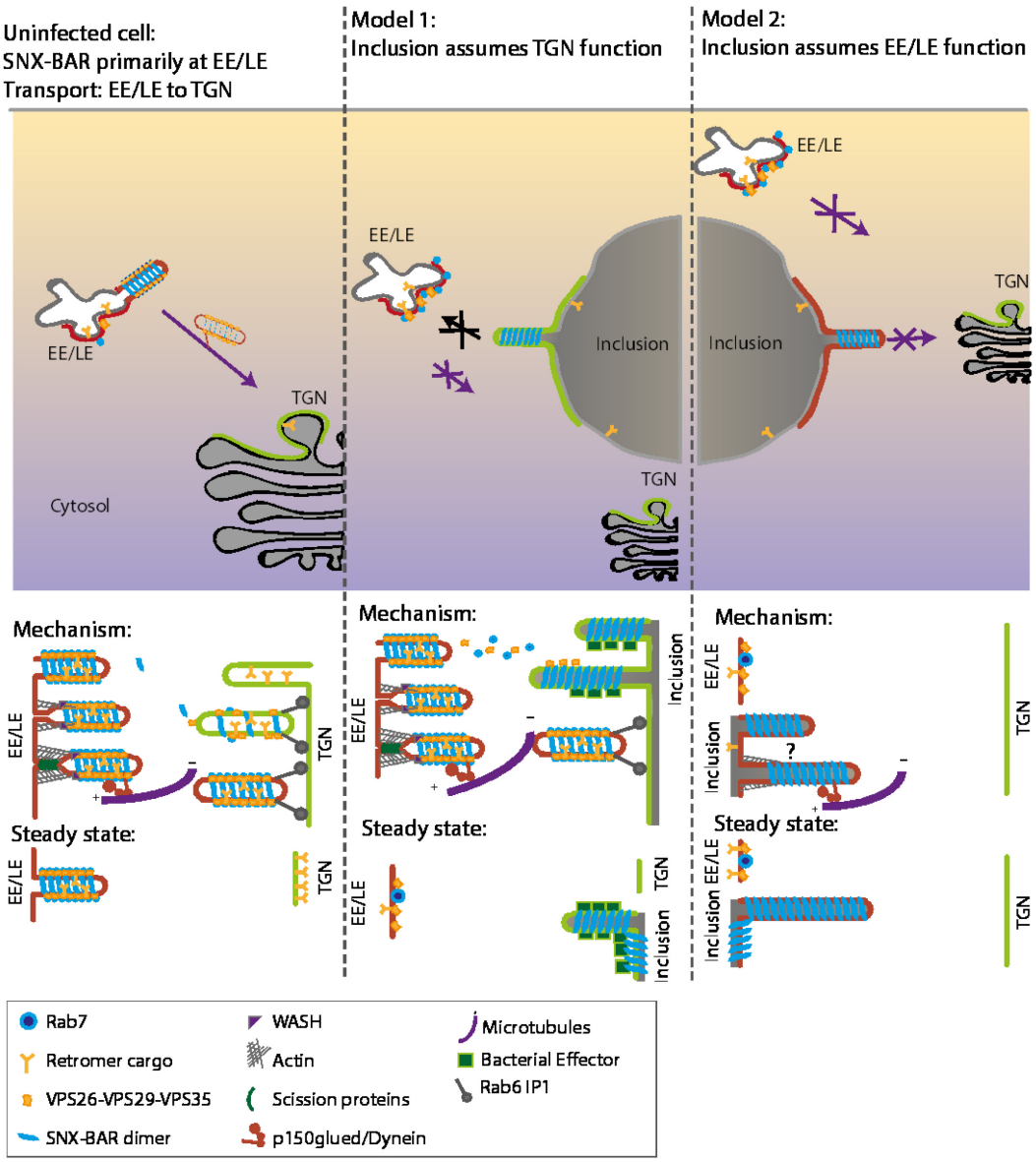

Figure 4.5: Models of SNX-BAR function in *C. trachomatis* infections
Two models of SNX-BAR recruitment to the inclusion of *C. trachomatis.* For both models the change in the initial mechanism of SNX-BAR mediated sorting is depicted, along with an illustration of the consequential steady state. Both models are described in the main text.

Another intriguing mechanism could be that the endosomal maturation pathway is stalled at the transition state from EE to LE, which coincides with the switch of Rab5 to Rab7 on the endosomal membrane and is thought to be the point at which SNX-BAR mediated retromer transport is initiated (van Weering, Verkade *et al.* 2012). This mechanism is compatible with the second model presented. In line with this model, a reason for the strong recruitment of SNX-BAR could be the early and sustained modulation of PtdIns species on the inclusion membrane by yet unidentified effectors. The recruitment of SNX-BAR proteins in this case would possibly be accidental and coincide with the recruitment of other PtdIns dependent effectors.

The modulation of PtdIns species is observed in many PV dwelling intracellular bacteria. One well established mechanism by which *S.* Typhimurium modulates the PtdIns metabolism at the early

SCV by the T3SS secreted effector Stabilisation of plasmid protein B (SopB) (Hernandez, Hueffer *et al.* 2004), which leads to avoidance of phagosome lysosome fusion (Bakowski, Braun *et al.* 2010). Most recently it was suggested that SopB reduces levels of the negatively charged PtdIns(4,5)P(2) and phosphatidylserine on the SCV and thereby alters recruitment of several host proteins, including Rab proteins, to change its intracellular fate (Bakowski, Braun *et al.* 2010). Several characterized effectors of *L. pneumophila* also interact with the host PtdIns metabolism (Hilbi, Weber *et al.* 2011). The effector retromer interactor decorating LCVs (RidL) inhibits retrograde trafficking to the LCV by strongly binding VPS29 and PtdIns(3)P, thereby possibly competing for SNX binding at the endosomal membrane to inhibit functional assembly of the retromer complex (Finsel, Ragaz *et al.* 2013).

Mycobacteria, reduce the levels of PtdIns(3)P on the MCV surface by two complementary mechanisms. One is the secretion of the PtdIns phosphatases Secreted acid phosphatase M (SapM) (Vergne, Chua *et al.* 2005) and *M.tuberculosis* Protein Tyrosine Phosphatase B (MptpB) (Beresford, Patel *et al.* 2007). The second strategy is the use of a toxic glycosylated PtdIns analogon called lipoarabinomannan (LAM) and its precursor PtdIns mannoside (PIM) (Chua, Vergne *et al.* 2004). LAM inhibits the activation of the PtdIns 3 kinase hVPS34 by calmodulin kinase II dependent mechanism (Vergne, Chua *et al.* 2003), which in turn prevents the delivery of vATPase and acidic hydrolases to the MCV (Fratti, Chua *et al.* 2003). PIM on the other hand promotes fusion with early endosomes, thereby circumventing the trafficking block induced by reduction of PtdIns(3)P, presumably to acquire sufficient membrane for continued growth of the MCV (Vergne, Fratti *et al.* 2004).

Taken together, the modulation of the host cell PtdIns metabolism by *Chlamydia* is very likely, given our observations of SNX-BAR recruitment in combination with the widespread nature of such mechanisms among PV dwelling pathogens. Arguments for this hypothesis are that we found an additional six PtdIns binding proteins in the proteome of the inclusion in addition to the five SNX proteins (Annexin A2, CERT, Inositol 1,4,5-trisphosphate receptor type 3, Phosphatidylinositol glycan anchor biosynthesis class U protein, Proflilin-1, and Rab35) and six PtdIns metabolizing enzymes (Phosphatidylinositol 3-kinase regulatory subunit beta, ARF1/ARF3, GPI transamidase component PIG-T, Lysophospholipid acyltransferase 7, Phosphatidylinositol glycan anchor biosynthesis class U protein, and Phosphatidylinositide phosphatase SAC1). The published data on PtdIns distribution in infected cells (Moorhead, Jung *et al.* 2010), which excluded recruitment of the PtdIns(3)P binding FYVE domain to the inclusion, however, does not strongly support this hypothesis.

The formation of extensive SNX positive tubules that we observed in infections (Figure 3.20), has previously been described for *Salmonella* and in this case is SopB dependent (Bujny, Ewels *et al.*

2008), suggesting it to be dependent on the modulation of PtdIns metabolism. These fibers are distinct from the widely known *Salmonella* induced fibers, emanating from its intracellular vacuole (Schroeder, Mota *et al.* 2011). Similar fibers have been reported as IncA fibers in infections of *C. trachomatis* (Bannantine, Stamm *et al.* 1998, Brown, Skeiky *et al.* 2002), and were suggested to be instrumental in the formation of secondary inclusions, which can form in the absence of bacteria contained therein and furthermore promote the segregation of inclusions into daughter cells during mitosis (Suchland, Rockey *et al.* 2005). In our experiments, IncA did colocalize with SNX fibers, although not completely and both appeared to be formed of individual and fused vesicles extending along a common path, presumably microtubules (Figure 3.20), indicating that the origin and function of these fibers is tightly linked. IncA is a major facilitator of homotypic fusion of inclusions (Hackstadt, Scidmore-Carlson *et al.* 1999, Fields, Fischer *et al.* 2002) but is also known to be dispensable for chlamydial infections (Johnson and Fisher 2013) albeit effects on clinical manifestations of the infection (Suchland, Jeffrey *et al.* 2008). Furthermore, different strains of *Chlamydia* are known to have largely different amounts of IncA fibers and secondary inclusions (Suchland, Jeffrey *et al.* 2008). This suggests that the relevance of IncA fibers and concomitantly SNX fibers is possibly not evident in cell culture in a single round of infection in our setting and different approaches to probing the relevance of SNX-BAR for the infection need to be looked into in future studies.

Ultimately, these hypotheses can only be proven or disproven by further research into the nature of the inclusion, including mechanistic studies on SNX-BAR recruitment and possibly biochemical analysis of the PtdIns composition of the inclusion, which, with the inclusion purification procedure presented herein, has become a feasible approach.

4.4.5 Retro-2 is a potent inhibitor of bacterial progeny formation

Retro-2, a compound that inhibits retrograde trafficking from the endosomes to the TGN, severely affects bacterial progeny formation with the peak of IFU formation between 24 h and 36 h *p.i.,* while no direct toxicity to the bacteria was observed (Figure 3.24). We did not observe obvious changes in the localization of retromer cargo nor components of either subcomplex upon Retro-2 treatment (Figure 3.26), in line with a previous report on VPS26, SNX1 and SNX2 localisation upon treatment in non-infected cells (Stechmann, Bai *et al.* 2010). This finding in combination with the lack of effect on bacterial progeny formation of upon SNX knockdown, suggests that the inhibitory effect of Retro-2 on the infection occurs independently of the classical SNX-BAR retromer or is more completely inhibiting the routes required for chlamydial replication than the knockdown of SNX-BAR proteins. Nonetheless, it is a strong indication that some retrograde trafficking pathways indeed contribute to the progression of the infection at mid-infection, as the effects shown were observed when Retro-2 was added to the infection at 8 h *p.i.*, a time point at which the early steps of inclusion establishment are completed (Clausen, Christiansen *et al.* 1997). Furthermore, treatment of bacteria with Retro-2 prior to infection did not influence bacterial progeny formation (data not shown). The mechanism of action of Retro-2 is unclear but is believed to be mediated by binding to a yet unidentified host protein. Retro-2 was identified by screening for small molecules that inhibit the toxicity of ricin, Shiga-like toxins and cholera toxin B subunit (CTxB) (Stechmann, Bai *et al.* 2010). These toxins are, after uptake, transported along the retrograde pathway from the EE via the GA to the ER from where they are ultimately released into the cytosol. Surprisingly the compound does not affect compartment morphology of the TGN, endosomes or the ER and neither blocks trafficking of endogenous retrograde cargoes or other known intracellular trafficking pathways, but is very specific for the exogenous toxins and specifically block their transport from endosomes to the TGN (Stechmann, Bai *et al.* 2010). Surprisingly, the trafficking of the exogenous Shiga toxin depends fully on SNX1 whereas the CTxB does not (Bujny, Popoff *et al.* 2007), this therefore suggests that a either a SNX1 independent route is additionally inhibited by Retro-2, or the effect of Retro-2 is upstream of SNX1. Alternatively it might inhibit a downstream mechanism as the pathways converge. Ultimately, understanding the molecular mode of action of Retro-2 would greatly help to unravel the mechanisms that are contributing to the detrimental effect on bacterial progeny formation we observed.

In addition to the inhibition of retrograde trafficking of bacterial toxins, Retro-2 is effective at inhibiting the intracellular stages of development of human papilloma virus 16 (Lipovsky, Popa *et al.* 2013) as well as human and monkey polyomaviruses (Nelson, Carney *et al.* 2013) which both depend on retrograde trafficking. The most pronounced known effect of Retro-2 treatment on proteins involved in intracellular trafficking was the relocalization of syntaxin 5 and 6, two SNARE

proteins also involved in retrograde transport (Stechmann, Bai *et al.* 2010). This was assumed to be the basis for the detrimental effect of Retro-2 on the development of *Leishmania amazonensis* (Canton and Kima 2012), a parasitophorous vacuole dwelling organism shown to be sensitive to depletion of syntaxin 5 (Canton, Ndjamen *et al.* 2012). Syntaxin 6 was previously reported to recruited to the inclusion (Moore, Mead *et al.* 2011) and therefore might be one of the targets that should be studied further in Retro-2 treated infections. Lastly, the development of inhibitors of retrograde trafficking has only started and efforts are underway to improve the current inhibitors (Noel, Gupta *et al.* 2013, Yu, Park *et al.* 2013), paving the way towards clinical use of these compounds. Most importantly, in mice, Retro-2 showed no apparent toxicity at doses effective for treatment of ricin intoxication, even before optimization (Stechmann, Bai *et al.* 2010), thereby already proving retrograde trafficking to be an attractive novel drug target for the treatment of a broad range of diseases, including infections with *C. trachomatis*.

4.5 Conclusions and outlook

This work showed the feasibility of a systematic approach for probing the host pathogen interactome of *C. trachomatis* using state of the art proteomics in combination with traditional organelle purification techniques. Using this approach, we were able to identify and quantify over three hundred proteins that were not reported previously to be inclusion localized. These data for the first time allowed an unbiased and quantitative assessment of the inclusion proteome. This dataset is an important resource for all groups involved in the research of host pathogen interactions of *Chlamydia.* Furthermore, the protocol for the isolation of inclusions presented herein is an important tool for probing host pathogen interactions independently of the host cell context and presents a basis for the rapid establishment of inclusion isolation procedures for other strains and species of *Chlamydia*, enabling comparative analysis of host-pathogen interactions on a global level.

In the systematic analysis of our data, we were able to confirm previous reports on the recruitment of proteins implied in several membrane trafficking pathways, including a significant but poorly characterized contribution of ER derived proteins to the inclusion proteome. We furthermore identified retrograde trafficking as a hitherto not described factor in chlamydial infections.

Detailed analysis of the proteins identified to be involved in retrograde trafficking showed that SNX-BAR proteins are highly and specifically recruited to the inclusion by a mechanism which likely involves binding of PtdIns species on the inclusion, possibly in combination with their targeted modulation. We furthermore showed that retrograde trafficking is essential for the efficient intracellular replication of *Chlamydia* using the recently described inhibitor Retro-2.

Our current efforts focus on the mechanistic details of SNX-BAR recruitment, including its functional relevance and Retro-2 mediated inhibition in the infection context. Furthermore, we aim to assess the effects of Retro-2 treatment of inclusion in a global approach, by comparing treated and non-treated inclusions relatively.

Retrograde trafficking has recently been identified as involved in infections with the parasitic protozoan *Leishmania amazonensis* (Canton and Kima 2012), the Gram-positive bacteria *L. pneumophila* (Finsel, Ragaz *et al.* 2013) and even in the in entry of human papillomavirus (Lipovsky, Popa *et al.* 2013), underlining that retrograde trafficking is an important contributor to the interaction of intracellular pathogens and their eukaryotic hosts and deserves increased attention as drug target, as this research might lead to novel and effective therapies of a wide range of infectious diseases.

5. Bibliography

Abdelrahman, Y. M. and R. J. Belland (2005). "The chlamydial developmental cycle." FEMS Microbiol Rev **29**(5): 949-959.

Abromaitis, S. and R. S. Stephens (2009). "Attachment and entry of Chlamydia have distinct requirements for host protein disulfide isomerase." PLoS Pathog **5**(4): e1000357.

Agaisse, H. and I. Derre (2014). "The expression of the effector protein IncD in C. trachomatis mediates the recruitment of the lipid transfer protein CERT and the ER-resident protein VAPB to the inclusion membrane." Infect Immun.

Akporiaye, E. T., J. D. Rowatt, A. A. Aragon and O. G. Baca (1983). "Lysosomal response of a murine macrophage-like cell line persistently infected with Coxiella burnetii." Infect Immun **40**(3): 1155-1162.

Al-Younes, H. M., M. A. Al-Zeer, H. Khalil, J. Gussmann, A. Karlas, N. Machuy, V. Brinkmann, P. R. Braun and T. F. Meyer (2011). "Autophagy-independent function of MAP-LC3 during intracellular propagation of Chlamydia trachomatis." Autophagy **7**(8): 814-828.

Al-Younes, H. M., V. Brinkmann and T. F. Meyer (2004). "Interaction of Chlamydia trachomatis serovar L2 with the host autophagic pathway." Infect Immun **72**(8): 4751-4762.

Al-Younes, H. M., T. Rudel and T. F. Meyer (1999). "Characterization and intracellular trafficking pattern of vacuoles containing Chlamydia pneumoniae in human epithelial cells." Cell Microbiol **1**(3): 237-247.

Alix, E., S. Mukherjee and C. R. Roy (2011). "Subversion of membrane transport pathways by vacuolar pathogens." J Cell Biol **195**(6): 943-952.

Alvarez-Dominguez, C., A. M. Barbieri, W. Beron, A. Wandinger-Ness and P. D. Stahl (1996). "Phagocytosed live Listeria monocytogenes influences Rab5-regulated in vitro phagosome-endosome fusion." J Biol Chem **271**(23): 13834-13843.

Alzhanov, D. T., S. K. Weeks, J. R. Burnett and D. D. Rockey (2009). "Cytokinesis is blocked in mammalian cells transfected with Chlamydia trachomatis gene CT223." BMC Microbiol **9**: 2.

Aniento, F., N. Emans, G. Griffiths and J. Gruenberg (1993). "Cytoplasmic dynein-dependent vesicular transport from early to late endosomes." J Cell Biol **123**(6 Pt 1): 1373-1387.

Ashburner, M., C. A. Ball, J. A. Blake, D. Botstein, H. Butler, J. M. Cherry, A. P. Davis, K. Dolinski, S. S. Dwight, J. T. Eppig, M. A. Harris, D. P. Hill, L. Issel-Tarver, A. Kasarskis, S. Lewis, J. C. Matese, J. E. Richardson, M. Ringwald, G. M. Rubin and G. Sherlock (2000). "Gene ontology: tool for the unification of biology. The Gene Ontology Consortium." Nat Genet **25**(1): 25-29.

Attar, N. and P. J. Cullen (2010). "The retromer complex." Adv Enzyme Regul **50**(1): 216-236.

Baek, G. H., H. Cheng, V. Choe, X. Bao, J. Shao, S. Luo and H. Rao (2013). "Cdc48: A Swiss Army Knife of Cell Biology." J Amino Acids **2013**: 183421.

Bakowski, M. A., V. Braun and J. H. Brumell (2008). "Salmonella-containing vacuoles: directing traffic and nesting to grow." Traffic **9**(12): 2022-2031.

Bakowski, M. A., V. Braun, G. Y. Lam, T. Yeung, W. D. Heo, T. Meyer, B. B. Finlay, S. Grinstein and J. H. Brumell (2010). "The phosphoinositide phosphatase SopB manipulates membrane surface charge and trafficking of the Salmonella-containing vacuole." Cell Host Microbe **7**(6): 453-462.

Bannantine, J. P., R. S. Griffiths, W. Viratyosin, W. J. Brown and D. D. Rockey (2000). "A secondary structure motif predictive of protein localization to the chlamydial inclusion membrane." Cell Microbiol **2**(1): 35-47.

Bannantine, J. P., W. E. Stamm, R. J. Suchland and D. D. Rockey (1998). "Chlamydia trachomatis IncA is localized to the inclusion membrane and is recognized by antisera from infected humans and primates." Infect Immun **66**(12): 6017-6021.

Beatty, W. L. (2006). "Trafficking from CD63-positive late endocytic multivesicular bodies is essential for intracellular development of Chlamydia trachomatis." J Cell Sci **119**(Pt 2): 350-359.

Beatty, W. L. (2008). "Late endocytic multivesicular bodies intersect the chlamydial inclusion in the absence of CD63." Infect Immun **76**(7): 2872-2881.

Beeckman, D. S. and D. C. Vanrompay (2010). "Bacterial secretion systems with an emphasis on the chlamydial Type III secretion system." Curr Issues Mol Biol **12**(1): 17-41.

Behnia, R. and S. Munro (2005). "Organelle identity and the signposts for membrane traffic." Nature **438**(7068): 597-604.

Belfort, G. M. and K. V. Kandror (2003). "Cellugyrin and synaptogyrin facilitate targeting of synaptophysin to a ubiquitous synaptic vesicle-sized compartment in PC12 cells." J Biol Chem **278**(48): 47971-47978.

Belland, R., D. M. Ojcius and G. I. Byrne (2004). "Chlamydia." Nat Rev Microbiol **2**(7): 530-531.

Belland, R. J., G. Zhong, D. D. Crane, D. Hogan, D. Sturdevant, J. Sharma, W. L. Beatty and H. D. Caldwell (2003). "Genomic transcriptional profiling of the developmental cycle of Chlamydia trachomatis." Proc Natl Acad Sci U S A **100**(14): 8478-8483.

Beresford, N., S. Patel, J. Armstrong, B. Szoor, A. P. Fordham-Skelton and L. Tabernero (2007). "MptpB, a virulence factor from Mycobacterium tuberculosis, exhibits triple-specificity phosphatase activity." Biochem J **406**(1): 13-18.

Blagoev, B. and M. Mann (2006). "Quantitative proteomics to study mitogen-activated protein kinases." Methods **40**(3): 243-250.

Boncompain, G., C. Muller, V. Meas-Yedid, P. Schmitt-Kopplin, P. B. Lazarow and A. Subtil (2014). "The intracellular bacteria Chlamydia hijack peroxisomes and utilize their enzymatic capacity to produce bacteria-specific phospholipids." PLoS One **9**(1): e86196.

Bonifacino, J. S. and B. S. Glick (2004). "The mechanisms of vesicle budding and fusion." Cell **116**(2): 153-166.

Bonifacino, J. S. and R. Rojas (2006). "Retrograde transport from endosomes to the trans-Golgi network." Nat Rev Mol Cell Biol **7**(8): 568-579.

Brickman, T. J., C. E. Barry, 3rd and T. Hackstadt (1993). "Molecular cloning and expression of hctB encoding a strain-variant chlamydial histone-like protein with DNA-binding activity." J Bacteriol **175**(14): 4274-4281.

Brown, W. J., Y. A. Skeiky, P. Probst and D. D. Rockey (2002). "Chlamydial antigens colocalize within IncA-laden fibers extending from the inclusion membrane into the host cytosol." Infect Immun **70**(10): 5860-5864.

Brunham, R. C. and J. Rey-Ladino (2005). "Immunology of Chlamydia infection: implications for a Chlamydia trachomatis vaccine." Nat Rev Immunol **5**(2): 149-161.

Bugarcic, A., Y. Zhe, M. C. Kerr, J. Griffin, B. M. Collins and R. D. Teasdale (2011). "Vps26A and Vps26B subunits define distinct retromer complexes." Traffic **12**(12): 1759-1773.

Bujny, M. V., P. A. Ewels, S. Humphrey, N. Attar, M. A. Jepson and P. J. Cullen (2008). "Sorting nexin-1 defines an early phase of Salmonella-containing vacuole-remodeling during Salmonella infection." J Cell Sci **121**(Pt 12): 2027-2036.

Bujny, M. V., V. Popoff, L. Johannes and P. J. Cullen (2007). "The retromer component sorting nexin-1 is required for efficient retrograde transport of Shiga toxin from early endosome to the trans Golgi network." J Cell Sci **120**(Pt 12): 2010-2021.

Burton, M. J. and D. C. Mabey (2009). "The global burden of trachoma: a review." PLoS Negl Trop Dis **3**(10): e460.

Campbell-Valois, F. X., M. Trost, M. Chemali, B. D. Dill, A. Laplante, S. Duclos, S. Sadeghi, C. Rondeau, I. C. Morrow, C. Bell, E. Gagnon, K. Hatsuzawa, P. Thibault and M. Desjardins (2012). "Quantitative proteomics reveals that only a subset of the endoplasmic reticulum contributes to the phagosome." Mol Cell Proteomics **11**(7): M111 016378.

Campbell, L. A., A. Lee and C. C. Kuo (2006). "Cleavage of the N-linked oligosaccharide from the surfaces of Chlamydia species affects infectivity in the mouse model of lung infection." Infect Immun **74**(5): 3027-3029.

Canton, J. and P. E. Kima (2012). "Targeting host syntaxin-5 preferentially blocks Leishmania parasitophorous vacuole development in infected cells and limits experimental Leishmania infections." Am J Pathol **181**(4): 1348-1355.

Canton, J., B. Ndjamen, K. Hatsuzawa and P. E. Kima (2012). "Disruption of the fusion of Leishmania parasitophorous vacuoles with ER vesicles results in the control of the infection." Cell Microbiol **14**(6): 937-948.

Capmany, A., N. Leiva and M. T. Damiani (2011). "Golgi-associated Rab14, a new regulator for Chlamydia trachomatis infection outcome." Commun Integr Biol **4**(5): 590-593.

Carabeo, R. A., D. J. Mead and T. Hackstadt (2003). "Golgi-dependent transport of cholesterol to the Chlamydia trachomatis inclusion." Proc Natl Acad Sci U S A **100**(11): 6771-6776.

Carlton, J., M. Bujny, B. J. Peter, V. M. Oorschot, A. Rutherford, H. Mellor, J. Klumperman, H. T. McMahon and P. J. Cullen (2004). "Sorting nexin-1 mediates tubular endosome-to-TGN transport through coincidence sensing of high- curvature membranes and 3-phosphoinositides." Curr Biol **14**(20): 1791-1800.

Carlton, J. G., M. V. Bujny, B. J. Peter, V. M. Oorschot, A. Rutherford, R. S. Arkell, J. Klumperman, H. T. McMahon and P. J. Cullen (2005). "Sorting nexin-2 is associated with tubular elements of the early endosome, but is not essential for retromer-mediated endosome-to-TGN transport." J Cell Sci **118**(Pt 19): 4527-4539.

Casadevall, A. (2008). "Evolution of intracellular pathogens." Annu Rev Microbiol **62**: 19-33.

Centers for Disease Control and Prevention. (2010). "Chlamydial Infection." Sexually Transmitted Diseases Treatment Guidelines, 2010 Retrieved 26.03.14, 2014, from http://www.cdc.gov/std/treatment/2010/chlamydial-infections.htm.

Chen, C., D. Garcia-Santos, Y. Ishikawa, A. Seguin, L. Li, K. H. Fegan, G. J. Hildick-Smith, D. I. Shah, J. D. Cooney, W. Chen, M. J. King, Y. Y. Yien, I. J. Schultz, H. Anderson, A. J. Dalton, M. L. Freedman, P. D. Kingsley, J. Palis, S. M. Hattangadi, H. F. Lodish, D. M. Ward, J. Kaplan, T. Maeda, P. Ponka and B. H. Paw (2013). "Snx3 regulates recycling of the transferrin receptor and iron assimilation." Cell Metab **17**(3): 343-352.

Chen, X., J. A. Edwards, C. D. Logsdon, S. A. Ernst and J. A. Williams (2002). "Dominant negative Rab3D inhibits amylase release from mouse pancreatic acini." J Biol Chem **277**(20): 18002-18009.

Chi, R. J., J. Liu, M. West, J. Wang, G. Odorizzi and C. G. Burd (2014). "Fission of SNX-BAR-coated endosomal retrograde transport carriers is promoted by the dynamin-related protein Vps1." J Cell Biol **204**(5): 793-806.

Chiappino, M. L., C. Dawson, J. Schachter and B. A. Nichols (1995). "Cytochemical localization of glycogen in Chlamydia trachomatis inclusions." J Bacteriol **177**(18): 5358-5363.

Chin, E., K. Kirker, M. Zuck, G. James and K. Hybiske (2012). "Actin recruitment to the Chlamydia inclusion is spatiotemporally regulated by a mechanism that requires host and bacterial factors." PLoS One **7**(10): e46949.

Chua, J., I. Vergne, S. Master and V. Deretic (2004). "A tale of two lipids: Mycobacterium tuberculosis phagosome maturation arrest." Curr Opin Microbiol **7**(1): 71-77.

Clausen, J. D., G. Christiansen, H. U. Holst and S. Birkelund (1997). "Chlamydia trachomatis utilizes the host cell microtubule network during early events of infection." Mol Microbiol **25**(3): 441-449.

Cocchiaro, J. L., Y. Kumar, E. R. Fischer, T. Hackstadt and R. H. Valdivia (2008). "Cytoplasmic lipid droplets are translocated into the lumen of the Chlamydia trachomatis parasitophorous vacuole." Proc Natl Acad Sci U S A **105**(27): 9379-9384.

Collingro, A., P. Tischler, T. Weinmaier, T. Penz, E. Heinz, R. C. Brunham, T. D. Read, P. M. Bavoil, K. Sachse, S. Kahane, M. G. Friedman, T. Rattei, G. S. Myers and M. Horn "Unity in variety--the pan-genome of the Chlamydiae." Mol Biol Evol **28**(12): 3253-3270.

Collingro, A., P. Tischler, T. Weinmaier, T. Penz, E. Heinz, R. C. Brunham, T. D. Read, P. M. Bavoil, K. Sachse, S. Kahane, M. G. Friedman, T. Rattei, G. S. Myers and M. Horn (2011). "Unity in variety--the pan-genome of the Chlamydiae." Mol Biol Evol **28**(12): 3253-3270.

Cortes, C., K. A. Rzomp, A. Tvinnereim, M. A. Scidmore and B. Wizel (2007). "Chlamydia pneumoniae inclusion membrane protein Cpn0585 interacts with multiple Rab GTPases." Infect Immun **75**(12): 5586-5596.

Cox, J. and M. Mann (2008). "MaxQuant enables high peptide identification rates, individualized p.p.b.-range mass accuracies and proteome-wide protein quantification." Nat Biotechnol **26**(12): 1367-1372.

Cox, J. V., N. Naher, Y. M. Abdelrahman and R. J. Belland (2012). "Host HDL biogenesis machinery is recruited to the inclusion of Chlamydia trachomatis-infected cells and regulates chlamydial growth." Cell Microbiol **14**(10): 1497-1512.

Cozier, G. E., J. Carlton, A. H. McGregor, P. A. Gleeson, R. D. Teasdale, H. Mellor and P. J. Cullen (2002). "The phox homology (PX) domain-dependent, 3-phosphoinositide-mediated association of sorting nexin-1 with an early sorting endosomal compartment is required for its ability to regulate epidermal growth factor receptor degradation." J Biol Chem **277**(50): 48730-48736.

Cullen, P. J. and H. C. Korswagen (2012). "Sorting nexins provide diversity for retromer-dependent trafficking events." Nat Cell Biol **14**(1): 29-37.

Davis, C. H., J. E. Raulston and P. B. Wyrick (2002). "Protein disulfide isomerase, a component of the estrogen receptor complex, is associated with Chlamydia trachomatis serovar E attached to human endometrial epithelial cells." Infect Immun **70**(7): 3413-3418.

Dean, M., A. Rzhetsky and R. Allikmets (2001). "The human ATP-binding cassette (ABC) transporter superfamily." Genome Res **11**(7): 1156-1166.

Dehoux, P., R. Flores, C. Dauga, G. Zhong and A. Subtil (2011). "Multi-genome identification and characterization of chlamydiae-specific type III secretion substrates: the Inc proteins." BMC Genomics **12**: 109.

Delevoye, C., M. Nilges, P. Dehoux, F. Paumet, S. Perrinet, A. Dautry-Varsat and A. Subtil (2008). "SNARE protein mimicry by an intracellular bacterium." PLoS Pathog **4**(3): e1000022.

Derre, I., R. Swiss and H. Agaisse (2011). "The lipid transfer protein CERT interacts with the Chlamydia inclusion protein IncD and participates to ER-Chlamydia inclusion membrane contact sites." PLoS Pathog **7**(6): e1002092.

Di Paolo, G. and P. De Camilli (2006). "Phosphoinositides in cell regulation and membrane dynamics." Nature **443**(7112): 651-657.

Dong, N., Y. Zhu, Q. Lu, L. Hu, Y. Zheng and F. Shao (2012). "Structurally distinct bacterial TBC-like GAPs link Arf GTPase to Rab1 inactivation to counteract host defenses." Cell **150**(5): 1029-1041.

Doyle, M. J., M. P. Price and E. Frieden (1981). "Stabilization of amphibian and mammalian liver nuclei by zinc and other metal ions." Comp Biochem Physiol C **68C**(2): 115-120.

Drissi, R., M. L. Dubois and F. M. Boisvert (2013). "Proteomics methods for subcellular proteome analysis." FEBS J **280**(22): 5626-5634.

Dumoux, M., D. K. Clare, H. R. Saibil and R. D. Hayward (2012). "Chlamydiae assemble a pathogen synapse to hijack the host endoplasmic reticulum." Traffic **13**(12): 1612-1627.

Dunn, A. Y., M. W. Melville and J. Frydman (2001). "Review: cellular substrates of the eukaryotic chaperonin TRiC/CCT." J Struct Biol **135**(2): 176-184.

Eden, E., R. Navon, I. Steinfeld, D. Lipson and Z. Yakhini (2009). "GOrilla: a tool for discovery and visualization of enriched GO terms in ranked gene lists." BMC Bioinformatics **10**: 48.

Elwell, C. A., S. Jiang, J. H. Kim, A. Lee, T. Wittmann, K. Hanada, P. Melancon and J. N. Engel "Chlamydia trachomatis co-opts GBF1 and CERT to acquire host sphingomyelin for distinct roles during intracellular development." PLoS Pathog **7**(9): e1002198.

Elwell, C. A., S. Jiang, J. H. Kim, A. Lee, T. Wittmann, K. Hanada, P. Melancon and J. N. Engel (2011). "Chlamydia trachomatis co-opts GBF1 and CERT to acquire host sphingomyelin for distinct roles during intracellular development." PLoS Pathog **7**(9): e1002198.

Everett, K. D., R. M. Bush and A. A. Andersen (1999). "Emended description of the order Chlamydiales, proposal of Parachlamydiaceae fam. nov. and Simkaniaceae fam. nov., each containing one monotypic genus, revised taxonomy of the family Chlamydiaceae, including a new genus and five new species, and standards for the identification of organisms." Int J Syst Bacteriol **49 Pt 2**: 415-440.

Fadel, S. and A. Eley (2007). "Chlamydia trachomatis OmcB protein is a surface-exposed glycosaminoglycan-dependent adhesin." J Med Microbiol **56**(Pt 1): 15-22.

Faro, S. (1985). "Chlamydia trachomatis infection in women." J Reprod Med **30**(3 Suppl): 273-278.

Fields, K. A., E. Fischer and T. Hackstadt (2002). "Inhibition of fusion of Chlamydia trachomatis inclusions at 32 degrees C correlates with restricted export of IncA." Infect Immun **70**(7): 3816-3823.

Fields, K. A. and T. Hackstadt (2002). "The chlamydial inclusion: escape from the endocytic pathway." Annu Rev Cell Dev Biol **18**: 221-245.

Finsel, I., C. Ragaz, C. Hoffmann, C. F. Harrison, S. Weber, V. A. van Rahden, L. Johannes and H. Hilbi (2013). "The Legionella effector RidL inhibits retrograde trafficking to promote intracellular replication." Cell Host Microbe **14**(1): 38-50.

Fisher, D. J., R. E. Fernandez, N. E. Adams and A. T. Maurelli (2012). "Uptake of biotin by Chlamydia Spp. through the use of a bacterial transporter (BioY) and a host-cell transporter (SMVT)." PLoS One **7**(9): e46052.

Fisher, D. J., R. E. Fernandez and A. T. Maurelli (2013). "Chlamydia trachomatis transports NAD via the Npt1 ATP/ADP translocase." J Bacteriol **195**(15): 3381-3386.

Foster, L. J., C. L. de Hoog, Y. Zhang, Y. Zhang, X. Xie, V. K. Mootha and M. Mann (2006). "A mammalian organelle map by protein correlation profiling." Cell **125**(1): 187-199.

Franceschini, A., D. Szklarczyk, S. Frankild, M. Kuhn, M. Simonovic, A. Roth, J. Lin, P. Minguez, P. Bork, C. von Mering and L. J. Jensen (2013). "STRING v9.1: protein-protein interaction networks, with increased coverage and integration." Nucleic Acids Res **41**(Database issue): D808-815.

Fratti, R. A., J. Chua, I. Vergne and V. Deretic (2003). "Mycobacterium tuberculosis glycosylated phosphatidylinositol causes phagosome maturation arrest." Proc Natl Acad Sci U S A **100**(9): 5437-5442.

Friis, R. R. (1972). "Interaction of L cells and Chlamydia psittaci: entry of the parasite and host responses to its development." J Bacteriol **110**(2): 706-721.

Frost, A., V. M. Unger and P. De Camilli (2009). "The BAR domain superfamily: membrane-molding macromolecules." Cell **137**(2): 191-196.

Fugier, E., S. P. Salcedo, C. de Chastellier, M. Pophillat, A. Muller, V. Arce-Gorvel, P. Fourquet and J. P. Gorvel (2009). "The glyceraldehyde-3-phosphate dehydrogenase and the small GTPase Rab 2 are crucial for Brucella replication." PLoS Pathog **5**(6): e1000487.

Fujimoto, M. and T. Hayashi (2011). "New insights into the role of mitochondria-associated endoplasmic reticulum membrane." Int Rev Cell Mol Biol **292**: 73-117.

Galvez, T., J. Gilleron, M. Zerial and G. A. O'Sullivan (2012). "SnapShot: Mammalian Rab proteins in endocytic trafficking." Cell **151**(1): 234-234 e232.

Garin, J., R. Diez, S. Kieffer, J. F. Dermine, S. Duclos, E. Gagnon, R. Sadoul, C. Rondeau and M. Desjardins (2001). "The phagosome proteome: insight into phagosome functions." J Cell Biol **152**(1): 165-180.

Ghigo, E., M. I. Colombo and R. A. Heinzen (2012). "The Coxiella burnetii parasitophorous vacuole." Adv Exp Med Biol **984**: 141-169.

Ghosh, P., N. M. Dahms and S. Kornfeld (2003). "Mannose 6-phosphate receptors: new twists in the tale." Nat Rev Mol Cell Biol **4**(3): 202-212.

Gomez, T. S. and D. D. Billadeau (2009). "A FAM21-containing WASH complex regulates retromer-dependent sorting." Dev Cell **17**(5): 699-711.

Gotthardt, D., H. J. Warnatz, O. Henschel, F. Bruckert, M. Schleicher and T. Soldati (2002). "High-resolution dissection of phagosome maturation reveals distinct membrane trafficking phases." Mol Biol Cell **13**(10): 3508-3520.

Grassl, G. A. and B. B. Finlay (2008). "Pathogenesis of enteric Salmonella infections." Curr Opin Gastroenterol **24**(1): 22-26.

Grieshaber, N. A., E. R. Fischer, D. J. Mead, C. A. Dooley and T. Hackstadt (2004). "Chlamydial histone-DNA interactions are disrupted by a metabolite in the methylerythritol phosphate pathway of isoprenoid biosynthesis." Proc Natl Acad Sci U S A **101**(19): 7451-7456.

Grieshaber, S., J. A. Swanson and T. Hackstadt (2002). "Determination of the physical environment within the Chlamydia trachomatis inclusion using ion-selective ratiometric probes." Cell Microbiol **4**(5): 273-283.

Grieshaber, S. S., N. A. Grieshaber and T. Hackstadt (2003). "Chlamydia trachomatis uses host cell dynein to traffic to the microtubule-organizing center in a p50 dynamitin-independent process." J Cell Sci **116**(Pt 18): 3793-3802.

Grieshaber, S. S., N. A. Grieshaber, N. Miller and T. Hackstadt (2006). "Chlamydia trachomatis causes centrosomal defects resulting in chromosomal segregation abnormalities." Traffic **7**(8): 940-949.

Griffin, C. T., J. Trejo and T. Magnuson (2005). "Genetic evidence for a mammalian retromer complex containing sorting nexins 1 and 2." Proc Natl Acad Sci U S A **102**(42): 15173-15177.

Griffiths, G. and K. Simons (1986). "The trans Golgi network: sorting at the exit site of the Golgi complex." Science **234**(4775): 438-443.

Guermonprez, P., L. Saveanu, M. Kleijmeer, J. Davoust, P. Van Endert and S. Amigorena (2003). "ER-phagosome fusion defines an MHC class I cross-presentation compartment in dendritic cells." Nature **425**(6956): 397-402.

Gurumurthy, R. K., A. P. Maurer, N. Machuy, S. Hess, K. P. Pleissner, J. Schuchhardt, T. Rudel and T. F. Meyer (2010). "A loss-of-function screen reveals Ras- and Raf-independent MEK-ERK signaling during Chlamydia trachomatis infection." Sci Signal **3**(113): ra21.

Hackstadt, T., D. D. Rockey, R. A. Heinzen and M. A. Scidmore (1996). "Chlamydia trachomatis interrupts an exocytic pathway to acquire endogenously synthesized sphingomyelin in transit from the Golgi apparatus to the plasma membrane." EMBO J **15**(5): 964-977.

Hackstadt, T., M. A. Scidmore-Carlson, E. I. Shaw and E. R. Fischer (1999). "The Chlamydia trachomatis IncA protein is required for homotypic vesicle fusion." Cell Microbiol **1**(2): 119-130.

Hackstadt, T., M. A. Scidmore and D. D. Rockey (1995). "Lipid metabolism in Chlamydia trachomatis-infected cells: directed trafficking of Golgi-derived sphingolipids to the chlamydial inclusion." Proc Natl Acad Sci U S A **92**(11): 4877-4881.

Haggerty, C. L., S. L. Gottlieb, B. D. Taylor, N. Low, F. Xu and R. B. Ness (2010). "Risk of sequelae after Chlamydia trachomatis genital infection in women." J Infect Dis **201 Suppl 2**: S134-155.

Harbour, M. E., S. Y. Breusegem, R. Antrobus, C. Freeman, E. Reid and M. N. Seaman (2010). "The cargo-selective retromer complex is a recruiting hub for protein complexes that regulate endosomal tubule dynamics." J Cell Sci **123**(Pt 21): 3703-3717.

Harrison, M. S., C. S. Hung, T. T. Liu, R. Christiano, T. C. Walther and C. G. Burd (2014). "A mechanism for retromer endosomal coat complex assembly with cargo." Proc Natl Acad Sci U S A **111**(1): 267-272.

Harterink, M., F. Port, M. J. Lorenowicz, I. J. McGough, M. Silhankova, M. C. Betist, J. R. van Weering, R. G. van Heesbeen, T. C. Middelkoop, K. Basler, P. J. Cullen and H. C. Korswagen (2011). "A SNX3-dependent retromer pathway mediates retrograde transport of the Wnt sorting receptor Wntless and is required for Wnt secretion." Nat Cell Biol **13**(8): 914-923.

Hasegawa, A., L. F. Sogo, M. Tan and C. Sutterlin (2009). "Host complement regulatory protein CD59 is transported to the chlamydial inclusion by a Golgi apparatus-independent pathway." Infect Immun **77**(4): 1285-1292.

Hatch, G. M. and G. McClarty (1998). "Phospholipid composition of purified Chlamydia trachomatis mimics that of the eucaryotic host cell." Infect Immun **66**(8): 3727-3735.

Hatch, T. P., M. Miceli and J. E. Sublett (1986). "Synthesis of disulfide-bonded outer membrane proteins during the developmental cycle of Chlamydia psittaci and Chlamydia trachomatis." J Bacteriol **165**(2): 379-385.

Hediger, M. A., B. Clemencon, R. E. Burrier and E. A. Bruford (2013). "The ABCs of membrane transporters in health and disease (SLC series): introduction." Mol Aspects Med **34**(2-3): 95-107.

Heinzen, R. A. and T. Hackstadt (1997). "The Chlamydia trachomatis parasitophorous vacuolar membrane is not passively permeable to low-molecular-weight compounds." Infect Immun **65**(3): 1088-1094.

Heinzen, R. A., M. A. Scidmore, D. D. Rockey and T. Hackstadt (1996). "Differential interaction with endocytic and exocytic pathways distinguish parasitophorous vacuoles of Coxiella burnetii and Chlamydia trachomatis." Infect Immun **64**(3): 796-809.

Hernandez, L. D., K. Hueffer, M. R. Wenk and J. E. Galan (2004). "Salmonella modulates vesicular traffic by altering phosphoinositide metabolism." Science **304**(5678): 1805-1807.

Heuer, D., A. Rejman Lipinski, N. Machuy, A. Karlas, A. Wehrens, F. Siedler, V. Brinkmann and T. F. Meyer (2009). "Chlamydia causes fragmentation of the Golgi compartment to ensure reproduction." Nature **457**(7230): 731-735.

Hilbi, H., S. Weber and I. Finsel (2011). "Anchors for effectors: subversion of phosphoinositide lipids by legionella." Front Microbiol **2**: 91.

Hoffmann, C., I. Finsel, A. Otto, G. Pfaffinger, E. Rothmeier, M. Hecker, D. Becher and H. Hilbi (2013). "Functional analysis of novel Rab GTPases identified in the proteome of purified Legionella-containing vacuoles from macrophages." Cell Microbiol.

Hong, Z., Y. Yang, C. Zhang, Y. Niu, K. Li, X. Zhao and J. J. Liu (2009). "The retromer component SNX6 interacts with dynactin p150(Glued) and mediates endosome-to-TGN transport." Cell Res **19**(12): 1334-1349.

Horn, M. (2008). "Chlamydiae as symbionts in eukaryotes." Annu Rev Microbiol **62**: 113-131.

Horn, M., A. Collingro, S. Schmitz-Esser, C. L. Beier, U. Purkhold, B. Fartmann, P. Brandt, G. J. Nyakatura, M. Droege, D. Frishman, T. Rattei, H. W. Mewes and M. Wagner (2004). "Illuminating the evolutionary history of chlamydiae." Science **304**(5671): 728-730.

Hornig-Do, H. T., G. Gunther, M. Bust, P. Lehnartz, A. Bosio and R. J. Wiesner (2009). "Isolation of functional pure mitochondria by superparamagnetic microbeads." Anal Biochem **389**(1): 1-5.

Horwitz, M. A. (1983). "The Legionnaires' disease bacterium (Legionella pneumophila) inhibits phagosome-lysosome fusion in human monocytes." J Exp Med **158**(6): 2108-2126.

Houde, M., S. Bertholet, E. Gagnon, S. Brunet, G. Goyette, A. Laplante, M. F. Princiotta, P. Thibault, D. Sacks and M. Desjardins (2003). "Phagosomes are competent organelles for antigen cross-presentation." Nature **425**(6956): 402-406.

Huang da, W., B. T. Sherman and R. A. Lempicki (2009). "Systematic and integrative analysis of large gene lists using DAVID bioinformatics resources." Nat Protoc **4**(1): 44-57.

Hunter, S., P. Jones, A. Mitchell, R. Apweiler, T. K. Attwood, A. Bateman, T. Bernard, D. Binns, P. Bork, S. Burge, E. de Castro, P. Coggill, M. Corbett, U. Das, L. Daugherty, L. Duquenne, R. D. Finn, M. Fraser, J. Gough, D. Haft, N. Hulo, D. Kahn, E. Kelly, I. Letunic, D. Lonsdale, R. Lopez, M. Madera, J. Maslen, C. McAnulla, J. McDowall, C. McMenamin, H. Mi, P. Mutowo-Muellenet, N. Mulder, D. Natale, C. Orengo, S. Pesseat, M. Punta, A. F. Quinn, C. Rivoire, A. Sangrador-Vegas, J. D. Selengut, C. J. Sigrist, M. Scheremetjew, J. Tate, M. Thimmajanarthanan, P. D. Thomas, C. H. Wu, C. Yeats and S. Y. Yong (2012). "InterPro in 2011: new developments in the family and domain prediction database." Nucleic Acids Res **40**(Database issue): D306-312.

Huotari, J. and A. Helenius (2011). "Endosome maturation." EMBO J **30**(17): 3481-3500.

Hybiske, K. and R. S. Stephens (2007). "Mechanisms of Chlamydia trachomatis entry into nonphagocytic cells." Infect Immun **75**(8): 3925-3934.

Hybiske, K. and R. S. Stephens (2007). "Mechanisms of host cell exit by the intracellular bacterium Chlamydia." Proc Natl Acad Sci U S A **104**(27): 11430-11435.

Isberg, R. R., T. J. O'Connor and M. Heidtman (2009). "The Legionella pneumophila replication vacuole: making a cosy niche inside host cells." Nat Rev Microbiol **7**(1): 13-24.

Ishihama, Y., J. Rappsilber and M. Mann (2006). "Modular stop and go extraction tips with stacked disks for parallel and multidimensional Peptide fractionation in proteomics." J Proteome Res **5**(4): 988-994.

Janz, R. and T. C. Sudhof (1998). "Cellugyrin, a novel ubiquitous form of synaptogyrin that is phosphorylated by pp60c-src." J Biol Chem **273**(5): 2851-2857.
Jehl, M. A., R. Arnold and T. Rattei (2011). "Effective--a database of predicted secreted bacterial proteins." Nucleic Acids Res **39**(Database issue): D591-595.
Jewett, T. J., E. R. Fischer, D. J. Mead and T. Hackstadt (2006). "Chlamydial TARP is a bacterial nucleator of actin." Proc Natl Acad Sci U S A **103**(42): 15599-15604.
Johannes, L. and V. Popoff (2008). "Tracing the retrograde route in protein trafficking." Cell **135**(7): 1175-1187.
Johannes, L. and C. Wunder (2011). "Retrograde transport: two (or more) roads diverged in an endosomal tree?" Traffic **12**(8): 956-962.
Johnson, C. M. and D. J. Fisher (2013). "Site-specific, insertional inactivation of incA in Chlamydia trachomatis using a group II intron." PLoS One **8**(12): e83989.
Johnson, K. A., M. Tan and C. Sutterlin (2009). "Centrosome abnormalities during a Chlamydia trachomatis infection are caused by dysregulation of the normal duplication pathway." Cell Microbiol **11**(7): 1064-1073.
Kagan, J. C. and C. R. Roy (2002). "Legionella phagosomes intercept vesicular traffic from endoplasmic reticulum exit sites." Nat Cell Biol **4**(12): 945-954.
Kanai, Y., H. Segawa, K. Miyamoto, H. Uchino, E. Takeda and H. Endou (1998). "Expression cloning and characterization of a transporter for large neutral amino acids activated by the heavy chain of 4F2 antigen (CD98)." J Biol Chem **273**(37): 23629-23632.
Kinchen, J. M. and K. S. Ravichandran (2008). "Phagosome maturation: going through the acid test." Nat Rev Mol Cell Biol **9**(10): 781-795.
Knop, M., E. Aareskjold, G. Bode and V. Gerke (2004). "Rab3D and annexin A2 play a role in regulated secretion of vWF, but not tPA, from endothelial cells." EMBO J **23**(15): 2982-2992.
Koharudin, L. M., W. Furey, H. Liu, Y. J. Liu and A. M. Gronenborn (2009). "The phox domain of sorting nexin 5 lacks phosphatidylinositol 3-phosphate (PtdIns(3)P) specificity and preferentially binds to phosphatidylinositol 4,5-bisphosphate (PtdIns(4,5)P2)." J Biol Chem **284**(35): 23697-23707.
Kumar, Y., J. Cocchiaro and R. H. Valdivia (2006). "The obligate intracellular pathogen Chlamydia trachomatis targets host lipid droplets." Curr Biol **16**(16): 1646-1651.
Kumar, Y. and R. H. Valdivia (2008). "Actin and intermediate filaments stabilize the Chlamydia trachomatis vacuole by forming dynamic structural scaffolds." Cell Host Microbe **4**(2): 159-169.
Laemmli, U. K. (1970). "Cleavage of structural proteins during the assembly of the head of bacteriophage T4." Nature **227**(5259): 680-685.
Lawn, A. M., W. A. Blyth and J. Taverne (1973). "Interactions of TRIC agents with macrophages and BHK-21 cells observed by electron microscopy." J Hyg (Lond) **71**(3): 515-528.
Lee, B. Y., D. Jethwaney, B. Schilling, D. L. Clemens, B. W. Gibson and M. A. Horwitz (2010). "The Mycobacterium bovis bacille Calmette-Guerin phagosome proteome." Mol Cell Proteomics **9**(1): 32-53.
Leiva, N., A. Capmany and M. T. Damiani (2013). "Rab11-family of interacting protein 2 associates with chlamydial inclusions through its Rab-binding domain and promotes bacterial multiplication." Cell Microbiol **15**(1): 114-129.
Li, L. V., K. Bakirtzi, R. T. Watson, J. E. Pessin and K. V. Kandror (2009). "The C-terminus of GLUT4 targets the transporter to the perinuclear compartment but not to the insulin-responsive vesicles." Biochem J **419**(1): 105-112, 101 p following 112.
Li, Q., C. Jagannath, P. K. Rao, C. R. Singh and G. Lostumbo (2010). "Analysis of phagosomal proteomes: from latex-bead to bacterial phagosomes." Proteomics **10**(22): 4098-4116.
Li, Q., C. R. Singh, S. Ma, N. D. Price and C. Jagannath (2011). "Label-free proteomics and systems biology analysis of mycobacterial phagosomes in dendritic cells and macrophages." J Proteome Res **10**(5): 2425-2439.

Li, Z., C. Chen, D. Chen, Y. Wu, Y. Zhong and G. Zhong (2008). "Characterization of fifty putative inclusion membrane proteins encoded in the Chlamydia trachomatis genome." Infect Immun **76**(6): 2746-2757.

Liao, H. J. and G. Carpenter (2007). "Role of the Sec61 translocon in EGF receptor trafficking to the nucleus and gene expression." Mol Biol Cell **18**(3): 1064-1072.

Lipovsky, A., A. Popa, G. Pimienta, M. Wyler, A. Bhan, L. Kuruvilla, M. A. Guie, A. C. Poffenberger, C. D. Nelson, W. J. Atwood and D. DiMaio (2013). "Genome-wide siRNA screen identifies the retromer as a cellular entry factor for human papillomavirus." Proc Natl Acad Sci U S A **110**(18): 7452-7457.

Liu, X., M. Afrane, D. E. Clemmer, G. Zhong and D. E. Nelson (2010). "Identification of Chlamydia trachomatis outer membrane complex proteins by differential proteomics." J Bacteriol **192**(11): 2852-2860.

Luhrmann, A. and A. Haas (2000). "A method to purify bacteria-containing phagosomes from infected macrophages." Methods Cell Sci **22**(4): 329-341.

Lutter, E. I., A. C. Barger, V. Nair and T. Hackstadt (2013). "Chlamydia trachomatis inclusion membrane protein CT228 recruits elements of the myosin phosphatase pathway to regulate release mechanisms." Cell Rep **3**(6): 1921-1931.

Lutter, E. I., C. Martens and T. Hackstadt (2012). "Evolution and conservation of predicted inclusion membrane proteins in chlamydiae." Comp Funct Genomics **2012**: 362104.

Mabey, D. and R. W. Peeling (2002). "Lymphogranuloma venereum." Sex Transm Infect **78**(2): 90-92.

Majeed, M., K. H. Krause, R. A. Clark, E. Kihlstrom and O. Stendahl (1999). "Localization of intracellular Ca2+ stores in HeLa cells during infection with Chlamydia trachomatis." J Cell Sci **112 (Pt 1)**: 35-44.

Mari, M., M. V. Bujny, D. Zeuschner, W. J. Geerts, J. Griffith, C. M. Petersen, P. J. Cullen, J. Klumperman and H. J. Geuze (2008). "SNX1 defines an early endosomal recycling exit for sortilin and mannose 6-phosphate receptors." Traffic **9**(3): 380-393.

Mastroberardino, L., B. Spindler, R. Pfeiffer, P. J. Skelly, J. Loffing, C. B. Shoemaker and F. Verrey (1998). "Amino-acid transport by heterodimers of 4F2hc/CD98 and members of a permease family." Nature **395**(6699): 288-291.

Matsumoto, A. (1981). "Isolation and electron microscopic observations of intracytoplasmic inclusions containing Chlamydia psittaci." J Bacteriol **145**(1): 605-612.

Matsumoto, A., H. Bessho, K. Uehira and T. Suda (1991). "Morphological studies of the association of mitochondria with chlamydial inclusions and the fusion of chlamydial inclusions." J Electron Microsc (Tokyo) **40**(5): 356-363.

Maurer, A. P., A. Mehlitz, H. J. Mollenkopf and T. F. Meyer (2007). "Gene expression profiles of Chlamydophila pneumoniae during the developmental cycle and iron depletion-mediated persistence." PLoS Pathog **3**(6): e83.

McGough, I. J. and P. J. Cullen (2011). "Recent advances in retromer biology." Traffic **12**(8): 963-971.

Mecaskey, J. W., C. A. Knirsch, J. A. Kumaresan and J. A. Cook (2003). "The possibility of eliminating blinding trachoma." Lancet Infect Dis **3**(11): 728-734.

Menozzi, F. D., K. Pethe, P. Bifani, F. Soncin, M. J. Brennan and C. Locht (2002). "Enhanced bacterial virulence through exploitation of host glycosaminoglycans." Mol Microbiol **43**(6): 1379-1386.

Merino-Trigo, A., M. C. Kerr, F. Houghton, A. Lindberg, C. Mitchell, R. D. Teasdale and P. A. Gleeson (2004). "Sorting nexin 5 is localized to a subdomain of the early endosomes and is recruited to the plasma membrane following EGF stimulation." J Cell Sci **117**(Pt 26): 6413-6424.

Mills, S. D. and B. B. Finlay (1998). "Isolation and characterization of Salmonella typhimurium and Yersinia pseudotuberculosis-containing phagosomes from infected mouse macrophages: Y. pseudotuberculosis traffics to terminal lysosomes where they are degraded." Eur J Cell Biol **77**(1): 35-47.

Miserey-Lenkei, S., F. Waharte, A. Boulet, M. H. Cuif, D. Tenza, A. El Marjou, G. Raposo, J. Salamero, L. Heliot, B. Goud and S. Monier (2007). "Rab6-interacting protein 1 links Rab6 and Rab11 function." Traffic **8**(10): 1385-1403.

Mital, J., N. J. Miller, D. W. Dorward, C. A. Dooley and T. Hackstadt (2013). "Role for chlamydial inclusion membrane proteins in inclusion membrane structure and biogenesis." PLoS One **8**(5): e63426.

Mital, J., N. J. Miller, E. R. Fischer and T. Hackstadt (2010). "Specific chlamydial inclusion membrane proteins associate with active Src family kinases in microdomains that interact with the host microtubule network." Cell Microbiol **12**(9): 1235-1249.

Molleken, K., E. Becker and J. H. Hegemann (2013). "The Chlamydia pneumoniae invasin protein Pmp21 recruits the EGF receptor for host cell entry." PLoS Pathog **9**(4): e1003325.

Moore, E. R., E. R. Fischer, D. J. Mead and T. Hackstadt (2008). "The chlamydial inclusion preferentially intercepts basolaterally directed sphingomyelin-containing exocytic vacuoles." Traffic **9**(12): 2130-2140.

Moore, E. R., D. J. Mead, C. A. Dooley, J. Sager and T. Hackstadt (2011). "The trans-Golgi SNARE syntaxin 6 is recruited to the chlamydial inclusion membrane." Microbiology **157**(Pt 3): 830-838.

Moorhead, A. M., J. Y. Jung, A. Smirnov, S. Kaufer and M. A. Scidmore (2010). "Multiple host proteins that function in phosphatidylinositol-4-phosphate metabolism are recruited to the chlamydial inclusion." Infect Immun **78**(5): 1990-2007.

Moorhead, A. R., K. A. Rzomp and M. A. Scidmore (2007). "The Rab6 effector Bicaudal D1 associates with Chlamydia trachomatis inclusions in a biovar-specific manner." Infect Immun **75**(2): 781-791.

Moulder, J. W. (1991). "Interaction of chlamydiae and host cells in vitro." Microbiol Rev **55**(1): 143-190.

Mukhopadhyay, S., R. D. Miller and J. T. Summersgill (2004). "Analysis of altered protein expression patterns of Chlamydia pneumoniae by an integrated proteome-works system." J Proteome Res **3**(4): 878-883.

Munier-Lehmann, H., F. Mauxion and B. Hoflack (1996). "Function of the two mannose 6-phosphate receptors in lysosomal enzyme transport." Biochem Soc Trans **24**(1): 133-136.

Nagaraj, N., J. R. Wisniewski, T. Geiger, J. Cox, M. Kircher, J. Kelso, S. Paabo and M. Mann (2011). "Deep proteome and transcriptome mapping of a human cancer cell line." Mol Syst Biol **7**: 548.

Nelson, C. D., D. W. Carney, A. Derdowski, A. Lipovsky, G. V. Gee, B. O'Hara, P. Williard, D. DiMaio, J. K. Sello and W. J. Atwood (2013). "A retrograde trafficking inhibitor of ricin and Shiga-like toxins inhibits infection of cells by human and monkey polyomaviruses." MBio **4**(6): e00729-00713.

Nicholson, T. L., L. Olinger, K. Chong, G. Schoolnik and R. S. Stephens (2003). "Global stage-specific gene regulation during the developmental cycle of Chlamydia trachomatis." J Bacteriol **185**(10): 3179-3189.

Niu, Y., C. Zhang, Z. Sun, Z. Hong, K. Li, D. Sun, Y. Yang, C. Tian, W. Gong and J. J. Liu (2013). "PtdIns(4)P regulates retromer-motor interaction to facilitate dynein-cargo dissociation at the trans-Golgi network." Nat Cell Biol **15**(4): 417-429.

Noel, R., N. Gupta, V. Pons, A. Goudet, M. D. Garcia-Castillo, A. Michau, J. Martinez, D. A. Buisson, L. Johannes, D. Gillet, J. Barbier and J. C. Cintrat (2013). "N-methyldihydroquinazolinone derivatives of Retro-2 with enhanced efficacy against Shiga toxin." J Med Chem **56**(8): 3404-3413.

Nunes, P., D. Cornut, V. Bochet, U. Hasler, M. Oh-Hora, J. M. Waldburger and N. Demaurex (2012). "STIM1 juxtaposes ER to phagosomes, generating Ca(2)(+) hotspots that boost phagocytosis." Curr Biol **22**(21): 1990-1997.

Ong, S. E., B. Blagoev, I. Kratchmarova, D. B. Kristensen, H. Steen, A. Pandey and M. Mann (2002). "Stable isotope labeling by amino acids in cell culture, SILAC, as a simple and accurate approach to expression proteomics." Mol Cell Proteomics **1**(5): 376-386.

Ouellette, S. P., F. C. Dorsey, S. Moshiach, J. L. Cleveland and R. A. Carabeo (2011). "Chlamydia species-dependent differences in the growth requirement for lysosomes." PLoS One **6**(3): e16783.

Park, E. and T. A. Rapoport (2012). "Mechanisms of Sec61/SecY-mediated protein translocation across membranes." Annu Rev Biophys **41**: 21-40.

Park, J. G., J. N. Kahn, N. E. Tumer and Y. P. Pang (2012). "Chemical structure of Retro-2, a compound that protects cells against ribosome-inactivating proteins." Sci Rep **2**: 631.

Paumet, F., J. Wesolowski, A. Garcia-Diaz, C. Delevoye, N. Aulner, H. A. Shuman, A. Subtil and J. E. Rothman (2009). "Intracellular bacteria encode inhibitory SNARE-like proteins." PLoS One **4**(10): e7375.

Peeling, R. W. and R. C. Brunham (1996). "Chlamydiae as pathogens: new species and new issues." Emerg Infect Dis **2**(4): 307-319.

Perara, E., D. Ganem and J. N. Engel (1992). "A developmentally regulated chlamydial gene with apparent homology to eukaryotic histone H1." Proc Natl Acad Sci U S A **89**(6): 2125-2129.

Perfettini, J. L., J. C. Reed, N. Israel, J. C. Martinou, A. Dautry-Varsat and D. M. Ojcius (2002). "Role of Bcl-2 family members in caspase-independent apoptosis during Chlamydia infection." Infect Immun **70**(1): 55-61.

Pernas, L., Y. Adomako-Ankomah, A. J. Shastri, S. E. Ewald, M. Treeck, J. P. Boyle and J. C. Boothroyd (2014). "Toxoplasma Effector MAF1 Mediates Recruitment of Host Mitochondria and Impacts the Host Response." PLoS Biol **12**(4): e1001845.

Peter, B. J., H. M. Kent, I. G. Mills, Y. Vallis, P. J. Butler, P. R. Evans and H. T. McMahon (2004). "BAR domains as sensors of membrane curvature: the amphiphysin BAR structure." Science **303**(5657): 495-499.

Peters, J., D. P. Wilson, G. Myers, P. Timms and P. M. Bavoil (2007). "Type III secretion a la Chlamydia." Trends Microbiol **15**(6): 241-251.

Pfeffer, S. and D. Aivazian (2004). "Targeting Rab GTPases to distinct membrane compartments." Nat Rev Mol Cell Biol **5**(11): 886-896.

Pokrovskaya, I. D., J. W. Szwedo, A. Goodwin, T. V. Lupashina, U. M. Nagarajan and V. V. Lupashin (2012). "Chlamydia trachomatis hijacks intra-Golgi COG complex-dependent vesicle trafficking pathway." Cell Microbiol **14**(5): 656-668.

Prakriya, M., S. Feske, Y. Gwack, S. Srikanth, A. Rao and P. G. Hogan (2006). "Orai1 is an essential pore subunit of the CRAC channel." Nature **443**(7108): 230-233.

Puolakkainen, M., C. C. Kuo and L. A. Campbell (2005). "Chlamydia pneumoniae uses the mannose 6-phosphate/insulin-like growth factor 2 receptor for infection of endothelial cells." Infect Immun **73**(8): 4620-4625.

Ragaz, C., H. Pietsch, S. Urwyler, A. Tiaden, S. S. Weber and H. Hilbi (2008). "The Legionella pneumophila phosphatidylinositol-4 phosphate-binding type IV substrate SidC recruits endoplasmic reticulum vesicles to a replication-permissive vacuole." Cell Microbiol **10**(12): 2416-2433.

Rao, P. K., C. R. Singh, C. Jagannath and Q. Li (2009). "A systems biology approach to study the phagosomal proteome modulated by mycobacterial infections." Int J Clin Exp Med **2**(3): 233-247.

Rappsilber, J., Y. Ishihama and M. Mann (2003). "Stop and go extraction tips for matrix-assisted laser desorption/ionization, nanoelectrospray, and LC/MS sample pretreatment in proteomics." Anal Chem **75**(3): 663-670.

Rappsilber, J., M. Mann and Y. Ishihama (2007). "Protocol for micro-purification, enrichment, pre-fractionation and storage of peptides for proteomics using StageTips." Nat Protoc **2**(8): 1896-1906.

Rees, D. C., E. Johnson and O. Lewinson (2009). "ABC transporters: the power to change." Nat Rev Mol Cell Biol **10**(3): 218-227.

Rejman Lipinski, A., J. Heymann, C. Meissner, A. Karlas, V. Brinkmann, T. F. Meyer and D. Heuer (2009). "Rab6 and Rab11 regulate Chlamydia trachomatis development and golgin-84-dependent Golgi fragmentation." PLoS Pathog **5**(10): e1000615.

Rink, J., E. Ghigo, Y. Kalaidzidis and M. Zerial (2005). "Rab conversion as a mechanism of progression from early to late endosomes." Cell **122**(5): 735-749.

Robertson, D. K., L. Gu, R. K. Rowe and W. L. Beatty (2009). "Inclusion biogenesis and reactivation of persistent Chlamydia trachomatis requires host cell sphingolipid biosynthesis." PLoS Pathog **5**(11): e1000664.

Rockey, D. D., M. A. Scidmore, J. P. Bannantine and W. J. Brown (2002). "Proteins in the chlamydial inclusion membrane." Microbes Infect **4**(3): 333-340.

Rojas, R., S. Kametaka, C. R. Haft and J. S. Bonifacino (2007). "Interchangeable but essential functions of SNX1 and SNX2 in the association of retromer with endosomes and the trafficking of mannose 6-phosphate receptors." Mol Cell Biol **27**(3): 1112-1124.

Rojas, R., T. van Vlijmen, G. A. Mardones, Y. Prabhu, A. L. Rojas, S. Mohammed, A. J. Heck, G. Raposo, P. van der Sluijs and J. S. Bonifacino (2008). "Regulation of retromer recruitment to endosomes by sequential action of Rab5 and Rab7." J Cell Biol **183**(3): 513-526.

Romano, P. S., M. G. Gutierrez, W. Beron, M. Rabinovitch and M. I. Colombo (2007). "The autophagic pathway is actively modulated by phase II Coxiella burnetii to efficiently replicate in the host cell." Cell Microbiol **9**(4): 891-909.

Ruepp, A., B. Brauner, I. Dunger-Kaltenbach, G. Frishman, C. Montrone, M. Stransky, B. Waegele, T. Schmidt, O. N. Doudieu, V. Stumpflen and H. W. Mewes (2008). "CORUM: the comprehensive resource of mammalian protein complexes." Nucleic Acids Res **36**(Database issue): D646-650.

Russell, D. G., H. C. Mwandumba and E. E. Rhoades (2002). "Mycobacterium and the coat of many lipids." J Cell Biol **158**(3): 421-426.

Rzomp, K. A., A. R. Moorhead and M. A. Scidmore (2006). "The GTPase Rab4 interacts with Chlamydia trachomatis inclusion membrane protein CT229." Infect Immun **74**(9): 5362-5373.

Rzomp, K. A., L. D. Scholtes, B. J. Briggs, G. R. Whittaker and M. A. Scidmore (2003). "Rab GTPases are recruited to chlamydial inclusions in both a species-dependent and species-independent manner." Infect Immun **71**(10): 5855-5870.

Saka, H. A., J. W. Thompson, Y. S. Chen, Y. Kumar, L. G. Dubois, M. A. Moseley and R. H. Valdivia (2011). "Quantitative proteomics reveals metabolic and pathogenic properties of Chlamydia trachomatis developmental forms." Mol Microbiol **82**(5): 1185-1203.

Sauer, J.-D., M. A. Bachman and M. S. Swanson (2005). "The phagosomal transporter A couples threonine acquisition to differentiation and replication of Legionella pneumophila in macrophages." Proceedings of the National Academy of Sciences of the United States of America **102**(28): 9924-9929.

Schachter, J. and A. O. Osoba (1983). "Lymphogranuloma venereum." Br Med Bull **39**(2): 151-154.

Schachter, J., R. S. Stephens, P. Timms, C. Kuo, P. M. Bavoil, S. Birkelund, J. Boman, H. Caldwell, L. A. Campbell, M. Chernesky, G. Christiansen, I. N. Clarke, C. Gaydos, J. T. Grayston, T. Hackstadt, R. Hsia, B. Kaltenboeck, M. Leinonnen, D. Ojcius, G. McClarty, J. Orfila, R. Peeling, M. Puolakkainen, T. C. Quinn, R. G. Rank, J. Raulston, G. L. Ridgeway, P. Saikku, W. E. Stamm, D. T. Taylor-Robinson, S. P. Wang and P. B. Wyrick (2001). "Radical changes to chlamydial taxonomy are not necessary just yet." Int J Syst Evol Microbiol **51**(Pt 1): 249; author reply 251-243.

Schlessinger, A., P. Matsson, J. E. Shima, U. Pieper, S. W. Yee, L. Kelly, L. Apeltsin, R. M. Stroud, T. E. Ferrin, K. M. Giacomini and A. Sali (2010). "Comparison of human solute carriers." Protein Sci **19**(3): 412-428.

Schmitz-Esser, S., N. Linka, A. Collingro, C. L. Beier, H. E. Neuhaus, M. Wagner and M. Horn (2004). "ATP/ADP translocases: a common feature of obligate intracellular amoebal symbionts related to Chlamydiae and Rickettsiae." J Bacteriol **186**(3): 683-691.

Schramm, N., C. R. Bagnell and P. B. Wyrick (1996). "Vesicles containing Chlamydia trachomatis serovar L2 remain above pH 6 within HEC-1B cells." Infect Immun **64**(4): 1208-1214.

Schroeder, N., L. J. Mota and S. Meresse (2011). "Salmonella-induced tubular networks." Trends Microbiol **19**(6): 268-277.

Schwanhausser, B., D. Busse, N. Li, G. Dittmar, J. Schuchhardt, J. Wolf, W. Chen and M. Selbach (2011). "Global quantification of mammalian gene expression control." Nature **473**(7347): 337-342.

Scidmore, M. A. (2011). "Recent advances in Chlamydia subversion of host cytoskeletal and membrane trafficking pathways." Microbes Infect **13**(6): 527-535.

Scidmore, M. A. and T. Hackstadt (2001). "Mammalian 14-3-3beta associates with the Chlamydia trachomatis inclusion membrane via its interaction with IncG." Mol Microbiol **39**(6): 1638-1650.

Seaman, M. N., M. E. Harbour, D. Tattersall, E. Read and N. Bright (2009). "Membrane recruitment of the cargo-selective retromer subcomplex is catalysed by the small GTPase Rab7 and inhibited by the Rab-GAP TBC1D5." J Cell Sci **122**(Pt 14): 2371-2382.

Seaman, M. N., J. M. McCaffery and S. D. Emr (1998). "A membrane coat complex essential for endosome-to-Golgi retrograde transport in yeast." J Cell Biol **142**(3): 665-681.

Seaman, M. N. and H. P. Williams (2002). "Identification of the functional domains of yeast sorting nexins Vps5p and Vps17p." Mol Biol Cell **13**(8): 2826-2840.

Shannon, P., A. Markiel, O. Ozier, N. S. Baliga, J. T. Wang, D. Ramage, N. Amin, B. Schwikowski and T. Ideker (2003). "Cytoscape: a software environment for integrated models of biomolecular interaction networks." Genome Res **13**(11): 2498-2504.

Shaw, A. C., K. Gevaert, H. Demol, B. Hoorelbeke, J. Vandekerckhove, M. R. Larsen, P. Roepstorff, A. Holm, G. Christiansen and S. Birkelund (2002). "Comparative proteome analysis of Chlamydia trachomatis serovar A, D and L2." Proteomics **2**(2): 164-186.

Shaw, E. I., C. A. Dooley, E. R. Fischer, M. A. Scidmore, K. A. Fields and T. Hackstadt (2000). "Three temporal classes of gene expression during the Chlamydia trachomatis developmental cycle." Mol Microbiol **37**(4): 913-925.

Shevchuk, O., C. Batzilla, S. Hagele, H. Kusch, S. Engelmann, M. Hecker, A. Haas, K. Heuner, G. Glockner and M. Steinert (2009). "Proteomic analysis of Legionella-containing phagosomes isolated from Dictyostelium." Int J Med Microbiol **299**(7): 489-508.

Skipp, P., J. Robinson, C. D. O'Connor and I. N. Clarke (2005). "Shotgun proteomic analysis of Chlamydia trachomatis." Proteomics **5**(6): 1558-1573.

Sonnichsen, B., S. De Renzis, E. Nielsen, J. Rietdorf and M. Zerial (2000). "Distinct membrane domains on endosomes in the recycling pathway visualized by multicolor imaging of Rab4, Rab5, and Rab11." J Cell Biol **149**(4): 901-914.

Soupene, E., J. Rothschild, F. A. Kuypers and D. Dean (2012). "Eukaryotic protein recruitment into the Chlamydia inclusion: implications for survival and growth." PLoS One **7**(5): e36843.

Stadler, C., E. Rexhepaj, V. R. Singan, R. F. Murphy, R. Pepperkok, M. Uhlen, J. C. Simpson and E. Lundberg (2013). "Immunofluorescence and fluorescent-protein tagging show high correlation for protein localization in mammalian cells." Nat Methods **10**(4): 315-323.

Stechmann, B., S. K. Bai, E. Gobbo, R. Lopez, G. Merer, S. Pinchard, L. Panigai, D. Tenza, G. Raposo, B. Beaumelle, D. Sauvaire, D. Gillet, L. Johannes and J. Barbier (2010). "Inhibition of retrograde transport protects mice from lethal ricin challenge." Cell **141**(2): 231-242.

Stephens, R. S., S. Kalman, C. Lammel, J. Fan, R. Marathe, L. Aravind, W. Mitchell, L. Olinger, R. L. Tatusov, Q. Zhao, E. V. Koonin and R. W. Davis (1998). "Genome sequence of an obligate intracellular pathogen of humans: Chlamydia trachomatis." Science **282**(5389): 754-759.

Stephens, R. S., G. Myers, M. Eppinger and P. M. Bavoil (2009). "Divergence without difference: phylogenetics and taxonomy of Chlamydia resolved." FEMS Immunol Med Microbiol **55**(2): 115-119.

Strochlic, T. I., T. G. Setty, A. Sitaram and C. G. Burd (2007). "Grd19/Snx3p functions as a cargo-specific adapter for retromer-dependent endocytic recycling." J Cell Biol **177**(1): 115-125.

Sturgill-Koszycki, S., P. H. Schlesinger, P. Chakraborty, P. L. Haddix, H. L. Collins, A. K. Fok, R. D. Allen, S. L. Gluck, J. Heuser and D. G. Russell (1994). "Lack of acidification in Mycobacterium phagosomes produced by exclusion of the vesicular proton-ATPase." Science **263**(5147): 678-681.

Su, H., L. Raymond, D. D. Rockey, E. Fischer, T. Hackstadt and H. D. Caldwell (1996). "A recombinant Chlamydia trachomatis major outer membrane protein binds to heparan sulfate receptors on epithelial cells." Proc Natl Acad Sci U S A **93**(20): 11143-11148.

Suchland, R. J., B. M. Jeffrey, M. Xia, A. Bhatia, H. G. Chu, D. D. Rockey and W. E. Stamm (2008). "Identification of concomitant infection with Chlamydia trachomatis IncA-negative mutant and wild-type strains by genomic, transcriptional, and biological characterizations." Infect Immun **76**(12): 5438-5446.

Suchland, R. J., D. D. Rockey, S. K. Weeks, D. T. Alzhanov and W. E. Stamm (2005). "Development of secondary inclusions in cells infected by Chlamydia trachomatis." Infect Immun **73**(7): 3954-3962.

Sudhof, T. C. and J. E. Rothman (2009). "Membrane fusion: grappling with SNARE and SM proteins." Science **323**(5913): 474-477.

Swanson, A. F. and C. C. Kuo (1991). "Evidence that the major outer membrane protein of Chlamydia trachomatis is glycosylated." Infect Immun **59**(6): 2120-2125.

Swanson, M. S. and R. R. Isberg (1995). "Association of Legionella pneumophila with the macrophage endoplasmic reticulum." Infect Immun **63**(9): 3609-3620.

Taraska, T., D. M. Ward, R. S. Ajioka, P. B. Wyrick, S. R. Davis-Kaplan, C. H. Davis and J. Kaplan (1996). "The late chlamydial inclusion membrane is not derived from the endocytic pathway and is relatively deficient in host proteins." Infect Immun **64**(9): 3713-3727.

Tilney, L. G., O. S. Harb, P. S. Connelly, C. G. Robinson and C. R. Roy (2001). "How the parasitic bacterium Legionella pneumophila modifies its phagosome and transforms it into rough ER: implications for conversion of plasma membrane to the ER membrane." J Cell Sci **114**(Pt 24): 4637-4650.

Tipples, G. and G. McClarty (1993). "The obligate intracellular bacterium Chlamydia trachomatis is auxotrophic for three of the four ribonucleoside triphosphates." Mol Microbiol **8**(6): 1105-1114.

Tisdale, E. J., J. R. Bourne, R. Khosravi-Far, C. J. Der and W. E. Balch (1992). "GTP-binding mutants of rab1 and rab2 are potent inhibitors of vesicular transport from the endoplasmic reticulum to the Golgi complex." J Cell Biol **119**(4): 749-761.

Tjaden, J., H. H. Winkler, C. Schwoppe, M. Van Der Laan, T. Mohlmann and H. E. Neuhaus (1999). "Two nucleotide transport proteins in Chlamydia trachomatis, one for net nucleoside triphosphate uptake and the other for transport of energy." J Bacteriol **181**(4): 1196-1202.

Toh, H., K. Miura, M. Shirai and M. Hattori (2003). "In silico inference of inclusion membrane protein family in obligate intracellular parasites chlamydiae." DNA Res **10**(1): 9-17.

Tresse, E., F. A. Salomons, J. Vesa, L. C. Bott, V. Kimonis, T. P. Yao, N. P. Dantuma and J. P. Taylor (2010). "VCP/p97 is essential for maturation of ubiquitin-containing autophagosomes and this function is impaired by mutations that cause IBMPFD." Autophagy **6**(2): 217-227.

Tse, S. M., D. Mason, R. J. Botelho, B. Chiu, M. Reyland, K. Hanada, R. D. Inman and S. Grinstein (2005). "Accumulation of diacylglycerol in the Chlamydia inclusion vacuole: possible role in the inhibition of host cell apoptosis." J Biol Chem **280**(26): 25210-25215.

Ulsamer, A. G., P. L. Wright, M. G. Wetzel and E. D. Korn (1971). "Plasma and phagosome membranes of Acanthamoeba castellanii." J Cell Biol **51**(1): 193-215.

UniProt, C. (2014). "Activities at the Universal Protein Resource (UniProt)." Nucleic Acids Res **42**(Database issue): D191-198.

Urwyler, S., Y. Nyfeler, C. Ragaz, H. Lee, L. N. Mueller, R. Aebersold and H. Hilbi (2009). "Proteome analysis of Legionella vacuoles purified by magnetic immunoseparation reveals secretory and endosomal GTPases." Traffic **10**(1): 76-87.

van Ooij, C., G. Apodaca and J. Engel (1997). "Characterization of the Chlamydia trachomatis vacuole and its interaction with the host endocytic pathway in HeLa cells." Infect Immun **65**(2): 758-766.

van Ooij, C., L. Kalman, I. van, M. Nishijima, K. Hanada, K. Mostov and J. N. Engel (2000). "Host cell-derived sphingolipids are required for the intracellular growth of Chlamydia trachomatis." Cell Microbiol **2**(6): 627-637.

van Weering, J. R., P. Verkade and P. J. Cullen (2012). "SNX-BAR-mediated endosome tubulation is co-ordinated with endosome maturation." Traffic **13**(1): 94-107.

Vandahl, B. B., S. Birkelund, H. Demol, B. Hoorelbeke, G. Christiansen, J. Vandekerckhove and K. Gevaert (2001). "Proteome analysis of the Chlamydia pneumoniae elementary body." Electrophoresis **22**(6): 1204-1223.

Verbeke, P., L. Welter-Stahl, S. Ying, J. Hansen, G. Hacker, T. Darville and D. M. Ojcius (2006). "Recruitment of BAD by the Chlamydia trachomatis vacuole correlates with host-cell survival." PLoS Pathog **2**(5): e45.

Verges, M., F. Luton, C. Gruber, F. Tiemann, L. G. Reinders, L. Huang, A. L. Burlingame, C. R. Haft and K. E. Mostov (2004). "The mammalian retromer regulates transcytosis of the polymeric immunoglobulin receptor." Nat Cell Biol **6**(8): 763-769.

Vergne, I., J. Chua and V. Deretic (2003). "Tuberculosis toxin blocking phagosome maturation inhibits a novel Ca2+/calmodulin-PI3K hVPS34 cascade." J Exp Med **198**(4): 653-659.

Vergne, I., J. Chua, H. H. Lee, M. Lucas, J. Belisle and V. Deretic (2005). "Mechanism of phagolysosome biogenesis block by viable Mycobacterium tuberculosis." Proc Natl Acad Sci U S A **102**(11): 4033-4038.

Vergne, I., R. A. Fratti, P. J. Hill, J. Chua, J. Belisle and V. Deretic (2004). "Mycobacterium tuberculosis phagosome maturation arrest: mycobacterial phosphatidylinositol analog phosphatidylinositol mannoside stimulates early endosomal fusion." Mol Biol Cell **15**(2): 751-760.

Voeltz, G. K., W. A. Prinz, Y. Shibata, J. M. Rist and T. A. Rapoport (2006). "A class of membrane proteins shaping the tubular endoplasmic reticulum." Cell **124**(3): 573-586.

Wade, N., N. J. Bryant, L. M. Connolly, R. J. Simpson, J. P. Luzio, R. C. Piper and D. E. James (2001). "Syntaxin 7 complexes with mouse Vps10p tail interactor 1b, syntaxin 6, vesicle-associated membrane protein (VAMP)8, and VAMP7 in b16 melanoma cells." J Biol Chem **276**(23): 19820-19827.

Wang, X., D. Ma, J. Keski-Oja and D. Pei (2004). "Co-recycling of MT1-MMP and MT3-MMP through the trans-Golgi network. Identification of DKV582 as a recycling signal." J Biol Chem **279**(10): 9331-9336.

Wassmer, T., N. Attar, M. V. Bujny, J. Oakley, C. J. Traer and P. J. Cullen (2007). "A loss-of-function screen reveals SNX5 and SNX6 as potential components of the mammalian retromer." J Cell Sci **120**(Pt 1): 45-54.

Wassmer, T., N. Attar, M. Harterink, J. R. van Weering, C. J. Traer, J. Oakley, B. Goud, D. J. Stephens, P. Verkade, H. C. Korswagen and P. J. Cullen (2009). "The retromer coat complex coordinates endosomal sorting and dynein-mediated transport, with carrier recognition by the trans-Golgi network." Dev Cell **17**(1): 110-122.

Wehrl, W., V. Brinkmann, P. R. Jungblut, T. F. Meyer and A. J. Szczepek (2004). "From the inside out--processing of the Chlamydial autotransporter PmpD and its role in bacterial adhesion and activation of human host cells." Mol Microbiol **51**(2): 319-334.

Wehrl, W., T. F. Meyer, P. R. Jungblut, E. C. Muller and A. J. Szczepek (2004). "Action and reaction: Chlamydophila pneumoniae proteome alteration in a persistent infection induced by iron deficiency." Proteomics **4**(10): 2969-2981.

Wieland, H., S. Ullrich, F. Lang and B. Neumeister (2005). "Intracellular multiplication of Legionella pneumophila depends on host cell amino acid transporter SLC1A5." Mol Microbiol **55**(5): 1528-1537.

Wisniewski, J. R., A. Zougman and M. Mann (2009). "Combination of FASP and StageTip-based fractionation allows in-depth analysis of the hippocampal membrane proteome." J Proteome Res **8**(12): 5674-5678.

Wylie, J. L., G. M. Hatch and G. McClarty (1997). "Host cell phospholipids are trafficked to and then modified by Chlamydia trachomatis." J Bacteriol **179**(23): 7233-7242.

Wyrick, P. B. (2000). "Intracellular survival by Chlamydia." Cell Microbiol **2**(4): 275-282.

Wyrick, P. B. and E. A. Brownridge (1978). "Growth of Chlamydia psittaci in macrophages." Infect Immun **19**(3): 1054-1060.

Ye, Y., Y. Shibata, C. Yun, D. Ron and T. A. Rapoport (2004). "A membrane protein complex mediates retro-translocation from the ER lumen into the cytosol." Nature **429**(6994): 841-847.

Yu, S., J. G. Park, J. N. Kahn, N. E. Tumer and Y. P. Pang (2013). "Common pharmacophore of structurally distinct small-molecule inhibitors of intracellular retrograde trafficking of ribosome inactivating proteins." Sci Rep **3**: 3397.

Zeichner, S. L. (1982). "Isolation and characterization of phagosomes containing Chlamydia psittaci from L cells." Infect Immun **38**(1): 325-342.

Zeichner, S. L. (1983). "Isolation and characterization of macrophage phagosomes containing infectious and heat-inactivated Chlamydia psittaci: two phagosomes with different intracellular behaviors." Infect Immun **40**(3): 956-966.

Zhang, P., Y. Wu, T. Y. Belenkaya and X. Lin (2011). "SNX3 controls Wingless/Wnt secretion through regulating retromer-dependent recycling of Wntless." Cell Res **21**(12): 1677-1690.

Zhang, S. L., Y. Yu, J. Roos, J. A. Kozak, T. J. Deerinck, M. H. Ellisman, K. A. Stauderman and M. D. Cahalan (2005). "STIM1 is a Ca2+ sensor that activates CRAC channels and migrates from the Ca2+ store to the plasma membrane." Nature **437**(7060): 902-905.

Zhong, Q., C. S. Lazar, H. Tronchere, T. Sato, T. Meerloo, M. Yeo, Z. Songyang, S. D. Emr and G. N. Gill (2002). "Endosomal localization and function of sorting nexin 1." Proc Natl Acad Sci U S A **99**(10): 6767-6772.

6. Appendix

6.1 List of identified host proteins

Table 6.1: Host proteins that passed the threshold for SILAC enrichment after initial filtering

Protein ID = Uniprot ID of the first protein of the Majority protein column of a protein group, if more than one protein was indicated in the Majority protein group it is listed in Table 6.2. iBAQ LOG2 = log2 value of iBAQ enrichment Inc/Lysate, capped at 250 fold. PERC = percentage of iBAQ intensity in the respective experiment (LYS = Lysate, INC = Inclusion). SD = standard deviation of the indicated percentage/ratio divided by mean. LYS QF = Quantitative Flag of lysates (1 = 2 unique peptides per experiment and SD smaller than 0.5 of mean, 2 = less than 2 unique peptides in at least one experiment and SD smaller than 0.5 of mean, - = SD higher than 0.5 of mean, N = quantified only based on dataset from (Nagaraj, Wisniewski *et al.* 2011)). INC QF = Quantitative flag of inclusion proteins (1 if SD smaller than 0.5 of mean, - if higher). SEA pval = adjusted p-value of the SILAC exclusion approach. Q SEA = Qualifier of SILAC exclusion approach; 1 = first set, three SILAC ratios, 2 = second set, only two SILAC ratio. SILAC L/H = average of SILAC ratio L/H.

Protein ID	Protein name	Gene names	SILAC L/H	SILAC SD	SEA pval	Q SEA	iBAQ LOG2	INC PERC	INC SD	INC QF	LYS PERC	LYS SD	LYS QF
Q9NRG9	Aladin	AAAS	1.65	0.16	0.034	2	4.24	0.02	0.9	-	0	0.56	-
P49588	Alanine--tRNA ligase, cytoplasmic	AARS	2.56	0.14	0.003	1	-3.13	0.01	0.41	1	0.05	0.17	1
O95573	Long-chain-fatty-acid--CoA ligase 3	ACSL3	1.85	0.27	0.003	1	4.28	0.24	0.31	1	0.01	0.39	1
O43707	Alpha-actinin-4	ACTN4	1.67	0.16	0.003	1	-3.19	0.02	0.64	-	0.16	0.07	1
P61158	Actin-related protein 3	ACTR3	1.49	0.21	0.005	1	-0.51	0.03	0.65	-	0.04	0.16	1
Q13443	Disintegrin and metalloproteinase domain-containing protein 9	ADAM9	2.47	0.88	0.007	1	3.22	0.01	0.47	1	0		0
Q53EU6	Glycerol-3-phosphate acyltransferase 3	AGPAT9	2.26	0.15	0.034	2	6.42	0.09	0.7	-	0	0.37	3
Q6RW13	Type-1 angiotensin II receptor-associated protein	AGTRAP	8.22	0.01	0.034	2	6.25	0.37	0.15	1	0	0.45	3
P51648	Fatty aldehyde dehydrogenase	ALDH3A2	1.38	0.08	0.006	1	3.93	0.17	0.51	-	0.01	0.28	1
P04075	Fructose-bisphosphate aldolase A	ALDOA	1.88	0.28	0.003	1	0.19	0.52	0.5	-	0.46	0.22	1
P09972	Fructose-bisphosphate aldolase C	ALDOC	1.71	0.17	0.034	2	-0.27	0.03	0.27	1	0.03	0.01	1
Q9BT22	Chitobiosyldiphosphodolichol beta-mannosyltransferase	ALG1	2.05	0.23	0.034	2	6.85	0.02	0.54	-	0		0
Q9Y673	Dolichyl-phosphate beta-glucosyltransferase	ALG5	1.98	0.34	0.003	1	5.44	0.04	0.36	1	0	0.85	-
P04083	Annexin A1	ANXA1	2.16	0.17	0.003	1	-1.44	0.25	0.27	1	0.68	0.02	1
P07355	Annexin A2	ANXA2	1.79	0.35	0.003	1	-0.27	0.66	0.14	1	0.79	0.12	1
P08758	Annexin A5	ANXA5	1.95	0.33	0.034	2	-1.88	0.03	1	-	0.11	0.28	1
Q10567	AP-1 complex subunit beta-1	AP1B1	1.37	0.03	0.04	2	3.22	0.01	1.15	-	0	0.36	2
O43747	AP-1 complex subunit gamma-1	AP1G1	2.28	0.12	0.034	2	4.2	0.02	0.16	1	0	0.91	-
Q9HDC9	Adipocyte plasma membrane-associated protein	APMAP	1.88	0.18	0.003	1	4.13	0.06	0.79	-	0	0.2	1
P61204	ADP-ribosylation factor 3	ARF3	1.32	0.03	0.008	1	0.7	0.24	0.75	-	0.15	0.19	1
Q8N6T3	ADP-ribosylation factor GTPase-activating protein 1	ARFGAP1	2.12	0.05	0.003	1	3.16	0.04	0.88	-	0		N
P05089	Arginase-1	ARG1	5.68	0.14	0.034	2	7.97	0.08	1.32	-	0		N
O75915	PRA1 family protein 3	ARL6IP5	2.03	0.27	0.003	1	2.57	0.15	1.1	-	0.03	0.05	1
O15143	Actin-related protein 2/3 complex subunit 1B	ARPC1B	1.68	0.44	0.005	1	-0.52	0.03	0.43	1	0.04	0.18	1
O15144	Actin-related protein 2/3 complex subunit 2	ARPC2	1.41	0.03	0.037	2	-0.25	0.04	0.23	1	0.04	0.18	1
P59998	Actin-related protein 2/3 complex subunit 4	ARPC4	1.52	0.15	0.004	1	0.11	0.05	0.96	-	0.05	0.18	1
Q12797	Aspartyl/asparaginyl beta-hydroxylase	ASPH	1.54	0.12	0.004	1	3.64	0.22	0.82	-	0.02	0.29	1
Q6DD88	Atlastin-3	ATL3	1.93	0.14	0.034	2	2.11	0.01	0.47	1	0	0.64	-

Q9HD20	Probable cation-transporting ATPase 13A1	ATP13A1	1.63	0.31	0.004	1	5.05	0.01	0.92	-	0		0
P05023	Sodium/potassium-transporting ATPase subunit alpha-1	ATP1A1	2.49	0.4	0.034	2	-1.1	0.01	0.86	-	0.03	0.09	1
P16615	Sarcoplasmic/endoplasmic reticulum calcium ATPase 2	ATP2A2	2.09	0.21	0.003	1	4.12	0.26	0.43	1	0.02	0.35	1
O75787	Renin receptor	ATP6AP2	2.15	0.51	0.034	2	5.04	0.03	0.28	1	0		0
Q93050	V-type proton ATPase 116 kDa subunit a isoform 1	ATP6V0A1	2.86	0.17	0.003	1	5.51	0.02	0.41	1	0		0
P61421	V-type proton ATPase subunit d 1	ATP6V0D1	2.54	0.17	0.034	2	5.32	0.08	0.12	1	0	0.46	3
O75348	V-type proton ATPase subunit G 1	ATP6V1G1	1.75	0.12	0.034	2	2.16	0.03	0.34	1	0.01	0.18	3
Q9UBB4	Ataxin-10	ATXN10	1.54	0.15	0.004	1	0.91	0.04	0.51	-	0.02	0.21	1
Q9Y679	Ancient ubiquitous protein 1	AUP1	2.13	0.23	0.003	1	3.91	0.01	0.32	1	0	0.14	2
P25311	Zinc-alpha-2-glycoprotein	AZGP1	2.45	0.62	0.034	2	7.97	0.08	1.39	-	0		N
Q9UPN4	5-azacytidine-induced protein 1	AZI1	5.97	0.5	0.003	1	3.49	0.01	0.17	1	0		N
P61769	Beta-2-microglobulin	B2M	1.91	0.21	0.034	2	3.29	0.26	0.97	-	0.03	0.84	-
P80723	Brain acid soluble protein 1	BASP1	2.26	0.14	0.003	1	3.48	0.26	1.12	-	0.02	0.31	1
P51572	B-cell receptor-associated protein 31	BCAP31	1.87	0.25	0.003	1	2.66	0.08	0.66	-	0.01	0.78	-
P35613	Basigin	BSG	2.28	0.24	0.003	1	0.78	0.15	0.29	1	0.09	0.1	1
Q9UKR5	Probable ergosterol biosynthetic protein 28	C14orf1	2.18	0.52	0.003	1	5.03	0.14	0.54	-	0	1.1	-
Q969H8	UPF0556 protein C19orf10	C19orf10	1.92	0.19	0.003	1	4.02	0.45	0.75	-	0.03	0.16	1
P27797	Calreticulin	CALR	1.87	0.2	0.003	1	3.35	1.3	0.2	1	0.13	0.24	1
O43852	Calumenin	CALU	1.64	0.26	0.004	1	4.16	0.23	0.24	1	0.01	0.67	-
P27824	Calnexin	CANX	2.12	0.2	0.003	1	5.01	0.76	0.44	1	0.02	0.27	1
Q01518	Adenylyl cyclase-associated protein 1	CAP1	2.15	0.23	0.034	2	-2.56	0.01	0.15	1	0.04	0.3	1
P04632	Calpain small subunit 1	CAPNS1	1.83	0.29	0.003	1	-0.44	0.06	0.54	-	0.09	0.14	1
Q14444	Caprin-1	CAPRIN1	1.56	0.15	0.004	1	0.32	0.04	0.66	-	0.03	0.24	1
P52907	F-actin-capping protein subunit alpha-1	CAPZA1	2.26	0.37	0.003	1	0.25	0.05	0.43	1	0.04	0.35	1
P47756	F-actin-capping protein subunit beta	CAPZB	2.49	0.32	0.003	1	-0.65	0.04	0.33	1	0.06	0.22	1
Q96A33	Coiled-coil domain-containing protein 47	CCDC47	1.57	0.19	0.004	1	3.92	0.1	0.15	1	0.01	0.24	1
P78371	T-complex protein 1 subunit beta	CCT2	2.05	0.29	0.003	1	-0.79	0.07	0.26	1	0.11	0.16	1
P49368	T-complex protein 1 subunit gamma	CCT3	2	0.34	0.003	1	-0.43	0.09	0.34	1	0.12	0.13	1
P50991	T-complex protein 1 subunit delta	CCT4	1.94	0.37	0.003	1	-0.93	0.06	0.39	1	0.12	0.17	1
P48643	T-complex protein 1 subunit epsilon	CCT5	2.21	0.36	0.003	1	-1.84	0.03	0.48	1	0.12	0.05	1
P40227	T-complex protein 1 subunit zeta	CCT6A	2.31	0.37	0.003	1	-1.17	0.06	0.79	-	0.14	0.01	1
Q99832	T-complex protein 1 subunit eta	CCT7	2.14	0.31	0.003	1	-0.36	0.06	0.26	1	0.08	0.14	1
P50990	T-complex protein 1 subunit theta	CCT8	2.07	0.25	0.003	1	-0.71	0.06	0.52	-	0.1	0.04	1
P16070	CD44 antigen	CD44	2.56	0.32	0.003	1	-0.91	0.04	0.47	1	0.07	0.13	1
P13987	CD59 glycoprotein	CD59	4.3	0.23	0.034	2	2.6	0.44	0.73	-	0.07	0.5	-
P60953	Cell division control protein 42 homolog	CDC42	1.59	0.16	0.004	1	-1.32	0.04	0.34	1	0.1	0.13	1
Q9UPV0	Centrosomal protein of 164 kDa	CEP164	6.35	0.27	0.034	2	7.91	0.01	0.93	-	0		N
Q6P2H3	Centrosomal protein of 85 kDa	CEP85	6.6	0.53	0.003	1	7.97	0.31	0.5	-	0		N
P23528	Cofilin-1	CFL1	2.79	0.2	0.003	1	0.22	0.68	0.35	1	0.58	0.13	1

Q99653	Calcium-binding protein p22	CHP	2.21	0.24	0.003	1	3.69	0.12	0.72	-	0.01	0.55	-
Q8N5K1	CDGSH iron-sulfur domain-containing protein 2	CISD2	1.57	0.19	0.004	1	4.88	0.11	0.69	-	0	0.51	-
Q00610	Clathrin heavy chain 1	CLTC	3	0.26	0.003	1	2.08	0.27	0.53	-	0.06	0.07	1
Q9Y2B0	Protein canopy homolog 2	CNPY2	1.77	0.22	0.003	1	3.39	0.37	0.18	1	0.04	0.26	1
Q9Y5P4	Collagen type IV alpha-3-binding protein	COL4A3BP	9.41	0.04	0.003	1	7.97	0.96	0.44	1	0	0.89	-
P53621	Coatomer subunit alpha	COPA	1.97	0.32	0.003	1	2.62	0.07	0.55	-	0.01	0.19	1
Q9Y678	Coatomer subunit gamma-1	COPG1	1.45	0.1	0.037	2	-0.14	0	0.18	1	0	0.53	-
Q14019	Coactosin-like protein	COTL1	2.31	0.04	0.034	2	-2.64	0.03	0.8	-	0.2	0.33	1
Q6UXH1	Cysteine-rich with EGF-like domain protein 2	CRELD2	1.79	0.28	0.034	2	1.98	0.01	0.33	1	0		N
Q5TZA2	Rootletin	CROCC	1.46	0.05	0.004	1	3	0.04	0.44	1	0	0.56	-
Q1MSJ5	Centrosome and spindle pole-associated protein 1	CSPP1	4.37	0.26	0.003	1	7.97	0.03	0.77	-	0		N
P00167	Cytochrome b5	CYB5A	1.46	0.12	0.005	1	5.52	0.29	0.37	1	0.01	0.7	-
P13498	Cytochrome b-245 light chain	CYBA	1.91	0.17	0.034	2	4.48	0.04	0.74	-	0		0
Q16850	Lanosterol 14-alpha demethylase	CYP51A1	2.03	0.27	0.003	1	4.37	0.08	0.24	1	0	0.11	1
P61803	Dolichyl-diphosphooligosaccharide--protein glycosyltransferase subunit DAD1	DAD1	1.59	0.28	0.005	1	4.49	0.54	0.59	-	0.02	0.72	-
P81605	Dermcidin	DCD	17.19	0.25	0.003	1	7.97	1.99	1.26	-	0.01		N
Q14203	Dynactin subunit 1	DCTN1	2.07	0.19	0.034	2	1.45	0.01	0.83	-	0	0.21	1
Q9UJW0	Dynactin subunit 4	DCTN4	5.62	0.75	0.003	1	1.89	0.01	0.62	-	0		N
P39656	Dolichyl-diphosphooligosaccharide--protein glycosyltransferase 48 kDa subunit	DDOST	1.61	0.19	0.004	1	4.45	0.28	0.64	-	0.01	0.17	1
Q15392	Delta(24)-sterol reductase	DHCR24	2.09	0.11	0.003	1	5.1	0.19	0.72	-	0.01	0.18	1
Q9UBM7	7-dehydrocholesterol reductase	DHCR7	1.5	0.2	0.006	1	3.01	0.16	0.23	1	0.02	0.15	1
Q9C0G6	Dynein heavy chain 6, axonemal	DNAH6	2.76	1.22	0.034	2	#ZAHL!	0.02	1.39	-			-
P31689	DnaJ homolog subfamily A member 1	DNAJA1	1.5	0.25	0.006	1	0.67	0.04	0.6	-	0.03	0.64	-
Q9UBS4	DnaJ homolog subfamily B member 11	DNAJB11	1.78	0.07	0.034	2	5	0.13	0.13	1	0	0.99	-
Q8IXB1	DnaJ homolog subfamily C member 10	DNAJC10	1.51	0.02	0.034	2	3.61	0.01	0.22	1	0	0.77	-
Q13217	DnaJ homolog subfamily C member 3	DNAJC3	1.48	0.04	0.035	2	1.53	0.02	0.08	1	0.01		N
Q08554	Desmocollin-1	DSC1	8.92	0.22	0.034	2	7.97	0.12	0.72	-	0		N
Q02413	Desmoglein-1	DSG1	3.09	0.49	0.003	1	7.97	0.06	1.31	-	0		N
P15924	Desmoplakin	DSP	2.85	0.5	0.003	1	3.34	0.05	0.92	-	0	0.08	1
Q14204	Cytoplasmic dynein 1 heavy chain 1	DYNC1H1	1.46	0.23	0.007	1	0.01	0.01	0.64	-	0.01	0.09	1
Q13409	Cytoplasmic dynein 1 intermediate chain 2	DYNC1I2	1.86	0.24	0.003	1	1.24	0.01	0.39	1	0	0.31	1
Q15125	3-beta-hydroxysteroid-Delta(8),Delta(7)-isomerase	EBP	1.66	0.21	0.004	1	4.58	0.64	0.31	1	0.03	0.14	1
P68104	Elongation factor 1-alpha 1	EEF1A1	1.47	0.1	0.004	1	2.25	5.68	0.8	-	1.19	0.12	1
P29692	Elongation factor 1-delta	EEF1D	1.55	0.17	0.004	1	1.11	0.31	0.34	1	0.15	0.08	1
P26641	Elongation factor 1-gamma	EEF1G	1.6	0.24	0.004	1	1.25	0.25	0.11	1	0.11	0.23	1
P13639	Elongation factor 2	EEF2	1.66	0.25	0.004	1	-0.91	0.2	0.33	1	0.38	0.11	1
Q96C19	EF-hand domain-containing protein D2	EFHD2	1.58	0.03	0.034	2	-0.77	0.02	0.37	1	0.04	0.19	1

P00533	Epidermal growth factor receptor	EGFR	3.23	0.51	0.003	1	2.57	0.03	0.73	-	0	0.2	1
P05198	Eukaryotic translation initiation factor 2 subunit 1	EIF2S1	1.58	0.21	0.004	1	-0.38	0.04	0.33	1	0.05	0.11	1
P41091	Eukaryotic translation initiation factor 2 subunit 3	EIF2S3	1.69	0.26	0.004	1	-0.42	0.07	0.24	1	0.1	0.02	1
Q9BW60	Elongation of very long chain fatty acids protein 1	ELOVL1	1.88	0.17	0.034	2	3.55	0.05	0.38	1	0	0.8	-
P06733	Alpha-enolase	ENO1	2.47	0.18	0.003	1	-0.6	0.82	0.4	1	1.25	0.05	1
P29317	Ephrin type-A receptor 2	EPHA2	3.38	0.23	0.003	1	2.56	0.02	0.67	-	0	0.85	-
P07099	Epoxide hydrolase 1	EPHX1	1.89	0.2	0.003	1	3.51	0.33	0.16	1	0.03	0.54	-
Q12929	Epidermal growth factor receptor kinase substrate 8	EPS8	4.41	0.06	0.034	2	5.27	0.01	0.3	1	0	0.97	-
Q9NZ08	Endoplasmic reticulum aminopeptidase 1	ERAP1	1.87	0.43	0.005	1	2.38	0.01	0.29	1	0		N
O75477	Erlin-1	ERLIN1	1.71	0.03	0.034	2	2.26	0.03	0.29	1	0.01	0.29	1
O94905	Erlin-2	ERLIN2	2.16	0.18	0.003	1	6.87	0.12	0.3	1	0	0.77	-
Q7Z2K6	Endoplasmic reticulum metallopeptidase 1	ERMP1	1.6	0.16	0.004	1	2.61	0.01	0.39	1	0		0
Q96HE7	ERO1-like protein alpha	ERO1L	2.01	0.27	0.003	1	5.97	0.15	0.52	-	0	0.21	1
P30040	Endoplasmic reticulum resident protein 29	ERP29	1.84	0.19	0.003	1	4.64	0.61	0.17	1	0.02	0.23	1
Q9BS26	Endoplasmic reticulum resident protein 44	ERP44	1.85	0.18	0.003	1	4.19	0.05	0.36	1	0	0.76	-
P15311	Ezrin	EZR	1.5	0.08	0.004	1	3.21	0.8	0.16	1	0.09	0.33	1
Q9BZQ8	Protein Niban	FAM129A	2.7	0.43	0.003	1	2.04	0.01	0.54	-	0	0.49	1
Q658Y4	Protein FAM91A1	FAM91A1	4.29	0.37	0.034	2	6.55	0.02	0.43	1	0		0
Q14192	Four and a half LIM domains protein 2	FHL2	5.08	0.36	0.003	1	4.25	0.04	0.36	1	0	0.53	-
Q9Y3D6	Mitochondrial fission 1 protein	FIS1	1.6	0.03	0.034	2	4.17	0.06	0.58	-	0	0.54	-
Q96AY3	Peptidyl-prolyl cis-trans isomerase FKBP10	FKBP10	1.52	0.15	0.004	1	4.45	0.1	0.07	1	0	0.21	1
Q02790	Peptidyl-prolyl cis-trans isomerase FKBP4	FKBP4	2.05	0.25	0.003	1	-3.58	0.01	0.55	-	0.09	0.37	1
Q13045	Protein flightless-1 homolog	FLII	6.51	0.27	0.003	1	6.92	0.25	0.4	1	0	0.58	-
P15328	Folate receptor alpha	FOLR1	1.96	0.22	0.034	2	1.05	0.05	0.46	1	0.02	0.06	1
Q16658	Fascin	FSCN1	2	0.36	0.003	1	-3.27	0.01	0.65	-	0.09	0.18	1
Q14697	Neutral alpha-glucosidase AB	GANAB	1.81	0.22	0.003	1	3.69	0.41	0.3	1	0.03	0.1	1
P04406	Glyceraldehyde-3-phosphate dehydrogenase	GAPDH	1.67	0.28	0.004	1	1.14	2.82	0.33	1	1.28	0.22	1
Q9Y2T3	Guanine deaminase	GDA	2.22	0.21	0.034	2	-2.71	0.01	0.44	1	0.05	0.35	1
P50395	Rab GDP dissociation inhibitor beta	GDI2	1.6	0	0.034	2	-1.36	0.04	0.17	1	0.09	0.15	1
P08754	Guanine nucleotide-binding protein G(k) subunit alpha	GNAI3	4.27	0.38	0.003	1	2.84	0.19	0.07	1	0.03	0.16	1
Q5JWF2	Guanine nucleotide-binding protein G(s) subunit alpha isoforms XLas	GNAS	2.6	0.3	0.034	2	1.22	0.02	0.07	1	0.01	0.32	1
P62873	Guanine nucleotide-binding protein G(I)/G(S)/G(T) subunit beta-1	GNB1	2.15	0.08	0.003	1	2.71	0.15	0.65	-	0.02	0.23	1
P62879	Guanine nucleotide-binding protein G(I)/G(S)/G(T) subunit beta-2	GNB2	1.61	0.19	0.004	1	-0.01	0.03	0.55	-	0.03	0.07	1
Q9UBI6	Guanine nucleotide-binding protein G(I)/G(S)/G(O) subunit gamma-12	GNG12	2.59	0.28	0.003	1	3.32	0.33	0.88	-	0.03	0.64	-
P06744	Glucose-6-phosphate isomerase	GPI	1.7	0.16	0.034	2	-2.23	0.03	1.02	-	0.14	0.12	1

Q8TCT9	Minor histocompatibility antigen H13	HM13	2.08	0.15	0.003	1	3.95	0.1	0.27	1	0.01	0.57	-
P30519	Heme oxygenase 2	HMOX2	2.07	0.25	0.003	1	4.91	0.24	0.12	1	0.01	0.31	1
P07900	Heat shock protein HSP 90-alpha	HSP90AA1	1.99	0.49	0.003	1	-0.65	0.22	0.24	1	0.34	0.16	1
P08238	Heat shock protein HSP 90-beta	HSP90AB1	1.88	0.37	0.003	1	0	1.16	0.18	1	1.16	0.08	1
P14625	Endoplasmin	HSP90B1	1.71	0.19	0.003	1	3.94	1.14	0.06	1	0.07	0.1	1
P08107	Heat shock 70 kDa protein 1A/1B	HSPA1A	1.98	0.31	0.003	1	-0.1	0.23	0.56	-	0.24	0.19	1
P11021	78 kDa glucose-regulated protein	HSPA5	1.71	0.19	0.003	1	3.58	2.59	0.26	1	0.22	0.13	1
P11142	Heat shock cognate 71 kDa protein	HSPA8	1.91	0.27	0.003	1	0.29	0.7	0.16	1	0.57	0.11	1
P04792	Heat shock protein beta-1	HSPB1	1.56	0.32	0.007	1	-1.68	0.09	0.74	-	0.27	0.18	1
Q92598	Heat shock protein 105 kDa	HSPH1	2.19	0.18	0.003	1	-2.79	0.01	0.95	-	0.08	0.13	1
Q9Y4L1	Hypoxia up-regulated protein 1	HYOU1	1.75	0.19	0.003	1	3.7	0.1	0.19	1	0.01	0.48	1
P11717	Cation-independent mannose-6-phosphate receptor	IGF2R	3.48	0.38	0.003	1	5.43	0.01	0.69	-	0	0.98	-
Q27J81	Inverted formin-2	INF2	1.31	0.03	0.008	1	2.59	0.01	0.97	-	0	0.09	3
P17301	Integrin alpha-2	ITGA2	3.01	0.13	0.034	2	2.79	0.01	0.98	-	0	0.33	1
P23229	Integrin alpha-6	ITGA6	4.26	0.31	0.003	1	3.02	0.01	0.61	-	0	0.45	1
P16144	Integrin beta-4	ITGB4	3.46	0.17	0.003	1	2.63	0.01	0.81	-	0	0.4	1
Q14573	Inositol 1,4,5-trisphosphate receptor type 3	ITPR3	2.19	0.26	0.034	2	0.16	0	0.26	1	0		N
P14923	Junction plakoglobin	JUP	4.31	0.65	0.003	1	2.11	0.07	1.17	-	0.02	0.21	1
Q06136	3-ketodihydrosphingosine reductase	KDSR	1.98	0.02	0.034	2	3.53	0.03	0.33	1	0	0.16	3
Q8N766	Uncharacterized protein KIAA0090	KIAA0090	1.72	0.22	0.003	1	4.02	0.01	0.7	-	0	0.58	-
O94964	Uncharacterized protein KIAA0889	KIAA0889	2.54	0.77	0.003	1	6.08	0	0.76	-	0		N
P05783	Keratin, type I cytoskeletal 18	KRT18	1.45	0.13	0.005	1	-0.35	0.21	1.05	-	0.26	0.07	1
Q16787	Laminin subunit alpha-3	LAMA3	1.64	0.16	0.003	1	4.7	0	0.72	-	0	0.29	3
P00338	L-lactate dehydrogenase A chain	LDHA	2.14	0.3	0.003	1	-1.09	0.44	0.44	1	0.93	0.27	1
P07195	L-lactate dehydrogenase B chain	LDHB	1.98	0.34	0.003	1	-0.76	0.5	0.76	-	0.85	0.05	1
P01130	Low-density lipoprotein receptor	LDLR	4.17	0.33	0.034	2	6.28	0.07	0.44	1	0	0.26	1
Q32P28	Prolyl 3-hydroxylase 1	LEPRE1	1.36	0.03	0.006	1	4.59	0.02	0.41	1	0	0.27	2
Q8IVL5	Prolyl 3-hydroxylase 2	LEPREL1	2.08	0.05	0.034	2	3.7	0.02	0.19	1	0		N
P49257	Protein ERGIC-53	LMAN1	1.89	0.17	0.003	1	4.27	0.29	0.5	1	0.01	0.24	1
Q12907	Vesicular integral-membrane protein VIP36	LMAN2	1.94	0.23	0.003	1	2.97	0.05	0.35	1	0.01	0.25	1
Q8NF37	Lysophosphatidylcholine acyltransferase 1	LPCAT1	1.83	0.17	0.034	2	4.9	0.05	0.01	1	0	0.32	1
Q6P1A2	Lysophospholipid acyltransferase 5	LPCAT3	1.57	0.24	0.037	2	3.9	0.05	0.17	1	0	0.2	2
P30533	Alpha-2-macroglobulin receptor-associated protein	LRPAP1	1.62	0.08	0.034	2	4.6	0.07	0.45	1	0	0.46	1
Q96AG4	Leucine-rich repeat-containing protein 59	LRRC59	1.54	0.17	0.004	1	3.76	0.41	0.5	-	0.03	0.57	-
Q32MZ4	Leucine-rich repeat flightless-interacting protein 1	LRRFIP1	8.21	0.31	0.003	1	5.49	0.5	0.49	1	0.01	0.25	1
Q9H089	Large subunit GTPase 1 homolog	LSG1	1.87	0.4	0.004	1	5.16	0.01	0.23	1	0	0.3	2
Q9BRK4	Leucine zipper putative tumor suppressor 2	LZTS2	7.41	0.57	0.003	1	7.97	0.08	0.39	1	0		N
P20645	Cation-dependent mannose-6-phosphate receptor	M6PR	9.4	0.24	0.003	1	5.42	0.2	0.36	1	0	0.86	-
P55145	Mesencephalic astrocyte-derived neurotrophic factor	MANF	1.6	0.07	0.003	1	4.5	0.24	0.27	1	0.01	0.26	1

Q66K74	Microtubule-associated protein 1S	MAP1S	3.37	0.36	0.003	1	6.29	0.01	0.45	1	0	0.44	3
Q96N66	Lysophospholipid acyltransferase 7	MBOAT7	1.65	0.22	0.004	1	3.04	0.02	0.76	-	0	0.28	1
Q5JRA6	Melanoma inhibitory activity protein 3	MIA3	1.68	0.19	0.003	1	5.47	0.01	0.58	-	0	0.29	3
Q14165	Malectin	MLEC	1.69	0.18	0.003	1	3.66	0.08	0.41	1	0.01	0.41	1
Q8NB16	Mixed lineage kinase domain-like protein	MLKL	1.84	0.37	0.034	2	7.97	0.44	0.86	-	0	0.25	3
Q9NZM1	Myoferlin	MYOF	8.1	0.15	0.003	1	5.02	0.47	0.5	-	0.01	0.07	1
O15049	NEDD4-binding protein 3	N4BP3	6.97	0.33	0.034	2	7.97	0.01	0.32	1	0		N
Q13765	Nascent polypeptide-associated complex subunit alpha	NACA	1.42	0.09	0.039	2	-1.54	0.07	0.45	1	0.19	0.12	1
Q6PIU2	Neutral cholesterol ester hydrolase 1	NCEH1	2.1	0.15	0.034	2	5.8	0.23	0.76	-	0	0.69	-
Q92542	Nicastrin	NCSTN	3.84	0.24	0.034	2	4.69	0.01	0.03	1	0		N
Q9UMX5	Neudesin	NENF	1.77	0.05	0.034	2	3.34	0.04	0.26	1	0		N
Q6ZNB6	NF-X1-type zinc finger protein NFXL1	NFXL1	1.47	0.18	0.007	1	3.65	0	0.4	1	0		N
Q96D46	60S ribosomal export protein NMD3	NMD3	1.42	0.1	0.04	2	2.42	0.02	0.02	1	0	0.12	1
Q15738	Sterol-4-alpha-carboxylate 3-dehydrogenase, decarboxylating	NSDHL	1.98	0.26	0.003	1	4.83	0.04	0.59	-	0	0.68	-
P13674	Prolyl 4-hydroxylase subunit alpha-1	P4HA1	1.51	0.09	0.004	1	5.04	0.07	0.47	1	0	0.92	-
P07237	Protein disulfide-isomerase	P4HB	1.75	0.22	0.003	1	3.79	1.06	0.14	1	0.08	0.2	1
P22234	Multifunctional protein ADE2	PAICS	1.52	0.09	0.004	1	0.1	0.13	0.71	-	0.12	0.19	1
Q15154	Pericentriolar material 1 protein	PCM1	5.97	0.18	0.003	1	5.47	0.05	0.74	-	0		N
P30101	Protein disulfide-isomerase A3	PDIA3	1.88	0.22	0.003	1	4.1	1.21	0.26	1	0.07	0.17	1
P13667	Protein disulfide-isomerase A4	PDIA4	1.69	0.18	0.003	1	3.78	0.64	0.1	1	0.05	0.21	1
Q15084	Protein disulfide-isomerase A6	PDIA6	1.77	0.23	0.003	1	3.95	0.73	0.82	-	0.05	0.16	1
P07737	Profilin-1	PFN1	1.76	0.11	0.003	1	-1.47	0.37	0.49	1	1.01	0.12	1
P52209	6-phosphogluconate dehydrogenase, decarboxylating	PGD	2.27	0.34	0.034	2	-1.81	0.02	0.09	1	0.08	0.31	1
P00558	Phosphoglycerate kinase 1	PGK1	2.37	0.3	0.003	1	-2.6	0.04	1.11	-	0.27	0.21	1
O00264	Membrane-associated progesterone receptor component 1	PGRMC1	1.75	0.2	0.003	1	4.77	0.29	0.08	1	0.01	0.66	-
O15173	Membrane-associated progesterone receptor component 2	PGRMC2	1.74	0.26	0.003	1	3.24	0.2	0.19	1	0.02	0.42	1
Q969N2	GPI transamidase component PIG-T	PIGT	1.86	0.24	0.003	1	4.71	0.01	0.33	1	0	0.7	-
Q9H490	Phosphatidylinositol glycan anchor biosynthesis class U protein	PIGU	2.02	0.19	0.034	2	1.93	0.04	0.39	1	0.01		N
O00459	Phosphatidylinositol 3-kinase regulatory subunit beta	PIK3R2	3.22	0.05	0.034	2	5.95	0	0.74	-	0		N
P14618	Pyruvate kinase isozymes M1/M2	PKM2	2.76	0.27	0.003	1	-0.1	0.82	0.24	1	0.87	0.15	1
Q9Y446	Plakophilin-3	PKP3	2.34	0.18	0.003	1	3.65	0.02	0.7	-	0	0.82	-
O00592	Podocalyxin	PODXL	7.98	0.38	0.003	1	3.39	0.11	0.52	-	0.01	0.31	1
P16435	NADPH--cytochrome P450 reductase	POR	1.74	0.19	0.003	1	4.3	0.04	0.82	-	0	0.73	-
P23284	Peptidyl-prolyl cis-trans isomerase B	PPIB	1.88	0.18	0.003	1	4.21	3.09	0.41	1	0.17	0.23	1
P62140	Serine/threonine-protein phosphatase PP1-beta catalytic subunit	PPP1CB	5.46	0.43	0.003	1	3.26	0.47	0.38	1	0.05	0.17	1
O14974	Protein phosphatase 1 regulatory subunit 12A	PPP1R12A	3.18	0.19	0.003	1	7.28	0.65	0.23	1	0	1.41	-

P60510	Serine/threonine-protein phosphatase 4 catalytic subunit	PPP4C	2.27	0.18	0.034	2	4.77	0.04	0.45	1	0	1.11	-
Q8TF05	Serine/threonine-protein phosphatase 4 regulatory subunit 1	PPP4R1	4.08	0.06	0.034	2	7.33	0.03	0.16	1	0	0.69	-
Q5VT98	PRAME family member 20/21	PRAMEF20	16.81	1.19	0.034	2	#ZAHL!	0.55	1.37	-			-
Q06830	Peroxiredoxin-1	PRDX1	1.82	0.19	0.003	1	0.71	2.23	0.21	1	1.36	0.05	1
P32119	Peroxiredoxin-2	PRDX2	2.56	0.4	0.003	1	-0.69	0.11	0.21	1	0.18	0.21	1
Q13162	Peroxiredoxin-4	PRDX4	1.75	0.24	0.003	1	3.88	0.57	0.5	1	0.04	0.08	1
P30041	Peroxiredoxin-6	PRDX6	2.25	0.21	0.003	1	-1.04	0.21	0.12	1	0.43	0.13	1
Q05655	Protein kinase C delta type	PRKCD	7.44	0.25	0.003	1	7.14	0.11	0.71	-	0	0.01	3
P14314	Glucosidase 2 subunit beta	PRKCSH	1.9	0.23	0.003	1	4.68	1.06	0.1	1	0.04	0.26	1
P25786	Proteasome subunit alpha type-1	PSMA1	2.09	0.36	0.003	1	-1.79	0.02	0.85	-	0.07	0.25	1
P25788	Proteasome subunit alpha type-3	PSMA3	2.39	0.51	0.003	1	-1.42	0.02	1.16	-	0.06	0.25	1
O14818	Proteasome subunit alpha type-7	PSMA7	1.96	0.13	0.003	1	-1.85	0.05	0.61	-	0.17	0.14	1
P20618	Proteasome subunit beta type-1	PSMB1	1.54	0.11	0.034	2	-1.97	0.02	0.12	1	0.09	0.1	1
Q99436	Proteasome subunit beta type-7	PSMB7	2.08	0.1	0.034	2	-1.53	0.01	0.99	-	0.04	0.21	1
Q13200	26S proteasome non-ATPase regulatory subunit 2	PSMD2	1.44	0.04	0.036	2	-2.36	0.01	0.05	1	0.03	0.22	1
O14684	Prostaglandin E synthase	PTGES	1.68	0.04	0.034	2	4.29	0.08	0.71	-	0		0
Q15185	Prostaglandin E synthase 3	PTGES3	1.52	0.03	0.034	2	-2.18	0.05	0.88	-	0.23	0.15	1
Q9P035	3-hydroxyacyl-CoA dehydratase 3	PTPLAD1	1.85	0.13	0.034	2	4.74	0.13	0.14	1	0	0.45	1
P61026	Ras-related protein Rab-10	RAB10	2.32	0.26	0.003	1	6.12	1.39	0.14	1	0.02	0.43	1
Q15907	Ras-related protein Rab-11B	RAB11B	7.91	0.3	0.003	1	6.47	3.89	0.34	1	0.04	0.14	1
Q6IQ22	Ras-related protein Rab-12	RAB12	4.47	0.19	0.003	1	6.93	0.13	0.31	1	0		N
P51153	Ras-related protein Rab-13	RAB13	1.74	0.33	0.034	2	4.99	0.1	0.65	-	0	0.49	3
P61106	Ras-related protein Rab-14	RAB14	6.12	0.15	0.003	1	6.93	2.34	0.75	-	0.02	0.03	1
Q9H0U4	Ras-related protein Rab-1B	RAB1B	1.45	0.07	0.004	1	2.74	0.31	0.39	1	0.05	0.19	1
O00194	Ras-related protein Rab-27B	RAB27B	1.63	0.12	0.003	1	5.22	0.12	0.34	1	0	0.6	-
P61019	Ras-related protein Rab-2A	RAB2A	2.26	0.15	0.003	1	5.61	1.8	0.43	1	0.04	0.04	1
Q15286	Ras-related protein Rab-35	RAB35	1.66	0.12	0.003	1	3.75	0.07	0.34	1	0.01	0.51	-
O95716	Ras-related protein Rab-3D	RAB3D	1.55	0.13	0.004	1	5.7	0.03	0.34	1	0		0
P20340	Ras-related protein Rab-6A	RAB6A	1.64	0.26	0.005	1	4.44	1.08	0.12	1	0.05	0.25	1
P61006	Ras-related protein Rab-8A	RAB8A	2.01	0.08	0.003	1	5.17	0.38	0.15	1	0.01	0.6	-
P63000	Ras-related C3 botulinum toxin substrate 1	RAC1	2.85	0	0.034	2	3.05	0.32	0.24	1	0.04	0.47	1
P62826	GTP-binding nuclear protein Ran	RAN	1.62	0.27	0.004	1	-2.02	0.11	0.56	-	0.45	0.08	1
P61224	Ras-related protein Rap-1b	RAP1B	1.38	0.11	0.007	1	2.33	0.23	0.06	1	0.05	0.33	1
P61225	Ras-related protein Rap-2b	RAP2B	4.28	0.41	0.003	1	4.64	0.15	0.37	1	0.01	0.21	1
Q15293	Reticulocalbin-1	RCN1	1.7	0.25	0.004	1	3.77	0.53	0.2	1	0.04	0.13	1
Q8TC12	Retinol dehydrogenase 11	RDH11	1.56	0.16	0.004	1	2.58	0.03	0.32	1	0	0.22	1
Q00765	Receptor expression-enhancing protein 5	REEP5	2.67	0.25	0.003	1	4.96	0.26	0.6	-	0.01	0.81	-
O15258	Protein RER1	RER1	1.82	0.21	0.034	2	4.81	0.09	0.5	1	0	0.89	-

P08134	Rho-related GTP-binding protein RhoC	RHOC	1.82	0.13	0.003	1	6.65	0.35	0.21	1	0	0.01	3
P84095	Rho-related GTP-binding protein RhoG	RHOG	1.39	0.12	0.006	1	5.27	0.08	0.52	-	0	0.13	3
P05388	60S acidic ribosomal protein P0	RPLP0	1.45	0.18	0.006	1	1.96	0.41	0.35	1	0.11	0.24	1
P05387	60S acidic ribosomal protein P2	RPLP2	1.42	0.06	0.004	1	1.6	1.38	0.68	-	0.45	0.25	1
P04843	Dolichyl-diphosphooligosaccharide--protein glycosyltransferase subunit 1	RPN1	1.71	0.17	0.003	1	3.48	0.28	0.19	1	0.02	0.11	1
P04844	Dolichyl-diphosphooligosaccharide--protein glycosyltransferase subunit 2	RPN2	1.6	0.18	0.004	1	3.28	0.23	0.34	1	0.02	0.18	1
Q9NQC3	Reticulon-4	RTN4	2.78	0.32	0.003	1	3.58	0.11	0.27	1	0.01	0.53	-
Q9HCY8	Protein S100-A14	S100A14	4.12	0.47	0.034	2	2.16	0.16	0.37	1	0.04	0.28	1
P26447	Protein S100-A4	S100A4	1.77	0.13	0.034	2	-3.2	0.07	0.19	1	0.69	0.65	-
P06703	Protein S100-A6	S100A6	1.56	0.21	0.005	1	-2.36	0.27	0.13	1	1.37	0.46	1
P06702	Protein S100-A9	S100A9	9.52	0.47	0.034	2	7.97	1.31	1.08	-	0		N
Q9NTJ5	Phosphatidylinositide phosphatase SAC1	SACM1L	2.24	0.24	0.003	1	4.08	0.04	0.04	1	0	0.24	1
O14828	Secretory carrier-associated membrane protein 3	SCAMP3	6.87	0.61	0.003	1	5.93	0.45	0.45	1	0.01	0.67	-
Q99470	Stromal cell-derived factor 2	SDF2	1.79	0	0.034	2	4.49	0.04	0.31	1	0		0
Q9BRK5	45 kDa calcium-binding protein	SDF4	1.45	0.01	0.036	2	2.91	0.03	0.3	1	0	0.57	-
P67812	Signal peptidase complex catalytic subunit SEC11A	SEC11A	1.87	0.13	0.003	1	5.44	0.12	0.79	-	0	0.59	-
O75396	Vesicle-trafficking protein SEC22b	SEC22B	1.88	0.07	0.034	2	3.26	0.16	0.05	1	0.02	0.34	1
P61619	Protein transport protein Sec61 subunit alpha isoform 1	SEC61A1	1.49	0.15	0.005	1	1.65	0.09	0.58	-	0.03	0.2	1
Q9UGP8	Translocation protein SEC63 homolog	SEC63	1.52	0.11	0.004	1	3.53	0.02	0.71	-	0	0.08	2
P36952	Serpin B5	SERPINB5	1.84	0.1	0.034	2	-2.54	0.01	0.14	1	0.04	0.18	1
P50454	Serpin H1	SERPINH1	1.56	0.15	0.004	1	3.45	0.44	0.31	1	0.04	0.46	1
P31947	14-3-3 protein sigma	SFN	3.3	0.17	0.003	1	-1.16	0.07	0.34	1	0.16	0.11	1
Q8TE82	SH3 domain and tetratricopeptide repeat-containing protein 1	SH3TC1	3.4	1.21	0.034	2	#ZAHL!	0.11	1.34	-			-
O60292	Signal-induced proliferation-associated 1-like protein 3	SIPA1L3	6.4	0.13	0.003	1	7.97	0.03	0.6	-	0		N
O15427	Monocarboxylate transporter 4	SLC16A3	3.61	0.27	0.034	2	-0.85	0.01	0.35	1	0.01	0.21	1
P08195	4F2 cell-surface antigen heavy chain	SLC3A2	2.44	0.15	0.003	1	0.34	0.11	0.77	-	0.08	0.04	1
Q01650	Large neutral amino acids transporter small subunit 1	SLC7A5	2.85	0.09	0.034	2	0.87	0.07	0.75	-	0.04	0.8	-
Q15599	Na(+)/H(+) exchange regulatory cofactor NHE-RF2	SLC9A3R2	1.99	0.22	0.034	2	0.93	0.01	0.59	-	0.01	0.33	1
Q13596	Sorting nexin-1	SNX1	3.97	0.25	0.003	1	7.3	0.36	0.89	-	0	0.23	1
O60749	Sorting nexin-2	SNX2	3.35	0.24	0.003	1	5.16	0.34	0.24	1	0.01	0.28	1
O95219	Sorting nexin-4	SNX4	1.73	0.31	0.034	2	2.18	0	0.41	1	0		N
Q9Y5X3	Sorting nexin-5	SNX5	3.25	0.15	0.003	1	7.4	0.32	0.55	-	0	0.55	-
Q9UNH7	Sorting nexin-6	SNX6	4.65	0.34	0.003	1	5.83	0.07	0.36	1	0	1.07	-
Q9Y6A9	Signal peptidase complex subunit 1	SPCS1	1.86	0.16	0.003	1	3.41	0.14	0.99	-	0.01	1.11	-
P61009	Signal peptidase complex subunit 3	SPCS3	1.66	0.03	0.034	2	5.79	0.26	0.48	1	0	1.27	-
O43291	Kunitz-type protease inhibitor 2	SPINT2	2.01	0.1	0.003	1	3.84	0.06	0.47	1	0	0.79	-

O15270	Serine palmitoyltransferase 2	SPTLC2	1.61	0.28	0.007	1	6.05	0	1	-	0		0
Q13501	Sequestosome-1	SQSTM1	1.46	0.05	0.004	1	3.14	0.06	0.63	-	0.01	0.05	1
Q9Y5M8	Signal recognition particle receptor subunit beta	SRPRB	1.76	0.2	0.003	1	4.49	0.26	0.06	1	0.01	0.13	1
Q13586	Stromal interaction molecule 1	STIM1	14.28	0.38	0.003	1	7.97	0.45	0.56	-	0		N
Q9P246	Stromal interaction molecule 2	STIM2	5.84	0.29	0.003	1	6.39	0.07	1.2	-	0		N
P31948	Stress-induced-phosphoprotein 1	STIP1	2.12	0.67	0.003	1	-0.14	0.07	0.97	-	0.08	0.11	1
P46977	Dolichyl-diphosphooligosaccharide--protein glycosyltransferase subunit STT3A	STT3A	1.43	0.16	0.008	1	3.67	0.06	0.75	-	0	0.07	1
Q8TCJ2	Dolichyl-diphosphooligosaccharide--protein glycosyltransferase subunit STT3B	STT3B	1.72	0.22	0.003	1	4.78	0.06	0.65	-	0	0.27	1
Q12846	Syntaxin-4	STX4	3.39	0.19	0.034	2	3.37	0.02	0.49	1	0		N
O15400	Syntaxin-7	STX7	3.23	0.61	0.003	1	3.48	0.04	0.41	1	0		N
Q8NBJ7	Sulfatase-modifying factor 2	SUMF2	1.85	0.21	0.003	1	4.76	0.11	0.14	1	0	0.05	1
O43760	Synaptogyrin-2	SYNGR2	10.38	0.1	0.003	1	6.8	1.75	0.67	-	0.02	0.32	2
Q16563	Synaptophysin-like protein 1	SYPL1	6.5	0.16	0.003	1	5.07	0.17	0.43	1	0	0.37	1
P26639	Threonine--tRNA ligase, cytoplasmic	TARS	2.56	0.22	0.003	1	-2.05	0.02	0.92	-	0.09	0.2	1
P17987	T-complex protein 1 subunit alpha	TCP1	2.99	0.35	0.003	1	-1.14	0.06	0.1	1	0.12	0.16	1
Q9NZ01	Trans-2,3-enoyl-CoA reductase	TECR	2.01	0.28	0.003	1	3.7	0.18	0.33	1	0.01	0.78	-
Q9Y6I9	Testis-expressed sequence 264 protein	TEX264	1.68	0.15	0.034	2	2.52	0.01	0.58	-	0		N
P02786	Transferrin receptor protein 1	TFRC	11.84	0.18	0.003	1	5.29	1.66	0.43	1	0.04	0.15	1
P29401	Transketolase	TKT	1.8	0.42	0.004	1	-3.56	0.03	0.36	1	0.34	0.21	1
P49755	Transmembrane emp24 domain-containing protein 10	TMED10	1.74	0.21	0.003	1	1.86	0.09	0.8	-	0.03	0.38	1
Q7Z7H5	Transmembrane emp24 domain-containing protein 4	TMED4	1.43	0.07	0.037	2	3.27	0.03	0.29	1	0	0.4	2
Q9Y3B3	Transmembrane emp24 domain-containing protein 7	TMED7	1.5	0.05	0.034	2	3.75	0.06	0.07	1	0	0.65	-
Q9BVK6	Transmembrane emp24 domain-containing protein 9	TMED9	1.81	0.19	0.003	1	2.08	0.05	0.65	-	0.01	0.9	-
P57088	Transmembrane protein 33	TMEM33	1.77	0.33	0.034	2	4.82	0.04	0.23	1	0	0.67	-
Q9BTV4	Transmembrane protein 43	TMEM43	2.04	0.27	0.003	1	5.53	0.06	0.44	1	0	0.71	-
Q9NYL9	Tropomodulin-3	TMOD3	3.32	0.12	0.003	1	5.18	0.18	0.42	1	0	1.02	-
Q9H3N1	Thioredoxin-related transmembrane protein 1	TMX1	2.06	0.24	0.003	1	4.67	0.26	0.11	1	0.01	0.85	-
Q9Y320	Thioredoxin-related transmembrane protein 2	TMX2	2.06	0.32	0.003	1	6.61	0.03	1	-	0		0
O43399	Tumor protein D54	TPD52L2	2.67	0.46	0.003	1	1.45	0.09	0.58	-	0.03	0.49	1
P60174	Triosephosphate isomerase	TPI1	1.69	0.16	0.003	1	-2.66	0.06	0.74	-	0.39	0.15	1
P07951	Tropomyosin beta chain	TPM2	1.76	0.19	0.003	1	0.9	0.1	0.27	1	0.05		N
P06753	Tropomyosin alpha-3 chain	TPM3	3.4	0.12	0.003	1	-0.04	0.1	0.24	1	0.1	0.28	1
P67936	Tropomyosin alpha-4 chain	TPM4	2.1	0.11	0.003	1	3.52	2.83	0.61	-	0.25	0.11	1
Q6Q0C0	E3 ubiquitin-protein ligase TRAF7	TRAF7	1.98	0.75	0.04	2	5.77	0.01	1.07	-	0		N
O95881	Thioredoxin domain-containing protein 12	TXNDC12	1.72	0.21	0.003	1	4.55	0.34	0.3	1	0.01	0.3	1
Q8NBS9	Thioredoxin domain-containing protein 5	TXNDC5	1.71	0.24	0.003	1	3.26	0.37	0.35	1	0.04	0.01	1
Q9BZV1	UBX domain-containing protein 6	UBXN6	2.6	0.05	0.034	2	2.94	0.03	1.19	-	0		N

Q9NYU2	UDP-glucose:glycoprotein glucosyltransferase 1	UGGT1	1.77	0.25	0.003	1	4.12	0.04	0.36	1	0	0.18	1
Q15836	Vesicle-associated membrane protein 3	VAMP3	6.01	0.43	0.003	1	5.53	0.96	0.64	-	0.02	0.15	1
Q9BV40	Vesicle-associated membrane protein 8	VAMP8	4.88	0.23	0.003	1	3.86	0.22	0.15	1	0.02	0.53	-
Q9P0L0	Vesicle-associated membrane protein-associated protein A	VAPA	4.22	0.25	0.003	1	6.69	1.77	0.14	1	0.02	0.14	1
O95292	Vesicle-associated membrane protein-associated protein B/C	VAPB	3.9	0.32	0.003	1	5.69	0.8	0.26	1	0.02	0.41	3
P26640	Valine--tRNA ligase	VARS	1.43	0.17	0.006	1	-0.86	0.02	0.95	-	0.03	0.09	1
P18206	Vinculin	VCL	1.98	0.47	0.004	1	-2.05	0.01	0.54	-	0.05	0.15	1
P55072	Transitional endoplasmic reticulum ATPase	VCP	2.64	0.11	0.003	1	3.54	0.84	0.48	1	0.07	0.16	1
Q8N0U8	Vitamin K epoxide reductase complex subunit 1-like protein 1	VKORC1L1	1.98	0.24	0.034	2	4.78	0.09	0.01	1	0	0.53	-
Q9UBQ0	Vacuolar protein sorting-associated protein 29	VPS29	2.74	0.27	0.003	1	1.84	0.07	0.43	1	0.02	0.55	-
Q96QK1	Vacuolar protein sorting-associated protein 35	VPS35	3.28	0.43	0.003	1	1.1	0.03	0.38	1	0.01	0.32	1
P67809	Nuclease-sensitive element-binding protein 1	YBX1	1.36	0.07	0.006	1	0.38	0.25	0.54	-	0.19	0.13	1
P31946	14-3-3 protein beta/alpha	YWHAB	3.3	0.11	0.003	1	1.67	0.51	0.36	1	0.16	0.96	-
P62258	14-3-3 protein epsilon	YWHAE	5.12	0.18	0.003	1	2.99	4.14	0.2	1	0.52	0.12	1
P61981	14-3-3 protein gamma	YWHAG	2.49	0.16	0.003	1	1.83	0.35	0.52	-	0.1	0.09	1
Q04917	14-3-3 protein eta	YWHAH	2.67	0.19	0.003	1	1.11	0.1	0.53	-	0.05	0.07	1
P27348	14-3-3 protein theta	YWHAQ	2.57	0.31	0.003	1	0.77	0.14	0.3	1	0.08	0.08	1
P63104	14-3-3 protein zeta/delta	YWHAZ	4.24	0.19	0.003	1	2.38	3.36	0.63	-	0.65	0.06	1
O75844	CAAX prenyl protease 1 homolog	ZMPSTE24	2.22	0.3	0.003	1	4.88	0.07	0.42	1	0	0.49	2
A6NL28	Putative tropomyosin alpha-3 chain-like protein		2.12	0.61	0.006	1	-0.26	0.02	0.32	1	0.02	0.31	1

Table 6.2: Protein groups identified in the inclusion proteome

Proteins that were identified as part of a protein group with more than one protein in the Majority Protein ID column

UNIPROT ID	Protein names	Gene names
P07355	Annexin A2;Putative annexin A2-like protein	ANXA2;ANXA2P2
P61204	ADP-ribosylation factor 3;ADP-ribosylation factor 1	ARF3;ARF1
P05023	Sodium/potassium-transporting ATPase subunit alpha-1;Sodium/potassium-transporting ATPase subunit alpha-3	ATP1A1;ATP1A3
O75348	V-type proton ATPase subunit G 1;V-type proton ATPase subunit G 2	ATP6V1G1;ATP6V1G2
P60953	Cell division control protein 42 homolog;Rho-related GTP-binding protein RhoQ	CDC42;RHOQ
P68104	Elongation factor 1-alpha 1;Putative elongation factor 1-alpha-like 3	EEF1A1;EEF1A1P5
P41091	Eukaryotic translation initiation factor 2 subunit 3;Putative eukaryotic translation initiation factor 2 subunit 3-like protein	EIF2S3;EIF2S3L
P62879	Guanine nucleotide-binding protein G(I)/G(S)/G(T) subunit beta-2;Guanine nucleotide-binding protein subunit beta-4	GNB2;GNB4
P08238	Heat shock protein HSP 90-beta;Putative heat shock protein HSP 90-beta-3	HSP90AB1;HSP90AB3P
Q5VT98	PRAME family member 20/21;PRAME family member 4;PRAME family member 9/15;PRAME family	PRAMEF20;PRAMEF4;PRAMEF9;PRAMEF23;PRAMEF5;PRAMEF6

	member 23;PRAME family member 5;PRAME family member 6	
O14818	Proteasome subunit alpha type-7;Proteasome subunit alpha type-7-like	PSMA7;PSMA8
Q9H0U4	Ras-related protein Rab-1B;Putative Ras-related protein Rab-1C	RAB1B;RAB1C
P61006	Ras-related protein Rab-8A;Ras-related protein Rab-8B	RAB8A;RAB8B
P63000	Ras-related C3 botulinum toxin substrate 1;Ras-related C3 botulinum toxin substrate 2;Ras-related C3 botulinum toxin substrate 3	RAC1;RAC2;RAC3
P05388	60S acidic ribosomal protein P0;60S acidic ribosomal protein P0-like	RPLP0;RPLP0P6
P61619	Protein transport protein Sec61 subunit alpha isoform 1;Protein transport protein Sec61 subunit alpha isoform 2	SEC61A1;SEC61A2
Q8TE82	SH3 domain and tetratricopeptide repeat-containing protein 1;SH3 domain and tetratricopeptide repeat-containing protein 2	SH3TC1;SH3TC2

Table 6.3: GO Term enrichment based on GO for cellular compartments (GOCC)

The top 50 categories are shown, based on p-values. Enrichment was generated using GOrilla as described in the materials and methods section.

GO Term	Description	P-value	FDR q-value	Enrichment
GO:0031982	vesicle	6.95E-55	8.26E-52	2.61
GO:0044421	extracellular region part	7.13E-55	4.24E-52	2.63
GO:0031988	membrane-bounded vesicle	3.22E-54	1.27E-51	2.62
GO:0043230	extracellular organelle	1.69E-51	5.03E-49	2.7
GO:0065010	extracellular membrane-bounded organelle	1.69E-51	4.02E-49	2.7
GO:0070062	extracellular vesicular exosome	1.69E-51	3.35E-49	2.7
GO:0044432	endoplasmic reticulum part	1.76E-47	2.99E-45	4.5
GO:0098589	membrane region	8.38E-40	1.24E-37	4.07
GO:0044444	cytoplasmic part	4.23E-36	5.58E-34	1.55
GO:0005789	endoplasmic reticulum membrane	3.97E-32	4.71E-30	4.28
GO:0005783	endoplasmic reticulum	2.48E-31	2.68E-29	4.29
GO:0098588	bounding membrane of organelle	2.90E-30	2.88E-28	2.75
GO:0016020	membrane	4.02E-29	3.67E-27	1.89
GO:0016023	cytoplasmic membrane-bounded vesicle	6.27E-28	5.32E-26	4.45
GO:0042470	melanosome	2.97E-27	2.35E-25	8.97
GO:0048770	pigment granule	2.97E-27	2.20E-25	8.97
GO:0031410	cytoplasmic vesicle	2.07E-26	1.45E-24	4.05
GO:0031090	organelle membrane	4.39E-25	2.89E-23	2.25
GO:0044425	membrane part	5.00E-25	3.13E-23	2
GO:0005788	endoplasmic reticulum lumen	7.96E-23	4.73E-21	7.66
GO:0016021	integral component of membrane	7.41E-19	4.19E-17	2.19
GO:0044433	cytoplasmic vesicle part	5.25E-16	2.83E-14	3.95
GO:0005615	extracellular space	5.38E-14	2.78E-12	3.51
GO:0044422	organelle part	9.46E-13	4.68E-11	1.33
GO:0044446	intracellular organelle part	1.23E-12	5.86E-11	1.33
GO:0030659	cytoplasmic vesicle membrane	4.49E-12	2.05E-10	3.9
GO:0012506	vesicle membrane	2.32E-11	1.02E-09	3.69
GO:0043227	membrane-bounded organelle	1.06E-10	4.49E-09	1.22
GO:0002199	zona pellucida receptor complex	1.73E-10	7.10E-09	16.44
GO:0005832	chaperonin-containing T-complex	1.73E-10	6.86E-09	16.44
GO:0005886	plasma membrane	3.43E-10	1.32E-08	1.87
GO:0030176	integral component of endoplasmic reticulum membrane	4.54E-10	1.69E-08	7.05
GO:0044459	plasma membrane part	1.18E-09	4.25E-08	2.19

GO:0009986	cell surface	1.93E-09	6.74E-08	4.2
GO:0043226	organelle	3.85E-08	1.31E-06	1.16
GO:0044297	cell body	4.62E-08	1.53E-06	3.6
GO:0098590	plasma membrane region	5.58E-08	1.79E-06	3.57
GO:0005793	endoplasmic reticulum-Golgi intermediate compartment	8.01E-08	2.51E-06	5.94
GO:0043233	organelle lumen	4.00E-07	1.22E-05	2.3
GO:0031301	integral component of organelle membrane	4.99E-07	1.48E-05	3.84
GO:0030141	secretory granule	5.42E-07	1.57E-05	4.48
GO:0031974	membrane-enclosed lumen	6.91E-07	1.96E-05	2.2
GO:0008250	oligosaccharyltransferase complex	1.22E-06	3.38E-05	12.33
GO:0044431	Golgi apparatus part	2.93E-06	7.91E-05	2.21
GO:0005575	cellular_component	3.13E-06	8.27E-05	1.04
GO:0048471	perinuclear region of cytoplasm	3.83E-06	9.89E-05	2.25
GO:0005829	cytosol	5.27E-06	1.33E-04	1.42
GO:0070013	intracellular organelle lumen	5.43E-06	1.34E-04	2.18
GO:0030136	clathrin-coated vesicle	9.03E-06	2.19E-04	4.11

Table 6.4: GO Term enrichment based on GO for biological processes (GOBP)

The top 50 categories are shown, based on p-values. Enrichment was generated using GOrilla as described in the materials and methods section.

GO Term	Description	P-value	FDR q-value	Enrichment
GO:0006457	protein folding	8.01E-19	7.28E-15	4.96
GO:0065008	regulation of biological quality	9.17E-17	4.17E-13	2.15
GO:0006986	response to unfolded protein	1.29E-16	3.91E-13	6.48
GO:0035966	response to topologically incorrect protein	4.66E-16	1.06E-12	6.22
GO:0034976	response to endoplasmic reticulum stress	1.01E-14	1.83E-11	5.84
GO:0044765	single-organism transport	4.90E-14	7.42E-11	1.96
GO:0051234	establishment of localization	1.34E-13	1.73E-10	1.77
GO:0045184	establishment of protein localization	2.53E-13	2.88E-10	2.2
GO:0006810	transport	4.39E-13	4.43E-10	1.76
GO:0042221	response to chemical	4.59E-13	4.17E-10	1.94
GO:0015031	protein transport	1.58E-12	1.30E-09	2.19
GO:0044699	single-organism process	1.97E-12	1.50E-09	1.25
GO:0010033	response to organic substance	4.54E-12	3.18E-09	2.01
GO:0050896	response to stimulus	1.03E-11	6.67E-09	1.49

GO:0051649	establishment of localization in cell	1.69E-11	1.02E-08	1.97
GO:0006984	ER-nucleus signaling pathway	5.82E-11	3.30E-08	6.01
GO:0007165	signal transduction	1.21E-10	6.48E-08	1.67
GO:1902582	single-organism intracellular transport	1.67E-10	8.42E-08	2.15
GO:0071702	organic substance transport	1.72E-10	8.24E-08	1.89
GO:0016192	vesicle-mediated transport	1.92E-10	8.72E-08	2.42
GO:0030968	endoplasmic reticulum unfolded protein response	4.99E-10	2.16E-07	6.08
GO:0046907	intracellular transport	6.70E-10	2.77E-07	1.97
GO:0050878	regulation of body fluid levels	6.96E-10	2.75E-07	2.96
GO:0034620	cellular response to unfolded protein	7.39E-10	2.80E-07	5.95
GO:0006184	GTP catabolic process	8.68E-10	3.16E-07	3.79
GO:1901069	guanosine-containing compound catabolic process	1.06E-09	3.72E-07	3.76
GO:0007599	hemostasis	1.18E-09	3.97E-07	3.08
GO:0035036	sperm-egg recognition	1.48E-09	4.79E-07	14.61
GO:0007339	binding of sperm to zona pellucida	1.48E-09	4.63E-07	14.61
GO:0035967	cellular response to topologically incorrect protein	1.57E-09	4.74E-07	5.7
GO:0044763	single-organism cellular process	1.93E-09	5.65E-07	1.26
GO:0046039	GTP metabolic process	2.34E-09	6.66E-07	3.64
GO:0050817	coagulation	3.41E-09	9.38E-07	3.02
GO:0007596	blood coagulation	3.41E-09	9.11E-07	3.02
GO:1901068	guanosine-containing compound metabolic process	4.98E-09	1.29E-06	3.52
GO:0006987	activation of signaling protein activity involved in unfolded protein response	5.26E-09	1.33E-06	6.58
GO:0009988	cell-cell recognition	7.00E-09	1.72E-06	13.15
GO:0019882	antigen processing and presentation	1.15E-08	2.75E-06	3.61
GO:0032075	positive regulation of nuclease activity	1.24E-08	2.88E-06	6.22
GO:0051716	cellular response to stimulus	2.35E-08	5.33E-06	1.46
GO:0051084	'de novo' posttranslational protein folding	2.66E-08	5.90E-06	7.05
GO:0032069	regulation of nuclease activity	2.73E-08	5.91E-06	5.9
GO:0006928	cellular component movement	3.12E-08	6.59E-06	2.15
GO:0018196	peptidyl-asparagine modification	3.81E-08	7.87E-06	4.74
GO:0018279	protein N-linked glycosylation via asparagine	3.81E-08	7.69E-06	4.74
GO:0006487	protein N-linked glycosylation	6.58E-08	1.30E-05	4.58
GO:0048193	Golgi vesicle transport	6.85E-08	1.32E-05	3.31
GO:0048002	antigen processing and presentation of peptide antigen	1.02E-07	1.93E-05	3.58
GO:0042592	homeostatic process	1.02E-07	1.90E-05	2.3

Table 6.5: GO Term enrichment based on GO for molecular functions (GOMF)
GO terms with with a p-value below 0.01 are shown.

GO Term	Description	P-value	FDR q-value	Enrichment
GO:0051082	unfolded protein binding	1.78E-13	4.88E-10	5.98
GO:0005515	protein binding	4.29E-10	5.86E-07	1.25
GO:0016860	intramolecular oxidoreductase activity	4.36E-10	3.98E-07	7.67
GO:0003924	GTPase activity	1.04E-09	7.09E-07	3.89
GO:0016864	intramolecular oxidoreductase activity, transposing S-S bonds	1.57E-08	8.58E-06	10.57
GO:0003756	protein disulfide isomerase activity	1.57E-08	7.15E-06	10.57
GO:0005525	GTP binding	2.12E-08	8.30E-06	3
GO:0032561	guanyl ribonucleotide binding	4.94E-08	1.69E-05	2.9
GO:0019001	guanyl nucleotide binding	5.66E-08	1.72E-05	2.88
GO:0005509	calcium ion binding	7.86E-08	2.15E-05	2.9
GO:0004576	oligosaccharyl transferase activity	9.40E-08	2.34E-05	12.79
GO:0003823	antigen binding	7.63E-07	1.74E-04	8.77
GO:0004579	dolichyl-diphosphooligosaccharide-protein glycotransferase activity	1.22E-06	2.58E-04	12.33
GO:0023026	MHC class II protein complex binding	1.53E-05	3.00E-03	11.74
GO:0023023	MHC protein complex binding	1.53E-05	2.80E-03	11.74
GO:0016853	isomerase activity	1.93E-05	3.30E-03	3.14
GO:0048029	monosaccharide binding	2.14E-05	3.44E-03	4.84
GO:0008092	cytoskeletal protein binding	2.52E-05	3.83E-03	1.97
GO:0019003	GDP binding	2.84E-05	4.08E-03	4.7
GO:0003779	actin binding	2.86E-05	3.91E-03	2.42
GO:0003674	molecular_function	3.12E-05	4.07E-03	1.06
GO:0005537	mannose binding	3.89E-05	4.83E-03	10.28
GO:0030246	carbohydrate binding	5.67E-05	6.74E-03	3.5
GO:0001948	glycoprotein binding	6.25E-05	7.12E-03	4.77
GO:0016705	oxidoreductase activity, acting on paired donors, with incorporation or reduction of molecular oxygen	7.09E-05	7.76E-03	3.65
GO:0019798	procollagen-proline dioxygenase activity	1.83E-04	1.92E-02	10.96
GO:0008426	protein kinase C inhibitor activity	2.23E-04	2.26E-02	16.44
GO:0008379	thioredoxin peroxidase activity	2.23E-04	2.18E-02	16.44
GO:0051920	peroxiredoxin activity	4.06E-04	3.83E-02	9.4
GO:0031543	peptidyl-proline dioxygenase activity	4.06E-04	3.71E-02	9.4
GO:0020037	heme binding	5.36E-04	4.73E-02	4.6
GO:0005488	binding	6.28E-04	5.36E-02	1.08
GO:0005102	receptor binding	7.29E-04	6.04E-02	1.73

GO:0030235	nitric-oxide synthase regulator activity	8.52E-04	6.86E-02	12.33

6.2 Abbreviations and Symbols

Where abbreviations for proteins were not defined in the text, the official gene symbol according to UniprotKB (UniProt 2014) was used. Uniprot identifiers for all identified host cell proteins are listed with their gene symbol in the appendix (Table 6.1).

Table 6.6: Abbreviations used in this thesis

Abbreviation	
(e)GFP	(enhanced) green fluorescent protein
AA	Amino acid
ABC	ATP-binding cassette
ACN	Acetonitrile
ACSL3	Long-chain-fatty-acid—CoA ligase 3
ACTB	Actin beta
ADP	Adenosine diphosphate
AmBic	Ammonium bicarbonate buffer
APS	Ammonium persulfate
ArtJ	arginine transport protein J
ATCC	American Type Culture Collection
ATP	Adenosine triphosphate
BAR	Bin/amphiphysin/Rvs
Bcl-2	B-cell lymphoma 2
BFA	Brefeldin A
BS3	(Suberic acid-bis-(3-sulfo-N-hydroxysuccinimide ester))
BSA	Bovine serum albumin
cDNA	complementary DNA
CERT	Ceramide transfer protein
CID	collision induced dissociation
CI-M6PR	cation independent mannose 6-phosphate receptor
CL	cleared lysate
COMC	Chlamydia outer membrane complex
COXI	Cytochrome C Oxidase Subunit I
CTP	Cytidine triphosphate
CTxB	cholera toxin B subunit
DAPI	4',6-diamidino-2-phenylindole
dFCS	dialyzed FCS
DMEM	Dulbecco's modified Eagle's medium
DMSO	Dimethyl sulfoxide
DNA	Deoxyribonucleic acid
DTT	Dithiothreitol
E1	first eluate
EB	Elementary body
ECL	Enhanced chemoluminescence
EE	early endosome
EEA1	early endosomal antigen 1
EGFR	epidermal growth factor receptor
EGTA	ethylene glycol tetraacetic acid
EL	endolysosome
ER	Endoplasmic reticulum
ERGIC	ER – Golgi intermediate compartment
ESI	electrospray ionization
et al.	et alia
EX	exocytosis
EXC	extracellular
EXV	exocytic vesicle
FASP	filter aided sample prepraration
.FASTA	File format

FCS	fetal calf serum
FLII	Protein flightless-1 homolog
FOV	field of view
FT	flow through
FW	forward
FYVE domain	Fab 1, YOTB, Vac 1 and EEA1 domain
G	ghost
G4V	GLUT4 containing vesicles
GA	Golgi apparatus
GAPDH	Glyceraldehyde 3-phosphate dehydrogenase
GET2020	Global elimination of trachoma by 2020
GO	Gene Ontology
GOBP	GO of biological processes
GOCC	GO of cellular compartments
GOMF	GO of molecular functions
GRP94	Glucose regulated protein of 94 kDa
GS15	Golgi SNARE with a size of 15 kDa
GST	Glutathione S-transferase
GTP	Guanosine triphosphate
H	heavy SILAC label
HeLa	Henrietta Lacks
HEPES	4-(2-hydroxyethyl)-1-piperazineethanesulfonic acid
HRP	Horseradish peroxidase
HSM	HEPES /sucrose/ magnesium buffer
HSMG	HEPES/sucrose/magnesium/EGTA
Hsp	Heat shock protein
IAA	Iodoacetamide
IB	intermediate body
iBAQ	intensity based absolute quantification
ID	identifier
IF	immunofluorescence
IFN- γ	interferon-γ
IFU	inclusion forming units
IM	Inclusion membrane
Inc	Inclusion protein
IPTG	isopropyl β-D-1-thiogalactopyranoside
IUPAC	International Union of Pure and Applied Chemistry
L	light SILAC label
LAMP	lysosomal associated membrane protein
LB	Luria-Bertani
LC-MS/MS	liquid chromatography coupled to tandem mass spectrometry
LCV	*Legionella* containing vacuole
LE	late endosome
LGV	Lymphogranuolma venereum
Luci	firefly luciferase
LY	lysosome
M6PR	mannose 6-phosphate receptor
MACS	Magnetic-activated cell sorting
MACS	magnet assisted cell sorting
MAP1-LC3	Microtubule-associated protein 1 light chain 3
MCS	membrane contact sites
MCV	*Mycobacteria* containing vacuole
Mito	mitochondria
MOI	multiplicity of infection
MOMP	major outer membrane protein
MTOC	microtubule organizing center
MVB	multivesicular body
MYOF	Myoferlin
N	Nucleus
NAD	nicotinamide adenine dinucleotide
NI	not infected
Npt	Nucleoside triphosphate transport protein

NSF	N-ethylmaleimide sensitive fusion protein
NT	not treated
OmcA	Small cystein-rich outer membrane protein A
OmcB	Small cystein-rich outer membrane protein B
P	monophosphate
P	Peptides (only used in Tables)
P(2)	bisphosphate
P(3)	triphosphate
p.i.	post infectionem
p62	Nucleoporin 61
PAGE	polyacrylamide gel electrophoresis
PBS	phosphate buffered saline
PC	phosphatiylcholine
PCR	Polymerase chain reaction
PDI	protein disulfide isomerase
PFA	Paraformaldehyde
PI3K	Phosphatidylinositol-3 kinase
Pht	Phagosomal transporter
PKCδ	protein kinase C delta
PM	plasma membrane
Pmp	polymorphic membrane protein
PtdIns	phosphatidylinositol
PV	parasitophorous vacuole
PVDF	polyvinylidene difluoride
PX	phox homology
R^2	Pearson's R-squared correlation coefficient
Rab	Ras-like protein from rat brain
Rab6 IP1	Rab6 interacting protein 1
Rac1	Ras-related C3 botulinum toxin substrate 1
.raw	File format
RB	Reticulate body
RE	recycling endosome
RidL	retromer interactor decorating LCVs
RKI	Robert Koch Institut
RNA	Ribonucleic acid
RNAi	RNA interference
rpm	Revolutions per minute
RPMI	Roswell Park Memorial Institute medium
rRNA	ribosomal RNA
RT-QPCR	Real time - quantitative PCR
RV	reverse
Sam68	Src associated in mitosis of 68 kDa
SAX	strong anion exchange chromatography
SDS	sodium dodecyl sulfate
Sec61β	General Secretory Pathway protein 68
SI	*Le Système international d'unités*
SidC	substrate of Icm/Dot transporter C
SILAC	Stable isotope labeling by amino acids in cell culture
siRNA	short inhbiting RNA
SLC	solute carrier
SM	sphingomyelin
SMVT	sodium multivitamin transporter
SNARE	Soluble NSF attachment factor receptor
SNX	sorting nexin
SopB	Stabilisation of plasmid protein B
STAGE	stop and go extraction
STIM1	Stromal interaction molecule 1
STRING	Search Tool for the Retrieval of Interacting Genes/Proteins
SYNGR2	Synaptogyrin-2
T3SS	type three secretion system
TARP	translocated acin-recruiting phosphoprotein
TBE	Tris/Borate/EDTA

TBS	tris buffered saline
TBST	tris buffered saline supplemented with tween
TBST-M	tris buffered saline supplemented with tween and milk
TEM	transmission electron microscopy
TEMED	Tetramethylethylenediamine
TFA	Trifluoroacetic acid
TFRC	Transferrin receptor
TGN	trans Golgi network
tRNA	transfer RNA
trp	Tryptophan
UA	Urea buffer
UTP	Uridine-5'-triphosphate
UV/Vis	ultraviolet/ visible
VAMP	Vesicle-associated membrane protein
vATPase	vacuolar H+-ATPase
VCP	Valinosin-containing protein
VPI	validation by purified inclusions
VPI-LC	VPI in live cell microscopy
Vps	vacuolar protein sorting-associated protein
W1	first wash fraction
W2	second wash fraction
WASH	Wiskott-Aldrich syndrome protein and Scar homologue
WT	wild type
XIC	Extracted ion current
YFP	yellow fluorescent protein
zntA	zinc transporting ATPase

Table 6.7: List of symbols used in this thesis

Symbol	Name	Unit
µm	micrometer	10^{-6} m
nm	Nanometer	10^{-9} m
A	Absorbance	Relative unit
Da	Dalton	$1.660538921(73)\times10^{-27}$ kg
x g	times gravity (relative centrifugal force)	9.81 m/s^2
h	hour	3600 s
G	gauge	see EN ISO 6009
mg	milli gram	10^{-6} kg
min	minute	60 s
ml	milli liter	10^{-6} m^3
mM	milli molar	mol/m^3
pH	-	$-\log_{10}([H^+])$
RT	room temperature	25 °C (as defined by IUPAC)
S	Svedberg	10^{-13}
V	Volt	SI unit

6.3 List of Figures

6.4 List of Tables

Acknowledgements

An dieser Stelle möchte ich mich bei den Personen bedanken, welche durch ihre professionelle Unterstützung, diese Arbeit erst möglich gemacht haben.

Zuerst möchte ich mich bei **Dr. Dagmar Heuer** für die Betreuung meiner Doktorarbeit bedanken, bei welcher sie mir nicht zuletzt die Freiheit gelassen hat mein eigenes Projekt zu erdenken und zu verwirklichen.

Prof. Dr. Thomas F. Meyer und die Max Planck Gesellschaft haben diese Arbeit mithilfe eines Stipendiums ermöglicht, Danke!

Für die grossartige Unterstützung bei den kleinsten Elementen dieser Arbeit möchte ich **Dr. Sebastian Banhart** danken, welcher entscheidend dazu beigetragen hat, dass die konfokalen Aufnahmen brillant geworden sind.

Anke Herrmann verdient spezielle Anerkennung für ihre unermüdliche Hilfe im Labor und den nicht versiegenden Nachschub an hochprozentigen Schokoladenprodukten.

Sophia Koch, **Laura Rose**, **Andrea Martini** und **Verena Keil** waren gerne für ein Spässchen zu haben und hatten auch im Labor immer ein helfendes Händchen.

Dr. Michael Laue, **Dr. Kazimierz Madela**, **Jeanette Piesker** und **Gudrun Holland** möchte ich für die elektronenmikroskopischen Aufnahmen danken.

Dr. Frank Schmidt und **Dr. Nico Jehmlich** danke ich für die wertvolle Messzeit an ihrer Orbitrap, die grossartigen Fischbrötchen in Greifswald werde ich zudem nie vergessen.

Dr. Toni Aebischer für Korrekturen und hilfreiche Kritik über meine ganze Zeit als Doktorand.

Durch ihre niemals nachlassende persönliche Unterstützung haben zudem folgende Personen entscheidend zur Fertigstellung dieser Arbeit beigetragen:

Melanie Weber für Verständnis, Geduld und alles andere

Hans Peter Aeberhard für mein Studium

Michaela Scherhaufer für unerschöpfliche Motivation

Hugo Aeberhard, **Lilly Aeberhard-Salvisberg, Willhelma und Siegfried Gröbacher** für ihr Vertrauen und ihre Unterstützung

Mena, **Michi** und **Philipp** für da z sy, wenns näch brucht!

Publications

Articles

Banhart S., E. Saied, A. Martini, S. Koch, **L. Aeberhard**, K. Madela, C. Arenz, and D. Heuer (2014). "Improved plaque assay identifies a novel anti-Chlamydia ceramide derivative with altered intracellular localization." Antimicrob Agents Chemother. (Accepted Manuscript)

Poster presentations and talks

Proteome analysis of the *Chlamydia trachomatis* intracellular vacuole identifies novel associated proteins (Poster)

Lukas Aeberhard, Sebastian Banhart, Nico Jehmlich, Frank Schmidt and Dagmar Heuer

Deutscher Chlamydien Workshop, Berlin, 2014

Proteome analysis of the *Chlamydia trachomatis* intracellular vacuole identifies novel associated proteins (Poster and talk)

Lukas Aeberhard, Sebastian Banhart, Nico Jehmlich, Frank Schmidt and Dagmar Heuer

EMBO Workshop „Integrating omics approaches to host-pathogen interactions“, Liverpool, 2013

Characterization of the interaction of *Chlamydia psittaci* with the Golgi apparatus (Poster)
Lukas Aeberhard, Julia Heymann, Thomas F. Meyer and Dagmar Heuer
Nationales Symposium für Zoonosenfoschung, Berlin, 2012

Berlin, September 2014 Lukas Aeberhard

Selbstständigkeitserklärung

Ich erkläre hiermit, dass ich die vorliegende Arbeit selbständig und nur unter Verwendung der angegebenen Hilfen und Hilfsmittel nach §7, Absatz 3 der Promotionsordnung vom 6. Juli 2009 der Mathematisch- Naturwissenschaftlichen Fakultät I der Humboldt Universität zu Berlin angefertigt habe. Wurden Ergebnisse in Kooperation produziert, ist dies entsprechend angegeben.

Berlin, im September 2014 Lukas Aeberhard